Extended application of timber for gates of existing locks

N.J. Groeneveldt
03/11/2021

TU Delft

Iv-Infra

This page intentionally left blank

Extended application of timber for gates of existing locks

By

N.J. Groeneveldt

in partial fulfilment of the requirements for the degree of

Master of Science

in Civil Engineering

Delft University of Technology
Faculty: Civil Engineering and Geosciences
Track: Structural Engineering
Specialization: Hydraulic Structures
Student number: 4487591
03/11/2021

Thesis committee:	Dr.ir. G.J.P. Ravenshorst	TU Delft
	Dr.ir. P.C.J. Hoogenboom	TU Delft
	Dr.ing. M.Z. Voorendt	TU Delft
	Ing. D.W. Alsemgeest	Iv-Infra B.V.
	Ir. Y. Yao	Iv-Infra B.V.

This page intentionally left blank

Preface

This thesis document is the final phase of my studies to obtain a Master of Science degree at the Delft University of Technology. While writing this thesis, I broadened my knowledge and also gained experience in the engineering sector at an engineering company. Additionally, I have learned a lot about myself during this period. Several people have supported me in multiple ways throughout the graduation and, therefore, I want to share my gratitude.

I would like to thank my graduation committee for the meetings we've had. Feedback during these meetings has helped me to find my way within the extensive subject of this thesis. The COVID-19 pandemic made it unique and is the reason why we had only one in-person meeting.

Secondly, I want to thank Iv-Groep and my colleagues of Iv-Infra for the opportunity to work on this subject and providing me with the knowledge and workplace. Special thanks to my daily supervisors Yirui and Dennis. Your guidance was very helpful and very much appreciated.

A special thanks goes to my family, girlfriend and friends for their support throughout this journey and, on occasion, tense period. Thanks for listening to my whining and distracting me when I needed it. I wouldn't have been able to complete this without you.

Non scholae, sed vitae discimus

N.J. Groeneveldt
Sliedrecht, November 2021

List of symbols

A	area
$E_{0,mean}$	mean modulus of elasticity parallel to the grain
$E_{0,k}$	characteristic modulus of elasticity parallel to the grain
$E_{90,mean}$	mean modulus of elasticity perpendicular to the grain
$E_{90,mean}$	mean modulus of elasticity perpendicular to the grain
F	force
F_{ax}	characteristic axial withdrawal capacity of the fastener
$F_{v,Rk}$	load carrying capacity per shear plane per fastener
G_{mean}	mean shear modulus
I	moment of inertia
K_{SLS}	slip modulus in serviceability limit state
K_{ULS}	slip modulus in ultimate limit state
M	bending moment
$M_{y,Rk}$	characteristic value for yield moment
N	normal force
V	shear force
W	resultant force of hydraulic load
a	distance to the neutral axis
b	width
d	diameter
$f_{c,0,k}$	characteristic compression strength parallel to the grain
$f_{c,90,k}$	characteristic compression strength perpendicular to the grain
$f_{h,i,k}$	characteristic embedment strength
$f_{m,k}$	characteristic bending strength for glue laminated beam
$f_{t,0,k}$	characteristic tensile strength parallel to the grain
$f_{t,90,k}$	characteristic tensile strength perpendicular to the grain
$f_{u,k}$	characteristic tensile strength of fasteners
$f_{v,k}$	characteristic shear strength
g	gravitational constant
h	height
k	shear modulus of fastener
k_c	instability factor
k_{crit}	factor used for lateral buckling
k_{def}	deformation factor
k_h	height factor
k_l	stress distribution factor for curved beams
k_m	stress distribution factor
k_{mod}	modification factor for duration of load and moisture content
k_r	reduction factor for curving lamellae
k_y or k_z	instability factor
l	length
p	hydrostatic pressure
$p_{1,2,3}$	wave pressure
p_u	uplift pressure
q	distributed load

r	radius of curvature
s	spacing of the fasteners
t	thickness
u	deflection
z	distance to the centre of gravity
$\alpha_{1,2,3}$	pressure coefficients
α_{ap}	angle in the middle of tapered beam
β	ratio of embedment strength of mechanically jointed beams
β_c	straightness factor
γ	loss factor of mechanically jointed theory
γ_f	load factor
γ_m	material factor
γ_m	specific weight of the mitre gate
λ	slenderness
$\lambda_{1,2,3}$	modification factors for the geometry of a wind wave loaded structure
λ_{rel}	relative slenderness
ρ_k	characteristic density
ρ_m	density of the mitre gate
ρ_{mean}	mean density
ρ_w	density of water
$\sigma_{c,0,d}$	design compressive stress parallel to the grain
$\sigma_{m,d}$	design bending stress
$\sigma_{t,0,d}$	design tensile stress parallel to the grain
τ_d	design shear stress
$\Psi_{2,1}$	factor for quasi-permanent value of variable action

Abstract

Many navigation locks in the Netherlands under management and maintenance of Rijkswaterstaat need to be replaced or renewed in a sustainable way before 2050. In order to achieve this goal, Rijkswaterstaat is planning to renew as sustainable and cost-effective as possible. Most of the navigation lock gates that have been renewed in the last decades are made in steel, especially mitre gates. However, timber is a more sustainable material than steel to replace the navigation lock gates. The goal of this thesis is to find out why timber is scarcely used for the renewal of mitre gates with a navigation lock chamber wider than 12 metres and to extend the application of timber in an innovative way for the renewal of existing mitre gates to replace steel mitre gates.

First, the structural layout of the mitre gates was analysed. Further research has shown that the steel design of mitre gates is more profitable than the current timber design for lock chambers above 12 metres width, because all the existing timber mitre gates are made by solid timber beams, which have limited availability due to the required dimensions. Further, the mortise and tenon joint of the main girders and posts is one of the challenges and critical parts of timber structures. Recent innovations, such as timber lamination, crossed or not, increases the strength and stiffness characteristics and creates more freedom in the design of the cross section size and shape, which makes timber a construction material that could be more competitive with other often used construction materials, steel for example. Since the mitre gates need to withstand the loads in both vertical and horizontal directions, cross laminated timber can be efficient. In building engineering, laminated timber is usually glued, however, for hydraulic engineering, this is not possible yet as no adhesive is appropriate in a wet environment. It is therefore chosen to further investigate the possibility of applying mechanically jointed cross laminated timber in a mitre gate.

The eastern navigation lock of Sambeek is considered as a suitable case study location to investigate. This lock chamber has a width of 16 metres, a water retaining height of 8.44 metres and a maximum differential head of 4.2 metres. The results of the preliminary design for this mitre gate consists of a dowel cross laminated skin plate, semi-ellipse web plates and three layered laminated curved girders. The skin plate in the renewed design contains layers in vertical and horizontal directions to transfer the load in both directions. Furthermore, the skin plate contains diagonally orientated layers to replace the steel strut and tension bar. The girder of the mitre gate is curved to create the biggest stiffness halfway the width of the mitre gate and spare the used amount of timber sideways. The web of the redesign is the connector of the skin plate and the girder. The challenge of the mortise and tenon joint is solved by directly supporting the girder towards the lock chamber wall. This results in a skin plate of 6 layers; all with a thickness of 25 mm. The skin plate has 2 horizontally orientated, 2 vertically orientated and 2 diagonally orientated layers. The curved laminated girder has 3 lamellae each 100 millimetres thick and the distance to the skin plate and girder varies between 0 and 300 mm. In between the girder and skin plate, a web plate of 150 millimetres thick is constructed. The girder and web plate are repetitive elements with a centre to centre distance of 1.5 metres vertically.

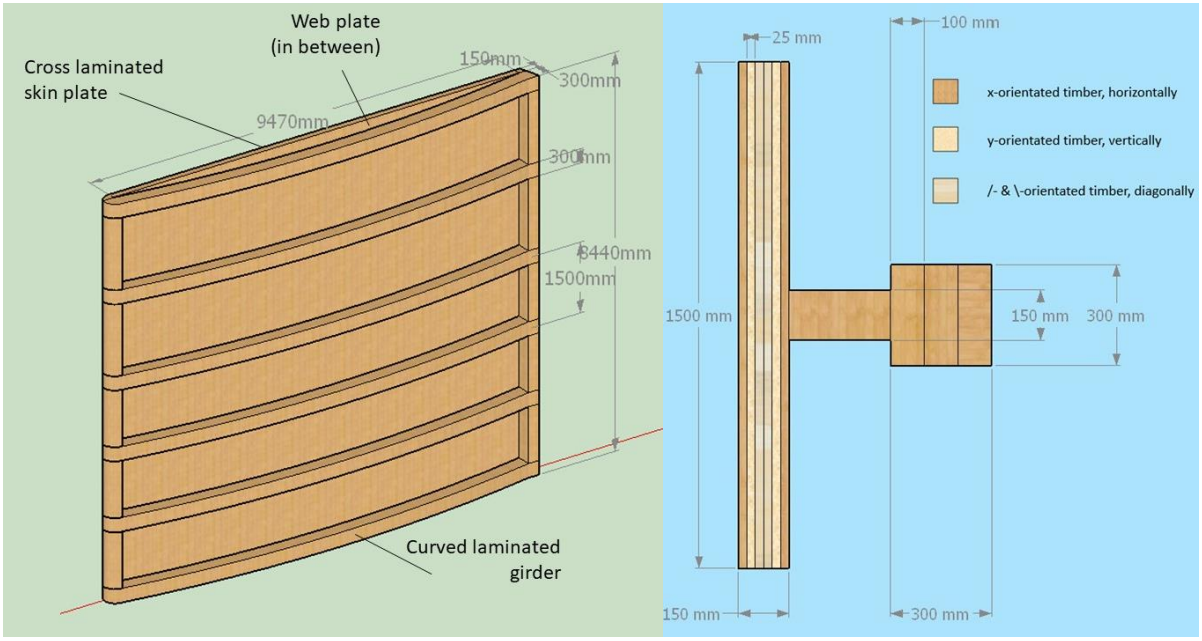

Figure 1: Overview (left) and repetitive cross section (right) of final preliminary design of the mitre gate for eastern Sambeek navigation lock

To verify the preliminary redesign, the mitre gate is modelled in a finite element program. In this finite element program, the mitre gate is built up of beam elements, and the interaction of the timber elements and fasteners is simulated with springs. For the closed mitre gate, the global outcomes of the model and preliminary design are consistent, but the interaction between the fasteners and timber elements in the dowel cross laminated skin plate requires further research. Furthermore, it can be concluded that the use of cross laminated timber is an equivalent replacement of the steel strut and tension bar to resist the self-weight of the mitre gate.

Based on the performed research in this thesis, the renewed design of timber mitre gates is at an early stage but attainable for the future. The mitre gate with cross laminated timber skin plate works as efficient as the steel gate and is more sustainable. However, the challenge remains in the connection of the timber elements and further research is needed to make the design feasible. The development in the material and connection method would make timber mitre gates more attractive during the choice of design.

Table of Contents

1. Introduction

In this chapter, the motivation of the thesis is written in the first section. The problem analysis is defined in the second section. It contains the general functioning of a navigation lock, inventory of common type of navigation lock gates and the application range of these common navigation lock gates. The end of this chapter contains the problem statement.

1.1 Motivation of the thesis

Hydraulic engineers in the Netherlands are challenged to come up with new sustainable and cost-effective designs or innovations for sluices. The majority of these sluices are navigation locks. Navigation locks are built for transport to overcome water level differences. According to Rijkswaterstaat, the Dutch directorate-general for public works and water management, 52 of the 137 navigation locks under management and maintenance of Rijkswaterstaat need to be replaced before 2050 (Rijkswaterstaat, 2016). 37 of them will reach their end of lifetime, whereas for the other 15 locks the capacity will not be sufficient in the future. To do so Rijkswaterstaat have set up a program called 'MultiWaterWerk', with the goal to standardize the design of the lock gates to decrease the Life Cycle Cost (LCC), optimize availability and reliability and have more insight in costs and construction time (Rijkswaterstaat, 2016). On the other hand, as stated by Willems & Busscher (2014), it seems difficult to realise the standardization since locks have many characteristics, for example, the width, length, height, material and operating mechanism of the lock. Even though there seems no consensus on the execution of the standardization of lock gates yet, the 'MultiWaterWerk' program proves that, although slow, innovation and sustainability are increasingly important (Willems & Busscher, 2014).

Historically, most lock gates were made from timber. Only recently has there been a trend that newly built hydraulic structures, lock gates especially, were constructed from steel, without really considering other possible materials. In building engineering, bridge engineering specifically the same trend was visible mid-20th century, steel was almost the only used construction material. Over time, concrete and timber became competitive with steel. Timber became particularly competitive due to sustainability aspects and quality improvements. Cross laminated timber is an example of the quest for more sustainable and innovative timber structures. Cross laminated timber consists of at least 3 perpendicular placed wood plates which are mainly are glued together (Wallner-Novak, Koppelhuber, & Pock, 2014). This ensures that the limitation with respect to the dimensions of timber disappear and the direction of loading becomes less important. Nowadays, almost all the cross laminated timber is made from softwoods. The use of softwood, which is less strong than hardwood, could be a reason why cross laminated timber is not used in hydraulic engineering yet. It could also be that the hydraulic engineering is less innovation supporting than the building engineering and is lagging a few decennia in material point of view (Willems and Busscher, 2014).

In this thesis, timber is chosen to be investigated for multiple reasons. First of all, steel is already roughly studied for standardizing lock gates by Levinson (2018). Secondly, timber has developed quite a lot over the last decades. Bridges with large spans and multi-storey buildings for example have been built from timber in the last decade. These developments show the possibility of application of timber to hydraulic structures beyond the scale where it's currently limited to. Moreover, timber is more sustainable than steel and other materials, thus timber becomes more attractive due to the fact that sustainability becomes more and more important in engineering. An example of the sustainable advantage of timber over steel is that the material production and disposal of timber results in half to two-thirds of the CO_2 equivalent emissions as for the same concrete or steel building (Buchanan, John, & Love, 2013). The sustainable advantage could even help to reach the goal of the Paris Agreement to reduce the CO_2 emission by 40% (United Nations, 2015). Apart from the sustainable part, by investigating the possibility of using cross laminated timber for larger scale of hydraulic structures, such as lock gates, may be interesting for all the stakeholders, like government, contractors, designers,

etc., and eventually applied in the renovation of mitre gates. This thesis explores the possibilities of timber innovations like cross laminated timber for lock gates.

1.2 Problem analysis

1.2.1 Functioning of navigation locks in general

A navigation lock is a structure that bridges the height difference of waterways. The navigation lock has three primary functions. The first primary function of a navigation lock is to enable transfer of ships. The second primary function is to maintain a water level difference in the waterways, for example, for flood defence purpose. The last primary function of a navigation lock gate is to manage the water quality of the separating waterways. The structural elements of a common navigation lock are shown in Figure 2 (Molenaar W. F., 2020).

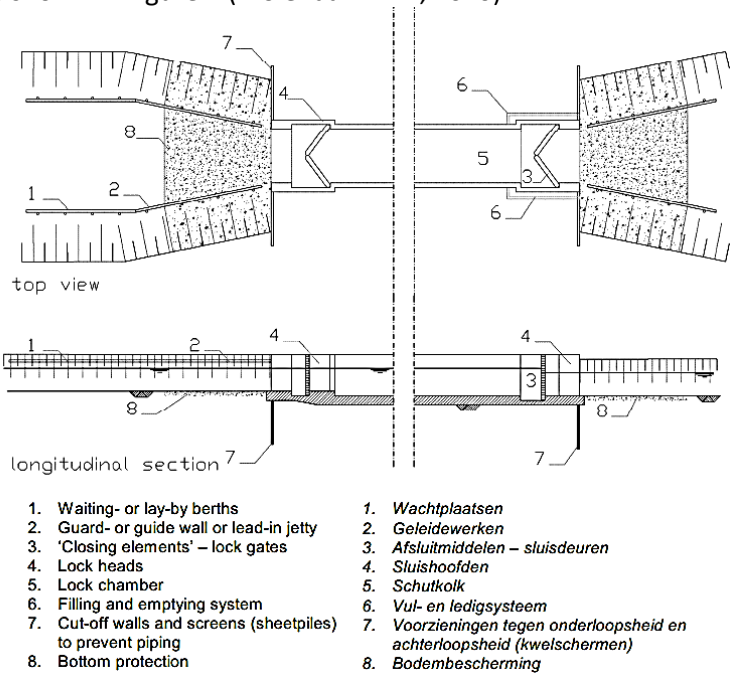

Figure 2: Layout of a navigation lock with mitre gates (Molenaar and Voorendt, 2020)

The operation of a navigation lock is always in one direction. This direction can be from upstream to downstream and vice versa, but it is impossible to do it simultaneously. The operation of a common navigation lock is as follows: a ship coming from downstream must wait to enter the lock chamber at berths. If the water level in the lock chamber is the same as the water level downstream, where the ship is waiting, the lock gate downstream opens and the ship can sail into the chamber and moors to the lock head. The lock gate closes and the water inside the chamber can be levelled to the water level upstream. After that, the upstream gate is opened and the ship can sail out the lock chamber and continues its way. The operation of the navigation lock from upstream to downstream is opposite of the operation from downstream to upstream.

1.2.2 Inventory of common type of lock gates

Different navigation lock gate types are used worldwide. In the Netherlands, the three most common types of navigations lock gates are mitre gates, rolling gates and lift gates. A description and layout of these gates is given below. The load distribution of the three most common navigation lock gate types is given in Appendix B.

Mitre gates

The mitre gate is named after the shape of the gate. They consist of two symmetric doors which rotate around the vertical axis. The driving mechanism is connected to the mitre gate on the high water side. If closed, the doors lean against each other at a gradient of about 1:3, with the point towards the high

water level (Glerum, et al., 2000). The first constructed mitre gates were able to retain the water in one direction, however, now sometimes mitre gates are able to retain the water in both directions. Advantages of mitre gates are the economic use of material, narrow gate recess in the chamber wall and simple operating mechanisms. Disadvantages are the exact dimensions and the sensitivity to ice, debris and collision in the direction of the point. Most of the mitre gates are made in steel and timber. The common layout of a steel and timber mitre gate is shown in Figure 3 and Figure 4, respectively.

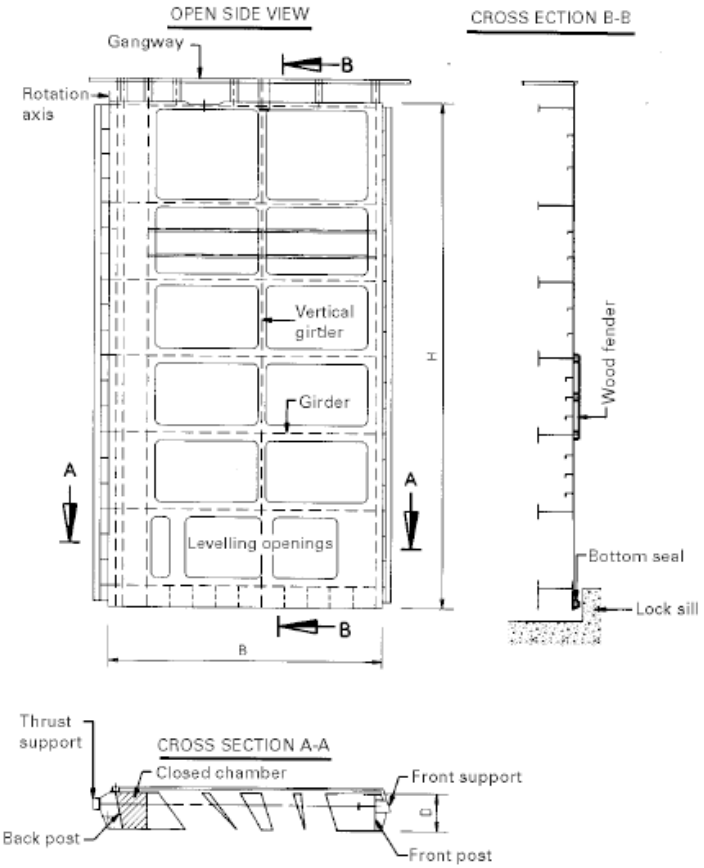

Figure 3: Steel mitre gate (Daniel and Paulus, 2019)

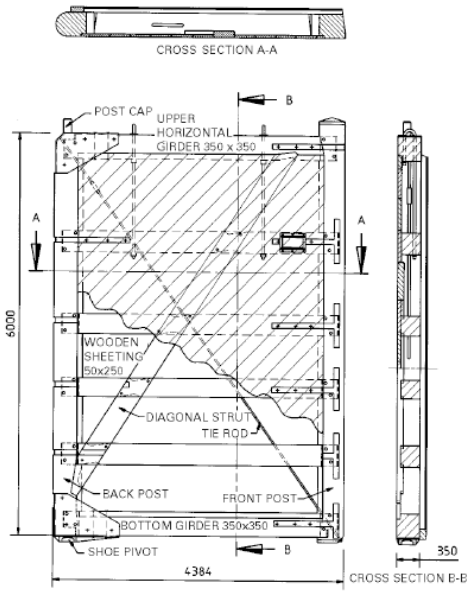

Figure 4: Timber mitre gate (Daniel and Paulus, 2019)

Lift gates

The lift gate is a gate that is lifted vertically between two towers positioned at both sides of the chamber walls. To reduce the operational mechanism, counter weights are used. Advantage of the lift gate is that it takes up little space of the chamber, can retain bilaterally and has little sensitivity to ice and debris. Disadvantages are the relatively small vertical clearances compared to other structures and complicated and expensive superstructure and operation mechanism.

The layout of a lift gate is almost the same as for a mitre gates and contains the following components: skin plate, horizontal girders, end girders and vertical posts if the cladding range is too big (Glerum, et al., 2000).

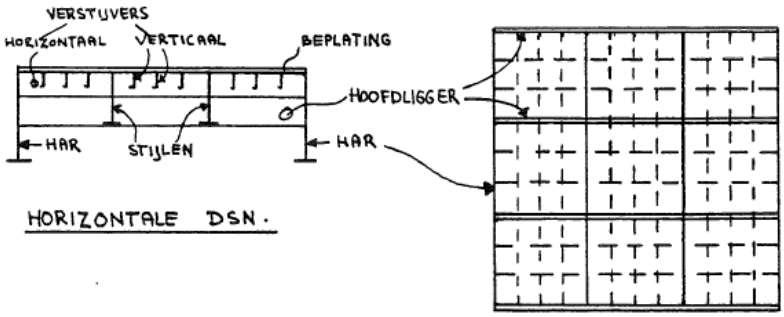

Figure 5: Steel lift gate (Molenaar and Voorendt, 2020)

Rolling gates

The rolling gate is a horizontally moving gate on rolling carriages. This type of gate is preferred for locks with big widths, because the construction and maintenance costs of the gate are quite high due to the complexity of the rolling gates. The first rolling gate was constructed at the end of the 16th century as a replacement of the lift gate (Arends, 1994). The movement of the rolling gate has always been a challenge. The introduction of float control chambers to reduce the weight of the gate contributed in a light operating mechanism. Another advantage of the rolling gate is the possibility of two-sided water retaining. Disadvantages are the big gate recess and expensive gate guiding system in construction and maintenance.

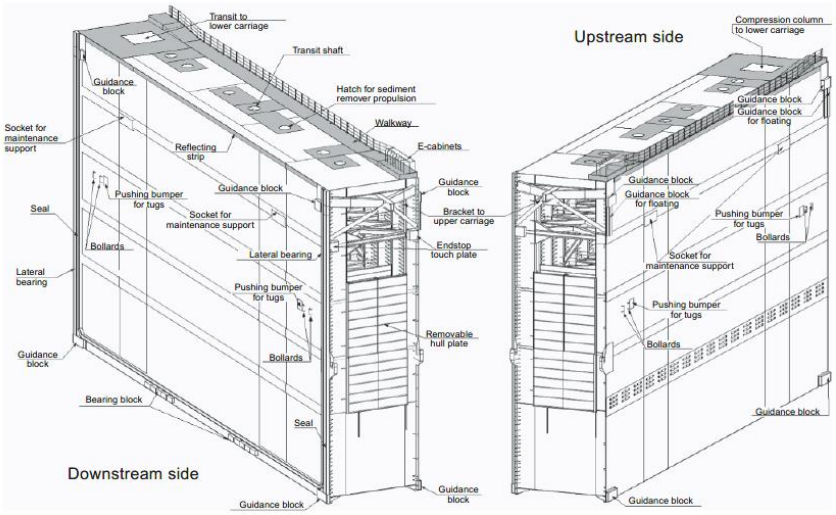

Figure 6: Rolling gates from the Panama Canal (Iv-infra, unpublished)

A detailed design of the Panama gates is shown in Figure 6.

1.2.3 Application range of each gate type

As told before in the previous section the mitre, rolling and lift gate are the most applied types of gates in the Netherlands. In general, it could be said that the choice of the type of gate mainly depends on the width of passage of the navigation lock, the requirements set for the gate as retaining structure and the requirements with regard to gate movement (Glerum, et al., 2000).

In preliminary design, the potential types of lock gates are based on the width of the navigation lock. The width for which the mitre, rolling and lift gate can be chosen is shown in the table below. In this table, two different types of locks are shown. The marine lock is located in a marine environment and therefore has large dimensions in most cases. The inland navigation lock is mainly limited to a maximum width of 24 metres due to the classification of inland waterways (Glerum, et al., 2000).

	Mitre gate	**Rolling gate**	**Lift gate**
Marine lock	< 24 m	> 16 m	
Inland navigation lock	< 24 m	16 – 24 m	10 – 24 m

Table 1: Application width of mitre, rolling and lift gates per lock type

The maximum width of the mitre gate is limited by the driving mechanism. A mitre gate in a lock wider than 24 metre needs a driving mechanism that is way too expensive to be able to compete with the rolling gate. The lift gate is not be chosen either in marine environment because of the limited vertical clearance. Hence, for extreme wide locks the rolling gate is the only economically attractive possibility as lock gate. The final design of the type of lock gate is chosen based on construction and maintenance costs, reliability and safety and other requirements of the client (Glerum, 1992).

As told in the Introduction, Rijkswaterstaat has set up the 'Multiwaterwerk' program where the goal is to decrease the Life Cycle Cost (LCC), optimize availability and reliability and have more insight in costs and construction time. The standardization of the entire lock is difficult. A more recent shift to renew the navigation lock in a more cost efficient way is to modularize navigation lock gates. Modularization is possible if locks are clustered. Therefore, Wilschut, Etman, Rooda, & Vogel (2019) have built a Dependency Structure Matrix based on a clustering algorithm to find lock commonalities for locks under management and maintenance of Rijkswaterstaat. This resulted into 7 different clusters. In each cluster, a lot of lock parameters are similar. To find out the application range of lock gates with different materials and different gate types, data of the 'Multiwaterwerk' is used. The clusters and some important characteristics are shown in Table 2.

	Type of gate	Material	Width range (m)
Cluster 1	26 mitre gates	5 timber gates 21 steel gates	11 - 18.1
Cluster 2	12 mitre gates	8 timber gates 4 steel gates	6 – 9.8
Cluster 3	14 rolling gates	All steel gates	9 - 50
Cluster 4	1 mitre gate 14 lift gates	All steel gates	7.5 - 24
Cluster 5	13 mitre gates	2 timber gates 10 steel gates 1 FRP[1] gates	6 - 20
Cluster 6	16 mitre gates 1 lift gate 2 rolling gates	6 timber gates 12 steel gates 1 FRP[1] gates	7.5 - 18
Cluster 7	26 square mitre gates	3 timber gates 20 steel gates 3 timber & steel gates	7 - 24
Total	68 mitre gates 15 lift gates 16 rolling gates 26 square mitre gates	24 timber gates 96 steel gates 2 FRP[1] gates 3 timber & steel gates	6 – 50

Table 2: Type of gate, material and width range of clusters made by Wilschut et al. (2018)

An extensive overview of the gates clustered by Wilschut et al. (2019) under management and maintenance of Rijkswaterstaat can be found in Appendix A. From the table above, it can be seen that in each cluster except for cluster two, most gates are steel gates.

1.3 Problem statement

Many navigation locks of Rijkswaterstaat need to be replaced or renewed in a sustainable way before 2050. Rijkswaterstaat is planning to do the renovation of the navigation lock gates as sustainable and cost effective as possible. Timber is a more sustainable material than steel to replace the navigation lock gates. However, steel is used more often to replace mitre gates. The problem therefore is that the renovation of the navigation locks is not done as sustainable as possible.

[1] FRP is fibre reinforced plastic

2. Thesis approach

In Chapter 2 the objective, scope, research questions and thesis outline are given. Section 2.1 gives the objective of this thesis. After setting up the objective of this thesis, the scope is defined in Section 2.2. The research questions of the thesis are given in Section 2.3. The methodology is described in the fourth section. Finally, Section 2.5 gives the total outline of the thesis.

2.1 Objective

This thesis aims to do research about timber mitre gates and aims to increase the number of timber mitre gates. The goal of this thesis was to find out why timber is scarcely used for renovation of mitre gates wider than 12 metres and to extend the application of timber in an innovative way for the renewal of existing mitre gates to replace steel mitre gates.

2.2 Scope

For this thesis, the lock gates under management and maintenance of Rijkswaterstaat are taken into account. The three most appearing navigation lock gates under management and maintenance of Rijkswaterstaat are mitre gates, lift gates and rolling gates. From the overview of the application range of lock gates in Section 1.2.3, we can conclude that more than half of the navigation gates under management and maintenance of Rijkswaterstaat are mitre gates, 68 of the 125 navigation locks in operation more precisely. Furthermore, it can be seen that 96 of the navigation lock gates are made of steel and only 24 gates are made of timber.

Mitre gates are chosen for the renewed design of the lock gate in this thesis for multiple reasons. First and most important of all, mitre gates are chosen because they have the biggest potential implementation range. Secondly, the lift gates are slightly outdated due to the restrictions with the vertical clearance and the expensive superstructure. Finally, the rolling gate is designed for big widths and the design of rolling gates is very detailed, so it seems more logical to first investigate the possibility to replace the smaller and less detailed mitre gates with the use of timber and if that succeeds, the rolling gates could be replaced in a more sustainable way.

When taking a closer look at the mitre gates, it stands out that almost every mitre gate above a width of 12 metres is made of steel. Hence, the width range of 12 to 24 metres seems to be a potential range to implement the more sustainable timber mitre gates, as 38 steel mitre gates are constructed in this width range. Therefore, the scope of this thesis is limited to mitre gates of Rijkswaterstaat with lock chambers widths between 12 and 24 metres. In Figure 7, all the mitre gates within the scope of this thesis are shown.

Figure 7: Mitre gate locations within the scope of the research

2.3 Research questions

To achieve the objective of this thesis the main research question was formulated:

In what way can timber be used optimally within the mitre gates of existing navigation locks, to resist the acting loads under different circumstances?

To answer the main research question, sub questions were set up:
Q1: *How is a timber mitre gate schematized to optimize the force distribution and what is the effect on the materialization?*
Q2: *What does the design of an optimized timber mitre gate look like for an existing situation out of the current application range?*
Q3: *How can the design of the renewed optimized timber mitre gate be modelled in a finite element modelling program and what are the differences with the analytical design?*

2.4 Methodology

This thesis contains a literature review, preliminary design exercise and a finite element modelling of the design. The content for each chapter in this thesis is described below.

Literature review

1. In the first chapter of the literature review the loads on a mitre gate are described and the load distribution in the current design of the mitre gate is analysed. The answer on the first sub question is mainly retrieved by published literature and marginally by unpublished information of various engineering firms. With the schematization of the loads the challenges of the common design of the timber mitre gates are found.
2. The second part of the literature review contains information about timber and innovative use of timber. The characteristics of timber and the effects of innovations on these characteristics are prescribed. The information is required to apply in the redesign of the mitre gate.

Preliminary design of mitre gate

3. For the preliminary design of a renewed mitre gate, a case study location is chosen. This location contains a non-timber mitre gate in the scope of this thesis. In the preliminary design a solution is found for the challenges of the now common design of a timber mitre gate first. After this, the innovations for the challenges are implemented in the redesign of the timber mitre. The preliminary design of the timber lock gate is made to investigate if it is possible to design a timber mitre gate out in the scope of this research. The preliminary design is done by hand.
4. The second part of the preliminary design contains the more detailed design of the mitre gate. The most critical locations in the design are examined and worked out in detail. After the second part of the preliminary design the complete answer on the second sub question is given.

Modelling of the design

5. The preliminary design of the mitre gate is modelled in SCIA Engineer. The outcomes of the Finite Element Modelling are compared to the analytical model. First, a single element of the redesigned mitre gate is simply modelled in multiple ways to gain insight in the modelling behaviour of the timber innovation. The outcomes of the different test models are compared and the most appropriate test model is used for the final model of the total mitre gate.
6. The final modelling of the total redesign of the mitre gate is the second part of modelling the design. The boundary conditions of the mitre gate are worked out in more detail compared to the test models. The results of the model are compared to the outcomes of the analytical preliminary design, this will provide an answer on the last sub question.

2.5 Thesis outline

The outline of the thesis is shown in Figure 8. As can be seen this thesis contains 9 chapters that answers three sub questions to answer the main research question.

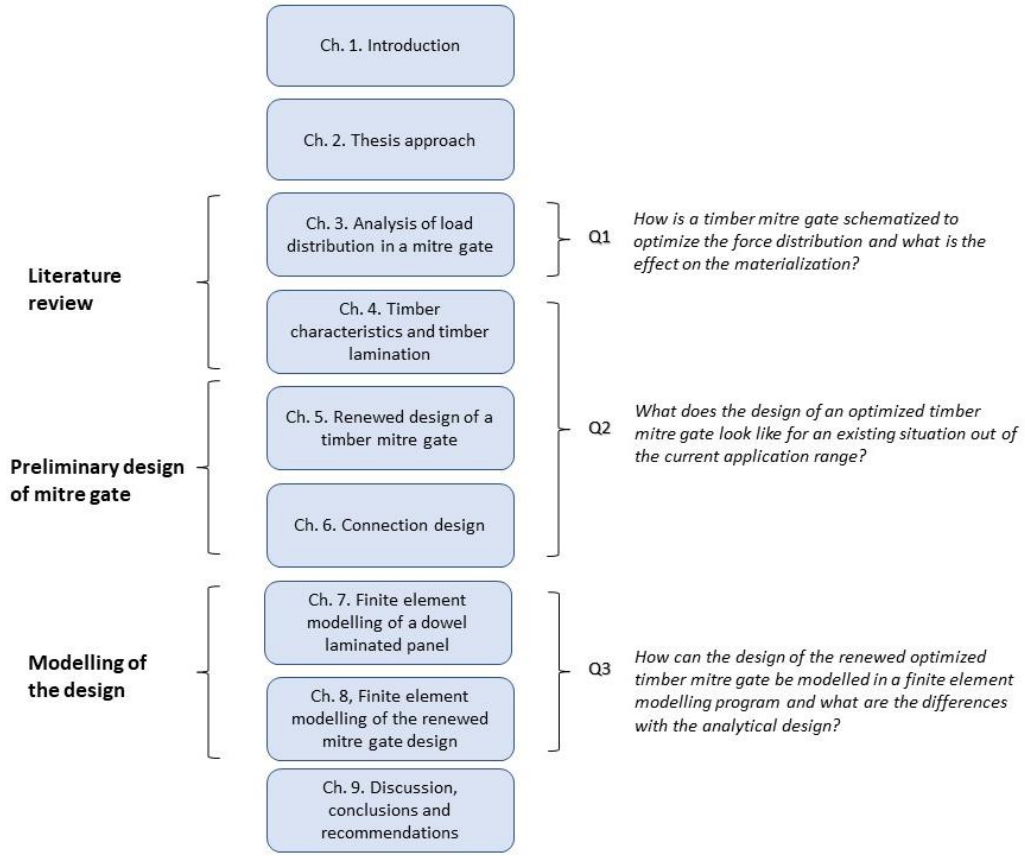

Figure 8: Thesis layout

3. Analysis of load distribution in a mitre gate

This chapter focuses on the loads on a mitre gate. First, Section 3.1 describes all the different loads on a mitre gate. The transversal load distribution of the mitre gate is described in Section 3.2 and the frontal load distribution is explained in the third section of Chapter 3. These previous sections provide insight in the current load distribution. In Section 3.4 the challenges of the current design of the timber mitre gate are given. Finally, Section 3.5 answers the first sub question*: How can a timber mitre gate be schematized to optimize the load distribution and what is the effect on the materialization?*

3.1 Loads on a mitre gate

To understand the load distribution in the mitre gate, three situations of the mitre gate can be considered. The gate can be in opened position, closed position and moving position from open to closed or vice versa.

In opened position the gate is in the lock recess. In the opened position the most critical situation is when a ship is passing by the gate and shortly ensures a water level difference between the water in the lock and the water behind the gate in the recess. The driving mechanism keeps the gate in opened position, which results in torsion in the gate. The water level difference due to passing ship is in order of few decimetres in navigation locks, together with the wind load this is a relatively small load and therefore the loads on the gate are not critical compared to other situations. Besides that the driving mechanism is out of scope of this research and therefore the opened situation of the mitre gate will not be studied into detail further.

In closed position the mitre gate is exposed to the following loads:

- Self-weight
- Uplift pressure
- Hydrostatic pressure
- Wind waves pressure
- Collision impact
- Ice load
- Other loads

During opening and closing of the gate the following loads can act on the mitre gate:

- Self-weight
- Uplift pressure
- Wind waves pressure
- Collision impact
- Ice load
- Obstacle load
- Other loads

For the strength verification of the mitre gate the loads are multiplied with different load factors. These load factors for different load combinations are defined in the '*Richtlijn Ontwerp Kunstwerken*' composed by Rijkswaterstaat, the tables with the load factors for closed and opening or closing situations are shown below.

Tabel 5-8: Belastingscombinaties Keermiddelen gesloten

belastingcombinatie Belasting	A	B	C	D	E	F	G	H	I
Eigen gewicht (F0,F1,F2)	1,25	1,25	1,25	1,25	1,25	1,25	1,25	1,25	1,25
Max pos vervalbelasting (MHW) (F10) Windgolfbelasting bij MHW (F13)	1,5								
Max neg verval (F11) Windgolfbelasting bij max neg verval (F13)		1,5							
Vervalbelasting bij max schutpeil (F12) Windgolfbelasting bij max schutpeil (F13) translatiegolf bij max schutpeil (F15)			1,5	1,2	1,2	1,2	1,2	1,0	1,0
Verkeersbelasting /bordesbelasting (F16)	1,2	1,2	1,2	1,5	1,2	1,2	1,2	1,0	1,0
Windbelasting	1,65	1,65	0,5	0,5	0,5	0,5	0,5	0,5	0,5
Voorspankracht uit bew. Werk (F33)	1,2	1,2	1,2	1,2	1,2	1,2	1,2	1,0	1,0
Schroefstraal schip					1,5				
IJsdruk (F53)					0,8	1,5			
Krachtsopbouw langs de draaias; zie (1.9)							1,5		
Aanvaren deur (F54)								1,0	
Lekraken drijfkist (F55)									1,0

Tabel 5-9: Belastingscombinaties openen/sluiten keermiddelen

belastingcombinatie Belasting	J	K	L	M	N
Eigen gewicht (F0,F1,F2)	1,4	1,25	1,25	1,25	1,25
Belastingen uit het bew.werk	1)	1)	2)	3)	1)
Hydraulische belastingen tijdens bewegen + wind (restverval, windgolven. Translatiegolven, wind, golfweerstand e.d) (F13+F14 +F15+F20+F22+F23+F24)	4)	4)			4)
Massakrachten (keermiddel + water) (F21+F30+F31)	4)	4)	4)	4)	4)
Obstakels (F40)			1,25		
Ijsdruk / ijsgewicht (F53)		1,5			
Falen besturingssysteem				1,25	
Krachtsopbouw langs de draaias; zie (1.9)					1,5

1) Voor de rekenwaarde van de belastingen uit het bewegingswerk wordt verwezen naar paragraaf 5.10 (4) "Belastingen op bewegingswerken"
2) Voor de rekenwaarde van de belastingen uit het bewegingswerk wordt verwezen naar paragraaf 5.10 (1.7) 'Belastingen door obstakels"
3) Gerekend mag worden bij hydraulische bewegingswerken met de overstortdruk x 1,20
4) Voor de belastingcombinaties en belastingsfactoren wordt verwezen naar paragraaf 5.10 (4) "Belastingen op bewegingswerken"

Figure 9: Load factors for closed (top) and opening or closing situation (bottom) (Richtlijn Ontwerp Kunstwerken, 2017)

3.1.1 Self-weight

The load due to the self-weight of the mitre gate is due to the gravity. This load is permanent present and is calculated by multiplying the volume of the gate with the specific weight of the gate.

$$F_{self-weight} = V * \gamma_m = V * \rho_m * g$$

V [m^3] = volume
γ_m [N/ m^3] = specific weight of the mitre gate
ρ_m[kg/ m^3] = density of the mitre gate
g [m^2/s] = gravitational constant

3.1.2 Uplift pressure

The uplift pressure is a result of the Archimedes' principle. The part of the mitre gate that is submerged experiences a buoyant force by the water. The uplift pressure is usually permanently present, only if the navigation lock is emptied for maintenance or other exceptional cases where there is no water in the navigation lock or river the uplift pressure is not present. The uplift pressure can be calculated with:

$$p_U = \rho_w * g * \frac{h_1 + h_2}{2} * t_d$$

Where:
p_U [kN/m] = uplift pressure per metre width
ρ_w [kg/m^3] = density of water
g [m^2/s] = gravitational constant
h_1 [m] = water depth on high water side
h_2 [m] = water depth on low water side
t_d [m] = thickness of the gate

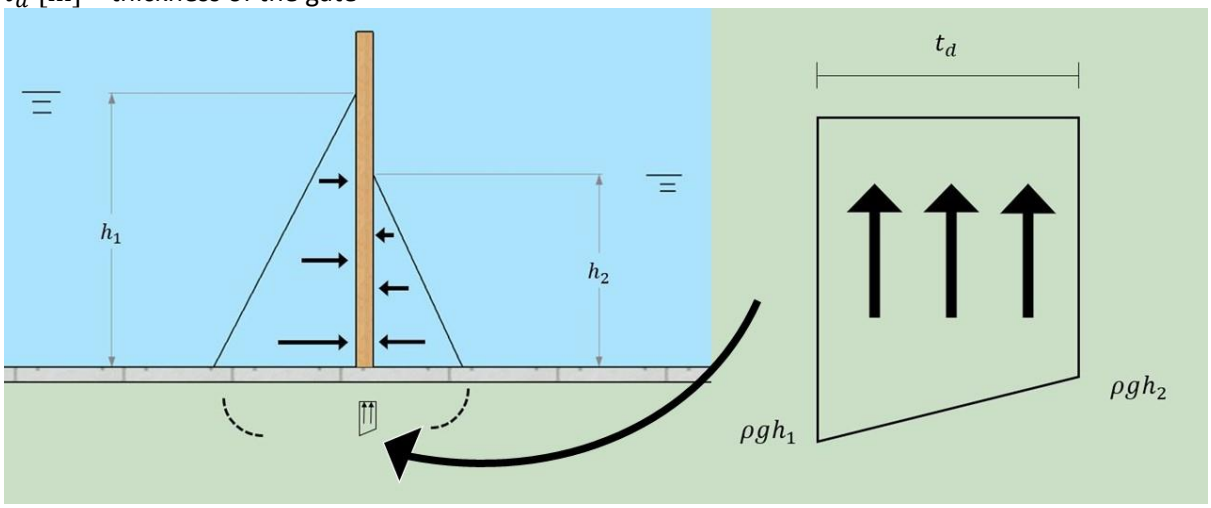

Figure 10: Side view of uplift pressure on a mitre gate, with the explanation (left) and the zoom in of the uplift pressure (right)

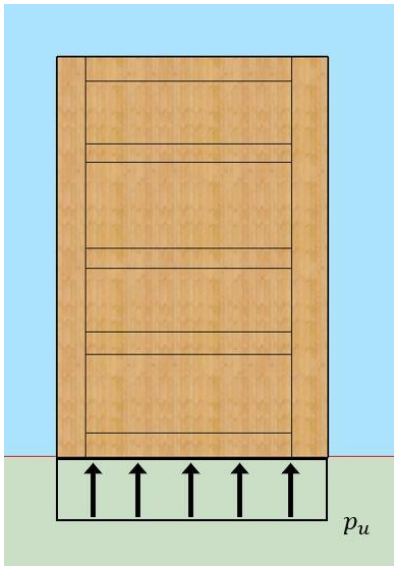

Figure 11: Front view of uplift pressure on mitre gate

3.1.3 Hydrostatic pressure

The hydrostatic pressure is a pressure on the mitre gate that builds up linearly from the top water level to the bottom. This pressure usually exists on both sides of the mitre gate, because water is present on both sides of the mitre gate. Like the uplift pressure the only absence of hydrostatic pressure is if the navigation lock is emptied. The formula for the calculation of the hydrostatic pressure is:

$$p = \rho_w * g * h$$

Where:
p $[\mathrm{N/m^2}]$ = hydrostatic pressure
ρ_w $[\mathrm{kg/m^3}]$ = density of water
h $[\mathrm{m}]$ = pressure head
g $[\mathrm{m^2/s}]$ = gravitational constant

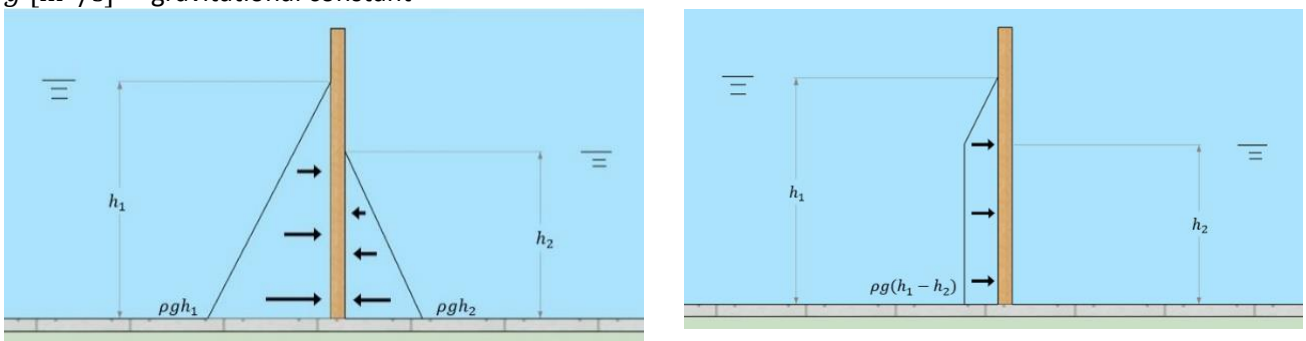

Figure 12: Hydrostatic pressure on a mitre gate (left) and resultant of hydrostatic pressure on a mitre gate (right)

3.1.4 Wind waves pressure

The pressures due to waves that act on a mitre gate generated by the wind are called wind waves. The wind wave load is greatest if close to sea or in open area. Wave can be breaking and non-breaking. Breaking of waves occurs when waves approach the coast, breaking is caused by the change of the water depth. In engineering the wave height of the breaking wave is added as an extra pressure to the hydrostatic pressure. As depicted in Section 2.2 the mitre gates in the scope are inland waterways and so the waves are not breaking. For non-breaking waves Voorendt and Molenaar (2020) mention five methods to calculate the load on the mitre gate if the waves are non-breaking. For the preliminary design a rule of thumb, linear theory and Sainflou method can be used. For the final design the method

of Rundgren and Goda can be used. The method of Goda gives the most precise values and is therefore elaborated (Technische Adviescommissie voor de Waterkeringen, 2003).

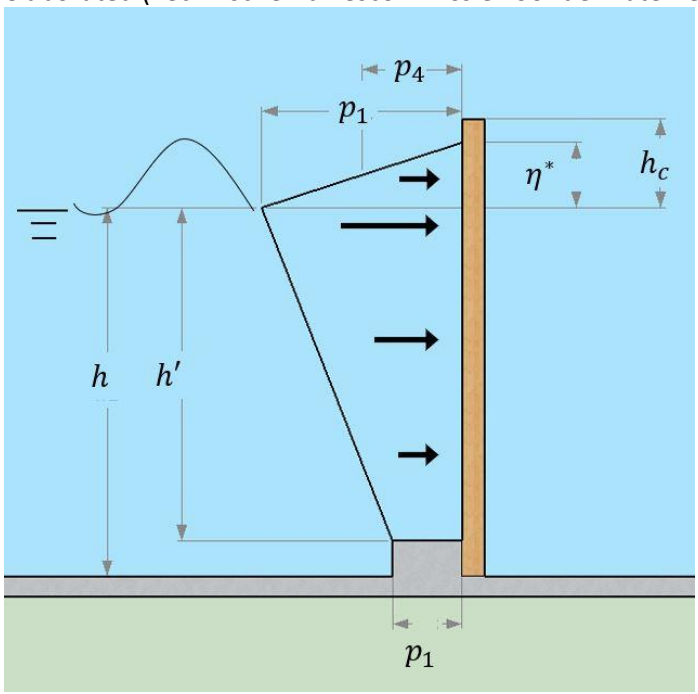

Figure 13: Wave pressure distribution with method of Goda

The wave pressures are:

$$p_1 = 0.5 * (1 + \cos(\beta)) * (\lambda_1 * \alpha_1 + \lambda_2 * \alpha_2 * \cos^2(\beta)) * \rho * g * H_D$$

$$p_3 = \alpha_3 * p_1$$

$$p_4 = \alpha_4 * p_1$$

Where:

$\beta =$ the angle of the incoming wave

$$\eta^* = 0.75 * (1 + \cos(\beta)) * \lambda_1 * H_D$$

$$\alpha_1 = 0.6 + 0.5 * \left(\frac{4\pi * \frac{h}{L_D}}{\sinh\left(4\pi * \frac{h}{L_D}\right)} \right)^2$$

$$\alpha_2 = \min\left(\frac{\left(1 - \frac{d}{h_b}\right) * \left(\frac{H_D}{d}\right)^2}{3}, \frac{2d}{H_D} \right)$$

$$\alpha_3 = 1 - \left(\frac{h'}{h}\right) * \left(1 - \frac{1}{\cosh\left(2\pi * \frac{h}{L_D}\right)} \right)$$

$$\alpha_4 = 1 - \frac{h_c^*}{\eta^*} \; if \; \eta^* > h_c \; and \; \alpha_4 = 0 \; if \; \eta^* < h_c$$

$$h_c^* = \min(\eta^*, h_c)$$

$\eta^*[\mathrm{m}] =$ Elevation to which the wave pressure is exerted

$H_D[\mathrm{m}] =$ design wave height

$L_D[\mathrm{m}] =$ design wave length

$p_1[\mathrm{N/m^2}] =$ Wave pressure at water level

$p_3[\mathrm{N/m^2}] =$ Wave pressure at bed level

$p_4[\mathrm{N/m^2}] =$ Wave pressure at top mitre gate or where load is exerted

$\alpha_1[-] =$ pressure coefficient for the wave length of the design wave

$\alpha_2[-]$ = pressure coefficient for the wave steepness
$\alpha_3[-]$ = pressure coefficient for the decrease in wave pressure over depth
$\lambda_1, \lambda_2, \lambda_3\ [-]$ = modification factors for the geometry of the structure, for mitre gates 1
$h\ [\mathrm{m}]$ = water depth before the sill
$h'\ [\mathrm{m}]$ = water depth on top of the sill
$h_c[\mathrm{m}]$ = height between water level and top of the mitre gate

The wind wave pressure mostly appears in combination with the hydrostatic pressure. An overview of the sum of the wind wave pressure defined by Goda and hydrostatic pressure is shown in Figure 14.

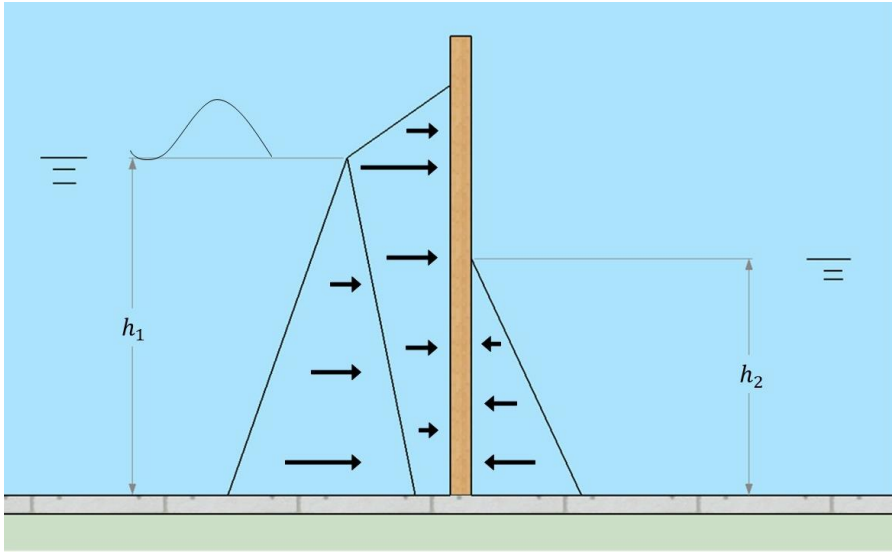

Figure 14: Wind wave and hydrostatic pressure on a mitre gate

Despite the more precise values that can be obtained from the method of Goda, in engineering most of the calculations are done with the conservative rule of thumb where the hydrostatic pressure of the significant wave height is added to the water level.

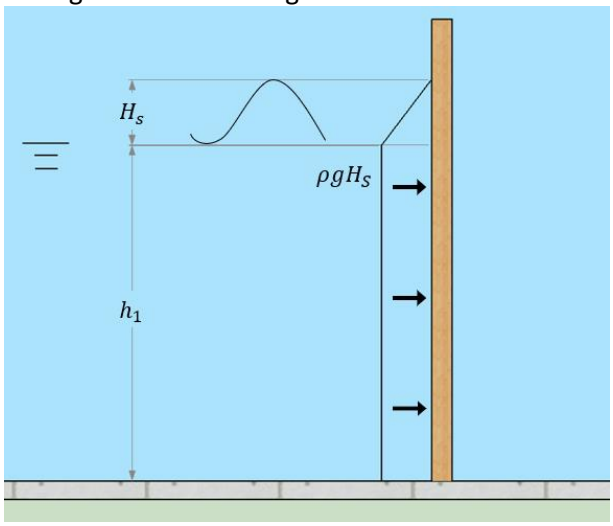

Figure 15: Pressure significant wave height

3.1.5 Collision impact

The collision of a ship is an exceptional load case for mitre gates. For the collision impact on timber mitre gates, insufficient literature is available (Ingenieursbureau Boorsma, 2020). Because of this absence, simplifications of collision impacts on timber mitre gates are made or the client accepts collision and provide an extra gate to replace the collided lock gate.

The schematization of the maximum impact of the collision by a ship is defined in 'Richtlijnen Ontwerp Kunstwerken 1.4'. In this guideline the kinetic energy that is generated by a ship is defined. The schematization implies that the ship provides a point load midway the gate or at the connection of the two gates. This load is applied on the mitre gate at the water level. Both simplifications are done on high water side and low water side, therefore the collision impact calculation contains four different calculations. These are shown in Figure 16. The impact from the low water side is less critical for the mitre gates than from the high water level. Due to the collision the gates are pushed open and the driving mechanism experiences most impact instead of the mitre gate itself.

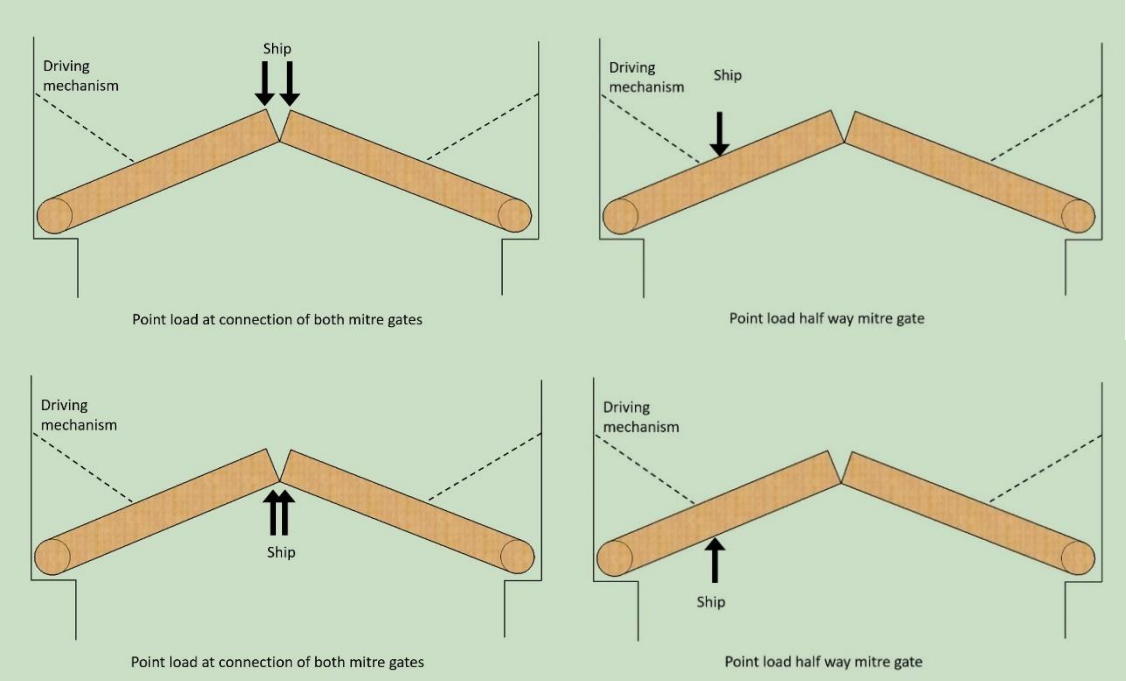

Figure 16: Collision situations on a mitre gate

3.1.6 Obstacle

This is a load that is caused by the driving mechanism when the gate is opening or closing. This load appear in four different situations: obstacle on the bed between mitre gate and gate recess, floating obstacle between mitre gate and gate recess, obstacle between the mitre gate and sill and a floating obstacle between the two closing mitre gates. The obstacle disturbs the movement of the mitre gates, while the driving mechanism is acting. This results in torsional moments in the mitre gate.

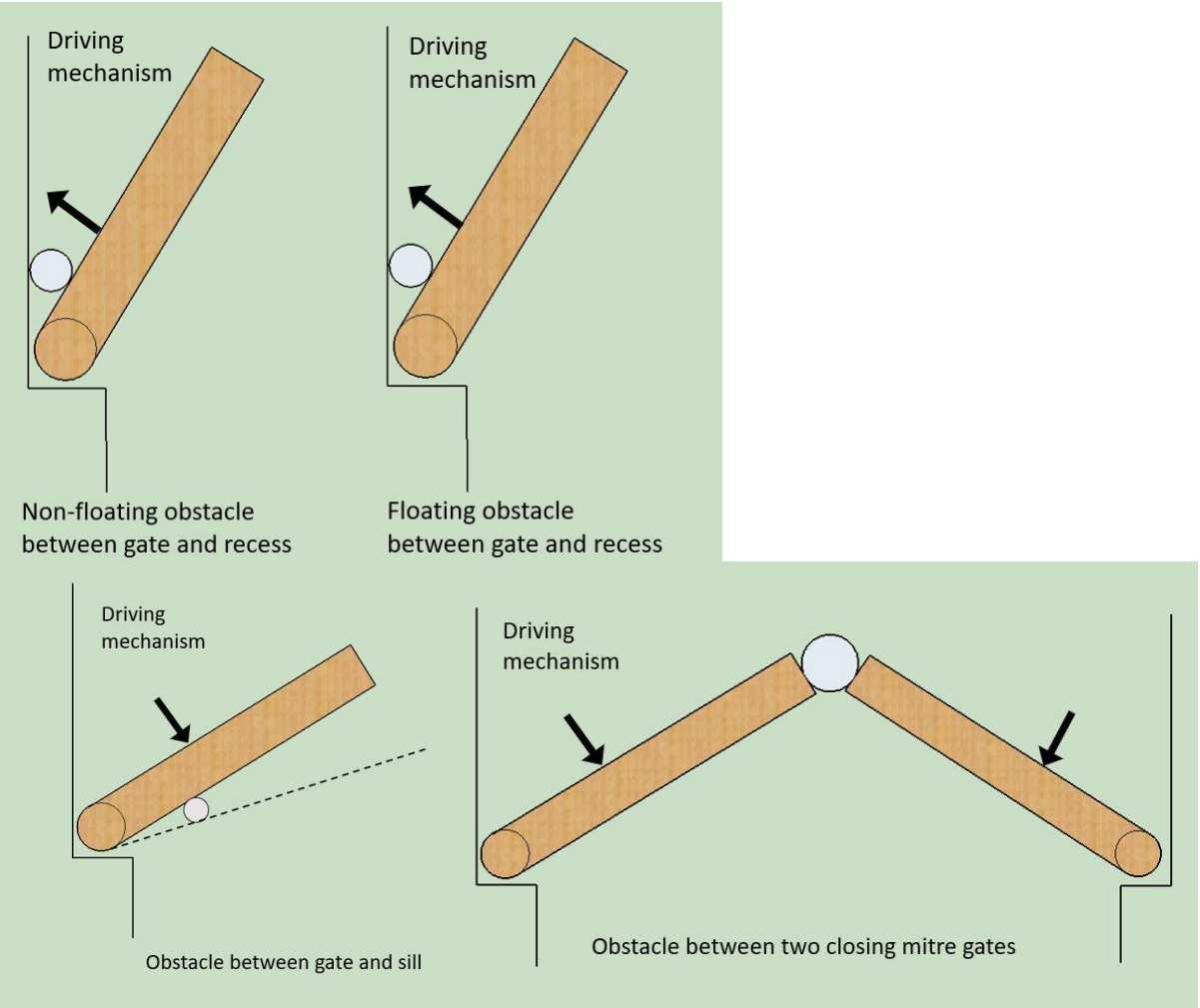

Figure 17: Obstacle schematizations

3.1.7 Ice load

The ice loads are the loads due to icing of the water level. Therefore this load is only applied on the mitre gate around the water level. According to Rijkswaterstaat this load should be calculated in two different load calculations. A horizontal longitudinal distributed load of 50 kN/m pointing 0.2 metres below water level in combination with a vertical distributed load of 10 kN/m on the horizontal beams pointing just below water level. This models the thermal expansion and grow of the ice.
The second load combination is a horizontal transversal distributed load of 50 kN/m acting at water level with the vertical distributed load of 10 kN/m on the horizontal beams pointing just below water level. This models the uplift and clinging of the ice.

Load combination	**Horizontal load**	**Vertical load**	**Modelling**
1	50 kN/m, 0.2 metres below water level	10 kN/m, first horizontal beam below water level	Thermal expansion and growth of ice
2	50 kN/m, at water level	10 kN/m, first horizontal beam below water level	Uplift and clinging of ice

Table 3: Ice load combinations

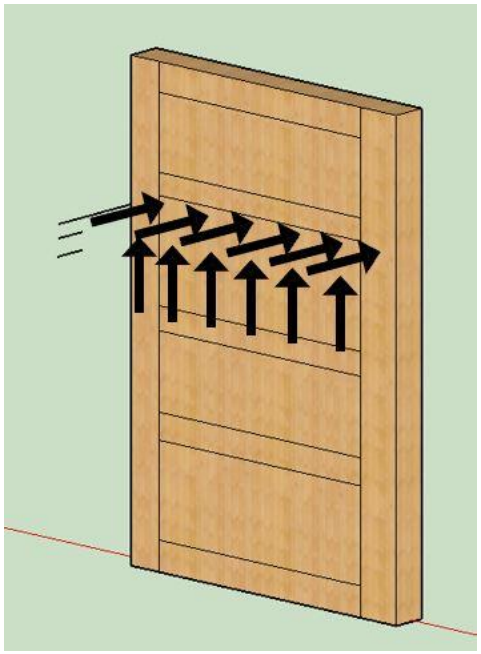

Figure 18: Ice load on a mitre gate

3.1.8 Other loads

Finally, some other dynamic loads are mentioned but not explained in detail because these are diverse with changing boundary conditions of the mitre gate or lock chamber and often not the most important loads on a mitre gate. These loads are: translation waves, driving mechanism prestressing, traffic load, mass inertia loads, ship propeller load, wind load and load due to earthquakes.

- Translation waves are caused by emptying or filling the lock chamber, tidal bores or other natural processes. This wave is in order of a few decimetres.
- Prestressing loads of the driving mechanism in case of closed gates. This is done by applying a small load on the gates to be sure that the gate is closed and is not going to leak.
- Traffic load should be taken into account if a mitre gate is intended for crossing the water.
- Mass inertia forces of the gate and the driving mechanism. These forces are taken by the driving mechanism and are therefore out of scope of this thesis.
- Ship propeller jet loads are generated by accelerating or decelerating vessels.
- The wind load is the load due to the wind on a closed gate. In the most critical load combination this load is normally not present, because the mitre gate is loaded by wind waves. The extended formula for the wind load is given in NEN-EN 1991-1-4.
- Earthquake load if the mitre gate is in earthquake area.

3.1.9 Conclusion loads on a mitre gate

The loads described in detail are summarized in the table below.

	Type of load	Direction of loading	Result in the mitre gate
Self-weight	Distributed	Vertical	Shear forces & bending moments
Uplift pressure	Distributed	Vertical	Shear forces
Hydrostatic pressure	Distributed	Perpendicular on gate	Shear forces & bending moments
Wind wave pressure	Distributed	Perpendicular on gate	Shear forces & bending moments
Collision impact	Point	Perpendicular on gate	Torsional moments & Shear forces
Ice load	Distributed	Perpendicular on gate & Vertical	Torsional moments, Shear forces & bending moments
Obstacle load	Point	Perpendicular on gate	Torsional moments & shear forces

Table 4: Result of loads on a mitre gate

For the schematization of the load distribution it can be concluded that most of the permanent loads on a mitre gate are distributed loads. So for the initial schematization of the mitre gate, distributed loads are taken into account. This distribution is as a starting point for the design. After finishing the design other less frequent appearing loads are considered and discussed how it could change the final design.

For the redesign of the mitre gate all the loads mentioned above cannot be taken into account. The governing load for the design of the mitre gate is the distributed load caused by the differential head. Other loads are not taken into account further on in this thesis.

3.2 Transversal load distribution

As told before, the mitre gate is pointed towards the high water level. In closed position the resultant of the hydrostatic pressure pushes the gate from high water level towards the low water level as can be seen in Figure 19.

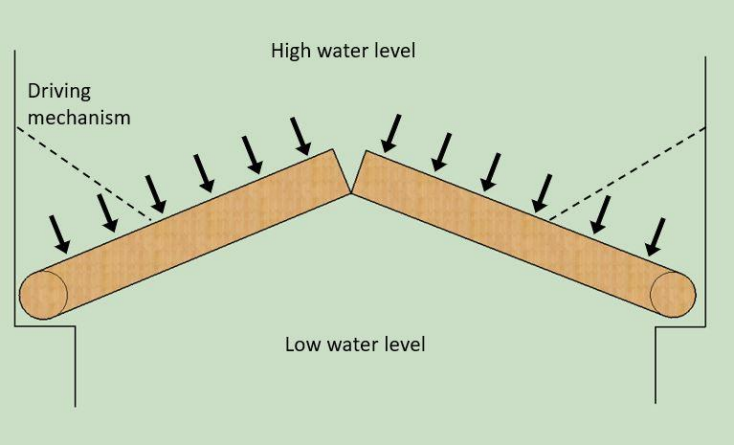

Figure 19: Closed mitre gate

In closed position both gates lean towards each other which provides a normal force in the mitre gate. The contact point of the two mitre gates is not in the centre of the mitre gate but below the centre of the mitre gate. This gives an eccentricity of the normal force. The eccentricity leads to a bending moment in the mitre gates. This bending moment is counterworking the bending moment of the water and therefore the maximum resistance of the mitre gate is increased.

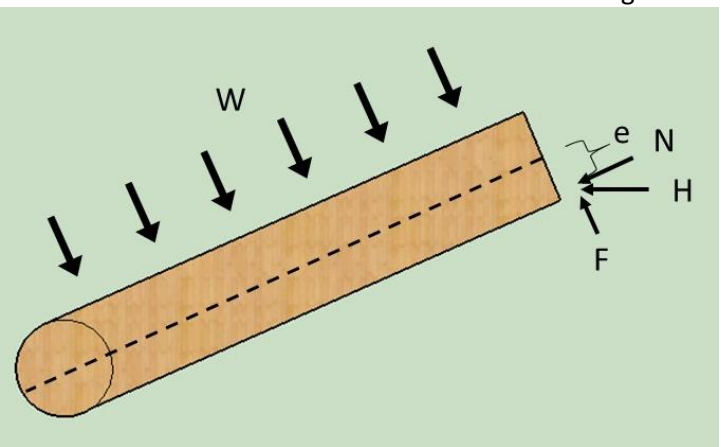

Figure 20: Transversal forces in a closed mitre gate

For the schematization of the top view calculations the mitre gates are schematized as simply supported beams. The loads acting on the mitre gate should be transferred sideways to the supports, here the lock head takes up the forces (Molenaar and Voorendt, 2019). In the schematization the

bearing between the two gates is represented by a support that transfers load perpendicular to the sailing direction. This can be seen in Figure 21. The bearings are usually not placed along the whole height of the mitre gate, rubber sealing prevent the gate from leakage.

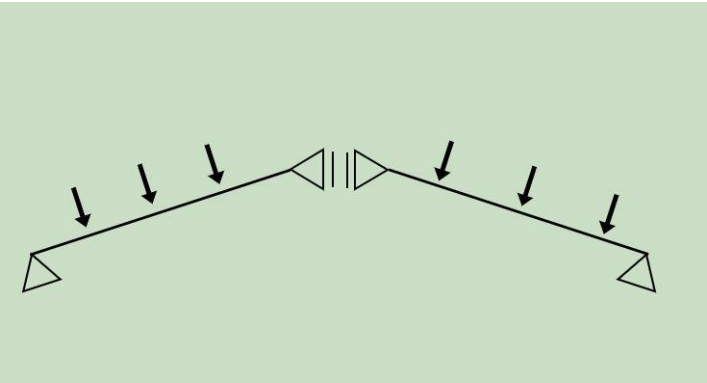

Figure 21: Top view schematization of closed mitre gates

3.3 Frontal load distribution

3.3.1 Leaf framing

The design of the mitre gate is such that the skin plate is located at the high water side. The skin plate distributes the load to the main girder. The load distribution between the component of the mitre gate is dependent on the framing of the mitre gate. The main girders can be placed either horizontally or vertically. If the main girders of the gates are horizontally framed, vertical stiffeners are applied to pass the hydraulic load to the horizontally framed main girders. The horizontally framed main girders pass the entire hydraulic load to the end post, which transfers the load to the lock chamber wall. Horizontally framed gates are economically more attractive if the width to height ratio is lower than 2. (Daniel & Paulus, 2019)

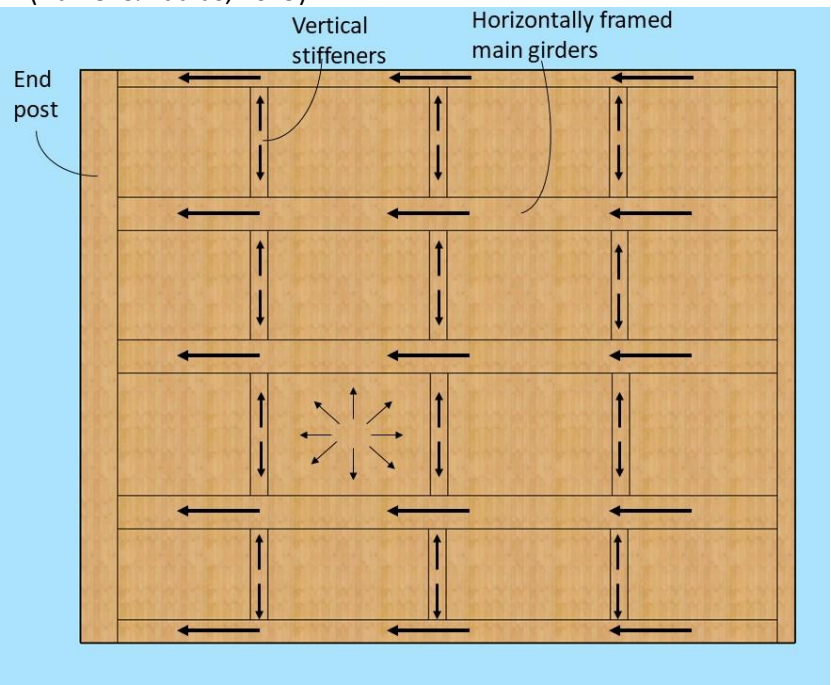

Figure 22: Horizontally framed mitre gate

A vertically framed gate passes the hydraulic load to the sill and end post through the top girder. The vertically framed gate is economical for wide but not deep navigation locks, when the width to height ratio is about 2 or higher. The span reduction of main girders in the vertically framed gates has a price. A large part of the hydraulic load shall be passed to the gate sill, which is the most uncertain

component of the structure. Because the sill can be exposed to settlements, sunken obstacles, deep draught vessels and is nearly inaccessible for inspection, maintenance or repair. Because of this, the vertically framed gates are rarely applied. Likewise, the width to height ratio is often lower than 2 in Europe (Daniel & Paulus, 2019). For the design of a mitre gate the bottom sill is not taken into account for the load distribution because: 'the contribution of sill to load transfer is sensitive to dimensional deviations and condition of both gate and sill during the entire service life and there are substantial risks that can disturb or prevent this contribution, such as floating or sunken obstacles, ice floes, small damages to contact lining, thermal expansion.' (Daniel & Paulus, 2019, p. 52)

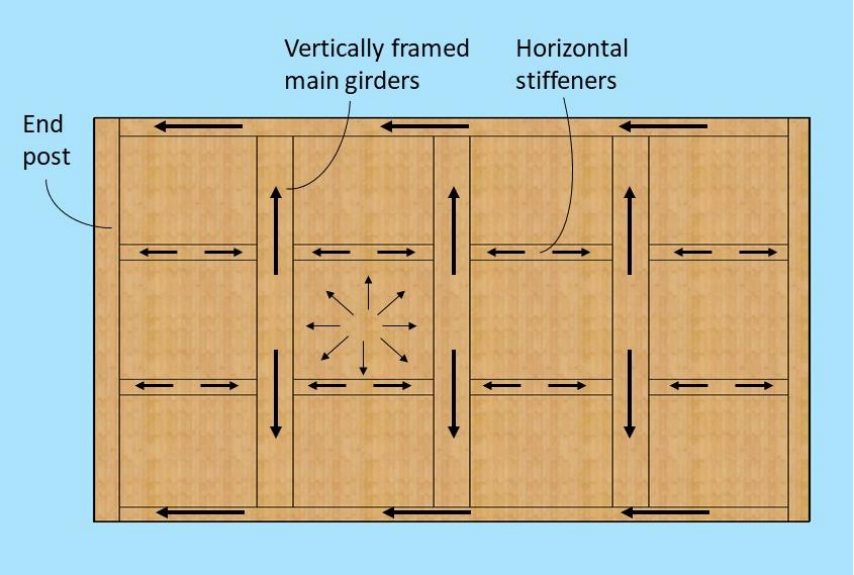

Figure 23: Vertically framed mitre gate

3.3.2 Structural system

For the transfer of the horizontal hydraulic load from the closed mitre gate to the lock chamber wall, two options are possible. Transfer of the load is possible through the pintle and through the end post in combination with transfer through the pintle. Daniel and Paulus (2019) mention two structural systems to schematize the load distribution of the mitre gate in the hinges, in practice the term hinge is used instead of pintle, these are: free-hinged and fixed-hinged. These two structural systems are defined for the hydraulic load transfer and lead to a different way of passing the load.

The free-hinged mitre gate is the most straight forward and cost effective system for mitre gates and therefore the most used system in Europe according to Daniel and Paulus (2019). The free-hinged mitre gate passes the hydraulic loads that build up through the end posts and hinges. The end post of the mitre gate is constructed with some clearances in the top and bottom hinges. The turning point of the end post is eccentric to minimize the wear of the end post. In case of centric turning points, friction between the end post and the gate recess lead to wear of the end post. The gate only fulfils the water retaining function in closed position due to the eccentricity of the rotation, if the gate is not closed the water can flow along the end post. The function of the clearance in closed position is that 'the growing differential water head not only locks the gate in mitering position, but also slightly lifts its front posts and releases the hinges, particularly their horizontal reactions. This is favourable because it spares the hinges and helps sealing the leakage. The end posts transfer the load to their contact surfaces as linear forces.' (Daniel & Paulus, 2019, p. 51) So for the schematization of the free-hinged mitre gate in closed position, the end post transfers the load as a uniform distributed load to the chamber wall of the navigation lock.

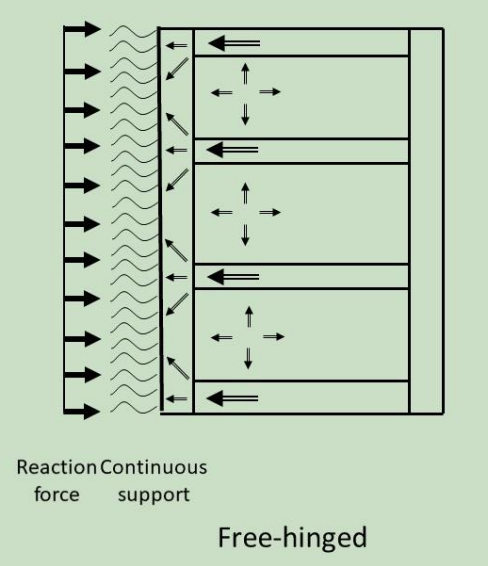

Figure 24: Front view of schematization of free-hinged end post with 4 horizontally main girders

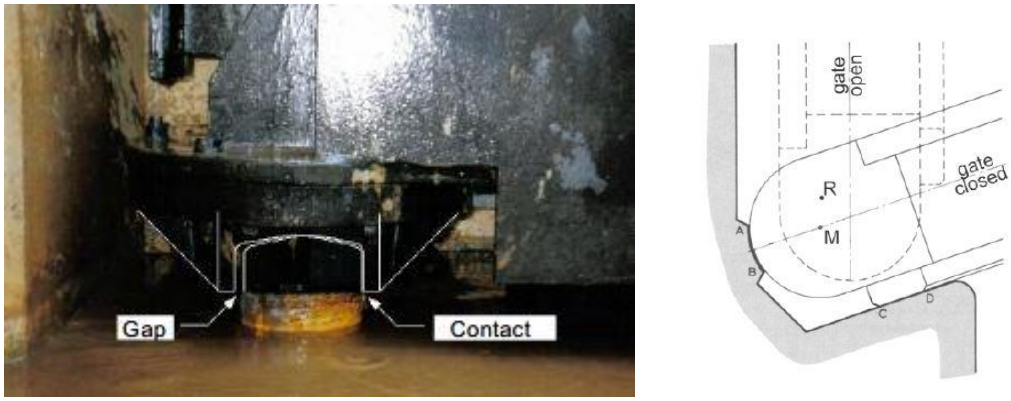

Figure 25: Hinge with clearance (left) (Daniel and Paulus, 2019) and top view hinge with clearance (right) (Moerbeek, 2017)

In Figure 24 a schematization is shown from a mitre gate with 4 horizontal main girders, a top and bottom girder and two intermediate girders. The loads from these girders are taken up by the end post and transferred to the chamber wall uniformly. In Figure 25 a side and top view of a hinge with clearance is shown, the white lines shows the gap in the hinge.

'However the systems of load transfer to the heel posts by free hinges have a common disadvantage. They rely on a horizontal sliding between two surfaces loaded by the entire own weight of the gate leaf. These surfaces are nearly inaccessible for maintenance, difficult to lubricate without pollution to the environment and exposed to various risks of submerged operation. Therefore, the fixed-hinged gate, that is, the gate without or nearly without hinge clearances, can prove better for several projects.' (Daniel & Paulus, 2019, p. 53).

The fixed-hinged gate has no clearance in the top and bottom hinge. The end post of the mitre gate cannot transfer load to the navigation lock pier and therefore the loads on the mitre gate are transferred to the hinges. The bundling of the loads in the hinges locally results in very high loads in the end post and hinges and therefore the end post should have bigger dimensions than in case of free-hinged gates. As a solution to decrease the load in the hinges, ball bearings are applied. The load distribution of a fixed-hinged mitre gate with 4 horizontal girders is shown in Figure 26.

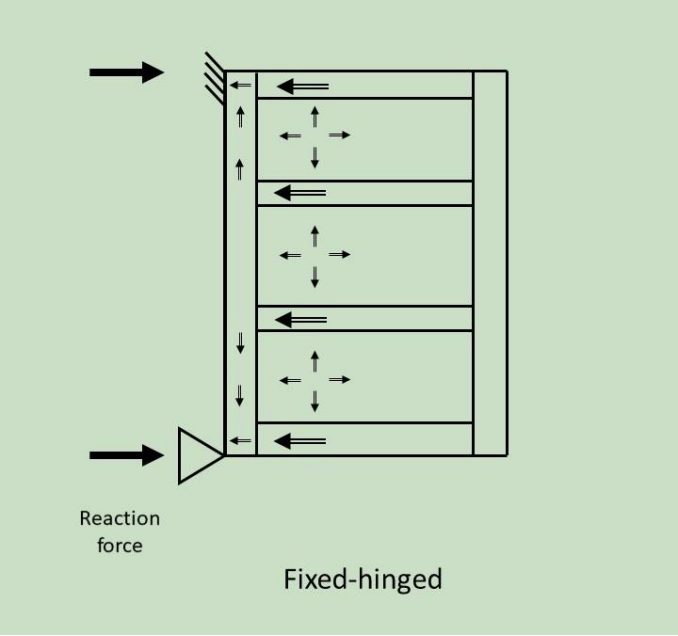

Figure 26: Front view of schematization of fixed-hinged end post with 4 horizontally main girders

According to Daniel & Paulus (2019) the choice between the free-hinged and fixed-hinged structural system is for a big part culture related. In the Netherlands and big parts of Europe the free-hinged system is in favor of the engineers. American engineers however usually give preference to the fixed-hinged structural system. Lastly as well as the cultural influence, the type of hydraulic loads on the mitre gate have an effect on the choice of structural system as well. If the load for example is more alternating the fixed-hinged method is more favorable because the alignment of the fixed-hinged mitre gate is more easy and does lead to less leakage.

For the vertical load transfer an important load during opening is the self-weight of the gate according to Molenaar and Voorendt (2020). The vertical reaction force of the bottom hinge (R_w) is equal to the weight of the mitre gate (W) to have vertical force equilibrium. To resist the bending moment caused by the self-weight, horizontal forces (R_M) occur in the top and bottom hinge of the mitre gate. As can be seen in Figure 27 these forces have an opposite direction. For big timber mitre gates the gate will tend to get out of square because of the relatively low stiffness of the timber mitre gate compared to steel. To prevent this, tension bars or struts are often applied from top hinge to the opposite bottom corner of the mitre gate. Another rarely applied solution is the use of roller support on the bottom corner of the mitre gate.

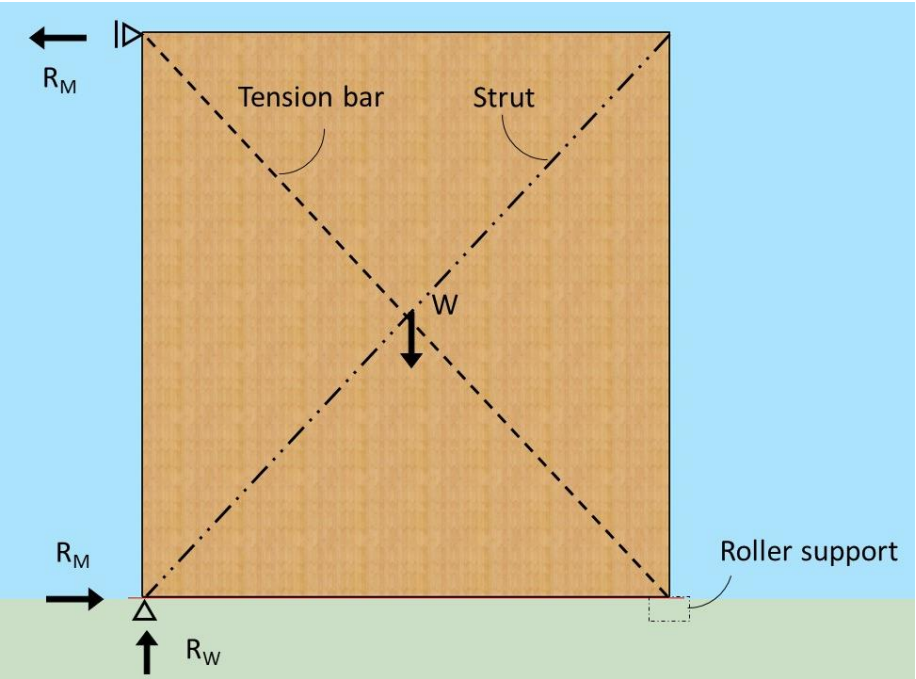

Figure 27: Vertical force distribution of a mitre gate

From the vertical and horizontal force distribution in a mitre gate it can be seen that the bottom hinge of the mitre gate is more critical than the top hinge because of the opposite working direction in the vertical force distribution. Furthermore the load on the bottom part of the mitre gate is more likely to be bigger as the hydrostatic pressure increases with depth.

3.4 Challenges of timber mitre gates

The current design of timber mitre gates has some challenges and is therefore not often applied for mitre gates with a chamber width above 12 metres. During knowledge sharing sessions in 2020 with researchers, several contractors and engineering companies of hydraulic structures the challenges of timber mitre gates were discussed. It came out that the main challenges are the available dimensions of structural timber and the conservatism of the Eurocode for the mortise tenon joint verification of the mitre gate (Ingenieursbureau Boorsma, 2020).

The first challenge implies that the required cross sections of the timber beams for the mitre gate are not available. The beams are thus not strong enough to withstand the loads on the mitre gate. Timber is a natural product and therefore dependent on the natural appearance in the forests. Nowadays, in hydraulic engineering azobé is most applied. According to constructor Wijma Kampen the azobé tree has a maximum diameter of 1.5 metre. The maximum cross section of a beam that can be applied as structural timber is 700x700 millimetres with a maximum length of 12 metres. The maximum length of an azobé beam is 18 metres. The maximum cross section with this length is 400x400 millimetres. These dimensions are not very wide appearing and therefore these beams have a long delivery time. In Figure 103 of Appendix C the availability of the cross section and length of the azobé beams are plotted against each other on the axis.

The second challenge is the conservatism of the Eurocode. Van de Kuilen and Blass (2005) mention that the shear strength of azobé is 2.7 times higher than the given shear strength in NEN-EN 338. Furthermore van Otterloo (2013) proved that the mortise and tenon joint verification in NEN-EN 1995 is not appropriate for hardwood mitre gates. A better verification for the mortise and tenon joint however is not yet taken up in the Eurocode. This is also shown in field tests with mitre gates in Stolwijk and Gouda. Here is concluded that the strength of the mitre gate was about 4 or 5 times higher than

the prescribed strength in the Dutch Eurocode. Hence some of the mitre gates in the Netherlands are verified with the German norm recently. (Stoop, Drop, Vlieger, & Donselaar-Gaal, 2013)

The challenges mentioned before do not always restrict the size of timber mitre gates as the Kattendijksluis in Antwerp, Belgium proves. This is the widest timber mitre gate in the world which has a chamber width of 24 metres, thus as told in Section 1.2.3, it is the utmost possible mitre gate. A single gate weights around 80 tons, is 13.9 metre wide and has a height of 9 metres, the Kattendijksluis is shown in Figure 28. The maximum differential head of the navigation lock is 2.3 metres according to the constructor of the Kattendijksluis Oosterhof Holman. The main girders of the Kattendijksluis are 13.7 metres long. To deal with the challenges the horizontal girders contain two beams which are mechanically jointed to create girders that resist the loads. The mortise and tenon joint is mechanically jointed as well. The mechanically jointed timber solution results in a heavy and expensive mitre gate, but the Kattendijksluis is part of the Belgian heritage and therefore the look should be preserved. (Beheersmaatschappij Antwerpen Mobiel, 2011) Because steel is a more economically attractive solution for wider mitre with the current design, timber mitre gates are scarce in navigation locks with a chamber above 12 metres.

Figure 28: Hoisting of Kattendijksluis (2011)

3.5 Conclusion analysis of load distribution in a mitre gate

In Chapter three the goal was to find an answer on the question: *How is a timber mitre gate schematized to optimize the force distribution and what is the effect on the materialization?* In Section 3.1 it came out that most of the loads on the mitre gate are distributed loads. Exact values of loads on the mitre gate were not given because these depend on the boundary conditions of the mitre gate. Further, we can conclude that the load distribution from the mitre gate to the lock chamber can be schematized in two ways, free-hinged and fixed-hinged. The free-hinged schematization results in a distributed transfer of loads to the lock chamber. The effect of this load transfer is that the load is almost equally spread over the timber end post and so equally transferred to the lock chamber wall. The fixed-hinged schematization transfers the load to the lock chamber wall via the top and bottom hinge of the mitre gate. This results in locally high peak loads. The free-hinged schematization of the mitre gate is usually used in the Netherlands because equally load distribution requires smaller dimensions for the mitre gate.

The mitre gate is usually constructed with horizontally framed main girders if the width to height ratio

is lower than two, which is the case in most of the Dutch waterways. In case of width to height ratio above two, vertically framed mitre gates are used. The sill of the navigation lock is not used for the loads distribution because this contains too much uncertainties (Daniel & Paulus, 2019). Furthermore the mitre gates lean towards each other and the alignment of the mitre gates is done in such a way that the sill is not distributing loads but retains the water retaining function.

Finally, in Chapter 3 the challenges of the design of timber mitre gates with chamber width above 12 metres are shown. These nowadays are: the availability of the required dimensions, the mortise and tenon joint verification. The challenges can be overcome by waiting for the required dimensions of the beams and mechanically jointing the timber gate but this increases the cost price of the mitre gate and makes steel a more economically attractive alternative like it is now.

4. Timber characteristics and timber lamination

In Chapter 4 general information about wood, timber and its characteristics are given in the first section. Section 4.2 4.1contains information about lamination. This section is divided in three parts to elaborate glue laminated timber, dowel laminated timber and cross laminated timber. The goal of this chapter is to obtain information of useful innovations for the renewed design of the mitre gate.

4.1 Characteristics of wood

Wood is a natural grown, organic material, comprising cells. The term wood is used when it is directly from the tree, timber is used when it has been processed for usage. The wood that is prescribed further is applicable for usage and therefore further on in this thesis the denomination timber is used. Timber is an anisotropic product which means that the strength and stiffness properties of wood differs in every direction due to the elongated cell structure and orientation of the cell walls. 'Parallel to the grain, in longitudinal direction of the tree stem, wood is particular strong, but conversely far lower at right angles to the grain, for example the tensile strength parallel to the grain is around 40 times higher than perpendicular to the grain.' (Blass & Sandhaas, 2017, p. 100). Timber is obtained from two categories of trees: deciduous trees, which is called, hardwood and conifers, called softwood. Hardwood is more evolved wood than softwood, thus hardwood contains more cell types than softwood, is stronger, heavier and therefore requires more extensive labour than softwood (Blass & Sandhaas, 2017). The microscopical difference of hardwood and softwood can be seen in the figure below.

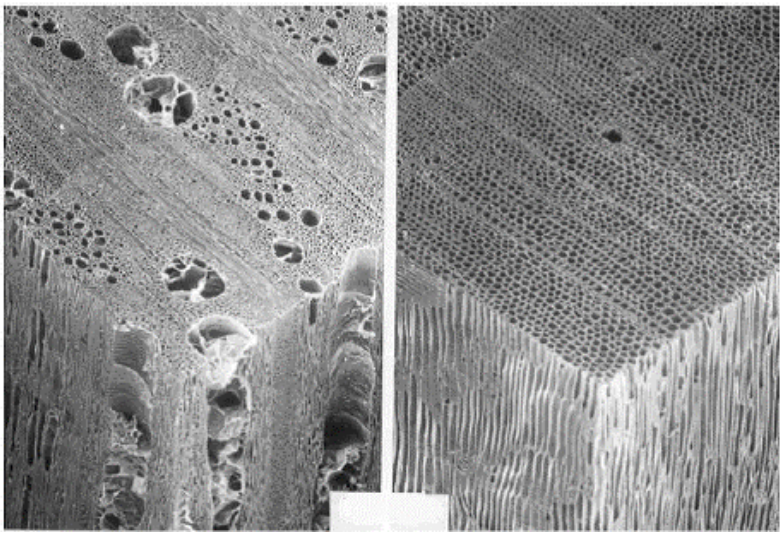

Figure 29: Microscopic structure of hardwood (oak, left) and softwood (spruce, right) (Blass & Sandhaas, 2017)

Like other construction materials, timber has different gradings. Two methods are used to classify the timber: visual grading and machine grading. In visual grading, the most important parameter that is used is the number of knots. In machine grading, the modulus of elasticity is analysed and used to grade the timber.

Timber is originally graded based on their bending strengths. In the grading of timber there are two categories: hardwood and softwood. The timber species that are classified as softwood have bending strengths between 14 and 50 N/mm^2, with corresponding classes C14 to C50. The hardwood species have bending strengths ranging from 18 to 80 N/mm^2 with classes D18 to D80. The NEN-EN 338 is expanded in 2016 with grading based on tension tests for softwood, classes T8 to T30. The extensive properties of each class is shown in Appendix C.

The values in the Eurocode contain large factors of safety because of the risk of timber degradation. Degradation of timber can occur due to irregularities in the tree. Because timber is a product of

nature, i.e. it is not produced under controlled circumstances, multiple irregularities can occur in the wood. Piths and knots are examples of irregularities that decrease the strength of the timber. Besides the irregularities of timber, biodegradation caused by, for example, insects, parasites or other micro-organisms decrease the strength of timber. The environmental durability and ways to classify wood based on this parameter is prescribed in NEN-EN 350. Hardwoods are inherently more resistant against fungi than softwood. A mitre gate is in wet environment, i.e. the timber of a mitre gate is permanent or regularly submerged in water. Therefore, natural durability 1 or 2 is required. This ensures that only some hardwood species can be applied in hydraulic engineering and softwood is hardly ever applied in hydraulic engineering. Softwood can however be used in environments with lower humidity, but it should first be treated for preservation.

There are many different species of wood that are used in engineering. The most frequently used softwood species are spruce, larch and pine. The most frequently used hardwoods are beech, oak and azobé. Oak used to be the most commonly used wood species in hydraulic engineering, but nowadays azobé is the most used species in this construction field.

4.2 Laminated timber elements

According to Blass and Sandhaas (2017), square timbers with a cross section of 150 x 450 millimetres up to 20 metres long were generally available. Nowadays these dimensions are more rare and thus increasing in price. Jointing timber elements is a solution for the increasing demand of longer timber elements dimensions. The most common ways of jointing are nails, dowels, bolts, screws, metal plates and glued finger joints. A solution to obtain larger cross sections and to make timber more homogeneous, is to laminate timber elements. The lamination of timber results in more homogeneous, thus stronger timber and reduces the probability to failure due to irregularities. This is also known as the laminating effect. 'The laminating effect is defined as the increase in strength of lumber laminations when bonded in a glue laminated beam compared with their strength when tested by standard test procedures' (Falk & Colling, 1995, p. 1). Another advantage of lamination is that it enables curving of the timber, so circular or parabolic shapes are possible to construct. This results in aesthetically seen prettier timber designs which is nowadays also an important as aesthetics becomes more and more important in designing. Lamination is done in two ways: Gluing and mechanically jointing with fasteners.

4.2.1 Glue laminated timber

Glued laminated timber is built up out of at least two lamellae arranged parallel to the grain. These lamellae can be in a range of 6 and 45 millimetres if finger joints are used. If exposed to dramatically fluctuating climates, lamellae of maximum 35 millimetres are recommended (Blass & Sandhaas, 2017). Without finger jointing the lamellae of the glue laminated beam are varying between 45 millimetres and 85 millimetres, usually a beam consists of 2 to 5 layers in this case. Lamination is mainly done of softwoods. The lamellae of softwoods are glued together with polyurethane (PU) or melamine urethane-formaldehyde (MUF). The current adhesive used for lamination is only applicable in dry environments. In case of wet environments gluing is not possible and lamination is done with mechanical fasteners, for example dowels or bolts. For glued laminated timber NEN-EN 14080 sets requirements. The characteristics for glue laminated timber are obtained from tests. In this norm softwood is only prescribed, according to Glavinić, Boko, Torić, & Vranković (2020) this is one of the reasons why hardwood glue lamination is not used often compared to softwood elements.

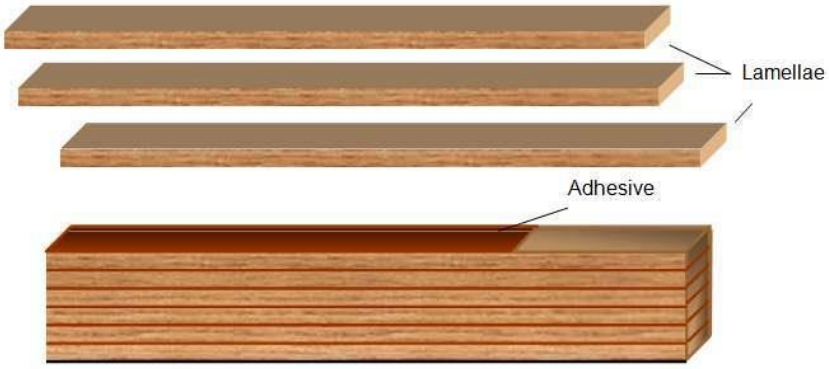

Figure 30: Glued laminated timber beam retrieved (Zangiácomo, Balanco, Christoforo, & Rocco Lahr, 2017)

4.2.2 Dowel laminated timber

For lamination of hardwood elements, dowel laminated timber is used, i.e. timber lamellae arranged parallel to each other penetrated with dowels. The holes for the dowels are drilled so the dowels can be hammered in the holes. Because dowel laminated timber is often used for hardwoods the dowels are often of steel. In case of low shear forces these dowels can be made of timber as well. The centre to centre distance of the dowels is usually in order of 100 to 300 millimetres and the dowels have roughly a diameter of 20 to 30 millimetres. (StructureCraft, 2021)

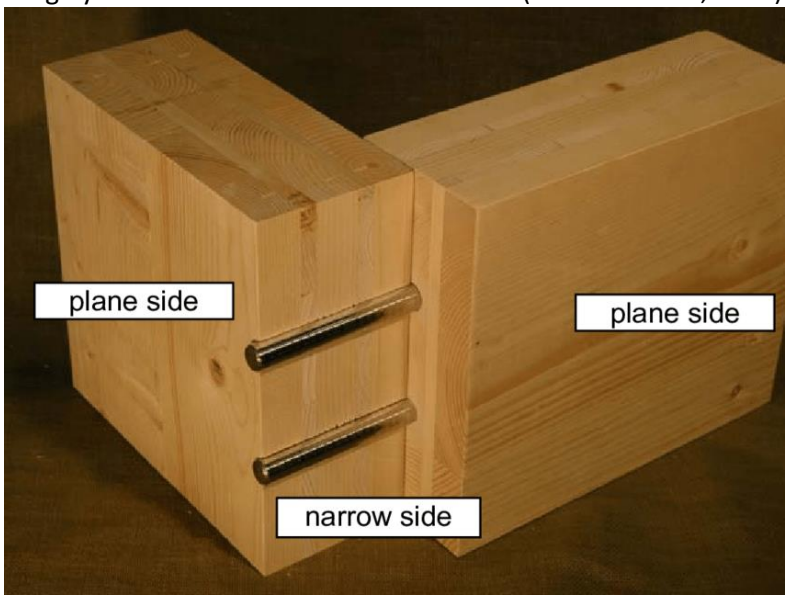

Figure 31: Example of dowel laminated timber (Uibel & Blass, 2007)

The analytical calculation of dowel laminated hardwoods can be done in two ways; The mechanically jointed beam theory of NEN-EN 1995 (γ-method) and the Shear Analogy Method. The γ-method is the more simple method to calculate mechanically jointed beams. A reduction coefficient, γ, is used for the calculation of the bending stiffness of the beam. The Shear Analogy Method of Kreuzinger (1999) can be used to calculate composed beams more accurately. In this method the composed beam is transformed to a single, fictitious and homogeneous beam (Blass & Sandhaas, 2017). The mechanically jointed beam theory of NEN-EN 1995 is only valid for three layered beams. However the γ-method has been extended by Schelling in 1982 and is valid for beams with infinite amount of layers (Schelling, 1982). For the analytical design of the mitre gate is chosen to use the most used γ-method. Based on the theory of linear elasticity the following assumptions of the γ-method are made for the analytical design:

- The beams are simply supported with a span ℓ. For continuous beams the expressions may be used with ℓ equal to 0.8 of the relevant span and for cantilevered beams with ℓ equal to twice the cantilever length.
- The individual parts (of wood, wood-based panels) are either full length or made with glued end joints.
- The individual parts are connected to each other by mechanical fasteners with a slip modulus of K.
- The spacing s between the fasteners is constant or varies uniformly according to the shear force between s_{min} and s_{max} with $s_{max} \leq 4s_{min}$.
- The load is giving a moment $M = M(x)$ varying sinusoidally or parabolically and a shear force $V = V(x)$.

An example of an azobé dowel laminated curved beam is the arch bridge in Frederikssund, Denmark seen on Figure 32.

Figure 32: Dowel laminated arch bridge, Frederikssund (Lesser Known Timber Species, 2020)

4.2.3 Cross laminated timber

A recently used addition for lamination of timber is the use of cross laminated timber, i.e., timber elements where the fibres of the lamellae are not placed parallel to each other, but orthogonal or under an angle. This placement is done to have better structural properties in multiple directions, thus to be able to have force distribution in multiple loading directions. Another advantage of cross laminated timber is that it is less prone to shrinkage and creep in case of temperature changes. Orthogonal placement of the fibres is mostly done, however it is possible to place under different angles as well. Cross laminated timber is usually built up of 3 to 8 layers. The thickness of these layers vary between 6 and 45 millimetres. Depending on the design of the construction the layers can be made of different timber species. Cross laminated timber panels have dimensions up to 16 x 3 x 0.5 metres (Wallner-Novak, Koppelhuber, & Pock, Cross-Laminated Timber Structural Design, 2014). For cross laminated timber the most used timber species in the Netherlands is pine.

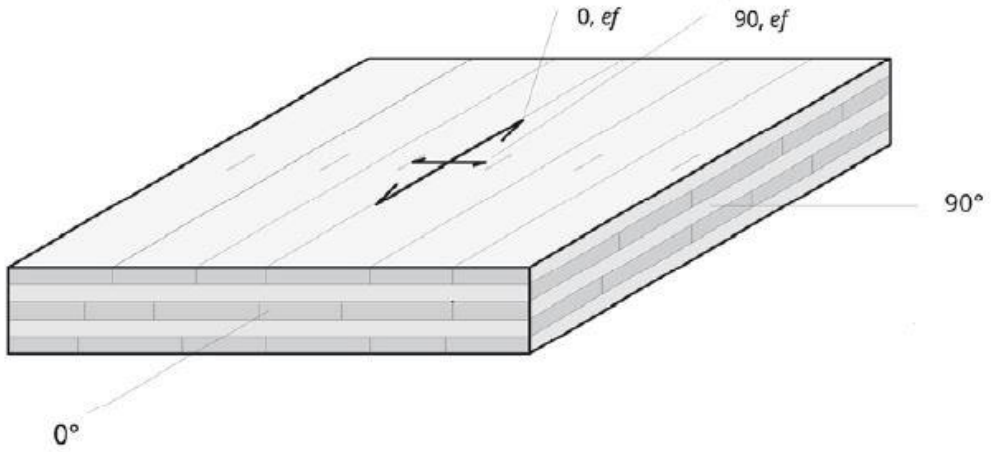

Figure 33: Cross laminated timber element (Wallner-Novak, Koppelhuber, & Pock, 2014)

Cross laminated timber is often glued together, dowel cross laminated timber is barely used. In 2021 a norm for cross laminated timber is released, NEN-EN16351. This norm for cross laminated timber is only applicable for glued softwood elements, yet no norm is available for hardwood cross laminated elements.

To summarize, lamination of timber increases the strength and stiffness characteristics and creates more freedom in the design of the cross section size and shape. Now, glue laminated timber made of softwood is mainly used in engineering. In wet environments, permanent or regularly exposed to water and so exposed to destructive organisms and/or salt, gluing is no option because no adhesive is appropriate for wet environments yet. Therefore lamination in wet environments is done with fasteners, dowels for example. The use of cross laminated timber results in better structural properties in multiple directions and is therefore able to distribute forces in multiple loading directions.

5. Renewed design of a timber mitre gate

In Chapter 5 a new preliminary design of a navigation lock gate is made for a case study location. The design of a timber mitre gate now is described as a 'stacked beam structure'. This means that the structure contains continuous horizontal massive timber beams with the required dimensions for the load-bearing capacity, a skin plate to retain the water and crossing diagonal tension and compression bars to avoid the gate out of square. This design has his challenges mentioned in Chapter 3 and is very costly for wider mitre gates because of the amount of used timber.

The goal of this thesis is to design a timber mitre gate in the new application range of navigation locks with a width of 12 to 24 metres. It is aimed to design a more economically attractive timber lock gate. The first section contains a description of boundary conditions of the case study location. In the second section the layout and the different components of the design are explained. The third section contains the mechanical properties of the different components of the mitre gate. In the fourth section the preliminary design verifications are presented. The last section contains the optimized preliminary design of the mitre gate.

5.1 Project information

The chosen case study location for the mitre gate has an average differential head and is a mitre gate in the scope. There is chosen to perform the analysis on a navigation lock with average dimensions within the scope on purpose. The locks with an average differential head are most likely to enhance to locks with both bigger and smaller differential heads and therefore could be adapted to most of the lock gates in the scope. In Table 1Table 20 of Appendix A it can be seen that the most appearing width for the mitre gates in the scope is 16 metres. This width is most appearing because the majority of the navigation locks in the scope are designed for CEMT-class Va or Vb. For inland waterways under management and maintenance of Rijkswaterstaat the average retaining maximum differential head is in order of 3 or 4 metres, according to Rijkswaterstaat.

Figure 34: Location of case study, Sambeek

With data provided from Rijkswaterstaat the eastern navigation lock Sambeek is chosen to perform the case study on. The navigation lock is designed for CEMT-class Vb has a chamber width of 16 metres and this gate has a levelling differential head of 3.1 metres. The water retaining differential head of the mitre gate is 4.2 metres, see Appendix Hydraulic boundaries of for more elaboration. As told earlier in the thesis the most economical gradient for the mitre gate is 1:3. The width of the gate

becomes: $l_{door} = 0.5 * w_{chamber} / \cos(1/3) + 1 = 9.47$ m. The extra metre width added to the gate is needed because of the recess of the lock chamber. The mitre gate is in wet environments and according to NEN-EN 1995-1-1 the mitre gate is classified as service class 3.

As told before the hydraulic boundary conditions have been established by Rijkswaterstaat. In here the water level, set up of wind waves and translation waves are summed up as one governing water level difference between the high water side and low water side. The load for the design of the mitre gate is the difference of hydrostatic pressure between the high and low water level sides. The water level on the upstream side is +11.9 metres NAP and the low water level is +7.7 metres NAP. The related load factor for the hydrostatic pressure from Richtlijn Ontwerp Kunstwerken 1.4 is 1.5, the differential head of 4.2 metres then results in a distributed load of 61.8 kN/m^2 due to the water level difference as can be seen below. This differential head is classified in the short-term load-duration class.

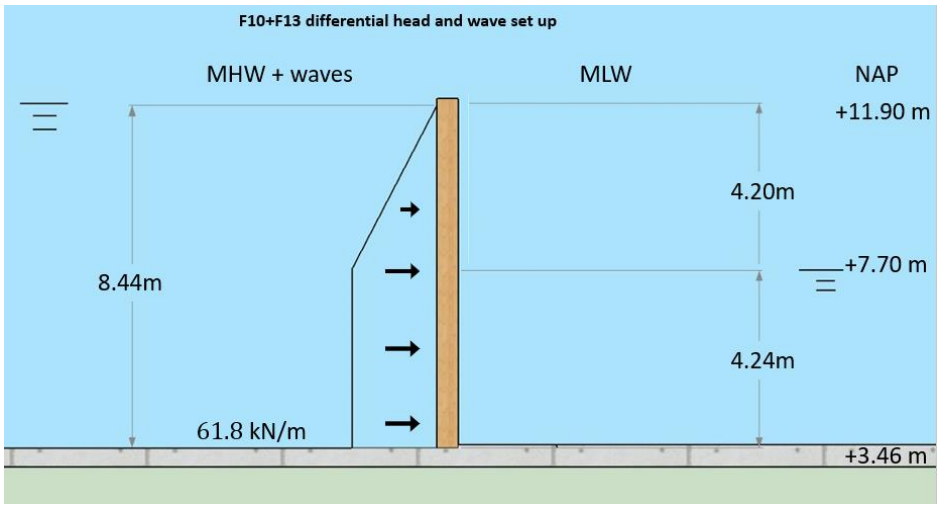

Figure 35: Hydrostatic pressure on mitre gate Sambeek lock

5.2 Design of the mitre gate in the new application area

From mechanics it turns out that the most economical designs usually follows the bending moment distribution of the construction. Because the lock gate is schematized as a simply supported beam and mainly loaded by the uniformly distributed hydraulic loading, the global bending moment distribution on the mitre gate is parabolic. Therefore halfway the mitre gate the bending moment is the maximum and at the supports the shear force is maximum.

The new design that is calculated is based on bridge engineering. In engineering it is often said that a mitre gate is a bridge tilted on his side. However, the layout of a timber mitre gate does not look like a bridge. There are multiple types of bridges such as: Arch bridges, truss bridges, cable bridges or suspension bridges. In timber engineering the joint is often a critical point in the design. This is because of the locally high shear, compression and normal force distribution and the different direction of the fibres of the jointing members (Blass & Sandhaas, 2017). Therefore the aim is to have a design with as little joints as possible, the truss bridge design is therefore not chosen to apply. Furthermore ties and cables are not possible for the design of a timber mitre gate. So to investigate if a 'bridge design' is suitable for the design of a timber mitre gate, an arched design is chosen for the case study.

5.2.1 Layout

The arch layout of the mitre gate contains three parts. As told in the introduction of this thesis, timber is more sustainable than steel. To have the most impact on sustainability all parts are made of azobé:

- The *skin plate* of the mitre gate usually ensures the retention of the water. As told before the design of the now common design of a mitre gate is a 'stacked beam' design, where in the global preliminary design only the girders are taken into account and the skin plate is left out.

Furthermore in the now common design the timber mitre gate contains steel tension bars or steel or timber struts, in the design of this research the goal is to design a mitre gate without external tension bars and struts. To do so, the skin plate has to bear forces in multiple directions, which is not favourable for timber. Therefore a cross laminated timber skin plate is used. As timber is most strong in the direction of the fibres, the layout of the plate has two crossed diagonal layers to replace the tension bar and strut, two horizontal layers and 2 vertical layers. As can be seen in Figure 36 from inner to outer the lamellae are in the following order: diagonal, vertical and horizontal. This is to create the biggest moment of inertia for the most heavily loaded direction. Because the skin plate is thicker due to the multiple layers the skin plate contributes in the calculation of this design.

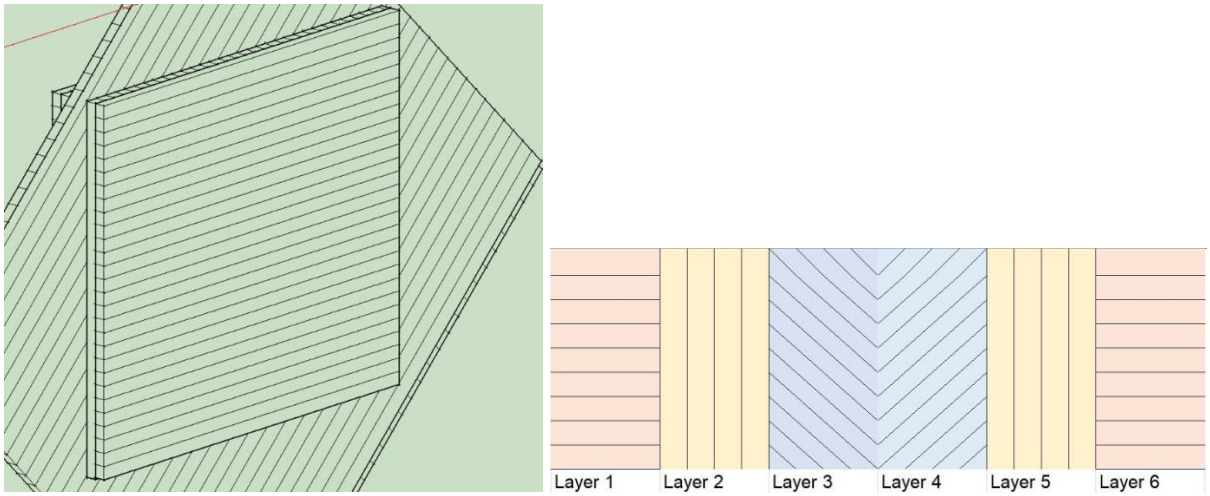

Figure 36: Build-up of cross laminated plate with extended diagonals for visual clarification (left) and cross section of layer sequence of skin plate (right)

- The main *girder* is the main contributor in the global transfer of forces. As told before to have an economical design the girder is curved. This results in a higher moment of inertia halfway the gate, which is favourable given the highest bending moment in the middle of the gate. Curving is only possible by laminating the girder. The lamellae are less thick and more easy to bend. Cross lamination of the lamellae has in this case no added value because the stresses are in the longitudinal direction of the mitre gate. The lamination of the girder further results in more easy available dimensions, which results in less waiting time thus cheaper girders.
- *Web plate* is the connection between the curved girder and skin plate. This plate avoids the beam from buckling and gives extra strength, stiffness and stability to the cross section. This plate contains some small drain holes, not shown in Figure 37, to let water fall down for the fluctuating water level. The reason to choose for a plate instead of connection blocks is that the joint of these plate is more easy compared to the joint of stiffener blocks with the girder and skin plate.

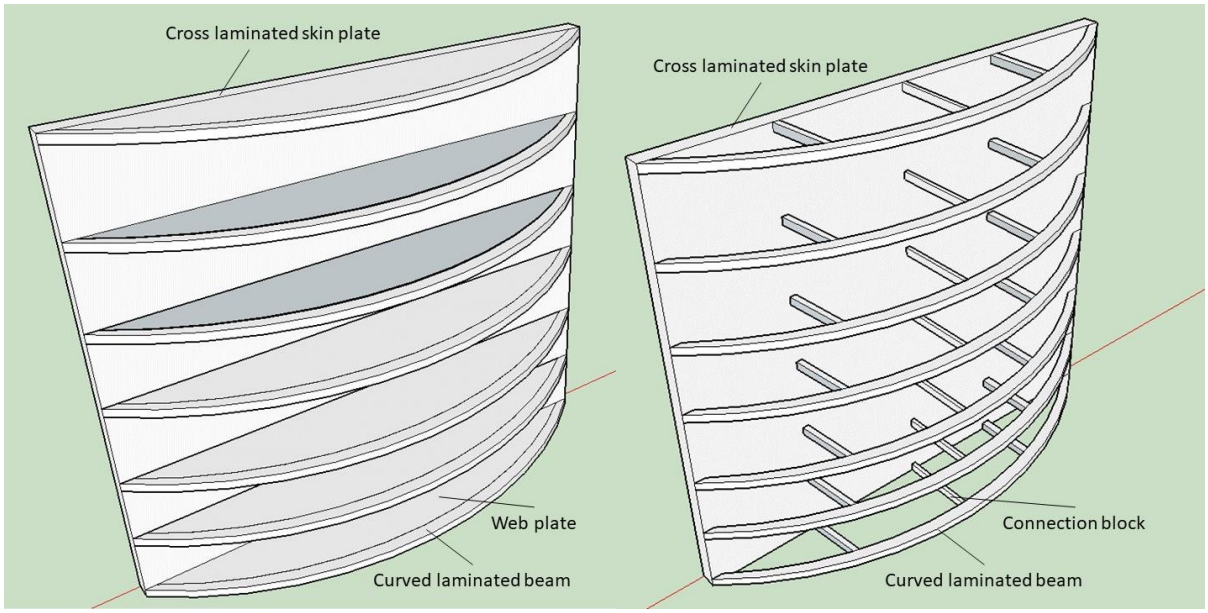

Figure 37: Design of mitre gate with chosen web plate (left) and not chosen connection blocks (right)

5.2.2 Global and local design

In the calculation the design is divided into two parts, the global and local design. The global design of the mitre gate is the schematization of the horizontal load transfer of the mitre gate. The local design is the schematized vertical load transfer of the mitre gate. For the horizontal design calculations the mitre gate is schematized as a simply supported beam over the width of the mitre gate which is loaded by a uniform distributed load. In here the curved laminated girder, connection plate and skin plate contribute in the transfer of forces. The vertical check of the mitre gate is schematized as a continuous beam with multiple supports. These supports are at the location of the curved laminated girder. The centre to centre distance between the curved laminated girders is the distance between the supports.

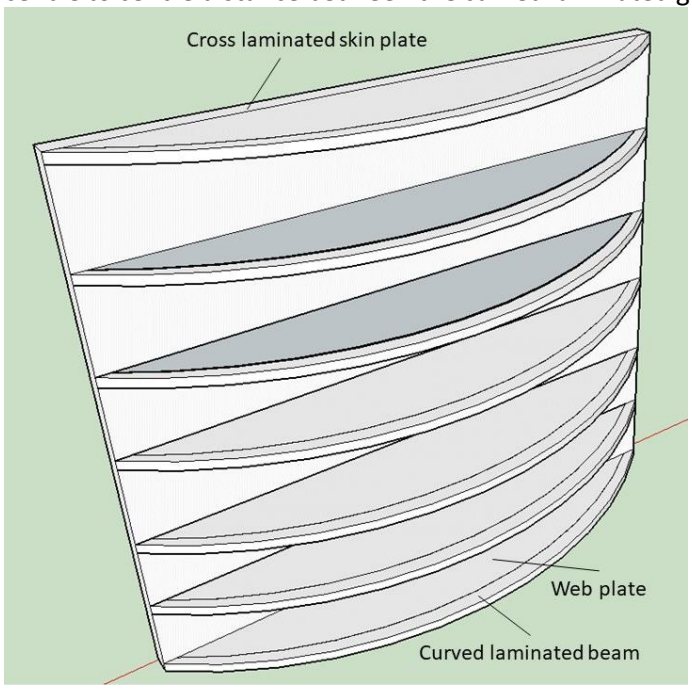

Figure 38: Mitre gate design

5.2.3 Implementations

The curved side is constructed on the high water side, this results in a counteracting bending moment compared to the bending moment of the hydraulic load. The contact point of the two gates leaning to each other is not in the centre of line of the cross section, so the normal force has an eccentricity which is counteracting the bending moment of the differential head. Another reason to design with a girder in compression is that a girder in compression makes installation of the girder at the posts more easily. The girders are connected to the post with metal strips connected by bolts. The mortise and tenon joint is checked further in detail during the design of the joints of Chapter 6. The lamination of the skin plate and girder is done with dowels. The connection of the connection plate with the girder and skin plate in done with bolts having the same diameter of the dowels of the lamination.

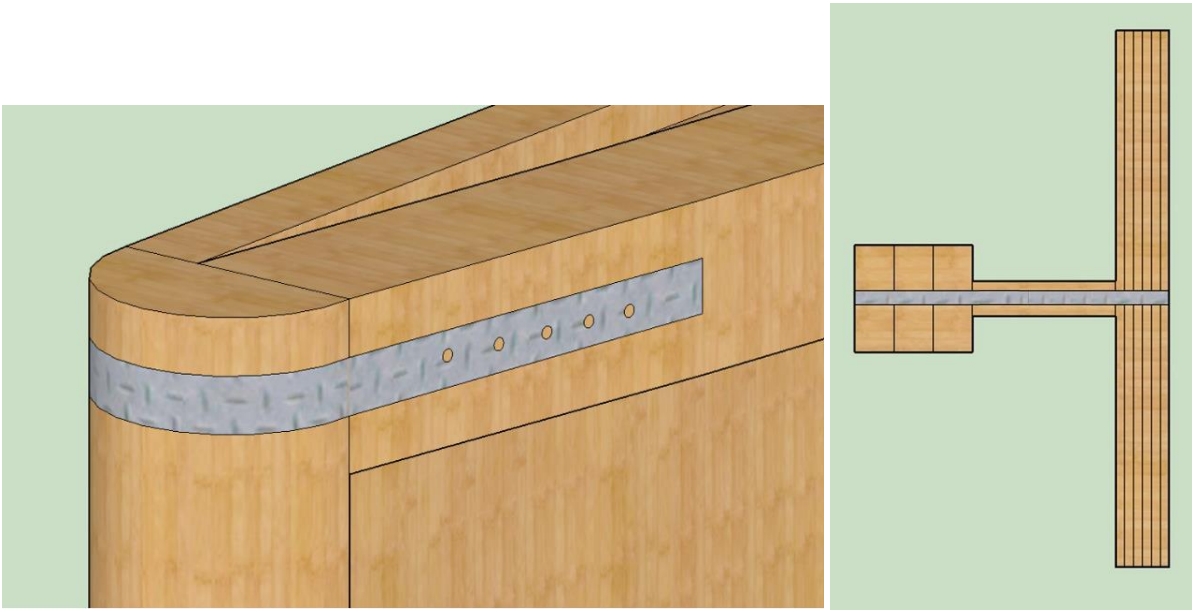

Figure 39: Detail girder post (left) and cross section with dowel (right)

5.3 Mechanical properties of design elements

Some of the elements of the mitre gate are not covered in the Eurocode or not existing at the moment. Azobé is nowadays the most used timber species for mitre gates, as it is the most economical efficient timber species when strength, stiffness and durability are considered. However azobé is not glued laminated yet, this is done with dowels. Only a few researches are done for glued lamination of hardwoods. Erhart et al., (2016) did research tests on laminated hardwood beech beams. In these tests it came out that theoretically GL40, GL48 and GL55 appear realistic and reachable with beech. While beech is classified as D40 in the standard. So the strength of the laminated element increases compared to non-laminated beech elements. However beech has natural durability of 5 and is therefore not applicable for the hydraulic engineering.
Further research on hardwood lamination is done by Hüpscher, 2019. These tests were done on iroko beams. He determined the bending and tension strength of iroko beams and laminated iroko beams. It came out that the finger joint was the most critical point of these glued laminated beams. The classification of strength class D40 for homogeneous iroko beams is correct. For the glued laminated beams it came out of tests that GL24h is a proper choice because the characteristic bending strength that came out of his tests was 42.3 N/mm^2. However, literature would suggest strength class GL32h (NEN-EN 14080, 2013) and GL36c (Frese & Blass, 2005).

Azobé is classified in strength class D70. The research mentioned above is done with softwoods or timber much less stronger than azobé is. Furthermore, yet no adhesive is existing that can be used in wet conditions. Therefore the decision is made to laminated the elements with dowels instead of gluing the lamination. This gives more realistic assumptions at the moment because lamination of

azobé is rarely done at all and gluing lamination of azobé would be unrealistic at the moment and setting up characteristics of this lamination gives a great deal of uncertainty and dubious assumptions. The cross laminated plate is built up of azobé lamellae D70, for the calculation of the cross laminated plate only the lamellae that are loaded in the direction of the fibres are included in the cross section.

An overview of the strength and stiffness characteristics of Azobé class D70 from the NEN-EN 338 are:

	Azobé D70	Unit
Characteristic bending strength $f_{m,k}$	70	(N/mm^2)
Char. tensile strength parallel to the grain $f_{t,0,k}$	42	(N/mm^2)
Char. tensile strength perpendicular to the grain $f_{t,90,k}$	0.6	(N/mm^2)
Char. compression strength parallel to the grain $f_{c,0,k}$	36	(N/mm^2)
Char. compression strength perpendicular to the grain $f_{c,90,k}$	12	(N/mm^2)
Char. shear strength $f_{v,k}$	5	(N/mm^2)
Mean modulus of elasticity parallel to the grain $E_{0,mean}$	20	(kN/mm^2)
Char. modulus of elasticity parallel to the grain $E_{0,k}$	16.8	(kN/mm^2)
Mean modulus of elasticity perpendicular to the grain $E_{90,mean}$	1.33	(kN/mm^2)
Mean shear modulus G_{mean}	1.25	(kN/mm^2)
Char. density ρ_k	800	(kg/m^3)
Mean density ρ_{mean}	960	(kg/m^3)

Table 5: Mechanical properties of design retrieved from NEN-EN 338

5.4 Preliminary design of the redesigned mitre gate

In this section the preliminary design of the redesigned mitre gate is shown. The comprehensive calculation of the preliminary design is shown in Appendix F. For the calculations a coordinate system is defined in Figure 40. The x-axis is along the width of the mitre gate, the y-axis is along the thickness of the mitre gate, for the height of the mitre gate the z-axis is used started from the bottom of the mitre gate.

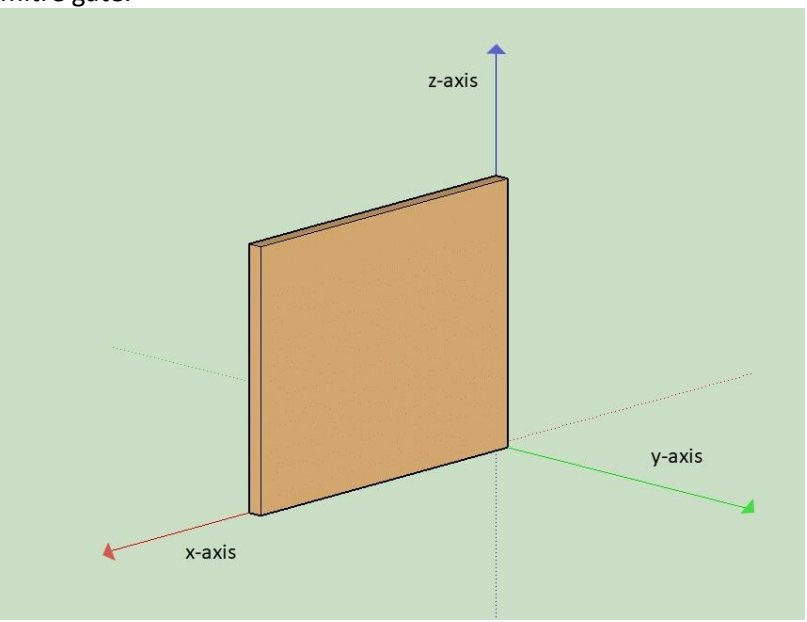

Figure 40: Coordinate system of the mitre gate

The calculation is done iteratively to receive an economical design. Multiple parameters like centre to centre distance of girders and web plate, thickness of skin plate and other dimensions of the girder and web plate have been optimized during calculation.

The differentiating parameters for the design of the mitre gate are:

1.	Centre to centre distance of the girders
2.	Thickness of the skin plate layers
3.	Thickness of the girder
4.	Height of the girder
5.	Maximum thickness of the web plate
6.	Height of the web plate

Table 6: Differentiating parameters during preliminary design

As in Figure 41 can be seen, the height of an element is defined in z-direction and the thickness in y-direction.

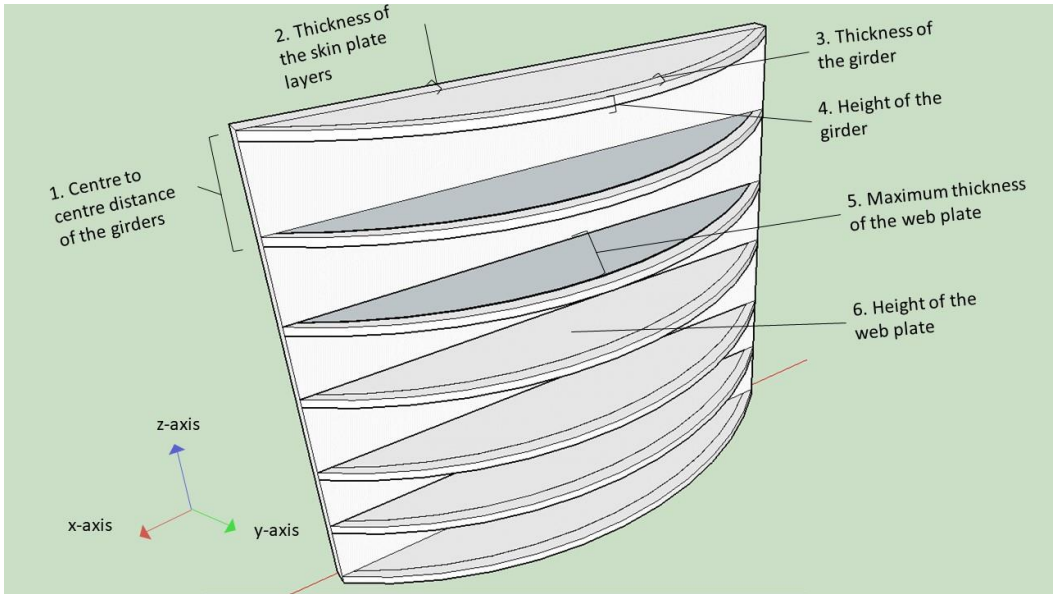

Figure 41: Differentiating parameters of preliminary design

5.4.1 Global and local design verifications

The bending moment in the global design are around the z-axis and therefore defined with the subscript z. In the local design it is around the y-axis so are marked with the subscript y. For the ultimate limit strength verification the design value of a strength parameter is calculated as the NEN-EN 1995 prescribes:

$$X_d = k_{mod} \frac{X_k}{\gamma_m}$$

X_d [x] = design value
k_{mod} [-] = modification factor for duration of load and moisture content, 0.7 for a timber mitre gate with short term loading in service class 3
γ_m [-] = material factor, 1.3 for sawn timber
X_k [x] = characteristic value
The depth factor k_h is not applied for the calculation as they are not valid. The depth factor for solid timber is only valid if $\rho_k \leq 700$ kg/m^3, the azobé used has a characteristic density of 800 kg/m^3. For laminated timber the depth factor is only valid for glue laminated timber.
Therefore an example of the compression strength parallel to the grain is:

$$f_{c,0,d} = k_{mod} \frac{f_{c,0,k}}{\gamma_m}$$

$f_{c,0,d}$ [N/mm^2] = design compression strength parallel to the grain
$f_{c,0,k}$ [N/mm^2] = characteristic compression strength parallel to the grain

For the ultimate limit design of the global and local design the NEN-EN 1995 prescribes the following verfications for bending moments in y- and z-direction:

$$6.11: \frac{\sigma_{m,y,d}}{f_{m,y,d}} + k_m \frac{\sigma_{m,z,d}}{f_{m,z,d}} \leq 1 \quad [1]$$

$$6.12: k_m \frac{\sigma_{m,y,d}}{f_{m,y,d}} + \frac{\sigma_{m,z,d}}{f_{m,z,d}} \leq 1 \quad [2]$$

$\sigma_{m,d}$ [N/mm^2] = design bending stress
$f_{m,d}$ [N/mm^2] = design bending strength
k_m = stress distribution factor, 0.7 for rectangular cross sections

For a cross section in compression the verification is:

$$6.2: \frac{\sigma_{c,0,d}}{f_{c,0,d}} \leq 1 \quad [3]$$

$\sigma_{c,0,d}$ [N/mm^2] = design compressive stress parallel to the grain
$f_{c,0,d}$ [N/mm^2] = design compression strength parallel to the grain

The shear verification is:

$$6.13: \frac{\tau_d}{f_{v,d}} \leq 1 \quad [4]$$

τ_d [N/mm^2] = design shear stress
$f_{v,d}$ [N/mm^2] = characteristic shear strength

For the combined bending moments and compression in the cross section the following verification should be met if the condition is met:

$$6.23: \frac{\sigma_{c,0,d}}{k_{c,y} f_{c,0,d}} + \frac{\sigma_{m,y,d}}{f_{m,y,d}} + k_m \frac{\sigma_{m,z,d}}{f_{m,z,d}} \leq 1 \; for \; \lambda_{rel,y} \geq 0.3 \quad [5]$$

$$6.24: \frac{\sigma_{c,0,d}}{k_{c,z} f_{c,0,d}} + k_m \frac{\sigma_{m,y,d}}{f_{m,y,d}} + \frac{\sigma_{m,z,d}}{f_{m,z,d}} \leq 1 \; for \; \lambda_{rel,z} \geq 0.3 \quad [6]$$

$k_{c,y}$ [-]= instability factor for a cross section in compression
$\lambda_{rel,y}$ [-] = relative slenderness of the cross section
For the used design it turns out that $\lambda_{rel,y} \leq 0.3$ & $\lambda_{rel,z} \leq 0.3$ so formula [5] and [6] are replaced by:

$$6.19: \left(\frac{\sigma_{c,0,d}}{f_{c,0,d}}\right)^2 + \frac{\sigma_{m,y,d}}{f_{m,y,d}} + k_m \frac{\sigma_{m,z,d}}{f_{m,z,d}} \leq 1 \quad [7]$$

$$6.20: \left(\frac{\sigma_{c,0,d}}{f_{c,0,d}}\right)^2 + k_m \frac{\sigma_{m,y,d}}{f_{m,y,d}} + \frac{\sigma_{m,z,d}}{f_{m,z,d}} \leq 1 \quad [8]$$

Curving of the construction provides some extra verifications as well. Some reduction of the bending strength should be taken into account as a result of curving the lamellae of the girder. Furthermore the bending stress should be multiplied with a redistribution factor for curving the girder.

$$6.41: \frac{k_l * \sigma_{m,y,d}}{k_r * f_{m,d}} \leq 1 \quad [9]$$

k_l [-] = stress distribution factor for curved beams
k_r [-] = reduction factor for curving lamellae
The clarification of the instability factor, relative slenderness, stress distribution factor and reduction factor for curving is shown in Preliminary design.
The flexural buckling stability of the girders is verified as well. According to section 6.3.3 of NEN-EN 1995, the bending moment around the strong y-axis and normal force in the beam should fulfil:

$$6.35: \left(\frac{\sigma_{m,y,d}}{k_{crit} f_{c,0,d}}\right)^2 + \frac{\sigma_{c,0,d}}{k_{c,z} f_{c,0,d}} \leq 1 \quad [10]$$

k_{crit} [-] = factor for flexural buckling

5.4.2 Cross sectional calculation

For the global calculation a height of 1.5 metres is taken for the design of a single slice. The cross section is varying along the width of this section, which is the width of the mitre gate. A sketch of the cross section of this slice halfway the width of the mitre gate is shown in Figure 42. On the left side the skin plate of the mitre gate is shown, the right element is the laminated girder. The web plate in between these components is varying of dimensions along the width of the mitre gate.

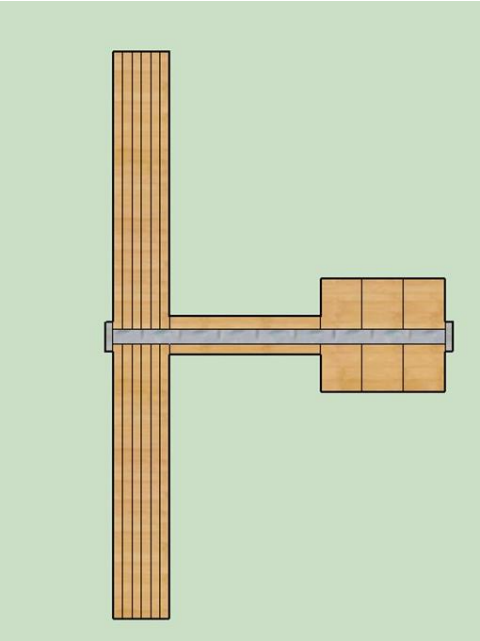

Figure 42: Sketch of the cross section of the slice during global design

As told before hardwood is yet impossible to glue in wet conditions, therefore the elements are jointed with dowels and bolts. To calculate the properties of the cross section, the mechanically jointed theory of the NEN-EN 1995 is used. As outlined in Section 4.2.2 the mechanically jointed beam theory has some assumptions. Furthermore this theory is only valid for the maximum three elements jointed. Mulder (2019, p. 19) however found out a simplification for the Schelling method, which is valid for more than 3 elements dowelled. To be able to obtain characteristics of the cross section the cross section for the global design is calculated in the following way. The total cross section for the global design is cut into three parts: 1. The cross laminated skin plate, 2. The web plate, 3. The laminated girder. The effective bending stiffness of the skin plate is calculated based on the simplification of the theory of Schelling (Mulder, 2019). The effective bending stiffness of the web plate is calculated in ordinary way for each rectangular solid element. The effective bending stiffness of the dowel laminated girder is obtained with the mechanically jointed theory of NEN-EN 1995. Expressed as formulas this is:

$$EI_{eff} = EI_{eff,skin\ plate} + \gamma_1 * E_{skin\ plate} * A_{skin\ plate} * a^2_{skin\ plate} + EI_{web\ plate} + \gamma_2 E_{web\ plate} A_{web\ plate} a^2_{web\ plate} + EI_{eff,curved\ girder} + \gamma_3 E_{curved\ girder} A_{curved\ girder} a^2_{curved\ girder}$$

$$EI_{eff,skin\ plate} = 2 * \sum_{i=1}^{3} (E_i * I_i + \gamma_i E_i A_i a_i^2)$$

$$EI_{eff,curved\ girder} = \sum_{i=1}^{3} (E_i * I_i + \gamma_i E_i A_i a_i^2)$$

E [N/mm^2] = modulus of elasticity
I [mm^4] = moment of inertia
With gamma according to NEN-EN 1995:

$$\gamma_1 = \gamma_3 = \frac{1}{1 + \frac{\pi^2 * E_i * A_i * s_i}{l_{ref}^2 * k}}$$

A [mm^2] = Area of the laminated beam
s [m] = spacing of the dowels
l_{ref} [mm] = reference length of the laminated beam
t [mm] = thickness of the lamellae
k [N/mm/m] = shear modulus

$$k = \frac{K_{ULS}}{s}$$

$$K_{ULS} = \frac{2}{3} K_{Ser}$$

$$K_{Ser} = \rho_m^{1.5} * \frac{d}{23} \text{ for dowels}$$

ρ_m [kg/m^3] = mean density of the connected elements
d [mm] = diameter of the dowel
K_{ULS} [N/mm] = slip modulus in ultimate limit state
K_{SLS} [N/mm] = slip modulus in serviceability limit state
The simplified shear reducing factors for the six layered skin plate are:

$$\gamma_1 = \gamma_6 = \frac{k * L^2 * (A_i^2 * E_i^2 * \pi^2 + 5 * A_i * k * E_i * L^2 * \pi^2 + 5 * k^2 * L^4)}{5 * (A_i^3 * E^3 * \pi^6 + A_i^2 * k * E_i^2 * L^2 * \pi^4 + 9 * A_i * k^2 * E_i * L^4 * \pi^2 + 2 * k^3 * L^6)}$$

$$\gamma_2 = \gamma_5 = \frac{2 * k^3 * L^6}{A_i^3 * E^3 * \pi^6 + A_i^2 * k * E_i^2 * L^2 * \pi^4 + 9 * A_i * k^2 * E_i * L^4 * \pi^2 + 2 * k^3 * L^6}$$

$$\gamma_3 = \gamma_4 = \frac{2 * (\pi^2 * E * A + 3 * k * L) * k^2 * L^4}{3 * (A_i^3 * E^3 * \pi^6 + A_i^2 * k * E_i^2 * L^2 * \pi^4 + 9 * A_i * k^2 * E_i * L^4 * \pi^2 + 2 * k^3 * L^6)}$$

The stress in the outer fibre of the girder according to NEN-EN 1995 becomes:

$$\sigma_{girder} = \frac{\gamma * E_{girder} * a_{girder} * M_{max}}{EI_{eff}}$$

$$\sigma_{m,girder} = \frac{0.5 * E_0 * h_{girder} * M_{max}}{EI_{eff}}$$

$$\sigma_{m,tot,girder} = \sigma_{girder} + \sigma_{m,girder}$$

The shear stress in the cross section is calculated as the mechanically jointed theory prescribes:

$$\tau_{max} = \frac{\gamma_{11} * E_1 * A_{11} * z_{11} + \gamma_{12} * E_2 * A_{12} * z_{12} + \gamma_{13} * E_3 * A_{13} * z_{13}}{b_{skinplate} * EI_{eff}} * V$$

5.4.3 Global design

As told before, for the preliminary design the hydraulic pressure of the water level difference is taken as the major load on the mitre gate. For simplicity reasons this pressure is taken uniform over the total height of the mitre gate. By leaning towards each other the mitre gates the differential head is resulting in a normal force in the mitre gate. The derivation of the normal force is done in Figure 95 of Appendix B: $N = \frac{W}{2\tan(1/3)}$. As already stated before this normal force is eccentric because the contact point of the mitre gates is not in the centre line of the mitre gates. The contact point of the mitre gates is shown in Chapter 6. For the determination of the dimensions of the cross section a repetitional cross section of the mitre gate is taken. This repetitional cross section contains the six-layered skin plate, one web plate and a three layered girder. For the calculation the centre to centre distance of the girders determines the width of the skin plate in one repetitional cross section. This centre to centre distance of the curved laminated girders is varied during the calculation. According to the NEN-EN

1995 the maximum effective width of the flange if shear lag is taken into account is $0.2 * l_{eff} = 0.2 * 9.5 = 1.9$ metres. After some iterations it came out that 1.5 metre centre to centre distance of the girders is an economically attractive distance for the girders. If the centre to centre distance increases the loads become high and the cross section should be relatively big to withstand the bending moment and normal force. If the centre to centre distance of the girders decreases the total amount of timber used for the mitre gate is big. In Figure 43 the global bending moment and load distribution of a simply supported beam with centre to centre distance of 1.5 metres can be seen.

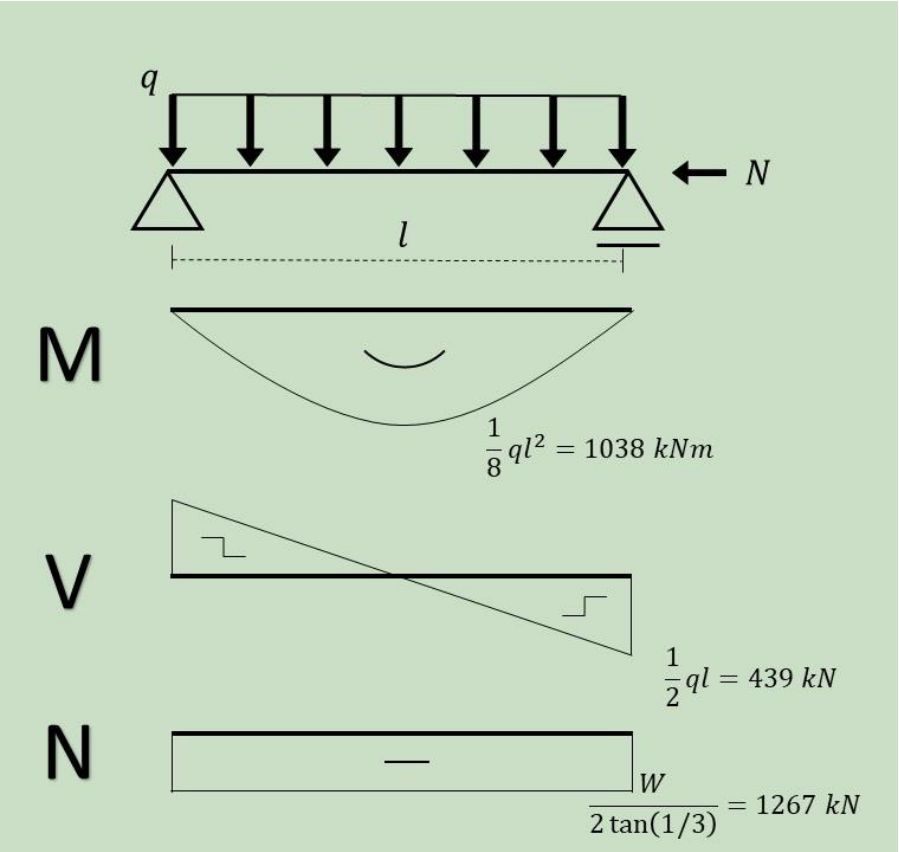

Figure 43: Bending moment and force diagrams of global design

5.4.4 Local design

The local design is for the local stability of the mitre gate, in this design the mitre gate is seen from aside. In the local design the mitre gate is schematized as a continuous beam with uniform distributed load over the total height of the mitre gate. The distributed load ensures a bending moment and shear force, no normal force is present. The schematization and the bending moment and force diagrams of the mitre gate are shown in Figure 44. The supports of the continuous beam are at the location where the web plate is connecting the curved girder and the skin plate.

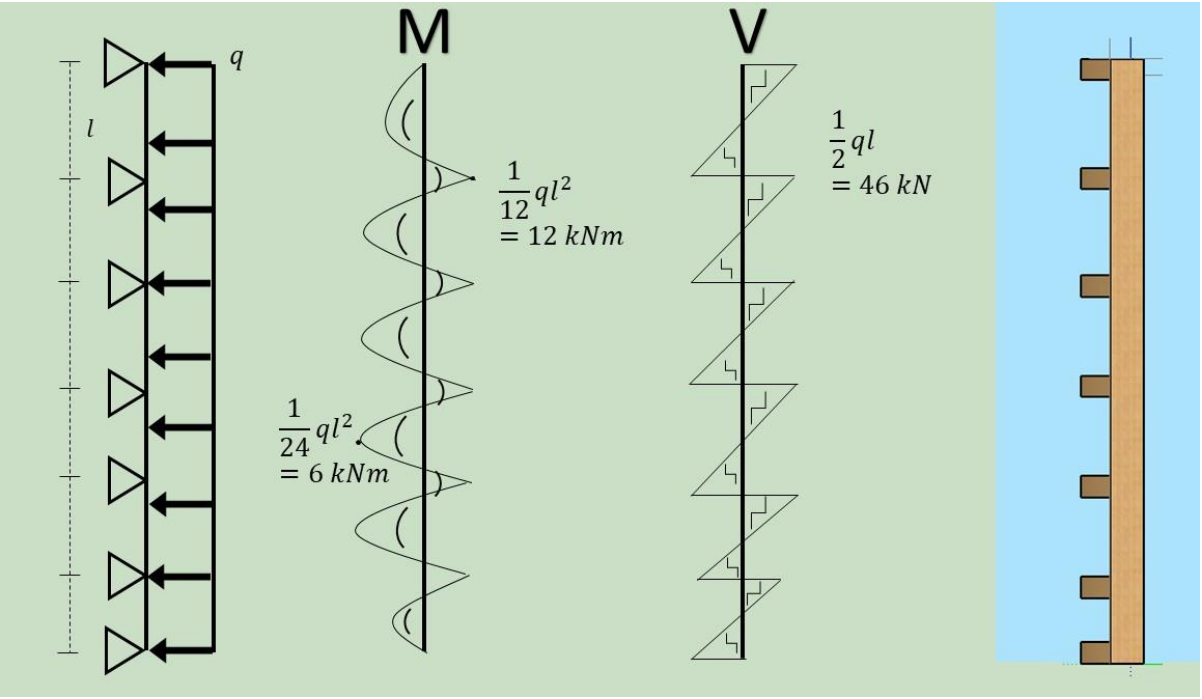

Figure 44: Bending moment and force diagrams of local design (side view of mitre gate)

For the design a slice of one metre width is taken to perform the local design on. So the dimensions of the cross section are b = 1000 millimetres, h = 25 millimetres. In the schematization can be seen that the supports of the continuous beam are at the location of the web plate and girder. Therefore the girder and web plate are not in the cross section for the local calculation. For this calculation the two outer (layer 1 & 6, horizontally orientated) and two inner (layer 3 & 4, diagonally orientated) layers of the cross laminated timber plate have no contribution in the strength of the plate as they are not loaded in their fibre direction and are therefore not taken into account in the cross section too. The effective layers of the cross section in the slice for the calculation can be seen in Figure 45.
The bending moment and shear force are maximum at the location of an intermediate girder. Along the width of the mitre gate the cross section consists of 2 active skin layers, layer 2 and 5. A slice of on metre is taken to perform the local design on so the cross section is b = 1000 millimetres, h = 25 millimetres.

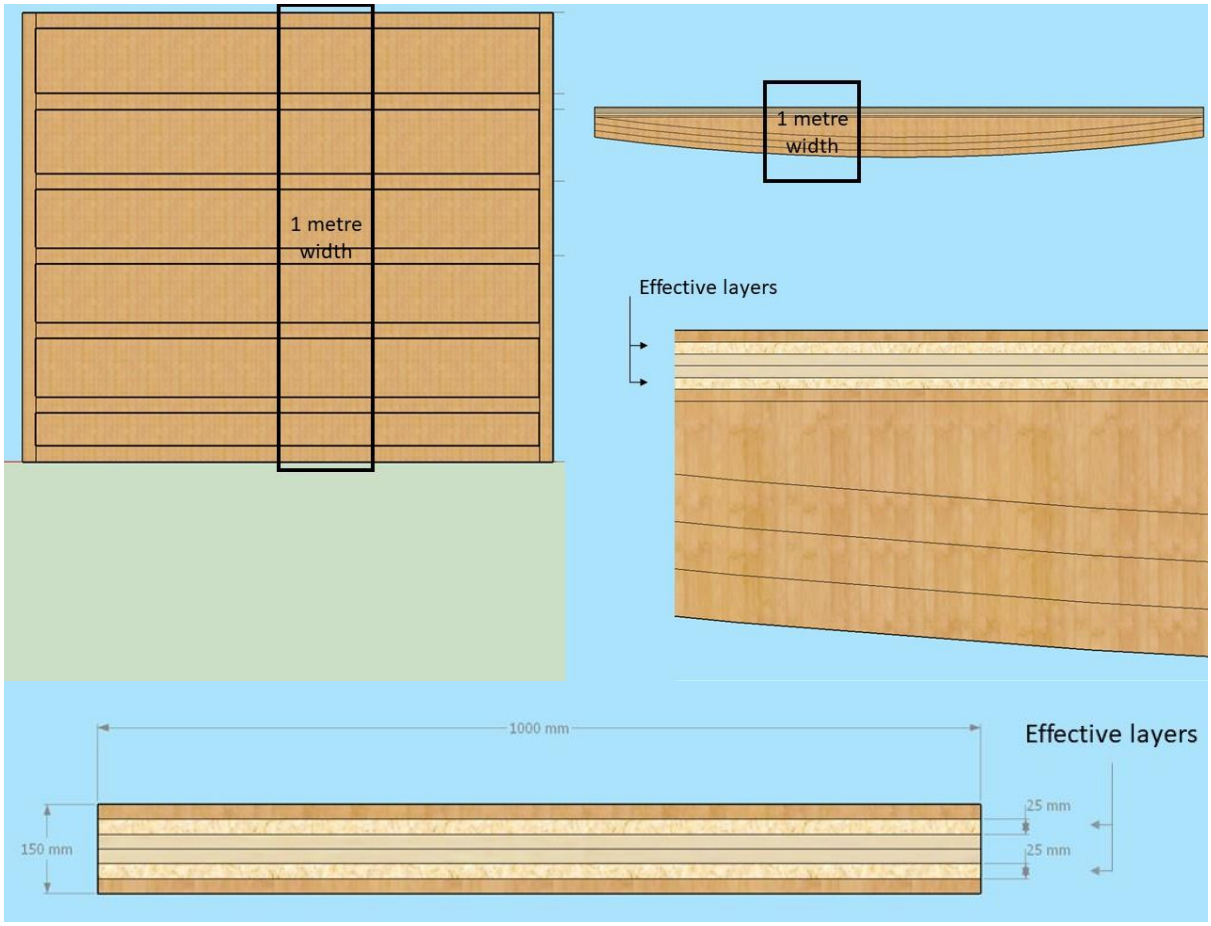

Figure 45: Derivation of cross sectional slice of local design

5.4.5 Deflection

The serviceable limit state is checked based on moments and deflection formulas of structural mechanics, also known as 'forget-me-nots'. These deflections are compared to the deflections obtained from the SCIA Engineer model. To estimate the deflection the gate is schematized as a simply supported beam with constant modulus of elasticity and moment of inertia over the width of the mitre gate. The initial deflection for a simply supported beam according to the formulas of structural mechanics is: $u_{inst,Q,1} = \frac{5ql^4}{384EI_{eff}}$. The final deflection for the gate loaded by the differential head is: $u_{fin,Q,1} = u_{inst,Q,1}(1 + \Psi_{2,1}k_{def})$.

Where:

k_{def} [-] = deformation factor, 2.0

$\Psi_{2,1}$ [-] = factor for quasi-permanent value of variable action, 0.8

The effective bending stiffness halfway the mitre gate according to the mechanically jointed beam theory is done in the same way as in Section 5.4.2, however the serviceability limit state is used for the slip modulus:

$$EI_{eff} = E_{skin\ plate} * I_{skin\ plate} + E_{stiffened\ plate} * I_{stiffened\ plate} + E_{curved\ girder} * I_{curved\ girder}$$

In here the Steiner's rule for the moment of inertia of the cross laminated timber skin plate and laminated girder has a reduction factor of γ described in NEN-EN 1995. The formula for the moment of inertia of the plate turns out to:

$$I_{skin\ plate} = I_{lamellae} + \gamma * A * z^2$$

$$I_{curved\ girder} = I_{lamellae} + \gamma * A * z^2$$

$I_{skin\ plate}$ [mm^4] = total moment of inertia of the skin plate

$I_{lamellae}$ [mm^4] = moment of inertia of a lamellae with the fibre in strongest direction (perpendicular to the direction of loading)

$I_{curved\ girder}$ [mm^4] = total moment of inertia of the curved girder
γ [-] = reduction factor for shear deformation
A [mm^2] = area of the lamellae
z [mm] = distance of the lamellae to the centre of gravity

5.4.6 Fastener verification

Lastly for the preliminary design the load on the fasteners is checked. According to NEN-EN 1995 the load on fasteners calculated with the mechanically jointed theory is taken as: $F = \frac{\gamma_i E_i A_i a_i s_i}{EI_{eff}} V$, where *i* is the number of the laminated element. Dowels and bolts are common used for lamination of timber, the selection of the fastener type for this thesis is done during the detailing described in Chapter 6.
For fasteners the characteristic load-carrying capacity in single shear is the minimum of six failure modes, the formula of this load-carrying capacity is shown below. The visual representation of the failure modes is shown in Figure 46.

$$F_{v,Rk} = min \begin{cases} f_{h,1,k} t_1 d \\ f_{h,2,k} t_2 d \\ \frac{f_{h,1,k} t_1 d}{1+\beta}\left[\sqrt{\beta + 2\beta^2\left[1+\frac{t_2}{t_1}+\left(\frac{t_2}{t_1}\right)^2\right]+\beta^3\left(\frac{t_2}{t_1}\right)^2} - \beta\left(1+\frac{t_2}{t_1}\right)\right] + \frac{F_{ax}}{4} \\ 1.05\frac{f_{h,1,k} t_1 d}{2+\beta}\left[\sqrt{2\beta(1+\beta)+\frac{4\beta(2+\beta)M_{y,Rk}}{f_{h,1,k} d t_1^2}} - \beta\right] + \frac{F_{ax}}{4} \\ 1.05\frac{f_{h,1,k} t_2 d}{1+2\beta}\left[\sqrt{2\beta^2(1+\beta)+\frac{4\beta(2+\beta)M_{y,Rk}}{f_{h,1,k} d t_1^2}} - \beta\right] + \frac{F_{ax}}{4} \\ 1.15\sqrt{\frac{2\beta}{1+\beta}}\sqrt{2M_{y,Rk} * f_{h,1,k} d} + \frac{F_{ax}}{4} \end{cases}$$

In here:
$f_{h,i,k}$ = embedding strength for bolts and dowels, $f_{h,i,k} = 0.082(1-0.001d)\rho_k$
β = ratio of embedding strength of the jointed beams, $\beta = \frac{f_{h,2,k}}{f_{h,1,k}} = 1$
$M_{y,Rk}$ = characteristic value for yield moment for bolts and dowels, $M_{y,Rk} = 0.3 f_{u,k} d^{2.6}$
F_{ax} is the characteristic axial withdrawal capacity of the fastener. According to the Johansen yield theory, this value differs for every type of fastener. For bolts this value is 25%, whereas it is 0% for dowels.

For fasteners in double shear the characteristic load-carrying capacity is the minimum of four failure modes, the formulas for the failure modes are:

$$F_{v,Rk} = min \begin{cases} f_{h,1,k} t_1 d \\ 0.5 f_{h,2,k} t_2 d \\ 1.05\frac{f_{h,1,k} t_1 d}{2+\beta}\left[\sqrt{2\beta(1+\beta)+\frac{4\beta(2+\beta)M_{y,Rk}}{f_{h,1,k} d t_1^2}} - \beta\right] + \frac{F_{ax}}{4} \\ 1.15\sqrt{\frac{2\beta}{1+\beta}}\sqrt{2M_{y,Rk} * f_{h,1,k} d} + \frac{F_{ax}}{4} \end{cases}$$

The visual representation of the failure modes is given below.

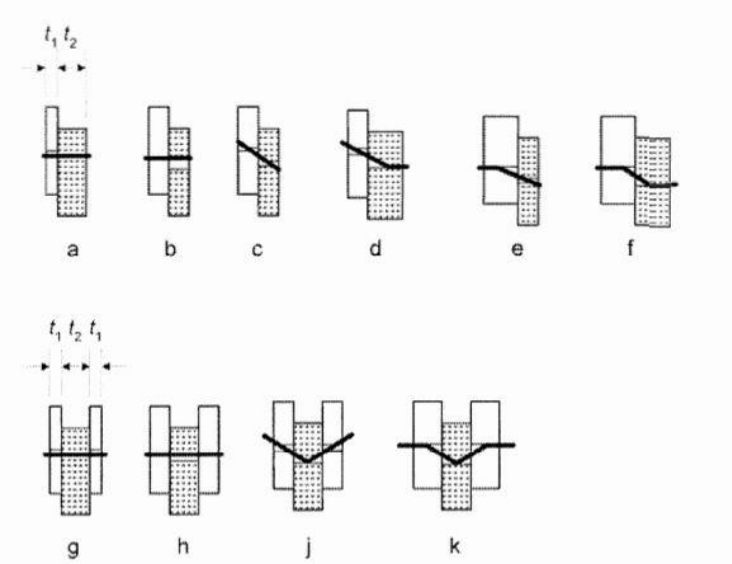

Figure 46: Failure modes of single shear (top) and double shear (bottom)

The characteristic the load-carrying capacity of the bolts in the mitre gate are different for the different parts of the mitre gate, skin plate, web plate and girder. The renewed design of the mitre gate contains over 2000 dowels and bolts with shear connections. These fasteners cannot be verified all in this thesis and a presumably governing situation is verified. This fastener is located at the lock chamber side where the shear force is maximum. When taking into account the design of the mitre gate, the laminated girder is expected to have the governing load on the fastener. The girder is in single shear for the design as the girder is in tension. In Figure 47 it can be seen that the dowel in the three layered girder is in single shear. For double shear the shear force in the two outer layers should have been orientated in the same direction.

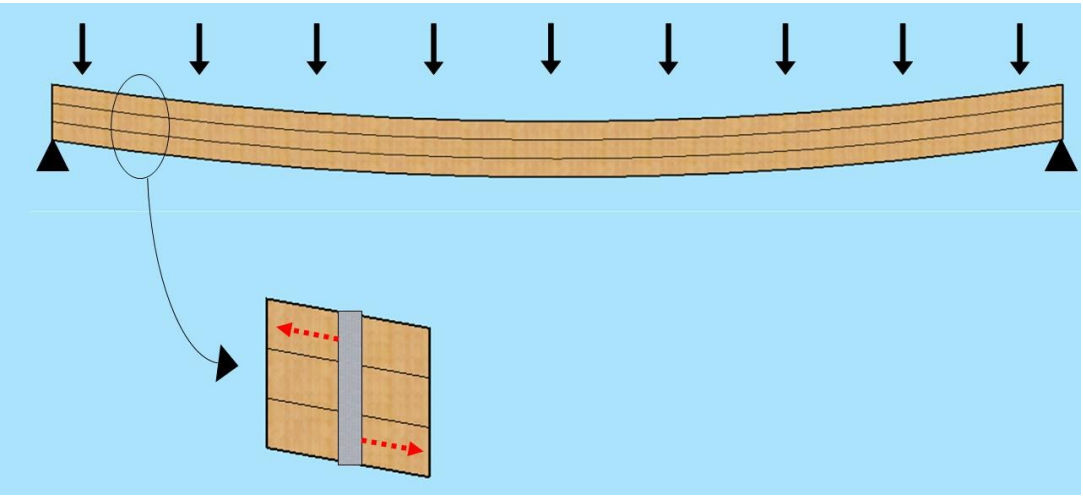

Figure 47: Explanation of single shear plane of fastener in laminated beam

The load-carrying capacity for each failure mode for the laminated girder are given in Table 7. The characteristic axial withdrawal capacity of the fastener is assumed as 0% :

Failure mode	$F_{v,Rk}$ **dowel of girder (kN)**
A	137.7
B	137.7
C	57.0
D	58.8
E	58.8
F	62.1

Table 7: Characteristics load-carrying capacity of fastener in laminated girder in single shear

The governing load-carrying capacity for the girder in single shear is the third failure mode with a characteristic load-carrying capacity of 57 kN. The design load-carrying capacity is $F_{v,d} = F_{v,Rk} * \frac{k_{mod}}{\gamma_m} = 30.7$ kN. This is more than the occurring load on the fastener in the laminated girder, which is 14 kN.

5.5 Optimized design

For the optimized design a unity check of 0.6 is aimed for the most critical verification in ultimate limit state. This is done because the calculations are preliminary design to have dimensions of the mitre gate and contain some simplifications. In the model of Chapter 7 the unity check can be somewhat higher or lower and to be safe the construction is able to fulfil the requirements, 0.6 is aimed for.

From the calculations the design results in a cross laminated plate of 6 layers each with a layer thickness of 25 millimetres. The cross laminated skin plate has 2 layers in each horizontal, vertical and diagonal direction, where the diagonals are crossing each other. The web plate is 150 millimetres thick and connects the plate with the girder. The calculation further results in a dowel laminated girder of 300 millimetres thick, which is 3 layers of 100 millimetres each. The most optimum centre to centre height of the girders is 1.5 metres for lower part of the gate where the uniform load is maximum. The loading on the top part of the mitre gate is lower and therefore the centre to centre distance of the girders can be bigger. Optimization of this distance is out of scope of this research. The laminated girder has a height of 300 millimetres. The girder is curved with a maximum spacing in the middle of the gate of 300 millimetres. So the maximum total thickness of the mitre gates is 750 millimetres. The radius of curvature of the laminated girder is 37.5 metres. The girder and plate connect at the end post which is the turning point of the gate.
From preliminary design it turns out that the deflection halfway the mitre gate is 23 millimetres instantaneously and the final deflection is 60, which is around L/150. The fastener check is verified and the dowels can withstand the loads that occur.

Zooming out of the design, the girder is laminated to be able to curve and decrease the amount of used timber instead of a solid beam. Cross laminated timber is applied to make the design more homogeneous, having less protruding and steel elements, due to the diagonal layers. The horizontal and vertical layers provide more stiffness and so a less thick mitre gate. A practical small win is that replacement of the lamellae is less labour extensive and less expensive. The lamellae of the skin plate at the water line should be replaced before reaching the end life of the mitre gate. Because the lamellae of the skin plate are placed horizontal instead of vertical, less lamellae have to be replaced.

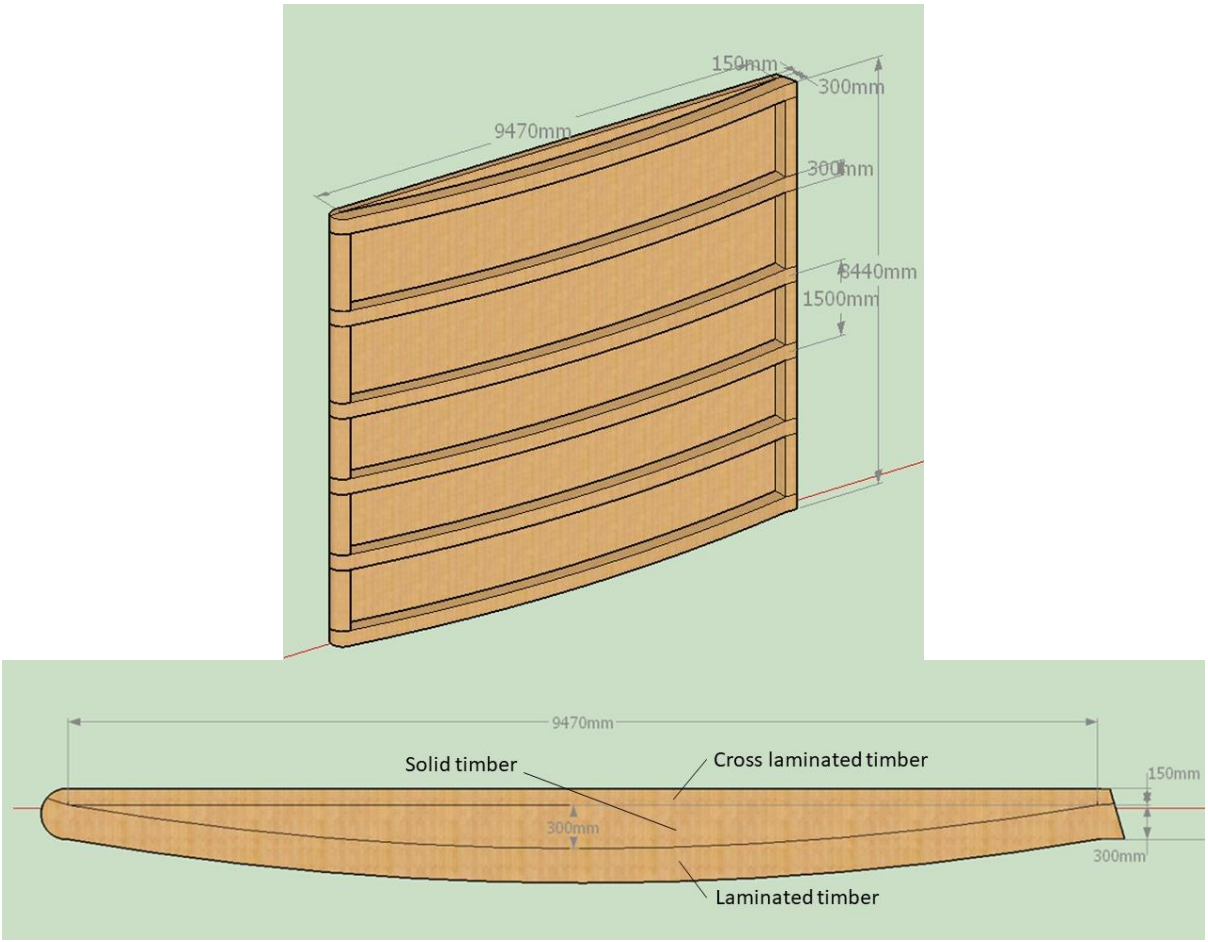

Figure 48: Overview (top) and top view (bottom) of design of mitre gate in Sambeek navigation lock

The unity checks of the formulas described in the preliminary design are shown in the table below.

Verification with Eurocode number	Location	Unity check
6.11: Double bending, y-axis dominant	Halfway the mitre gate, in curved girder	0.50
6.12: Double bending, z-axis dominant	Halfway the mitre gate, in curved girder	0.50
6.2: Compression	Halfway the mitre gate, in curved girder	0.40
6.13: Shear	At support, side of mitre gate	0.47
6.19: Double bending and compression, y-axis dominant	Halfway the mitre gate, in curved girder	0.60
6.20: Double bending and compression, z-axis dominant	Halfway the mitre gate, in curved girder	0.60
6.41: Curved bending moment	Halfway the mitre gate, in curved girder	0.27
6.35: Lateral stability, bending and compression	Halfway the mitre gate, in curved girder	0.39

Table 8: Unity checks design mitre gate

6. Design of timber mitre gate joints

In this chapter, the preliminary design of Chapter 5 is elaborated. The most important joints of the preliminary design of the previous chapter are detailed. The first section contains the joint of the skin plate, web plate, girder and post. The joint detail of the end and front post is slightly different as this section shows. In the next section the detailing of the cross section halfway the mitre gate is elaborated. This detail is the joint of the skin plate, web plate and girder. The location of these two described details are shown in Figure 49. The last detailing is done in the third section, in this section the detailing of the cross laminated skin plate is shown. In the last section of this chapter the current and previous chapter are summarized and an answer on the second sub question: *What does the design of an optimized timber mitre gate look like for an existing situation out of the current application range?* is given.

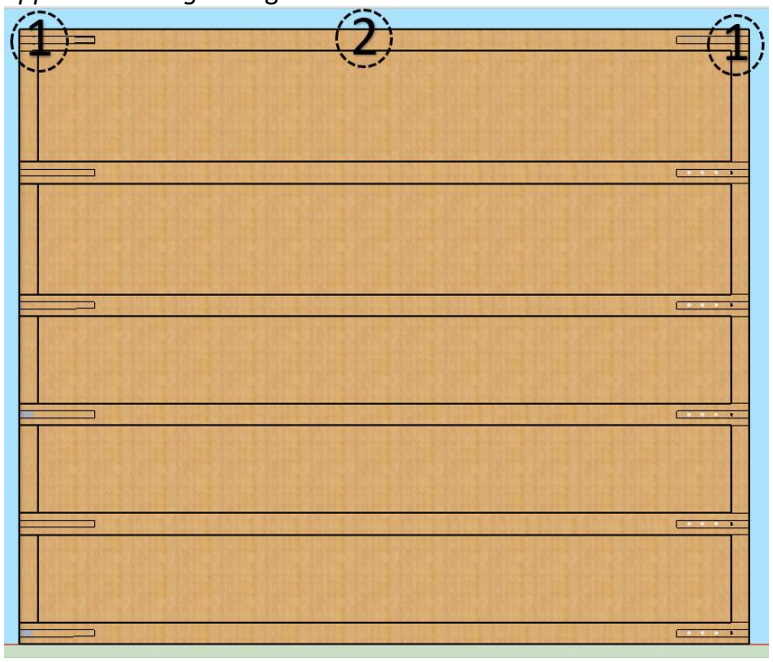

Figure 49: Locations of detailed joints

6.1 Joint post, girder and skin plate

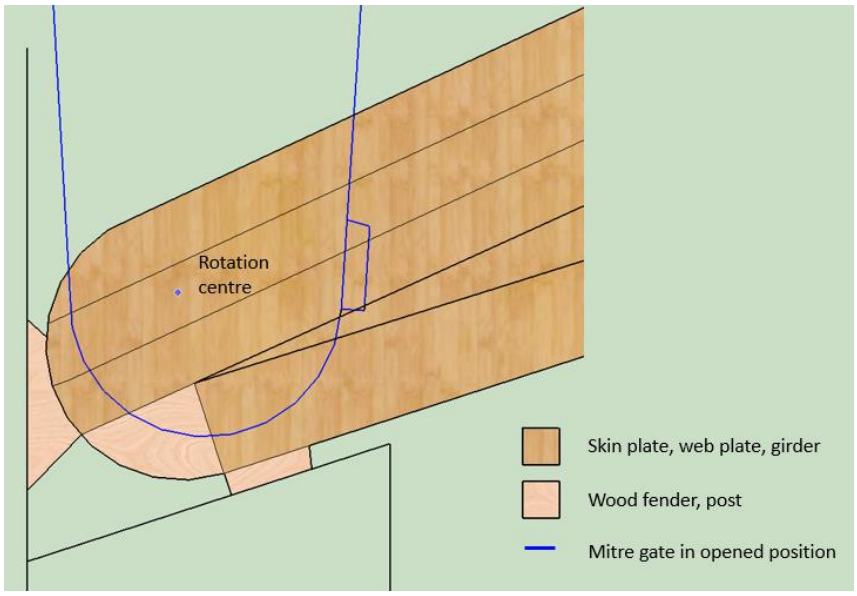

Figure 50: Mitre gate in opened and closed position

The first detail of Figure 49 is the detail where the post, girder, web plate and skin plate come together. As told earlier the common rotation centre of the mitre gate is located eccentric, so in case of movement of the mitre gate the mitre gate does not experience friction with the lock chamber. The eccentric rotation centre is also used for the new design of the mitre gate. In the schematization of the mitre gate the joint is defined as a support of a simply supported beam, thus the bending moment due to the differential head at the joint is zero, while the normal force and shear force are maximum. The shear force has to be distributed to the vertical connection of the lock chamber and the mitre gate. The normal force has to be distributed to the horizontal connection of the mitre gate and lock chamber. The now common design of this connection is the mortise and tenon joint. However this joint has his limitations. In the mortise and tenon joint the force of the girder should be transferred to the end post. This end post has orthogonally orientated fibres compared to the girder, which is less strong and thus is harder to verify as is explained in detail in Appendix G. As the shear and normal force are bigger with wider mitre gates this varication is met for wider gates or bigger differential head.

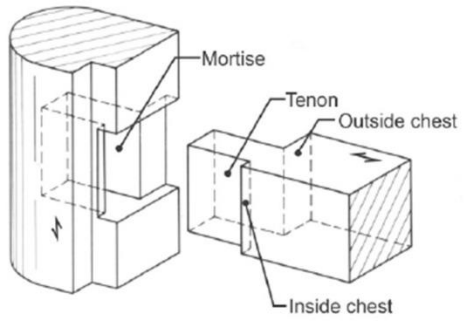

Figure 51: Common mortise and tenon joint (Van Leusden, 1991)

Therefore the distribution of the loads to the lock chamber is slightly changed. The girder is designed as continuous through the post. An advantage of this is that the distribution of the forces from the girder directly goes to the lock chamber. This would solve the problem of the mortise and tenon verification, because the fibres of the posts are orthogonally to the fibres of the girder. However the front and heel post do have a stability function as well. Therefore there is chosen to use the front and end posts but delete the mortise and tenon joint. The area of the girder is sawn out of the posts and stiffen the connection of the girder with the post and skin plate metal straps are used. Practical note is that the main goal of the mitre gate, the water retaining function, should be taken into account. With means that the gates should fit well towards each other and to the lock chamber, this is done by planing the wood very well.

Girder
The girder is mechanically jointed with bolts. By use of bolts the lamellae are connected to each other with shear. The girder of the mitre gate is in compression. The girder wants to shrink and move away from the end post.
Skin plate
The skin plate is mechanically jointed and built up of multiple different layers in different directions. Due to the fact that gluing is not possible in wet environment.

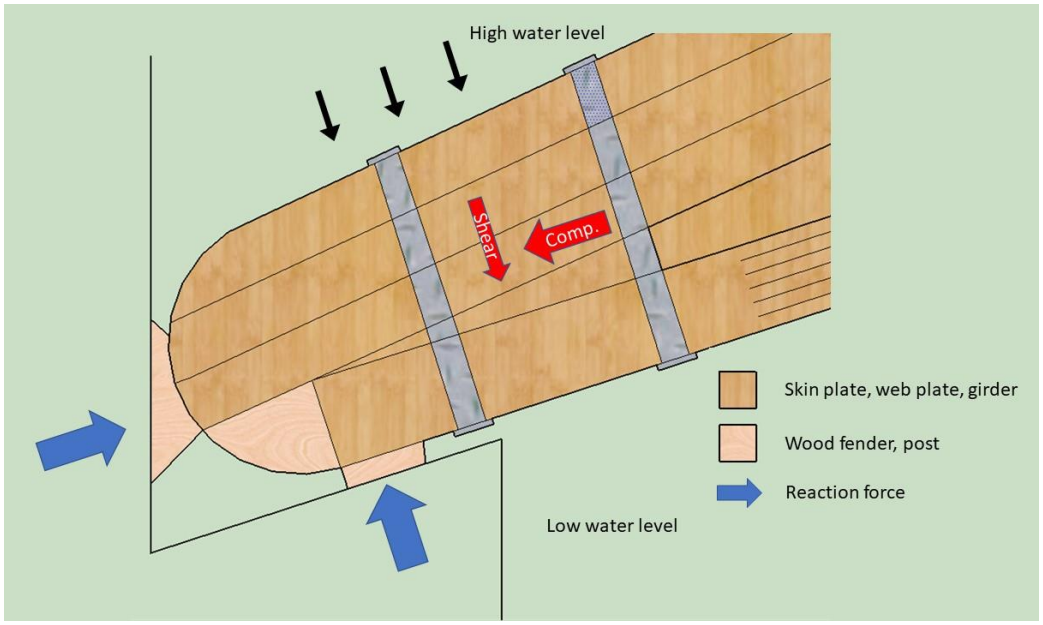

Figure 52: Force distribution of the end post, girder and skin plate detail

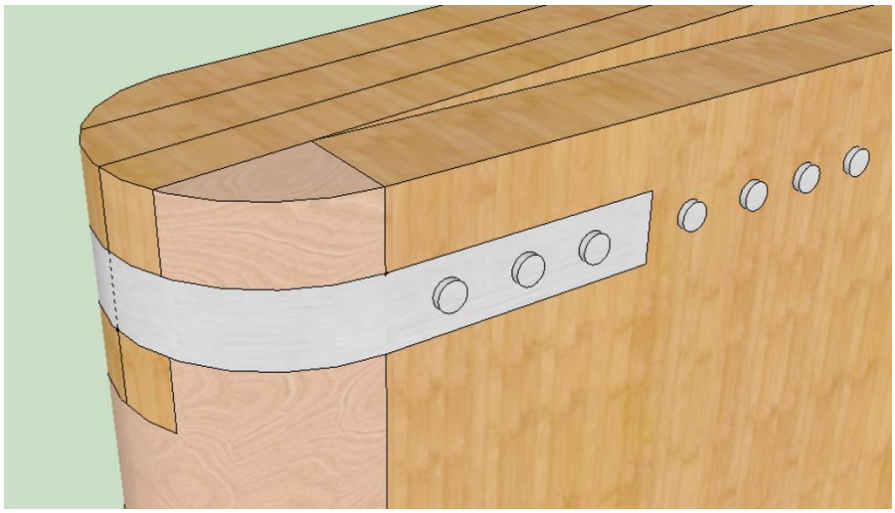

Figure 53: Overview of the post, girder and skin plate detail

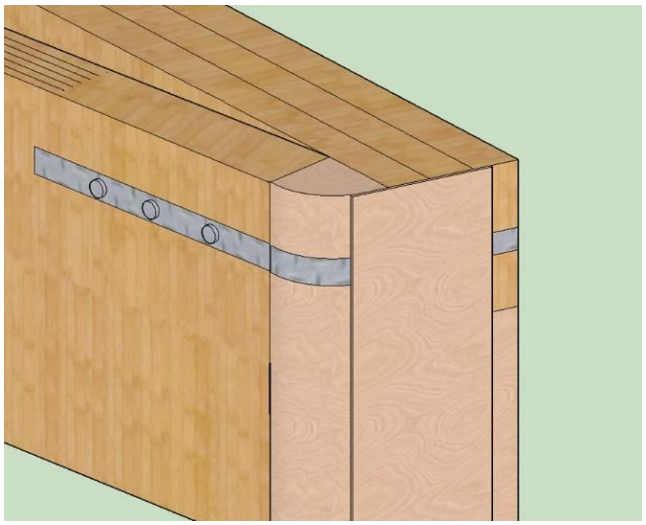

Figure 54: Overview of end post, skin plate, girder and web plate at connecting gate side

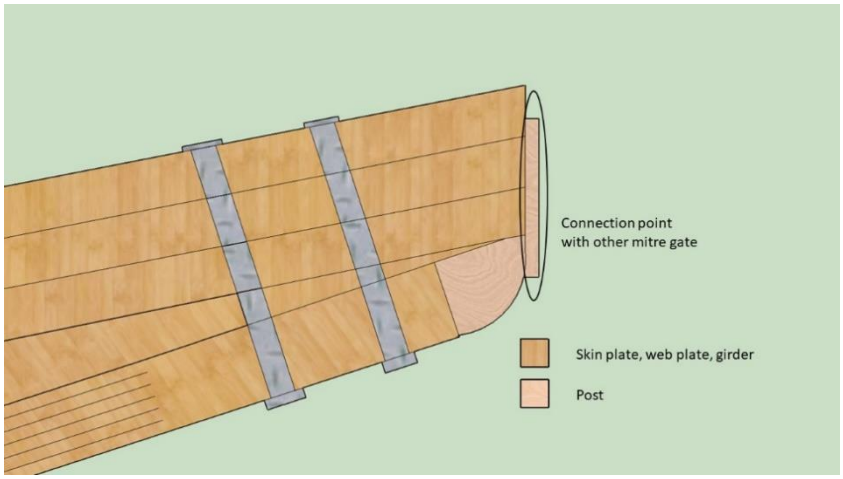

Figure 55: Top view of end post, skin plate, girder and web plate at connecting gate side

The connection of the end post with the skin plate, girder and web plate is modelled as a continuous supported element over the height of the post in case of closed situation. The contact points of the mitre gates is simulated as support over the total height as well. Although the connection of the posts is over the total height of the mitre gate, the more stiff girder is likely to distribute more forces. The top and bottom hinge are the supports of the total mitre gate during movement of the mitre gate.

6.2 Joint girder, web plate and skin plate

Halfway the mitre gate the bending moment and normal force are maximum and the shear force is zero. The differential head hydrostatic pressure results in a skin plate that is in tension and a girder in compression.

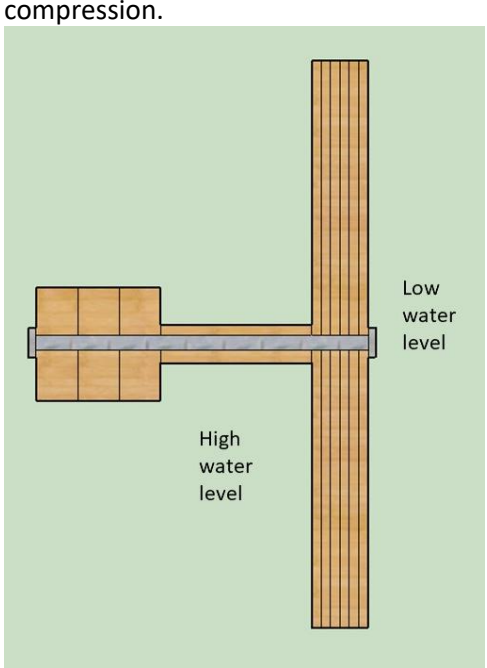

Figure 56: Detailed cross section halfway the mitre gate

6.3 Dowel laminated skin plate

The skin plate of the mitre gate is built up in 6 layers each of 25 millimetres thick. This skin plate is dowelled. An average spacing of the dowels is 200 to 300 millimetres for civil engineering. To connect all the different layers of the skin plate dowels are used. The design of a skin plate with lamellae of 200 millimetres wide for the x- and y-orientated lamellae is shown in the figures below.

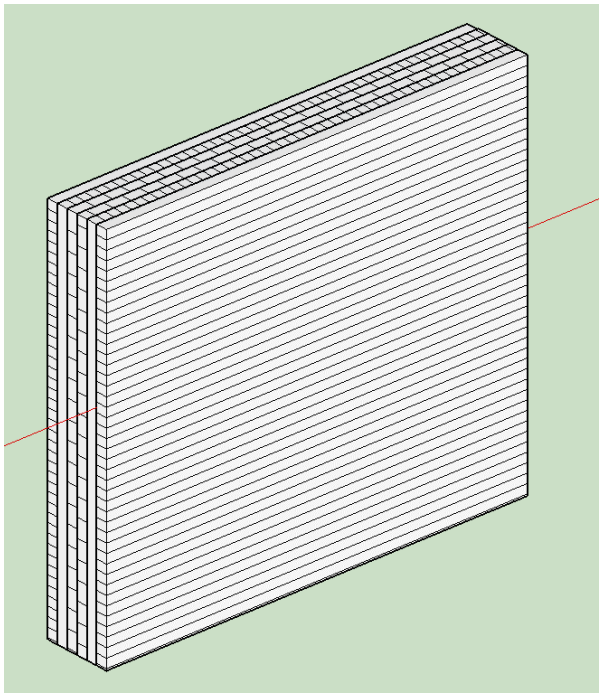

Figure 57: Overview of cross laminated skin plate with lamellae of 200 mm wide and diagonal lamellae of 200/√2 wide

The dowels should penetrate through the middle of the lamella of each layer to create the best interaction between the layers. With right placement of the skin plate layers small square squares with equal sides appear in the skin plate in the front view. The side of these square plates have a length that is equal to the width of the horizontal and vertical orientated layers divided by the square root of 2. So in case of width 200 the square plates that appear in the plate to be one plate has sides of $200/\sqrt{2}$. This length is equal to the width of the diagonal lamellae of the diagonals.

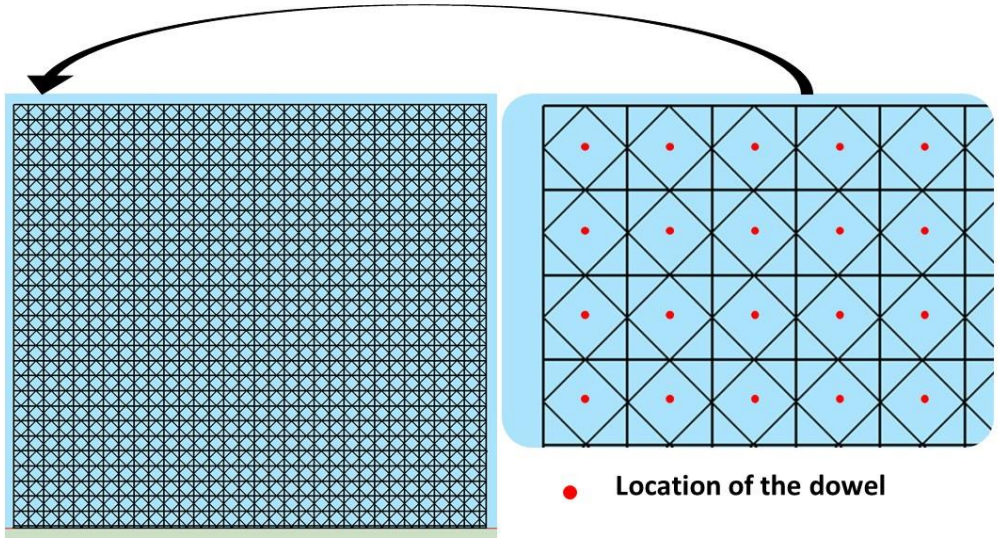

Figure 58: Front view of dowel locations in skin plate

In the figures the black lines are the sides of the lamellae, so the dowels are placed in the middle of the created rhombus, red dots in Figure 58.

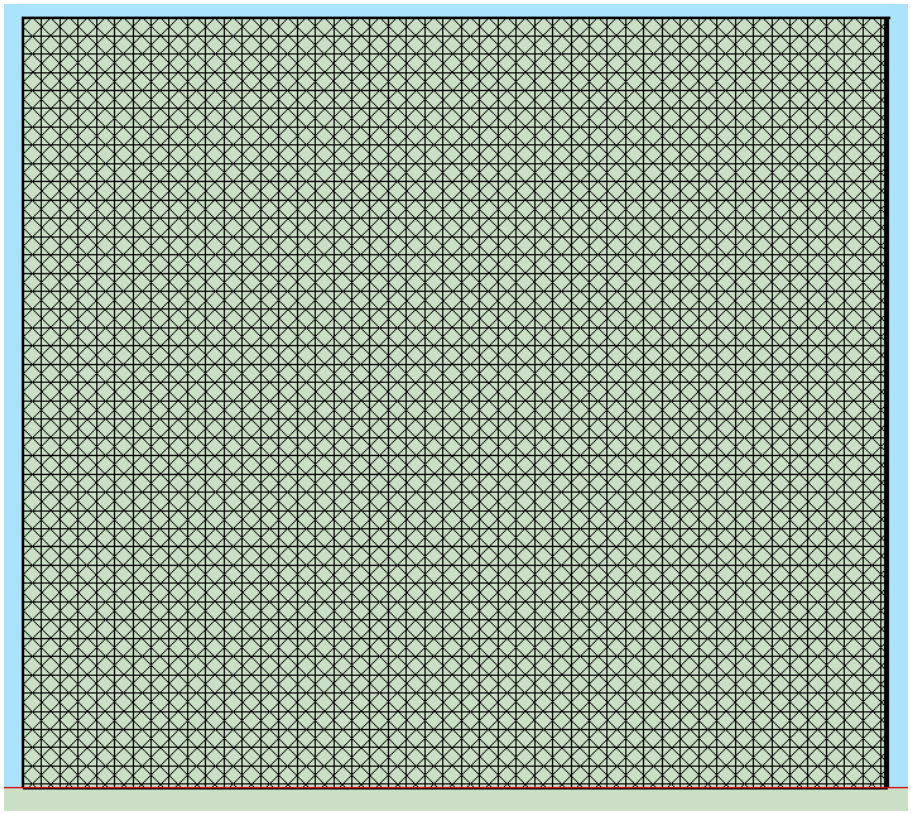

Figure 59: Front view of laminated skin plate with lamellae of 200 mm wide and diagonal lamellae of 200/√2 wide

6.4 Final design of mitre gate out of the current application range

To finalize the preliminary design and detailing of the mitre gate, the answer on the third sub question is given. The third sub question is: *What does the design of an optimized timber mitre gate look like for an existing situation out of the current application range?* For the design of a mitre gate out of the current application range, the eastern navigation lock of Sambeek is used. The navigation lock has a water retaining height of 8.44 metres, width of 16 metre and a mitre gate width of 9.47 metres. The design for a mitre gate with a width of 9.47 metres and a water retaining height of 8.44 metres consists of a dowel cross laminated skin plate, web plate and a laminated girder. The centre to centre distance of the girders, and also the web plate, is 1.5 metres. The dowel cross laminated skin plate consists of 6 layers with a thickness of 25 millimetres. The fibres of the six layers are placed in the following sequence: x-direction, y-direction, /-direction, \-direction, y-direction and x-direction. The width of the x- and y-orientated lamellae is 200 millimetres, the diagonal orientated layers have a width of 141 millimetres for practical reasons. The web plate of the mitre gate is a semi-ellipse plate with a thickness of 150 millimetres. The maximum height of the web plate is 300 millimetres halfway the mitre gate. The laminated girder is a curved three layered beam, each layer has a thickness of 100 millimetres and a height of 300 millimetres. The maximum distance between the girder and web plate is 300 millimetres halfway the mitre gate. The mortise and tenon joint in the mitre gate is avoided by continuation of the girder towards the lock chamber wall. The skin plate is mechanically jointed with dowels, the web plate and girder are connected with bolts. A visual representation of the design of the mitre gate for the eastern Sambeek navigation lock is shown in Figure 48.

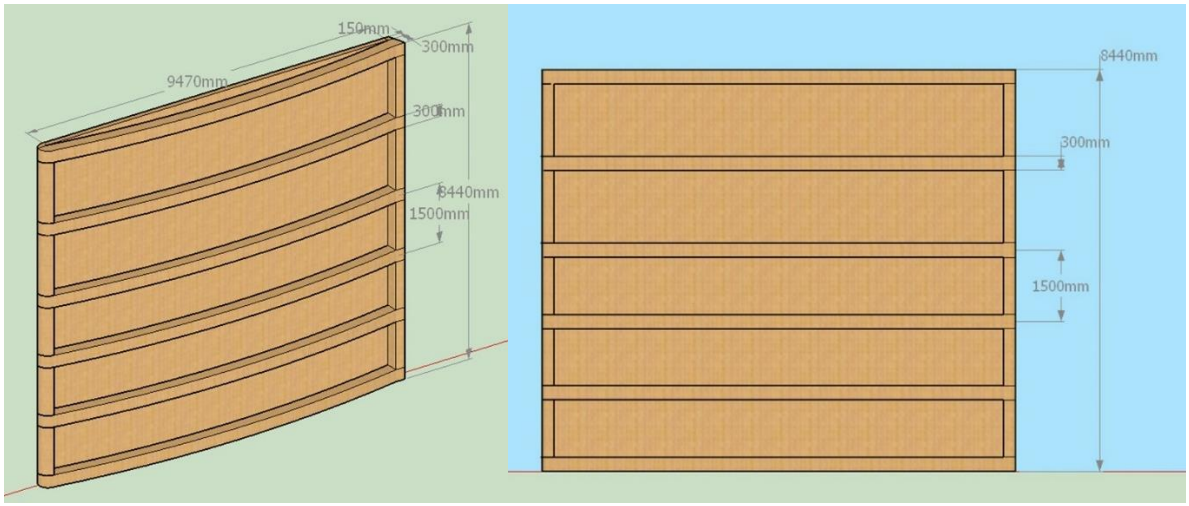

Figure 60: Overview of design (left) and front view design (right) of mitre gate Sambeek lock

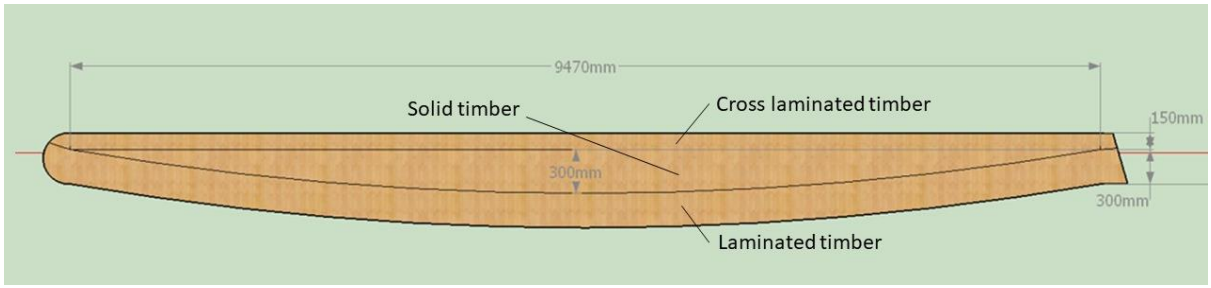

Figure 61: Top view design single mitre gate Sambeek lock

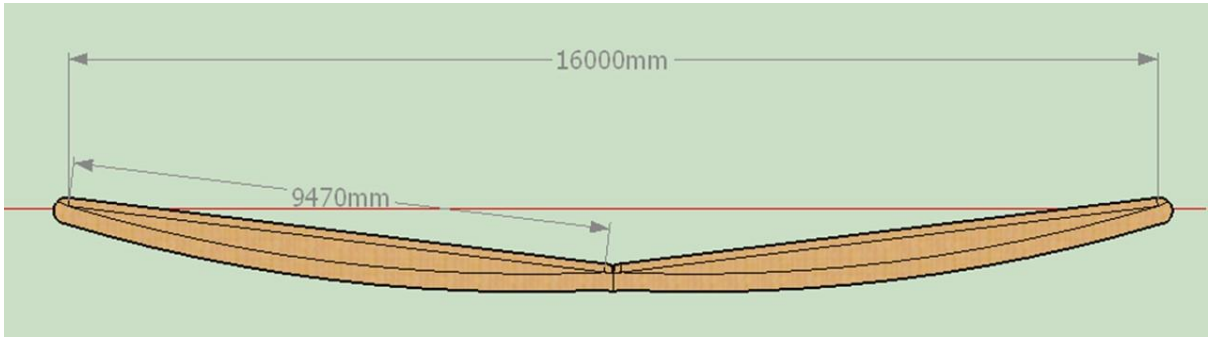

Figure 62: Top view double mitre gates Sambeek lock

7. Finite element modelling of a dowel laminated panel

Finite element modelling of dowel laminated timber is not done often and dowel cross laminated timber not often at all, hence some test models of a general dowel cross laminated panels made in SCIA Engineer are shown in this chapter. The layout and most important outcomes of the two dowel cross laminated test panels is given in Section 7.1. For the modelling of glued laminated timber orthotropic panels are common used (Wallner-Novak, Augustin, Koppelhuber, & Pock, 2018). Gluing however results in more homogeneous shear transfer than doweling where shear only is transferred by dowels. Therefore the panels of the test models are not modelled as one orthotropic plate but with beam elements connected with beam elements that simulate the dowels. The results of the test models are given in the second section of Chapter 7. Finally, the conclusions of the test models are given in Section 7.3.

For the readability of the following chapters a practical note is required. The cross sectional calculation in SCIA Engineer is done in the centre lines of the elements and thus the centre lines of the elements are shown in the program, while in the sketches and figures of the preliminary design, the outlines of the elements are shown.

7.1 Test models

To model the total mitre gate 2 test models are built to have insight in the behaviour of the dowel skin plate and to be able to evaluate the outcomes of the total mitre gate in SCIA Engineer.

The first model is the most simple model of a dowel cross laminated panel. The timber layers and dowels are modelled and automatically fully fixed by SCIA Engineer.

In the second model the interaction of the dowel with the panel layers is modelled based on the slip modulus of dowels from the NEN-EN 1995.

Model A	Dowel connection fixed by SCIA Engineer
Model B	Dowel connection based on the slip modulus of NEN-EN 1995

7.1.1 Test model basis

A model is a representation of a system. The best models are the models that represent the reality the best in the most clear way (Wee & Annema, 2014). Dowel laminated plates have not been modelled quite often so far. Therefore to model the dowelled skin plate as realistic as possible two test models are made and compared. The goal of these test models is to gain insight in the difference of the possible modelling of a dowel cross laminated panel.

The two models have the following characteristics in common. A test panel is made with supports on two sides hinged at x = 0, and a sliding support at x = 2. These supports are placed over the total y-direction of the mitre gate. The timber members in the models all have the same characteristics. The test panel is built up of 6 different timber layers. bottom to top orientated in: x-direction, y-direction, /-direction, \-direction, y-direction and x-direction. The numbering of these layers is from bottom to top, starting with layer 1 on z = 0 and layer 6 on z = 125 mm.

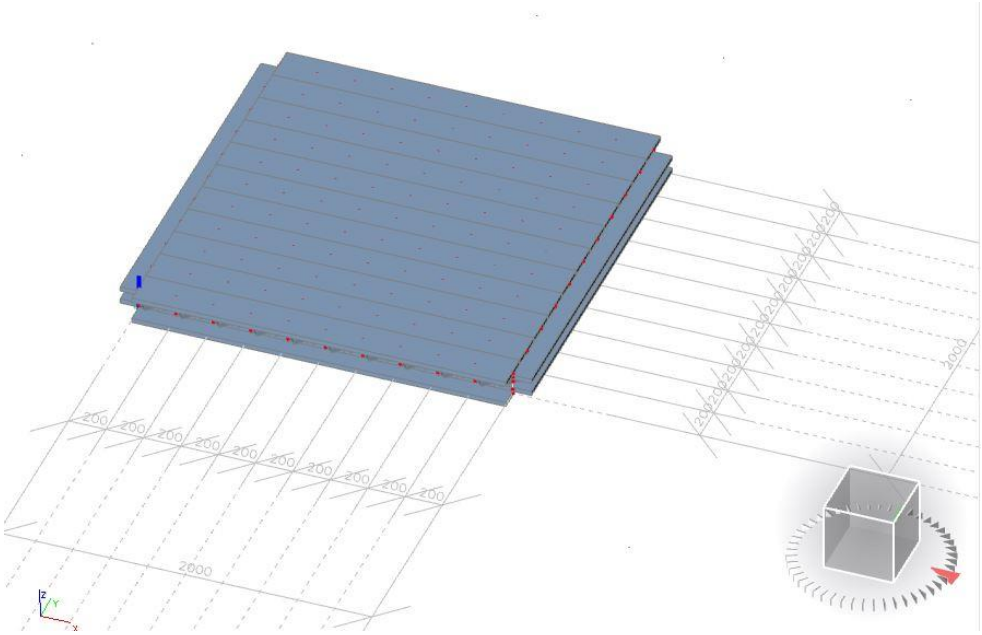

Figure 63: Layout of test model with dowel cross laminated panel

Each layer in x- and y-direction contains 11 lamellae next to each other. Each lamellae has a thickness of 25 millimetres and a width of 200 millimetres for the layers in x- and y-direction, the maximum centre to centre distance of the lamellae therefore is 2 metres. The diagonals have a width of 141 millimetres as is efficient for doweling earlier explained in Chapter 6.

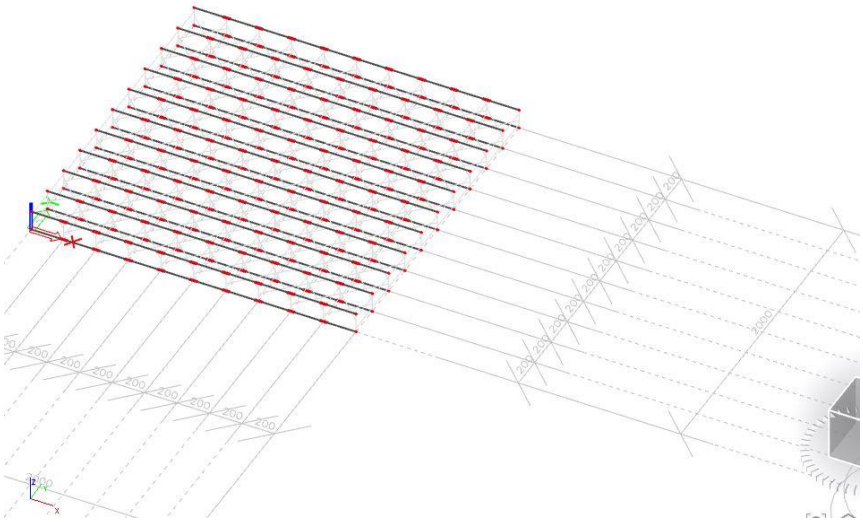

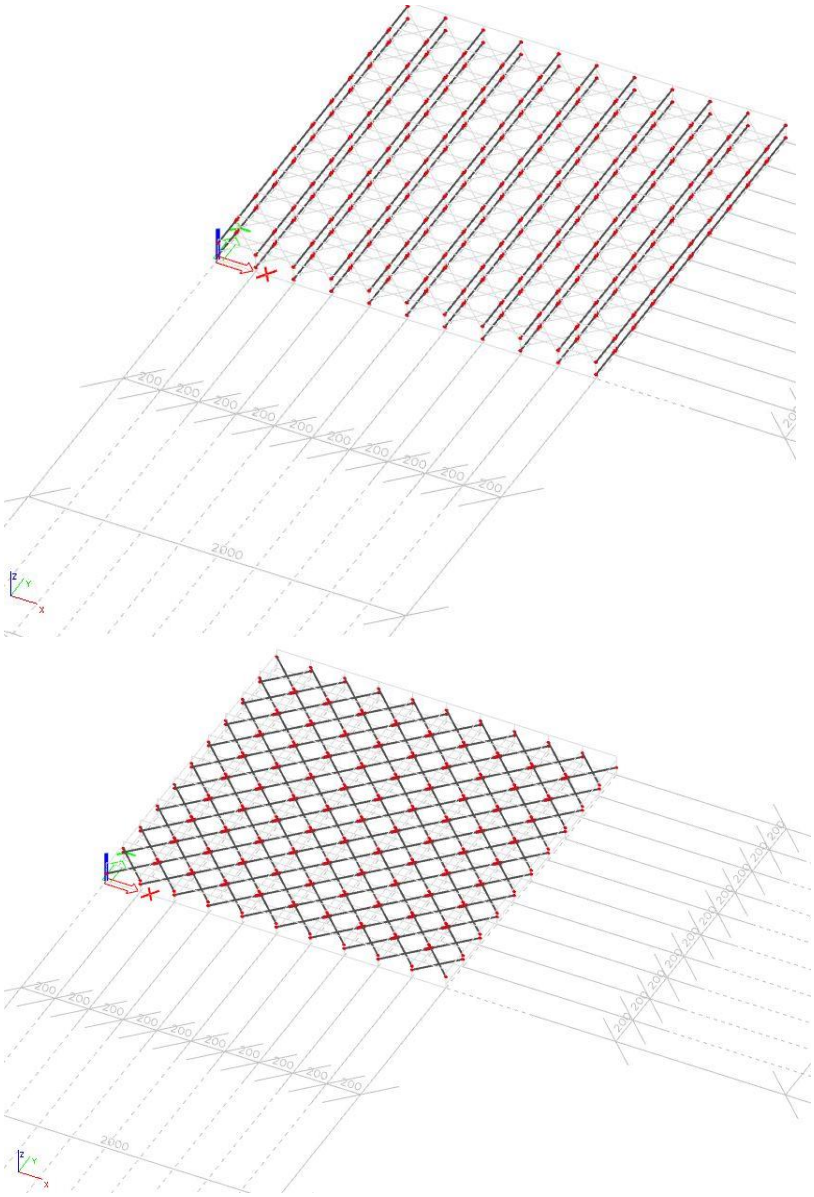

Figure 64: Input overview of layers of the test panel: x-orientated (first), y-orientated (second), diagonals (third)

The last similarity of both test models is that the dowels have a diameter of 30 millimetre and are placed with a centre to centre distance of 200 millimetres in both x- and y-direction. Modelling the dowels of the panel is done in different ways and these are prescribed later on in the thesis. Two different types of loading is used for the first models: the load on the structure is modelled with a distributed load of 50 kN/m over each lamellae in x-direction and an equivalent loading with point loads on the location of the dowels in the panel of 10 kN and point loads of 5 kN on the supports. The load is placed on the top layer of the panel, this is the sixth panel layer. See Figure 65 for the visual representation of the two different types of loading.

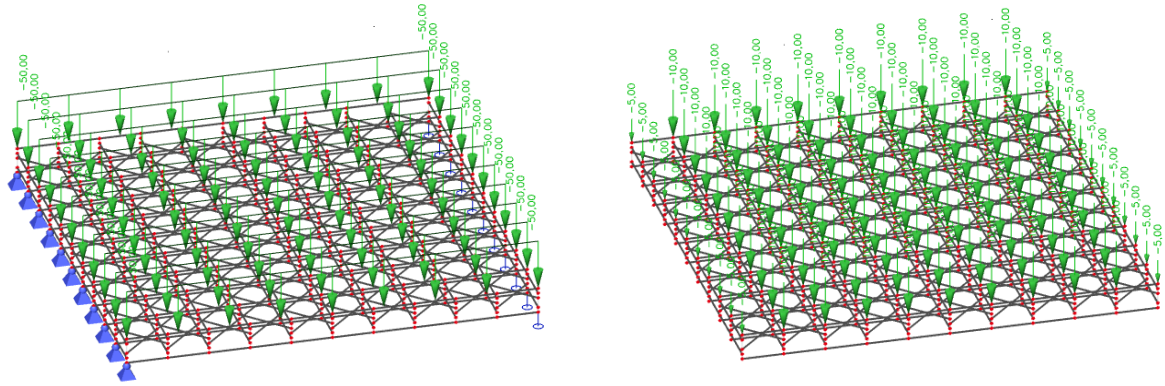

Figure 65: Loading of the panel: uniform distributed (left) and point loaded (right)

7.1.2 Model A: Fixed dowels connected as cross links

The first model contains dowels that are modelled as round steel pins. The dowels are fixed connected to the panel layers by cross links as it is named in SCIA Engineer. The steel circular dowels have a diameter of 30 millimetres and a common steel modulus of elasticity of 210.00 N/mm^2. The connection of the dowel with the panel layers is fixed everywhere and in every direction. In Figure 66 this is shown by the red characters. In this figure it can be seen that the end connection and intermediate connections in SCIA Engineer have different characters but the same stiffness. By fixing the connections of the lamellae with the dowel, the behaviour of the panel is comparable to a glued laminated timber panel.

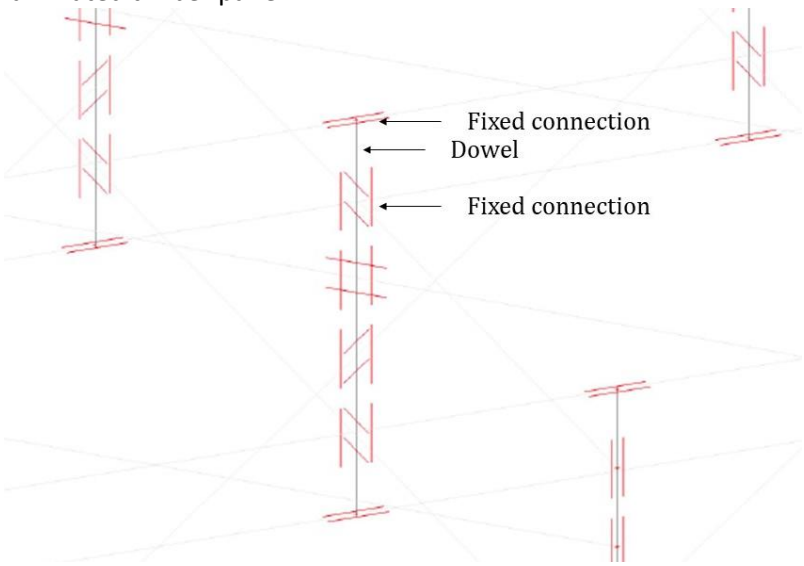

Figure 66: Dowel layout of model A, fixed connected dowel

Due to the fixed connections of the dowels with the panel layers the expectation is that the model is stiff. After calculation it turns out that the model is actually stiff, the maximum deflection of the panel is 23.6 millimetres halfway the span. The bending moment is as assumed mainly taken up by the layers in x-direction. The diagonals together take up 30% of the bending moment and the layers in y-direction barely contribute in bearing the bending moment. The shear force diagram of the x-orientated layer is an expected diagram with the shape of a 'forget-me-not' of a simply supported beam. The x-orientated layers bear most of the shear force and the diagonal and y-orientated bear 25% and 4% respectively. The dowels have high bending moments of 3 kNm and high shear forces of maximum 59 kN. The nodal displacement is in order of few millimetres, the maximum displacement of 2.6 is at the support, at x = 0 the top nodes and at x = 2 the bottom nodes.

Finally the first models shows that the different type of loading, uniform distributed load or point loads, have a minimal difference. It therefore can be concluded that the distance of the dowels is close enough to avoid unrealistic peaks in the results. Further on in this thesis the distributed load is used for modelling the differential head.

7.1.3 Model B: Divided dowels with translational spring at connection point of layers

In the second test model the connection of the dowel with the panel layers is modelled with the slip modulus K_{SLS} of NEN-EN 1995. This slip modulus is located at the connection point of two panel layers, i.e. halfway the centre lines of the skin layers. Therefore the dowel is split up in 10 parts, 5 dowel layers all with two parts. This is done to be able to model the slip spring at the location of the contact point of the timber panel layers. With this layout of the dowels, the dowels should be infinite stiff to avoid deformation of the dowel. In case of normal dowel stiffness, the dowel deform and the slip spring would not exactly be halfway the centre lines of the panel layers. Therefore the infinite modulus of elasticity is 21.000.000 N/mm^2. Furthermore the dowels remain circular with a diameter of 30 millimetres. The modelling and clarification is shown in Figure 67 and Figure 68.

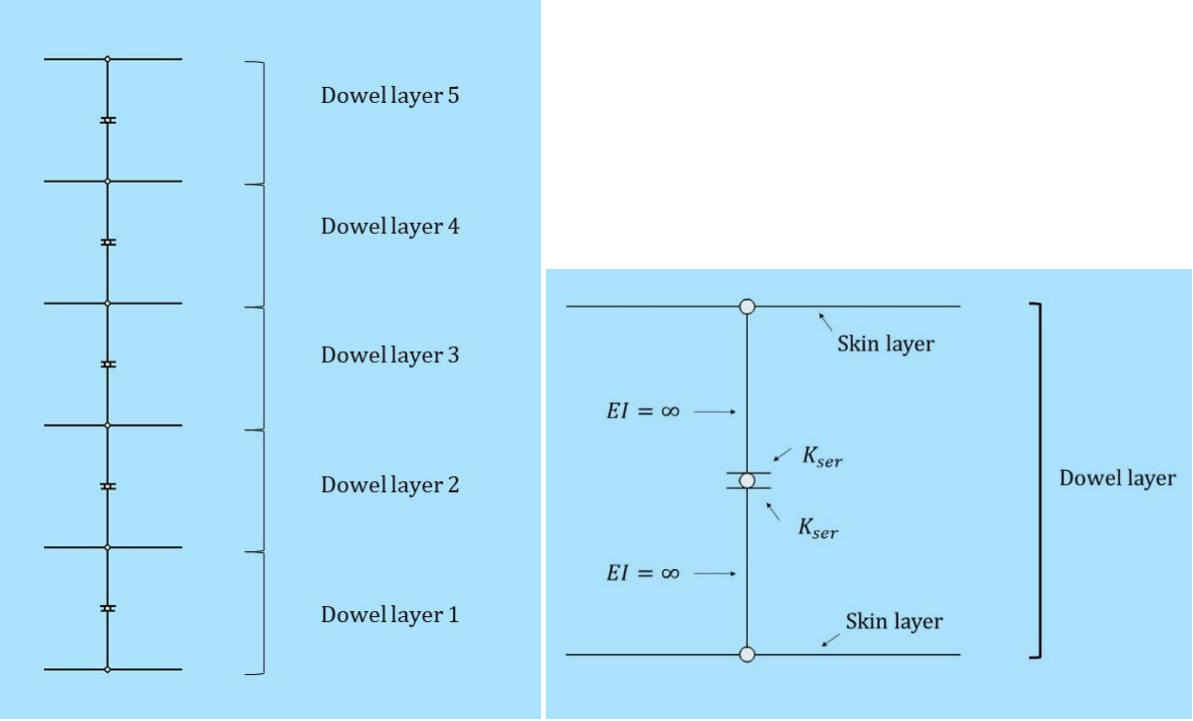

Figure 67: Visual explanation of dowel in model B

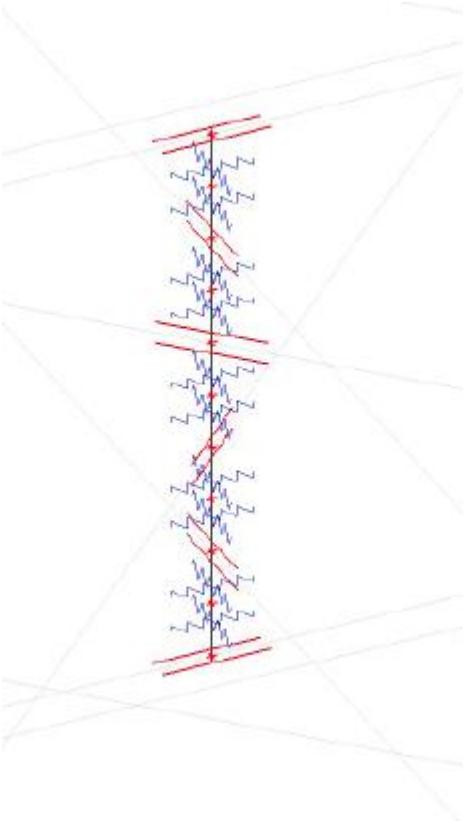

Figure 68: Dowel layout of model B in SCIA Engineer, Divided dowel with translational spring at connection point of layers

The outcomes of model B are:
Model B has a maximum deflection of 62 millimetres halfway the span. This is much more than model A, but expected because the connection of the dowels with the panel layers are modelled with springs. The x-orientated layers take up the most bending moments and have a maximum bending moment which is 20% higher than model A. Like in the first model, the y-orientated layers have a negligible share in the distribution of the bending moments, the moments only occur at the corners of the panel. Lastly, the diagonals distribute ±0.7 kNm, which is 30% less than the bending moment distributed in model A. The shear force of model B is mostly distributed by the x-orientated layers. The layers in y-direction again barely contribute in the distribution of the shear force and like in the bending moment diagram only occur in the corners of the panel. The shear force distribution of the diagonals is again around 30% decreased compared to the first model. The maximum bending moment in the dowels is ±2.9 kNm and linear distributed over the height of the dowel. The shear force of the dowel is maximum 51 kN and similar to previous models.

7.2 Results test models

In table 9 until Table 13 the numerical results of the test models are summarized. Table 14 shows the outcome per model and a comparison with the previous test model. The figures the test models are shown in Appendix H.
In the tables 9 until Table 13 the location of the maximum value is shown between brackets. The z-coordinate for the panel layers is clear as each layer has its own z-coordinate. Therefore, only the x- and y-coordinates are given behind the result between round brackets. For the dowels the z-coordinate is given as well between the round brackets. Figure 69 gives a visual clarification of the locations for the test model.

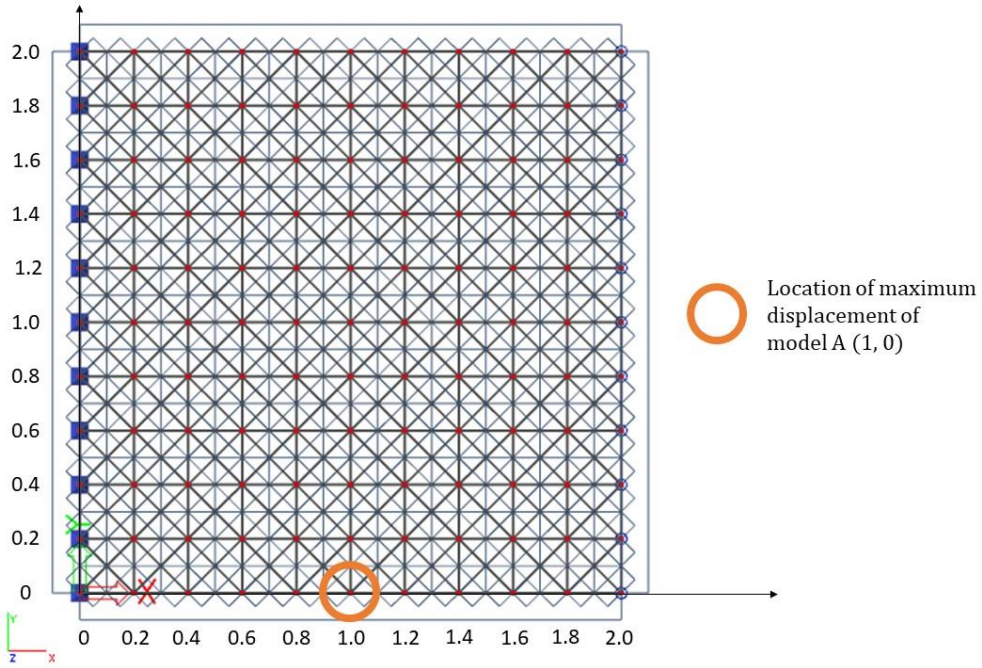

Figure 69: Top view test model with x,y-coordinate system with the maximum displacement of model A as an example

	Model A	Model B
Deflection [mm]	23.6 (1, 0)	62.1 (1, 0)
Rz [kN]	52.5 (2, 0.2)	52.6 (2, 0.2)

Table 9: Maximum deflection and support reaction of the test models

The x- and y-coordinates are given behind the result between round brackets.

	Model A	Model B
M_y layer 6 [kNm]	2.0 (0, 0) & -1.6 (0.2, 0)	2.4 (0, 0) & -1.9 (0.4, 0)
M_y layer 5 [kNm]	0.1 (1.4, 1.2) & - 0.1 (0.2, 1.8)	0.1 (0, 0) & -0.04 (0, 0.2)
M_y layer 4 [kNm]	1.0 (1.6, 1.8) & -1.0 (2, 1.8)	-0.7 (2, 1.8) & 0.7 (1.4, 2)
M_y layer 3 [kNm]	1.0 (1.8, 0) & -1.0 (2, 0.2)	-0.7 (0, 1.8) & 0.7 (1.6, 0)
M_y layer 2 [kNm]	0.1 (1.4, 1.2) & - 0.1 (0.2, 1.8)	0.1 (0, 0) & -0.04 (0, 0.2)
M_y layer 1 [kNm]	1.9 (2, 0) & -1.8 (1.8, 0)	2.2 (2, 0) & -1.7 (1.6, 0)

Table 10: Maximum bending moments in test models

	Model A	Model B
V_z layer 6 [kN]	-22.6 (0, 0) & 22.5 (2, 0)	-24.5 (0, 0) & 24.5 (2, 0)
V_z layer 5 [kN]	1.1 (1.8, 0)	0.7 (2, 2)
V_z layer 4 [kN]	6.8 (2, 1.8) & -6.8 (0.2, 0)	4.7 (2, 1.8) & -4.7 (0.2, 0)
V_z layer 3 [kN]	6.8 (0, 1.8) & -6.8 (1.8, 0)	4.7 (0, 1.8) & -4.7 (1.8, 0)

V_z layer 2 [kN]	-1.1 (1.6, 1.8)	-0.7 (0, 0)
V_z layer 1 [kN]	-17.7 (0, 0) & 18.2 (2, 0)	-19.5 (0, 0) & 19.5 (2, 0)

Table 11: Maximum shear force in the panel layers of test models

	Model A	Model B
N layer 6 [kN]	-195 (1, 0.6)	-180 (1, 1)
N layer 5 [kN]	4.5 (1, 0.6)	1 (1, 1)
N layer 4 [kN]	1.9 (0, 2)	-4 (1, 0.8)
N layer 3 [kN]	2.0 (1.8. 0)	4 (1 ,1)
N layer 2 [kN]	5.7 (2, 2)	-1 (1, 1)
N layer 1 [kN]	195 (1, 0.2)	180 (1, 1)

Table 12: Maximum normal force in the panel layers of test models

	Model A	Model B
M_y in dowel [kNm]	-3.0 (1.8, 0, 0) & 3.0 (0.2, 0, 0)	2.9 (0.4, 0, 0) & -2.9 (1.6, 0, 0)
V_z in dowels [kN]	-58.6 (0.2, 0, 0) & 59.6 (1.8, 0, 0)	-50.6 (0.4, 0) & 50.6 (1.6, 0)
Node displacement u_x [mm]	2.6 (0, y, 0.125) & (2, y, 0)	2.5 (0, 0.4, 0) & (2, 0.4, 0)

Table 13: Maximum bending moment, shear force and node displacement in the dowels of test models

*The local coordinate system of dowel layer 3 is rotated, so vector calculation is used to obtain the results in the global direction.

Model	Outcome
A	• Uniform distributed loading or point loading on dowels does not give significant different results. • High bending moments in connections of dowel with panel

B	• Stiff structure, deflection twice as big as the deflection of A.
	• X-orientated layers take up most of the loads, other layers are barely contributing. Dowels are more equally loaded over height
	• In comparison with B:
	  • Bending moment in x-orientated layers 40% higher.
	  • Other layers much less contribution in bending moment distribution.
	  • Shear force in upper x-layer 40% higher, lower layer similar.
	  • Shear force in y-orientated and diagonals much less, 20% and 50% less compared to the values C, respectively.
	  • Bending moment in dowels is high, similar to values of A, shear force almost equal over total height of the dowels.

Table 14: Outcomes of test models

7.3 Conclusions test models

General conclusions of the test models are:

- The deflection of the panel is highly dependent on the stiffness of the connection of the dowel with the panel layers.
- The support reactions of the models are similar to each other and almost equal to the expected support reaction of a simply supported beam loaded by an uniform load. The small difference in support reactions between the models is due to the different interactions of the lamellae of the panel with the dowels.

- The bending moment is mostly taken up by the x-orientated layers, with a maximum bending moment around 2 kNm. The bending moment distribution diagram contains jumps at the locations of the dowels, caused by the bending moments in the dowels. The shape of the bending moment distribution is similar to the structural mechanics moment formulas of a beam loaded by a distributed load.
- There is hardly any bending moment distribution in the y-orientated layers, if there is a bending moment it is at the location of the dowels, forced by the bending moment in the dowel.
- The shape of the bending moment diagram of the diagonal lamellae have a similar shape as the x-orientated layers, seen along the y-axis. In here too the jumps in the diagram come from the dowels. The maximum bending moment of the diagonals is less than the bending moments in the x-orientated layers for both model A and B.
- The shear force diagram in the x-orientated layers is similar to the expected diagrams of the structural mechanics diagrams of a simply supported beam, $V \approx \frac{1}{2} * q * l$. The small jumps in the diagram again are originated from the dowels. By loading only the top layer, the line is only linear at the top layer. The bottom x-layer is equal between the dowel because this layer is only connected at the location of the dowel. About 70 percent of the shear force is taken up by the x-orientated layers.
- The y-orientated layers contribute at the edges of the panel only, with maximum 5 percent of the total shear force distribution.
- The shape of the shear force diagram of the diagonals is similar to the x-orientated layers with maximum between, $V = \frac{1}{9} * q * l$ and $V = \frac{1}{23} * q * l$
- The normal force in the middle of the panel is higher than at the edges of the panel.
- The normal force in the layers 1,2 and 3 are opposite to normal force in layers 4, 5 and 6. The upper layers are in compression and the bottom layers are in tension.
- The normal force distribution diagrams are equal for both models.
- The bending moment diagram of the dowels is more or less linear from maximum at the top of the dowel to opposed maximum at the bottom of the dowel. The bending moments in the dowels are high in the models A & B, i.e. with stiff connections or stiff dowels. When using the less rigid connections or dowels the maximum bending moments decrease with 60 percent.
- The shear force in the dowels is zero halfway and increases towards the support. The maximum values is close to the support, but not exactly at the support. The shear force is maximum around the 50 kN and over the height of the dowel equal.
- The nodal displacement of both models is almost equal. The maximum nodal displacement is 2.5 millimetres.

Some final remarks of the results of the test panels are:

- Overall it looks like that the in y-direction are non-functional, however, these have been added in the preliminary design for the local design of the mitre gate. These layers therefore remain in the renewed design of the mitre gate.
- Lastly, it is expected that the order of diagonal placement could be important for preventing squaring because of an asymmetry in the cross section due to the diagonals. However, in the models it can be found that the deformation is in order of L/5000 and L/6700 for model A and B as Figure 70 shows. Therefore to avoid misunderstanding for the modelling of the redesign of the mitre gate the same order of diagonal placement is used as for the test models. This means that the third layer of the skin plate is \-orientated and the fourth layer of the skin plate is /-orientated, Chapter 8 explains the modelling of the mitre gate further.

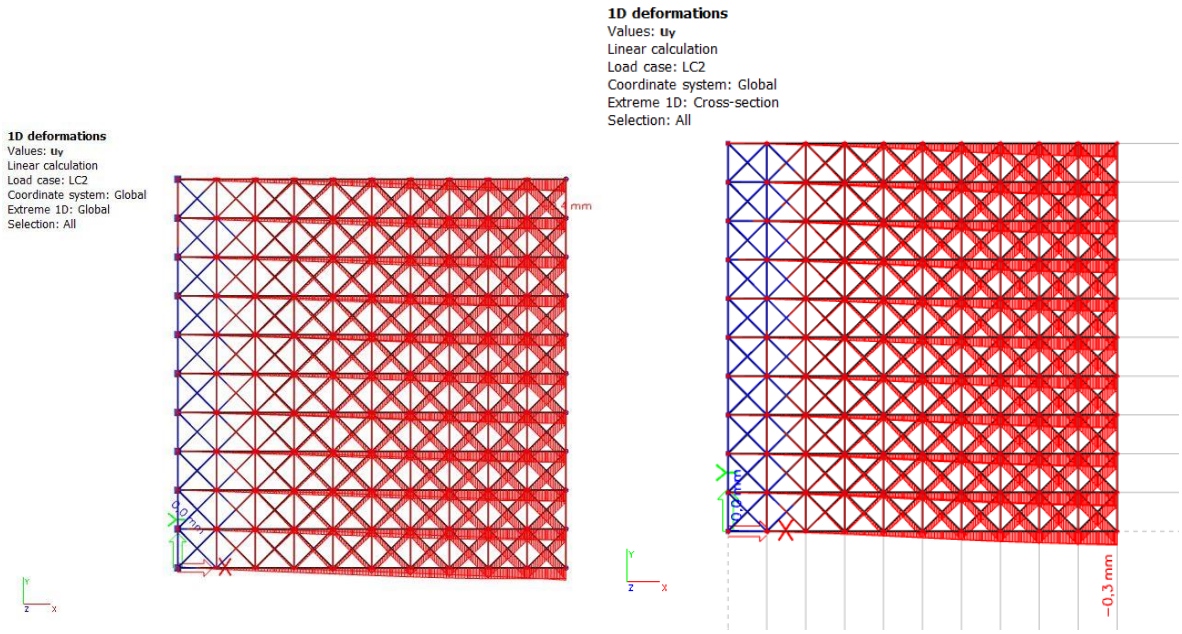

Figure 70: Deformation u_y, of model A (left), model B (right)

For the modelling of the renewed design model D is chosen to model the skin plate of the mitre gate. This model is chosen because the slip modulus of dowels is used in the preliminary design and therefore the second model is the most representative model to compare with the preliminary design. Also, the setup of the model is based on the slip modulus of the Eurocode and therefore model D is chosen.

8. Finite element modelling of the renewed mitre gate design

In this chapter, the design of the mitre gate for the case study location in Sambeek is modelled in SCIA Engineer and the results are compared to the preliminary design. The first section shows two situations, the closed situation and the opening or closing situation, for which the mitre gate is modelled. In Section 8.2 the outcomes of the closed mitre gate and the comparison of the cross sectional checks with the preliminary design are given. The results of the opening or closing mitre gate are shown in the third section of this chapter. This situation is made to test if the diagonal strut and tension bar can be replaced by the cross laminated timber skin plate. The conclusion of the modelling and answering the third sub question: *How can the design of the renewed optimized timber mitre gate be modelled in a finite element modelling program and what are the differences with the analytical design?* Is done in Section 8.4.

8.1 Modelling of final finite element model

For modelling the mitre gate, the dimensions of the case study location Sambeek are adjusted to practical dimensions. The lamellae of the skin plate are 200 millimetres wide and therefore the width of the gate is rounded off to 9.4 metres and the height of the mitre gate is rounded off to 8.4 metres. The centre to centre distance of the girders then becomes 1.4 metres, which results in 7 girders in total.

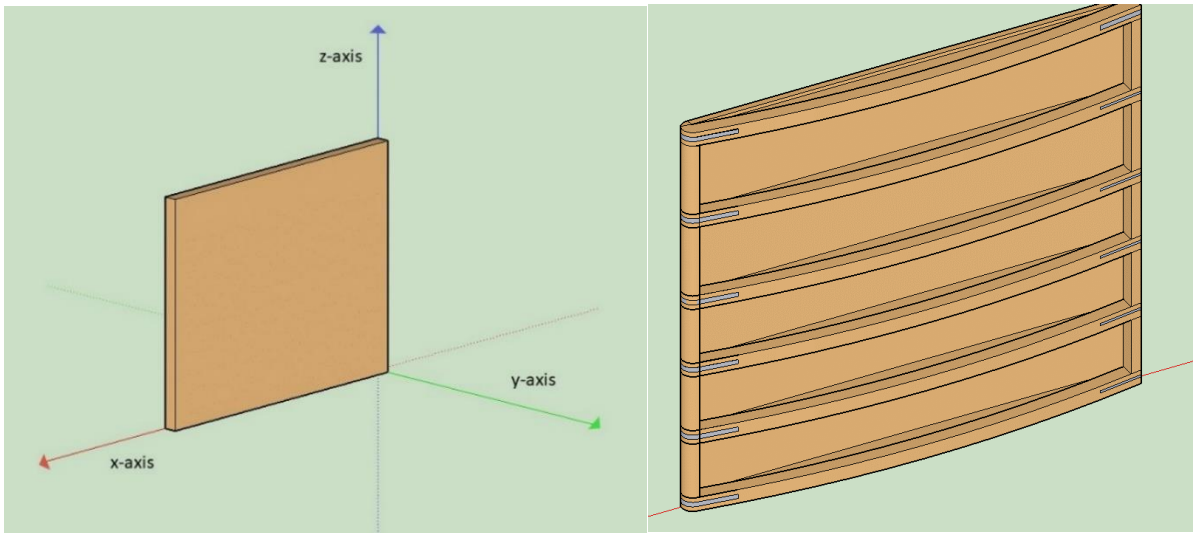

Figure 71: Mitre gate shown in global coordinate system

The **skin plate** is built up of 6 layers with the lamellae orientated in x-direction, y-direction, \-direction, /-direction, y-direction and x-direction starting from y=0 as can be seen in Figure 72. Each lamellae has a thickness of 25 millimetres and a width of 200 millimetres for the layers in x- and y-direction. The centre to centre distance of the x- and y-orientated layers is 200 millimetres over the total height and width, 8400 and 9400 millimetres respectively. The diagonals have a width and hence a centre to centre distance of 141 millimetres as is efficient for doweling earlier explained in Chapter 6.

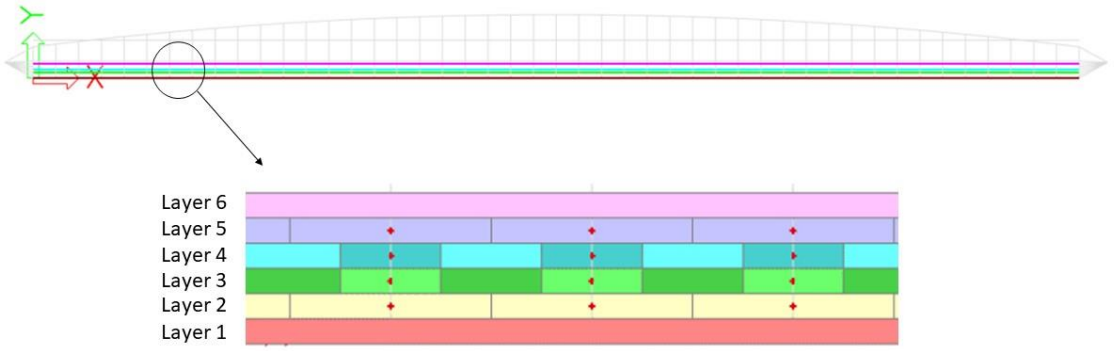

Figure 72: Top view of the skin plate of the final model in SCIA Engineer

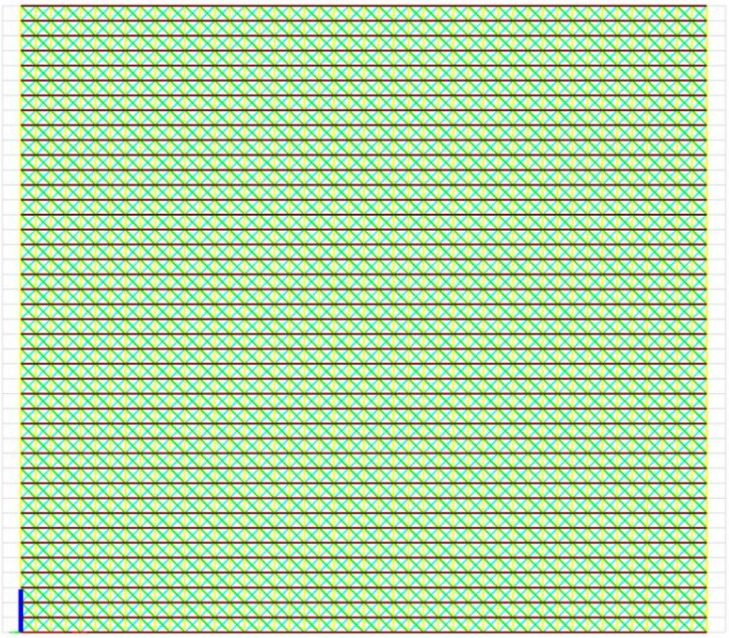

Figure 73: Front view of the skin plate of the final model in SCIA Engineer

The **dowels in the skin plate** are modelled as in the second test model of Section 7.1. So one dowel of the skin plate is cut off in five different layers, every dowel layer connecting two skin plate layers. Every dowel layer is represented by two infinite stiff members with end springs that contain the spring stiffness equal to the slip modulus of NEN-EN 1995. For the dowels in the skin plate this results in five dowels layers, every dowel layer having two dowels of 12.5 millimetres with springs halfway the dowel layer. Thus one dowel is represented by 10 infinite stiff steel members.

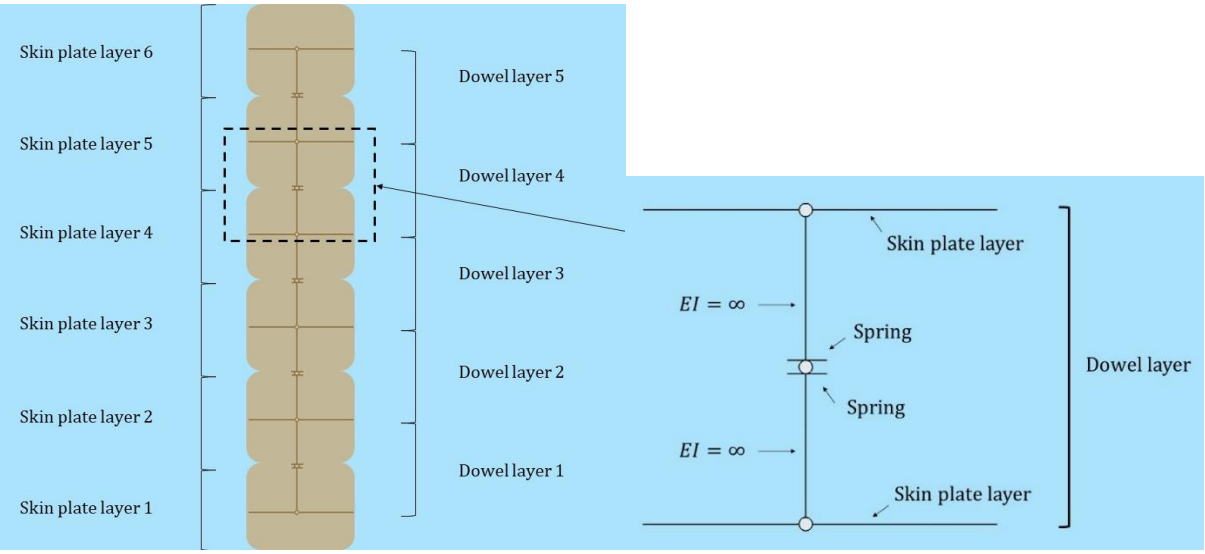

Figure 74: Visual explanation of dowel modelling of final model

The layout of the second test model is chosen for modelling the design of the total mitre gate because the slip modulus of dowels is also used in the preliminary design and therefore the second model is the most representative model to compare with the preliminary design. In NEN-EN 1995 is stated that the spring stiffness is different for both serviceability limit state and ultimate limit state. In SCIA Engineer it is not possible to link the different spring values to the calculations, only one spring stiffness can be allocated. As the preliminary design is contains more ultimate limit state checks, the spring stiffness of K_{ULS} is used. $K_{ULS} = \frac{2}{3} * K_{SLS} = \frac{2}{3} * \frac{30*800^{1.5}}{23} = 19676\ \mathrm{N/mm} = 19.676\ \mathrm{MN/m}$. The other connection point of the dowel, e.g. with the timber layer, is fully fixed. This is done to prevent rotation of the dowel between the skin plate layers, which would make the dowel like a pendulum. The dowel is infinite stiff to prevent deformation and maintain the distance of the skin plate layers.

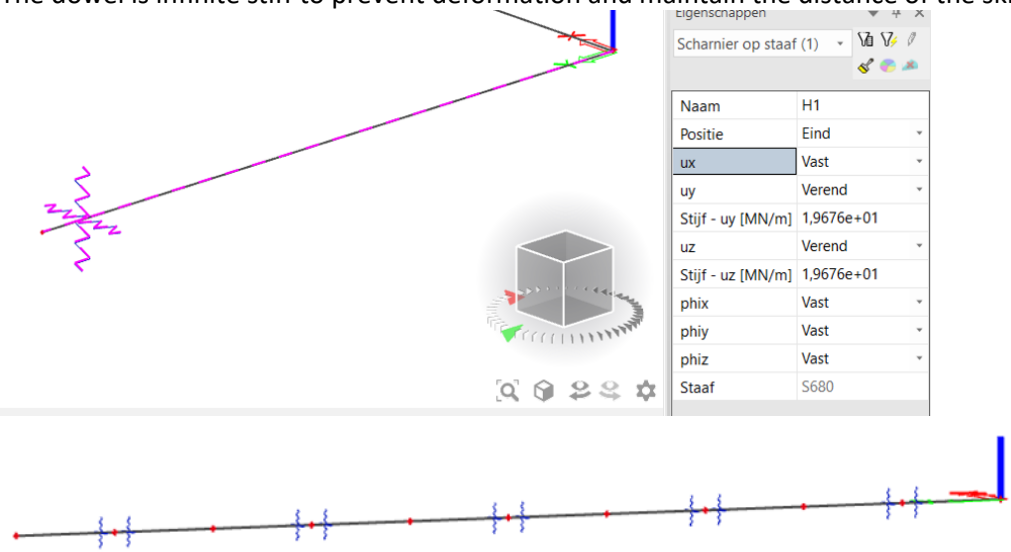

Figure 75: SCIA Engineer input of half dowel layer (top) and one total skin plate dowel, having 5 dowel layers (bottom)

For the bolts that connect the girder, web plate and skin plate the modelling is the same as for the dowels in the skin plate. The bolt is divided in 2 bolt layers and halfway the centre to centre distance of the timber elements a spring is modelled, with the slip modulus of the bolt. The slip modulus of bolts is the same as for the bolts in the skin plate, as NEN-EN 1995 prescribes.

The shape of the **web plate** is a semi-ellipse, seen from above. In SCIA Engineer this is not possible to model, so an approximation is required for the web plate. Modelling the web plate is approached by beams with an arbitrary profile, these beams have different cross sections at the beginning and at the end and increase linearly between the two cross sections. The total web plate is cut into 5 different arbitrary profiles mirrored halfway to approach the curve of the web plate. The representation of the web plate is shown in Figure 76.

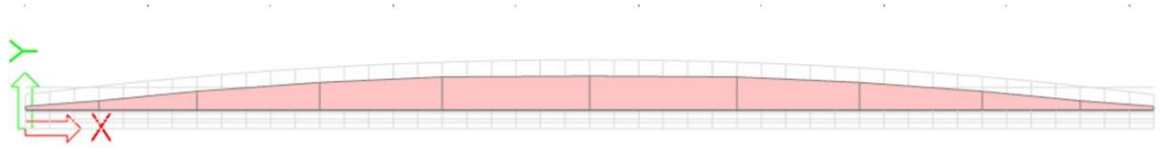

Figure 76: Top view of modelling web plate

For the dowelled three layered **girder** of the design an equivalent girder is modelled in SCIA Engineer. The equivalent girder is a fictitious homogeneous girder with the same bending stiffness as the dowelled girder. The mechanically jointed theory of NEN-EN 1995 is used for the computation of the equivalent girder. The gamma factor for three layered girder of the design is:

$$\gamma_1 = \gamma_3 = \frac{1}{1 + \frac{\pi^2 * E_i * A_i * s_i}{l_{ref}^2 * k}} = 0.882$$

The effective moment of inertia becomes:

$$I_{eff} = 3 * \frac{1}{12} * b * h^3 + 2 * \gamma * A * z^2 = 603 * 10^6 \text{ mm}^4$$

The equivalent girder has the same width of the girder of the design and therefore the height of the equivalent girder becomes:

$$I_{eff} = I_{eff,equivalent} = \frac{1}{12} * b * h_{equivalent}^3$$

$$h_{equivalent} = 289 \text{ mm}$$

Therefore the girder is modelled as an solid timber beam of 300 mm wide and a height of 289 mm. In SCIA Engineer curving of a continuous girder is possible by using catalogue blocks. This cuts the curved beam into parts that are slightly rotated to each other to obtain the curved shape. The length of the beam parts is equal to the spacing of the bolts, which is 200 millimetres.

Figure 77: Top view modelling girder in SCIA Engineer

The **posts** of the mitre gate are modelled as homogeneous timber beams, of 500 millimetres squared. The main function of the posts in the new design is to provide vertical stability to the mitre gate and to function as the turning point of the mitre gate. The placement of the centre line of the posts in the model is at the location of the horizontal supports. In the next sections the placement of the post is described in more detail.
For the description of the boundary conditions and the results of the modelling of the mitre gate, a clarification of the terminology is given in the figure below.

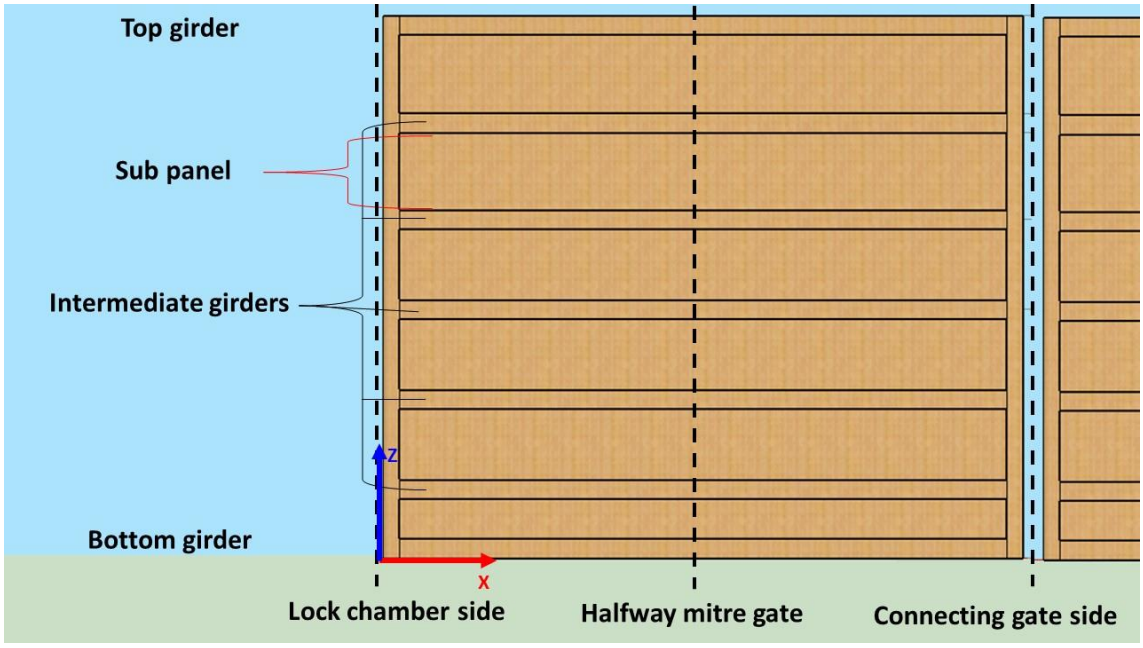

Figure 78: Clarification of the terminology of the mitre gate

8.1.1 Closed mitre gate

Boundary conditions:
The mitre gate is modelled into two different situations. The first situation is when the mitre gate is closed, the results of this situation are compared to the preliminary design. The second situation is when the mitre gate is closing or opening, this situation is made to see if the expectation that the cross laminated skin plate could be an useful solution to replace the diagonal strut and tension bar in the now common design of the mitre gate. The modelling of the supports is:
1: For the closed gate it is important that the eccentricity of the normal force is modelled in the right way. To have the same eccentricity as in the preliminary design the supports in x-direction, i.e. the direction of the width of the mitre gate, are placed at y = 137.5 mm. This is the location of the top of the sixth skin plate layer and bottom of the web plate. At the lock chamber side these supports are placed along the total height of the end post. The supports in y-direction at the lock chamber side are connected to the first layer of the skin plate. Likewise these supports are along the total height of the skin plate.

At the connecting gate side, the support is perpendicular to the sailing direction as can be seen in Figure 80. In the coordinate system in SCIA Engineer this is modelled as a support placed at the post in x-direction under an angle of 18 degrees with the mitre gate, see Figure 79 and Figure 82. This angle is obtained from the 1:3 gradient of the mitre gates leaning towards each other. The total supporting system of the closed mitre gate is shown in Figure 79. Like in the preliminary design the sill has no contribution in the transfer of forces in the model due to the unpredicted behaviour.

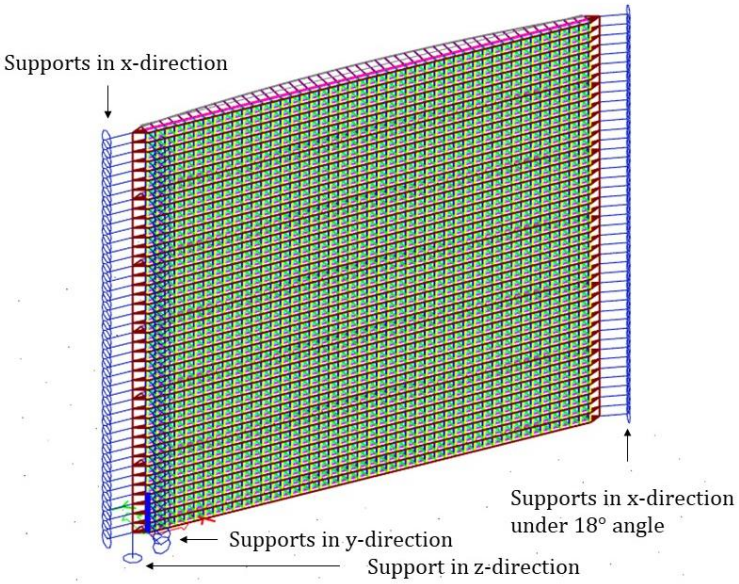

Figure 79: Supporting system closed mitre gate

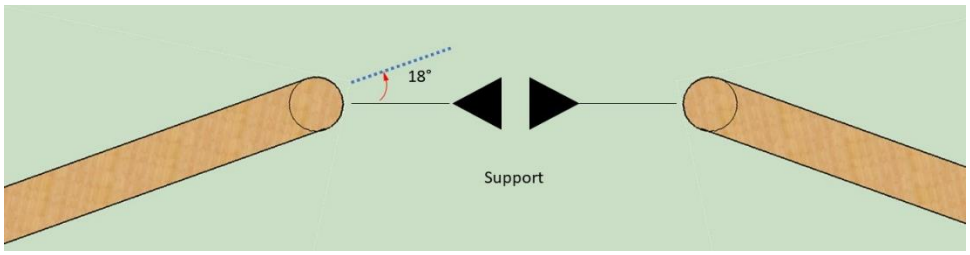

Figure 80: Visual explanation of support at connecting gate side

In Figure 81 and Figure 82 the top view of the lock chamber side and the connecting gate side is shown.

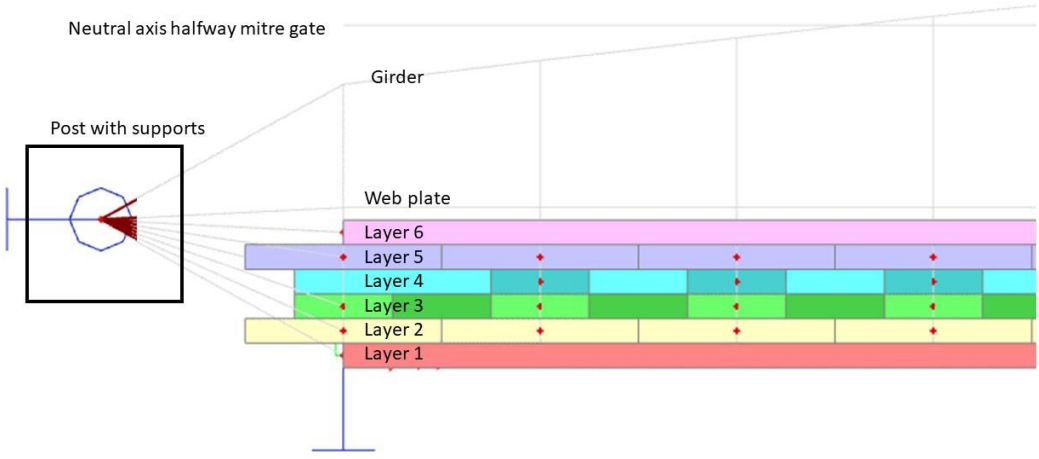

Figure 81: Top view of modelling support at lock chamber side

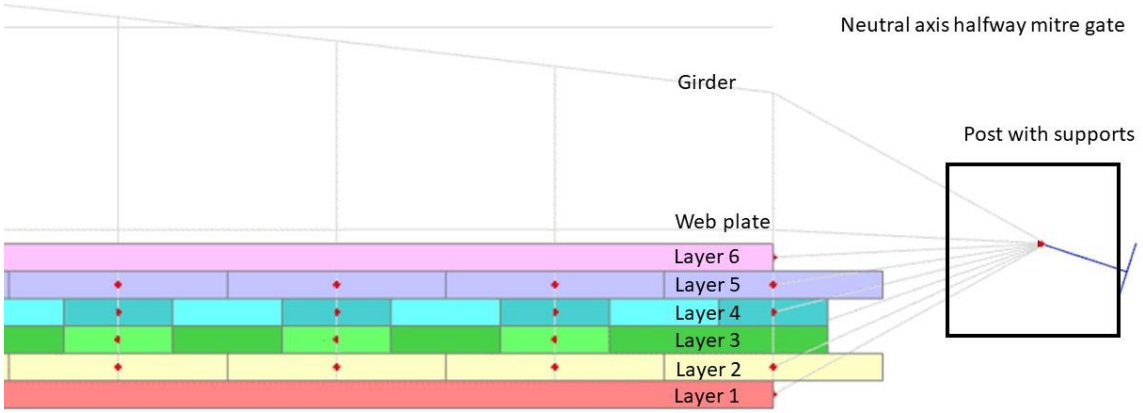

Figure 82: Top view modelling connecting gate side

Load case

For the first model, the closed mitre gate, the maximum differential head is the only load present. This is represented as line loads over the width of each lamellae. The line load in this model is in negative y-direction and is placed on the sixth layer of the skin plate. From the preliminary design it is clear that the design value of the load is defined as 61.8 kN/m^2. The load of the model is placed on 200 millimetre wide lamellae. Therefore the line load on every lamellae of the sixth layer is 12.36 kN/m. This load from the preliminary design is already multiplied with a load factor and therefore the load factor in SCIA Engineer is set up at 1. The input of the design load value instead is done on purpose because it reduces calculation time.

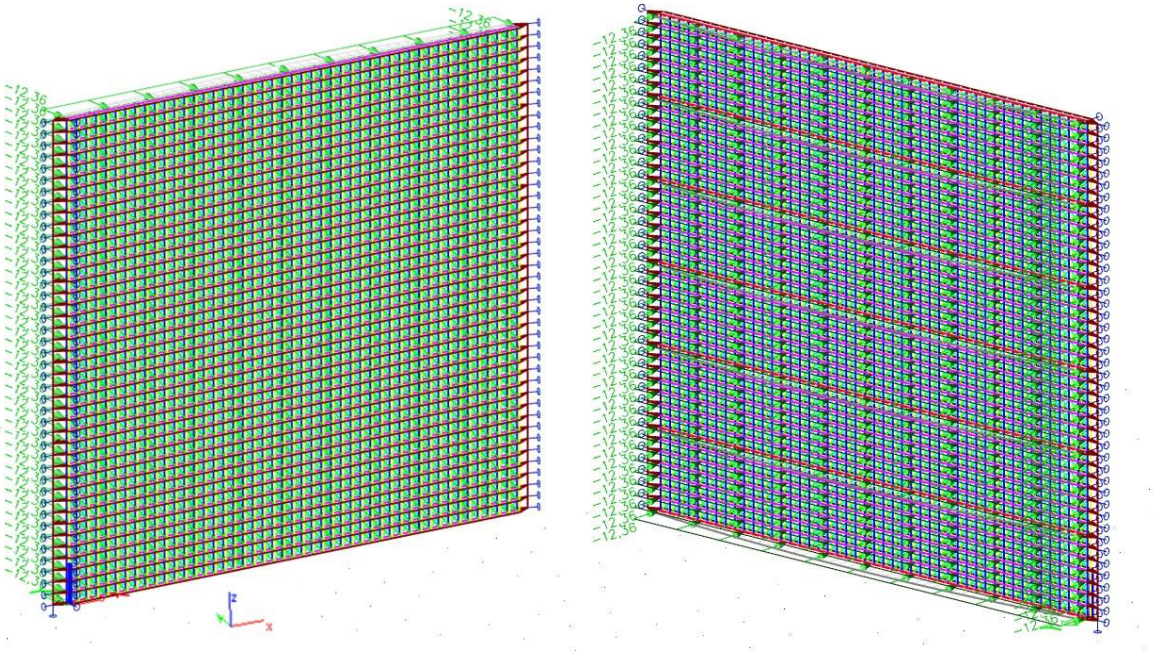

Figure 83: Modelling of load on closed mitre gate seen from low water side (left) and seen from high water side (right)

8.1.2 Opening or closing mitre gate

The second situation modelled in SCIA Engineer is during opening or closing of the mitre gate, in this situation the water level is equal at both sides. A mitre gate is only set in motion if the water levels are equal, but as described in Chapter 3 during motion multiple loads on a mitre gate are present. However, as for the preliminary design of the closed situation simplifications for the opening situation

are required. The only load that is taken into account is the self-weight of the structure. The timber elements and dowels of the second model are modelled in the same way as the first modelled situation with the maximum differential head, the only difference between these models are the loads and the supporting system. As the mitre gate is specified with clearance at the hinge, the supporting system of a mitre gate in opening or closing position is at the top and bottom hinge at the lock chamber side of the mitre gate. The bottom hinge is rigid in x-, y- and z-direction while the top hinge is rigid in x- and y-direction as can be seen in the figure below.

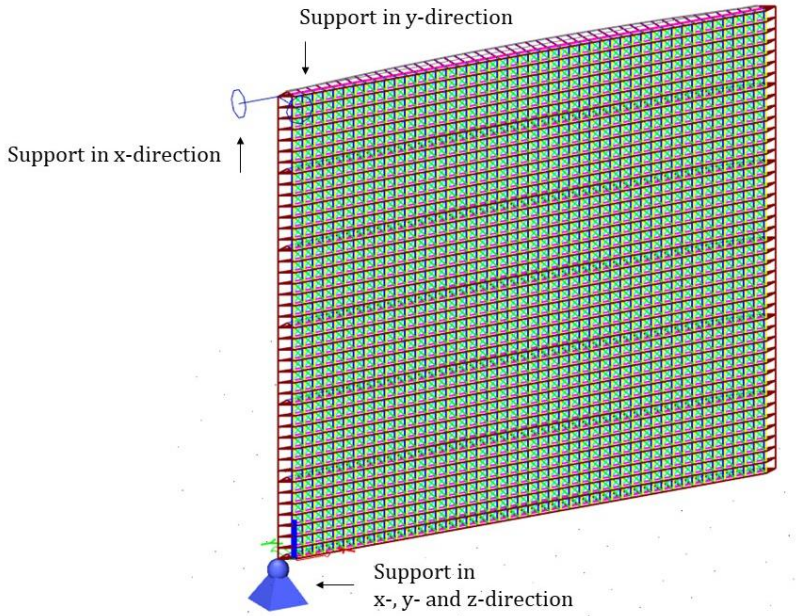

Figure 84: Modelling of supports for opening or closing mitre gate

The second model does not contain any extra inserted load. The self-weight of the mitre gate is the only load present in the model, this load is automatically executed by SCIA Engineer. During opening and closing of the mitre gate, water is present in the navigation lock, which ensures an uplift pressure due to the Archimedes' principle. However, this uplift pressure is not added in the model, because the actual weight of the mitre gate is higher as extra elements are added to the mitre gate in reality, for example to prevent for collision and to enable levelling. Because these elements of the mitre gate are not included in the design, the uplift pressure is not added in the second model.

8.2 Results closed mitre gate model & comparison with preliminary design

The results of the model of the closed mitre gate are given in this section. The cross sectional check is the only displayed result from the SCIA Engineer model, because to model the gate in SCIA Engineer, beams are split up and simplifications are made, for this reason the buckling checks for example are not reliable. Furthermore this section contains a comparison of the model and the preliminary design

8.2.1 Reaction forces and displacement of the mitre gate

The sum of the reaction forces in the model is consistent with the inserted load of the differential head. The resulting reaction forces in the SCIA Engineer model are shown in Figure 85, these are equal to the inserted load on the structure: $n_x * b_x * q = 43 * 9.2 * 12.6 = 4889.6$ kN.
Where:
n_x [-] = number of x-orientated lamellae
b_x [m] = width of x-orientated lamellae
q [kN/m] = distributed load on a single lamellae

Resultante

Lineaire berekening, Extreem : Globaal
Selectie : Alle
Belastingsgevallen : BG2

Belasting	Rx [kN]	Ry [kN]	Rz [kN]
BG2	0,0	4889,6	0,0

Figure 85: Sum of the reaction forces of SCIA Engineer model

The results of the reaction forces and displacements are summarized in the table below. The results are obtained from the output shown in Appendix J.

	Maximum value	Location
Ry top/bottom girder	267 kN	Connecting gate side
Ry intermediate girder	529 kN	Connecting gate side
Ry sub panel	-22 kN	Connecting gate side
Rx top/bottom girder	847 kNm	Lock chamber side
Rx intermediate girders	1628 kN	Lock chamber side & connecting gate side
Rx skin plate	72 kN	Lock chamber side
Uy sub panel	64 mm	Halfway mitre gate
Uy intermediate girders	59 mm	Halfway gate width
Uy top/bottom girders	-7 mm	Connecting gate side
Uy sub panel	-6 mm	Connecting gate side

Table 15: Support reactions and displacement from maximum differential head

The load distribution in both x- and y-direction is mainly done at the height of the girders. At the vertical, y-direction, and horizontal, x-direction, supports the reaction forces at the top and bottom side are approximately twice as small as the other reactions forces of the gate. The reason for this is that the top and bottom girder are half a slice and thus the skin plate has a height of only 750 millimetres, see the figure below.

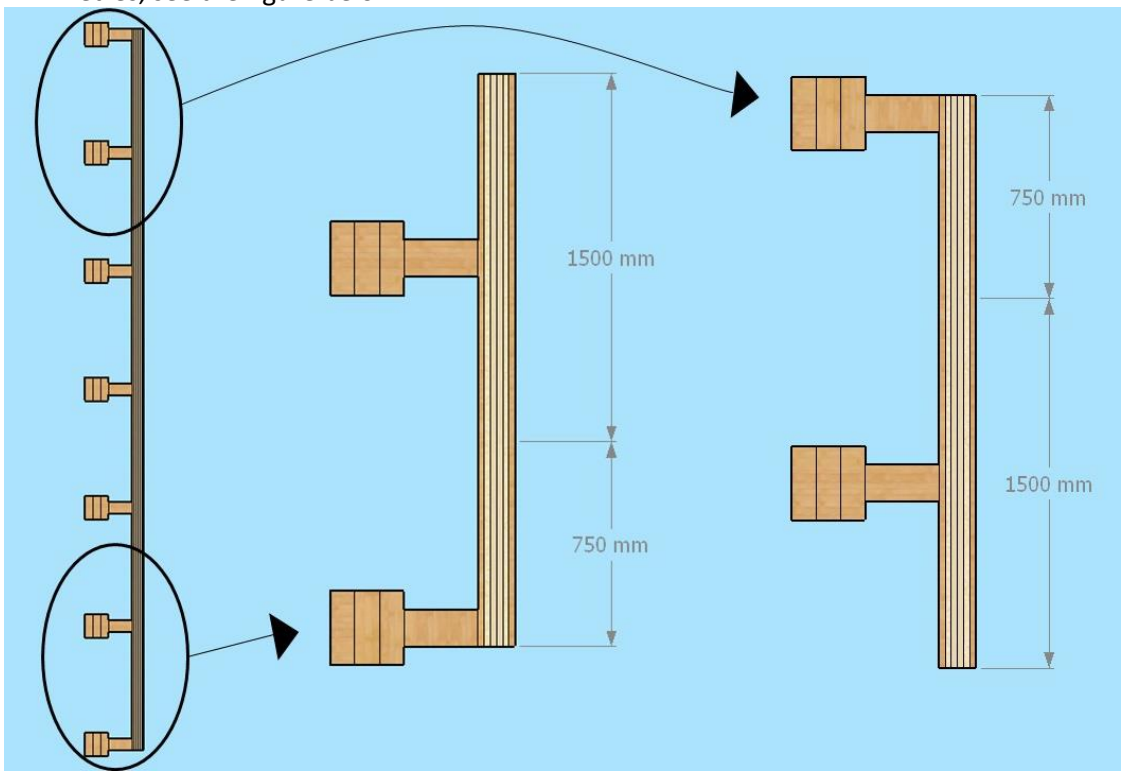

Figure 86: Side view mitre gate with zoom in of top (middle) and bottom girder (right)

In x-direction, the reaction force at the location of the girders are compression forces. The support reactions at the sub panels are tension forces of 60 to 70 kN and therefore increase the reaction force

at the girder. Almost all the horizontal load is transferred by the girders. Therefore the assumption that the load distribution is done over the total height of the mitre gate, is invalid for the design of the mitre gate. This however, does not lead to failure, because the girder is directly supporting on the lock chamber and loaded in the fibre direction as explained in Section 6.1.

The support reactions in x-direction are almost equal at both sides, in y-direction the reaction forces differ. In y-direction, the supports at the sub panels at the lock chamber side have negligible transfer, while the reaction force at the same height at the connecting mitre gate side is 4 to 5 times bigger. This reaction force however, is in negative direction and therefore increases the reaction force at the girders. The reason for this is that the placement of the support at the connection with the other mitre gate is schematized under an angle of 18 degrees. To have force equilibrium at the support this results in higher reaction forces in y-direction. This is shown Figure 87.

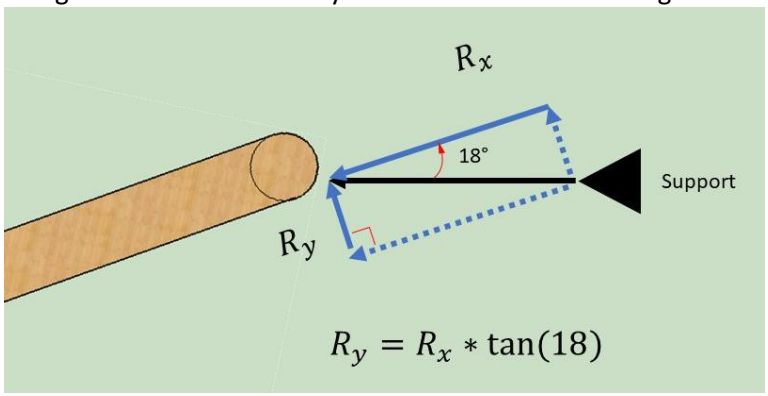

Figure 87: Derivation Ry SCIA Engineer model connecting mitre gate side

The values of the reaction forces in x-direction at the intermediate girders are on average 1625 kN. The global reaction force of the repeating slice in the preliminary design is 1267 kN. This is consistent with the model as the negative reaction forces of the sub panel decrease the global support: $1625 - 6 * 65 = 1235$ kN. The reaction forces in y-direction at the lock chamber side on the girders are on average 397 kN, adding the reaction force at the sub panel, 5 kN. $397 + 6 * 5 = 427$ kN. This is consistent with the reaction force at the support of the preliminary design, 439 kN. To summarise, the reaction forces of the model and the preliminary design are consistent.

The maximum displacement of the mitre gate in the model with a uniform distributed load is halfway the width of the mitre gate. Over the height of the gate, the displacement is maximum halfway the sub panel, due to the increased stiffness of the girders slightly lower at the height of the girders. The maximum displacement at the sub panels is 64 mm, in the direction of the load, negative y-direction. The maximum displacement of the gate at the height of the girder is 57 mm.
The displacement of the preliminary design is almost equal with maximum final deflection of 60 millimetres, L/150. However, these displacements are not reliable as the cross section of the preliminary design is taken as constant over the total width of the door, which is not the case as the girder and web plate differentiate along the width of the mitre gate. Furthermore in the SCIA Engineer model the value of the slip modulus at the dowels are modelled with ultimate limit state values, while displacements are serviceability limit state.
A remarkable displacement is at the connecting mitre gate side, the displacement is opposed of the load direction. This displacement is maximum 6.9 mm at the top of the mitre gate and this displacement is a likely result of the opposite support reaction Ry between the girders. In reality this displacement is not observed.

8.2.2 Internal forces in the mitre gate model

The results of the girders obtained from the SCIA Engineer model are summarized in the table below. The results are obtained from the output shown in J.

	Maximum value	Location
N top/bottom girder	-1102 kN	Halfway gate width
N intermediate girders	-1824 kN	Halfway gate width
My top/bottom girder	-123 kNm	lock chamber side
My top/bottom girder	57 kNm	Halfway gate width
My top/bottom girder	-84 kNm	mitre gate connection side
My intermediate girders	-222 kNm	lock chamber side
My intermediate girders	-88 kNm	Halfway gate width
My intermediate girders	-157 kNm	mitre gate connection side

Table 16: Internal forces in the girders from maximum differential head in SCIA Engineer

The normal force in the girders is almost constant over the width of the mitre gate. Like the support reactions, the normal force in the top and bottom girders are lower as these skin plate has half the width compared to skin plate at the intermediate girders. The bending moment distribution of the girder has a parabola shape of a uniform distributed load with an eccentric loaded normal force. The bending moment at the sides of the mitre gate is the eccentricity multiplied with the support reaction. The bending moment distribution is not symmetrical because the support reactions at the connecting mitre gate side are bigger than the lock chamber side. Furthermore in the bending moment distribution some small jump are observed at the location of the dowels, these are caused by the bending moments in the dowels.

The dimensioning of the girder is based on the maximum bending moment and the normal force in the middle span of the gate. In the preliminary design the representative normal force in the girder is:

$$N_{girder,calc} = \frac{N}{A_{eff,cross\ section}} * A_{eff,girder} = \frac{-1267}{2.1 * 10^5} * (300 * 289) = -523\ \text{kN}$$

While in the SCIA model a normal force of -1824 kN is obtained. The bending moment My of the preliminary design with the eccentric normal force taken into account is 787 kNm, while the bending moment of the model is only 88 kNm. These differences in internal forces result in a stress difference of around 3 and 2 for the normal stress and bending stress, respectively. The relatively small difference of bending stress compared to the difference in bending moments is due to the computation of the bending stiffness. In the preliminary design the theory of mechanically jointed beams is used and in SCIA this calculation is not applicable. The comparison of the maxima are shown in the table below.

	Preliminary design	SCIA model
N	-523 kN	-1824 kN
My	787 kNm	88 kNm
$\boldsymbol{\sigma_{c,girder}}$	6 MPa	21 MPa
$\boldsymbol{\sigma_{m,girder}}$	12.1 MPa	21.1 MPa

Table 17: Comparison of preliminary design and SCIA model results in the intermediate girder

Because the stresses in the SCIA model and preliminary design do not match, the unity checks of the preliminary design and the model in SCIA are not comparable. The governing check of the model with combined bending and axial compression, $\left(\frac{\sigma_{c,0,d}}{f_{c,0,d}}\right)^2 + k_m \frac{\sigma_{m,y,d}}{f_{m,y,d}} + \frac{\sigma_{m,z,d}}{f_{m,z,d}} \leq 1$, is 0.6 for the preliminary design and 1.73 in the SCIA model. As can be seen in Appendix J, with the outcomes of the SCIA model the girders do not meet the requirements of NEN-EN 1995.

The maximum internal forces in the skin plate layers are given in the table below.

Skin plate layer	Maximum tension (kN)	Maximum compression (kN)
1	62	N/A
2	11	-8
3	13	N/A
4	14	N/A

5	N/A	-19
6	68	-50

Table 18: Maximum normal forces in the skin plate layers

The maximum internal forces in the lamellae of the skin plate layers are higher than the internal forces of the preliminary design:

$$N_{skin\ plate,calc} = \frac{N}{A_{eff,cross\ section}} * A_{skin\ plate} = \frac{-1267}{2.1 * 10^5} * (200 * 25) = -30\ \text{kN}$$

Thus, the maximum unity checks for the skin plate layers are higher than the 0.6 aimed for in the preliminary design. The most critical location for every skin plate layer is at the height of the girder. The normal force and bending moments at the sub panels are low, therefore the unity checks in the skin plate are low at the height of the sub panels. The only location in the mitre gate that does not fulfil are the lamellae at the lock chamber and connecting mitre gate sides of the loaded sixth layer. The reason for this is that the bending moment at these sides are high and leads to an unity check above 1. However, for the design of the structure this is no problem as these lamellae are included in the joint design with metal straps as is explained in Section Joint post, girder and skin plate.

The maximum internal force in the web plate is shown in Table 19.

	Maximum value	**Location**
N top/bottom web plate	-46 kN	At 1/8th of gate width
N intermediate web plate	-115 kN	At 1/4th of gate width

Table 19: Maximum internal forces in web plate

In the preliminary design the maximum normal force in the web plate is more than doubled.

$$N_{web\ plate,calc} = \frac{N}{A_{eff,cross\ section}} * A_{web\ plate} = \frac{-1267}{2.1 * 10^5} * (300 * 150) = -272\ \text{kN}$$

Because the internal force in the web plate of the SCIA model are half the internal force of the preliminary design the unity checks for the web plate meet the requirements of NEN-EN1995. Only directly at the sides of the mitre gate this is not met, because the mesh of the web plate is very small and so the resistance is low. However, like with the skin plate, this is no problem as these sides are connected with metal straps as is explained in Chapter 6.

8.3 Results opening or closing mitre gate model

The extensive outcomes of the opening or closing mitre gate are shown in Appendix J. In this section, the outcomes are summarized and discussed. The total force due to the self-weight in SCIA Engineer, Fz is 1017.4 kN. The derivation of the self-weight is: $Fz = W * g = 103{,}710 * 9.81 = 1017{,}400\ \text{N} = 1017.4\ \text{kN}$. The self-weight of the mitre gate per construction material is shown in Figure 88.

Materiaallijst

Selectie: Alle
Sorteertype: Materiaal

Samenvatting

Materiaal	Massa [kg]	Oppervlak [mm²]	Volume [m³]
Staal	81236,7	168742936,1	1,0349e+01
Hout	22473,6	1227925065,5	2,3410e+01
Totaal	103710,3	1396668001,6	3,3759e+01

Opmerking: De waarde 'Oppervlak' vertegenwoordigt voor 1D-elementen de totale blootgestelde oppervlakte, en voor 2D-elementen correspondeert deze alleen met de oppervlakte van het vlak met het zwaartepunt.

Figure 88: Self-weight of the mitre gate design in SCIA Engineer

The horizontal reaction forces in SCIA Engineer are checked. From the overview of forces in Figure 89, it can be seen that the vertical forces introduce a couple that should be in equilibrium with the counterworking couple of the horizontal reaction forces, R_x.

$$\sum M = 0$$

$$W * 0.5 * b_{model} = 1017.4 * 0.5 * 9.7 = 4934 \text{ kNm}$$

$$R_x * h = 587.4 * 8.4 = 4934 \text{ kNm}$$

Where:

b_{model} [m] = width of the mitre gate from support to support

The outcome of the reaction force in SCIA Engineer meets the expected outcome of the horizontal support reactions.

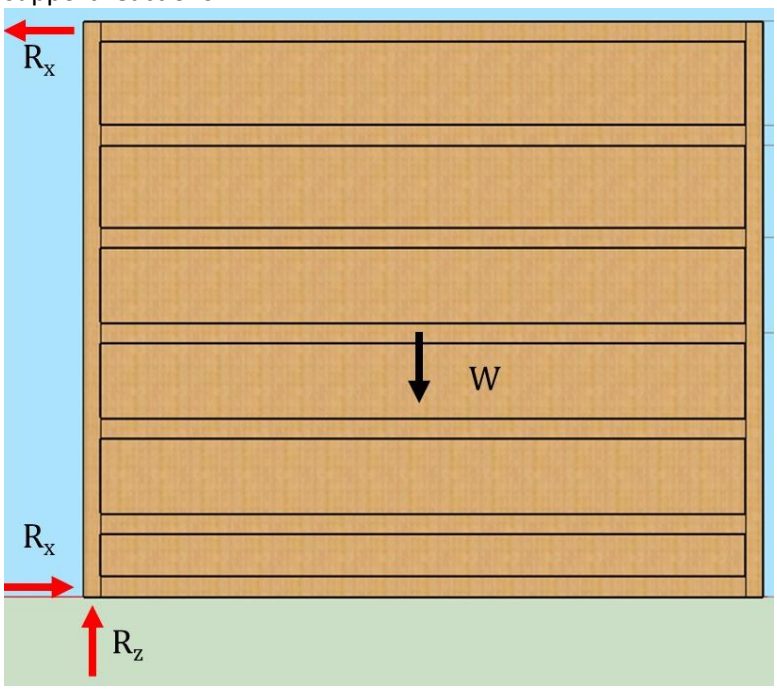

Figure 89: Overview of forces on the mitre gate during opening or closing.

The deflection of the opened mitre gate, uz, is 5.6 mm and equal over the height of the mitre gate. This deflection is increasing from the lock chamber side to the other end of the mitre gate. Again a remark is required because the ultimate limit state value of the spring stiffness is used in the model. The expected deflection of the mitre gate is higher as the spring stiffness of the serviceability limit state, K_{SLS}, is lower than K_{ULS}. But the magnitude of this deflection is not expected to be in order of multiple centimetres and so the mitre gate will not tend to go out of square.

The normal force in the skin plate layers, web plate and girder of the opening or closing mitre gate are summarized below. Overall the outcomes of the skin plate layers directed in the same direction are equal and therefore the layers in the same direction are discussed together.

Layer 1 and 6 are horizontally orientated and mainly loaded in the top and bottom lamellae of the skin plate. The top lamellae of each layer are loaded in tension, while the bottom lamellae of these skin plate layers are loaded in compression. The biggest normal force is present at the top and bottom hinge at the lock chamber side, 67 kN maximum.

Layer 2 and 5, vertically orientated, are barely contributing in the load transfer of the self-weight. The only lamellae that are loaded are the lamellae close to the lock chamber side, with an absolute maximum normal force of 24 kN.

The diagonals, layer 3 and 4, are equally loaded over the total skin plate. The diagonals connected to the top and bottom hinge are most heavily loaded.

Like for the first and sixth layer of the skin plate, the top and bottom web plate and top and bottom girder transfer the majority of the load. The intermediate web plates and girders barely contribute in the transfer of loads. The top girder and top web plate are loaded in tension and the bottom in compression as is expected from the reaction forces seen in Figure 89.

The unity checks of the opened/closing mitre gate are all below one. Only close to the bottom and top hinge the unity check of the first layer and web plate approaches 1, with a check of 0.85 and 0.87, respectively. As told in Section 8.2, the web plate has a very small area close to the hinge and therefore the unity check is relatively low. The reason for the high unity check of layer 1 is due to the fact that it is connected to the support and all the loads are transferred to this location. At the bottom and top hinge of a mitre gate the elements are made of steel because all the loads are transferred to the hinges during opening and closing. As the top and bottom hinge are not governing if they are made of steel, it can be concluded at first glance that the cross laminated timber is an interesting option for the replacement of the metal diagonal strut and tension bar.

8.4 Conclusion modelling optimized redesign of mitre gate

To summarize modelling of the modelling of the optimized redesign of the mitre gate the answer on the last sub question is given. The last sub question is: *How can the design of the renewed optimized timber mitre gate be modelled in a finite element modelling program and what are the differences with the analytical design?*
In this thesis a finite element model for the redesign of the mitre gate is made. As the design does contain innovations that are new in hydraulic engineering, the model made in this thesis is a starting point for modelling the innovations as dowel cross laminated skin plate or curved laminated girder. The mitre gate designed in Chapter 5 and 6 is modelled with beams and springs as interaction between the dowels and timber elements is expected. This interaction is done by the addition of springs with characteristics of the slip modulus.
The conclusions drawn from the model made in this thesis for the closed situation of the mitre gate are:

- Due to asymmetrical supporting system the reaction forces on the mitre gate are not similar in y-direction. This results in opposite support reactions at sub panel and displacement of sub panel against the loading direction. The global reaction forces of the model and preliminary design are consistent.
- The displacement of the model and the preliminary design equal each other in the model.
- The internal forces in the girder, N & My, do not match with the values of the preliminary design. An explanation for the difference is that the bending stiffness is derived according to the mechanically jointed theory for the preliminary design and the bending stiffness in SCIA Engineer does not contain loss factors of the mechanically jointed theory.
- The internal forces in the skin plate are halved the preliminary design, except for the lamellae at the supports. At the supports, peak loads occur in the lamellae. So the skin plate layers meet the requirements except for the supports.
- The joints at the lock chamber side or connecting gate side are from importance and now designed with metal straps at the girders. To be safe a metal strip at the skin plate layer is another option to resist peak loads.

The model with the opening or closing mitre gate shows that the use of cross laminated timber is an equivalent replacement of the steel strut and tension bar during opening or closing mitre gate. This models shows critical locations during opening and closing of the mitre gate at the top and bottom hinge. However, in the design these critical locations are equipped of steel.

9. Discussion, conclusions and recommendations

In this chapter, the discussion, conclusions and recommendations for further research are given. The main goal of this thesis was to find out why timber is scarcely used for renovation of navigation lock gates and to extend the application of timber in an innovative way for the renewal of navigation lock gates to replace steel gates.

Discussion

During the preliminary design stage several assumptions were made to simplify the design process but yet conservative, so that the dimensions of the structure and amount of material can be determined. Those assumptions are:

- The hydrostatic load acting on the mitre gate is simplified as equally distributed pressure over the full height of the mitre gate. In reality the hydrostatic pressure builds up linearly, from high water level until low water level and remains constantly to the bottom of the mitre gate, provided that the water density is equal on both sides of the gates, which is mostly the case for most of the mitre gates in this thesis. This assumption results in conservative results in the design.
- As stated in Section 4.2.2, the mechanically jointed beam theory contains some assumptions, which is applicable for the curved laminated girder. Nevertheless, for the cross laminated skin plate, the assumption of Mulder (2019) is only applicable for layers having equal characteristics. This however, is not the case for the cross laminated skin plate as the fibres of the lamination are placed in different directions. The characteristics of the layers of the skin plate are different. The differences in outcomes are described in detail in Appendix I. The preliminary fastener verification is done in the laminated girder done based on the maximum shear force on the fastener. Furthermore the calculation of the maximum force on a fastener is based on the mechanically jointed theory with fibres in equal direction. Accepting the dissimilarities of the mechanically jointed theory was the best possible option, as the other method for the calculation of the mechanically jointed mitre gate is the shear analogy method of Kreuzinger, this method is a better method for a final design instead of a preliminary design as is done in this thesis. The shear analogy method is better method for a final design of the mitre gate because it is more precise.
- The deflection in the preliminary design is calculated based on constant cross section along the width of the mitre gate. The actual cross section of the mitre gate however, varies along the width of the mitre gate, which means the real maximum deflection is expected to be higher than calculated in the preliminary design. Furthermore the ultimate limit state value of the slip modulus K_{ULS}, which is 2/3 of the serviceability limit state K_{SLS}, is applied in the finite element modelling, for the purpose of the strength and stability checks of the mitre gate. This leads to a smaller deformation than the outcomes of the finite element modelling.

For the verification in the finite element model, due to de limitation of the program, also several assumptions were made:

- In order to apply the slip modulus K_{ULS} at the interface between two skin plate layers, the dowel is divided into parts by applying springs at the element ends.
- The laminated girder is modelled as a solid girder with an equivalent moment of inertia of the three layered girder in the preliminary design.
- The connection of the post with the skin plate, web plate and girder is done with connecting dummy elements to enable the neutral axis of all mitre gate elements in the right position.
- The cross section of the web plate is divided into multiple trapezoidal parts to model the semi-ellipse shape.

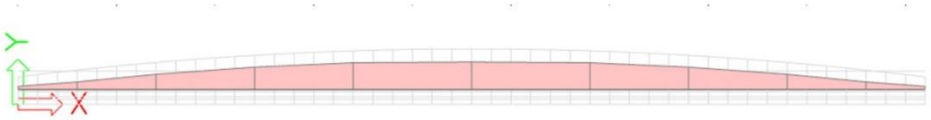

Figure 90: Top view of modelling web plate

One of the most important factors that affect the finite element results is the connection and the stiffness between the layers of the skin plate, the dowels. The dowels connecting the cross laminated timber layers of the mitre gate are modelled by infinite stiff dummy elements. A translation stiffness, determined by slip modulus according to the Eurocodes, is applied at the middle of each two layers, this is the real connecting location of the skin plate layers. The input and background of these values are based on experimental tests. However, a dowel can rotate, so it also has a rotational stiffness. The addition of the rotational stiffness makes the model affects the results of the finite element model. A proper model for doweled cross laminated timber contains both rotational and translational stiffness for the dowels. The elaborated explanation of the derivation of the rotational and translational springs in dowel cross laminated panels is shown in Appendix K. For this thesis the slip modulus of the test model is used as this can enables comparison of the preliminary design and the finite element model.

Conclusions

This thesis aimed to do research about timber mitre gates and aimed to increase the number of timber mitre gates. The goal of this thesis was to find out why timber is scarcely used for renovation of mitre gates wider than 12 metres and to apply timber in an innovative way for the renewal of existing mitre gates to replace steel mitre gates. The answers on the sub questions of the thesis and the main conclusions of these questions are given below.

Q1: *How is a timber mitre gate schematized to optimize the force distribution and what is the effect on the materialization?*

The load distribution from the mitre gate to the lock chamber wall is schematized in two ways, free-hinged and fixed-hinged. The free-hinged schematization results in a distributed transfer of loads to the lock chamber wall. The fixed-hinged schematization results in a load distribution to the lock chamber wall through the top and bottom hinge of the mitre gate. This gives high peak loads at the location of the top and bottom hinge. In the Netherlands the free-hinged schematization is most commonly used because the load is equally distributed over the total height of the mitre gate, which is favourable for the transfer of loads.

Framing of the mitre gate is based on the width to height ratio of the mitre gate. If the ratio is above two, vertically framed mitre gates are used. The Dutch waterways have a width to height ratio below two and therefore the horizontally framed mitre gate is used in the Netherlands. The sill of the navigation lock is not used to for the loads distribution because this contains too much uncertainties. The mitre gates lean towards each other and the alignment of the mitre gates is done in such a way that the sill contributes in the water retaining function but not in the load distribution.

The challenges of the current design of timber mitre gates with a lock chamber width above 12 metres are: the availability of the required dimensions and the mortise and tenon joint verification. The availability of timber challenge can be overcome by waiting for the required dimensions of the beams and mechanically jointing the timber mitre gate but this increases the cost price of the mitre gate and makes steel a more economically attractive alternative.

Q2: *What does the design of an optimized timber mitre gate look like for an existing situation out of the current application range?*

Lamination enables more homogeneous timber and allows curving and larger cross sections. For the optimized design of a mitre gate out of the current application range, the eastern navigation lock of Sambeek is used as case study location. The design for a mitre gate with a width of 9.47 metres, a water retaining height of 8.44 metres and a maximum differential head of 4.2 meters consists of a dowel cross laminated skin plate, web plate and a laminated girder. All these elements are made of azobé to have the most sustainable design. The centre to centre distance of the girders and the centre to centre distance of the web plates is 1.5 metres. The dowel cross laminated skin plate consists of 6 layers with a thickness of 25 millimetres each. The fibres of the six layers are placed in the following sequence: x-direction, y-direction, /-direction, \-direction, y-direction and x-direction. The width of the x- and y-orientated lamellae is 200 millimetres, the diagonal orientated layers have a width of 141 millimetres for optimal dowelling of the skin plate. The web plate of the mitre gate is a semi-ellipse plate with a thickness of 150 millimetres. The maximum height of the web plate is 300 millimetres halfway the mitre gate. The laminated girder is a curved three layered beam, each layer has a thickness of 100 millimetres and a height of 300 millimetres. Continuation of the girder through the end post results in avoiding the mortise and tenon joint. The maximum distance between the girder and web plate is 300 millimetres. Adhesives for wet environments are not available yet. Therefore, the skin plate is mechanically jointed with dowels, the web plate and girder are connected with bolts. The visual representation of the design of the mitre gate for the eastern Sambeek navigation lock is shown in Figure 91.

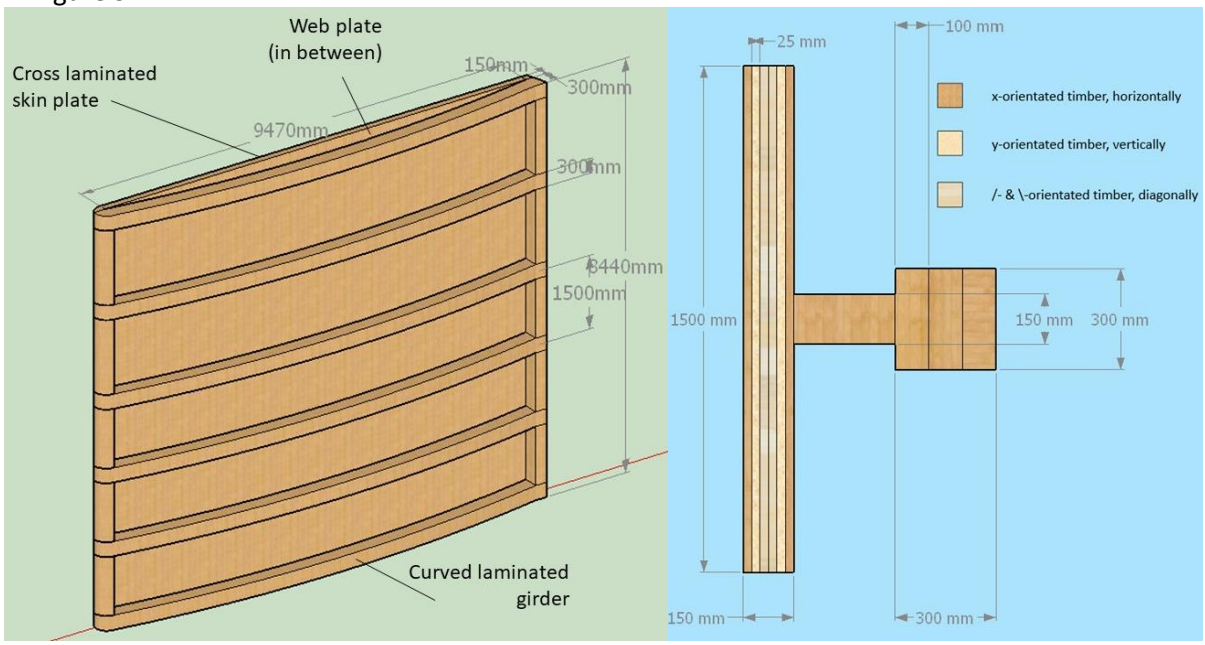

Figure 91: Overview and cross section of repeating slice of renewed design of mitre gate in Sambeek navigation lock

Q3*: How can the design of the renewed optimized timber mitre gate be modelled in a finite element modelling program and what are the differences with the analytical design?*

The model made in this thesis is a starting point for modelling the innovations as dowel cross laminated skin plate or curved laminated girder. The renewed optimized timber mitre gate design is modelled with beams and springs with characteristics of the slip modulus to model the interaction between the dowels and timber elements. For the closed mitre gate the global outcomes of the model and preliminary design are consistent, but the interaction between the fasteners and timber elements in the dowel cross laminated skin plate is not discernible. Furthermore it can be concluded that the use of cross laminated timber is an equivalent replacement of the steel strut and tension bar to resist the self-weight of the mitre gate. This only critical locations appear at the top and bottom hinge of the mitre gate but these hinges are equipped of steel.

Main research question*: In what way can timber be used optimally within the mitres gates of existing navigation locks, to resist the acting loads under different circumstances?*

For the renewed design of mitre gate out of the current application locks the use of laminated timber and cross laminated timber are innovations that can be used. The timber is used in a more spatial way, i.e. less solid and robust timber beams, but a cross section of timber elements with distance to the neutral axis is designed to increase the bending stiffness and decrease the amount of used timber. The skin plate of the mitre gate is a cross laminated timber plate to increase the strength of the mitre gate in orthogonal directions and replace the strut and tension bar, which decreases the amount of steel. Lastly, the design of the girder of the mitre gate can be directly supported to the lock chamber to load the timber in the strongest direction and solve the challenge of the mortise and tenon joint.

Recommendations

The final part of this thesis contains recommendations for future research. It is recommended to:

- Perform laboratory tests for the designed cross section of the preliminary design. Compare the outcomes of the laboratory tests with the repetitive cross section in the global design of the preliminary design.
- Perform more research on dowel cross laminated timber panels. Laboratory tests of dowel cross laminated timber panels will provide insight in the behaviour of the dowel cross laminated timber panel and the interaction of the dowels and timber layers.
- Execute a comparison design with glued laminated timber elements instead of mechanically jointed elements. Academic assumptions for the characteristics of a glued laminated plate are required but the modelling of glued laminated timber is more developed and could asses the design of this thesis in a better way.
- Carry out laboratory tests to obtain the stiffness of the rotational and translational springs in a dowel cross laminated timber panel described in Appendix K and model the design of the mitre gate with the rotational and translational spring. The interaction between the dowel cross laminated timber layers and dowels is modelled with the slip modulus of NEN-EN 1995 in this thesis, but the expectation is that a rotational and translational springs are a good representation too.
- Further develop the renewed design of the mitre gate. Final design of a timber mitre gate with dowel cross laminated timber skin plate requires more research. The design of the mitre gate in this thesis is a preliminary design of an averaged mitre gate in the scope of this thesis, based on an equally uniform distributed load on the mitre gate. The final renewed design of the mitre gate contains the described loads of Section 3.1.

References

Arends, G. (1994). *Sluizen en stuwen.* Delftse Universitaire Pers.

Beheersmaatschappij Antwerpen Mobiel. (2011). *Kattendijksluis in ere hersteld.* Nautin.

Bezuyen, K., Glerum, A., Kuiper, H., Kuiper, W., & Vrijling, J. (2000). *Constructieve Waterbouwkunde.* Delft: Lecture notes Delft University of Techonology.

Blass, H., & Sandhaas, C. (2017). *Timber Eningeering.* (R. Mort, Vert.) Karlsruhe: KIT Scientific Publishing.

Buchanan, A., John, S., & Love, S. (2013). Life cycle assessment and carbon footprint of multistorey timber buildings compared with steel and concrete buildings. *NZ Journal of Forestry, 57*, 9-18.

CUR. (2012). *CUR Rapport 166: Damwandconstructies.* CUR.

Daniel, R., & Paulus, T. (2019). *Lock gates and other closures in hydraulic projects.* Oxford: Butterworth-Heinemann.

Elling, R., Andeweg, B., Jong, J. d., & Swankhuisen, C. (2005). *Rapportagetechniek.* Groningen: Wolters Noordhoff.

Erhart, T., Fink, G., Steiger, R., & Frangi, A. (2016). Strength grading of European beech timber for the production of GLT & CLT. *INTER Proceedings*, 29-44.

Falk, R., & Colling, F. (1995). Laminating Effects in Glued-Laminated Timber Beams. *Journal of Structural Engineering*, 1857-1863.

Frese, M., & Blass, H. (2005). Beech glulam strength classes. *CIB-W18*.

Glavinić, I., Boko, I., Torić, N., & Vranković, J. (2020). Application of hardwood for glued laminated timber in Europe. *GRAĐEVINAR 72, 72*(7), 607-616.

Glerum, A. (1992). *Waterbouwkundige Kunstwerken.* Delft University of Techonology.

Glerum, A., Vrijburcht, A., Beem, R., Boogaard, A., Graaf, M. d., Heneberque, S., . . . Weijers, J. (2000). *Ontwerp van Schutsluizen.* Utrecht: Ministerie van Verkeer en Waterstaat, Directoraat-Generaal Rijkswaterstaat, Bouwdienst.

Ingenieursbureau Boorsma. (2020). *MultiWaterWerk Materialisatie sluisdeuren.* Rijkswaterstaat.

Kreuzinger, H. (1999). Platten, Scheiben und Schalen. Ein Berechnungsmodell fur . *Bauen mit Holz*, 34-39.

Kuilen, J. v., & Blass, H. (2005). Mechanical properties of azobé (Lophira alata). *European Journal of Wood and Wood Products, 63*, 1-10.

Larsen, H., & Enjily, V. (2011). *Practical design of timber structures to Eurocode 5.* London: ICE Publishing.

Lesser Known Timber Species. (sd). *Frederikssund*.

Leusden, B. v. (1996). *Duikers en sluizen.* Culemborg: Educaboek.

Levinson, M. (2018). *Standardization of mitre gates.* MSc thesis. Delft University of Technology.

Ministerie van Verkeer en waterstaat. (1992). *Aanvaarrisico's voor sluisdeuren.* Rotterdam: Rijkswaterstaat.

Molenaar, W. F. (2020). *Locks.* Delft: Delft University of Technology.

Molenaar, W., & Voorendt, M. (2020). *Hydraulic Structures.* Delft: Lecture notes Delft University of Technology.

Mulder, M. (2019). *Verificatieregels mechanisch verbonden ligger met meer dan 3 delen.* Unpublished manuscript.

Rijkswaterstaat. (2016). MultiWaterWerk. *Programma MultiWaterWerk* (pp. 1-61). Delft: De Bouwcampus.

Rijkswaterstaat. (2017). *Richtlijnen Ontwerp Kunstwerken 1.4.* Utrecht.

Rijkswaterstaat. (2020). *Richtlijnen Vaarwegen 2020.*

Romeijn, A. (2006). *Steel Bridges dictaat deel I.* Delft University of Technology.

Schelling, W. (1982). Zur Berechnung nachgiebig zusammengesetzter Biegeträger aus beliebig vielen Einzelquerschnitten. *Ingenieurholzbau in Forschung und Praxis*, 155-162.

Stoop, J., Drop, P., Vlieger, J. d., & Donselaar-Gaal, B. (2013, May). Houten sluisdeuren sterker dan rekenregels aangeven : sterkteproef bij Stolwijkerschutsluis. *Land + water : magazine voor civiele- en milieutechniek*, pp. 18-19.

StructureCraft. (2021, June). *Dowel Laminated Timber.* Opgehaald van StructureCraft: https://structurecraft.com/materials/mass-timber/dlt-dowel-laminated-timber

Technische Adviescommissie voor de Waterkeringen. (2003). *Leidraad Kunstwerken.* Delft: Nivo.

Uibel, T., & Blass, H. J. (2007). Edge Joints with Dowel Type Fasteners in Cross Laminated Timber.

United Nations. (2015). Paris Agreement. *Climate Change Conference.* Paris.

Veldhuis, A. (2020). *Integral Design Process of CLT Structures and Robotic Fabrication.* MSc Thesis Delft University of Technology.

Voorendt, M., & Molenaar, W. (2020). *Manual Hydraulic Structures.* Delft: Lecture notes Delft University of Technology.

Wallner-Novak, M., Augustin, M., Koppelhuber, J., & Pock, K. (2018). *Cross-Laminated Timber Structural Design Volume 2.* Vienna: proHolza Austria.

Wallner-Novak, M., Koppelhuber, J., & Pock, K. (2014). *Cross-Laminated Timber Structural Design.* Vienna: proHolz Austria.

Wee, B. v., & Annema, J. (2014). *Verkeer en vervoer in hoofdlijnen.* Bussum: Coutinho.

Willems, J., & Busscher, T. (2014). *De Nederlandse sluizensector: in de houdgreep? Rapport 1 voor MultiWaterWerk/Rijkswaterstaat.* Rijksuniversiteit Groningen. Faculteit Ruimtelijke Wetenschappen.

Wilschut, T., Etman, L., Rooda, J., & Vogel, J. (2019). Similarity, Modularity, and Commonality Analysis of Navigation Locks in the Netherlands. *Journal of Infrastructure Systems, 25*(1), 1-13. doi:https://doi.org/10.1061/(ASCE)IS.1943-555X.0000468

Zangiácomo, A., Balanco, G., Christoforo, A., & Rocco Lahr, F. (2017). Glued Laminated Timber Produced with Tropical Brazilian Wood Species. *British Journal of Applied Science and Technology*, 1-12.

Appendices

A. Clustering of lock gates

This appendix provides the detailed results of clustering the navigation locks done by Wilschut et al. in 2018 and the application area of the redesign of the mitre gate in this thesis.
The 7 clusters are made with a clustering algorithm based upon a Dependency Structure Matrix with the characteristics of the navigation locks. The outcomes of the clustering and the most important characteristics of the lock gates are given.

Cluster 1
The lock characteristics in this cluster are:

- Monodirectional water retention
- Single head high water retention
- Lock chamber width between 10 and 20 metre
- Mitre gates (primarily electro-hydraulic driving mechanism)
- Gate openings (primarily electro-hydraulic driven)

	Name	Type of gate	Material	Chamber Width
1	Sluis Heel west	Mitre gates	Steel	16
2	Noordersluis Grote oostelijke sluis	Mitre gates	Timber	12
3	Sluis Driel	Mitre gates	Steel	18
4	Schutsluis Belfeld oost (oude sluis)	Mitre gates	Steel	16
5	Zuidersluis	Mitre gates	Steel	18.1
6	Sluis 5	Mitre gates	Timber	12.6
7	Schutsluis Belfeld west	Mitre gates	Steel	16
8	Sluis Grave noord (nieuw)	Mitre gates	Steel	16
9	Sluis Panheel (nieuwe kolk)	Mitre gates	Steel	18.1
10	Zuidersluis	Mitre gates	Timber	12
11	Sluis 6	Mitre gates	Timber	12.6
12	Schutsluis Sambeek midden	Mitre gates	Steel	16
13	Kleine Sluis	Mitre gates	Steel	11
14	Spooldersluis	Mitre gates	Steel	14
15	Sluis Helmond	Mitre gates	Steel	12.6
16	Gaarkeuken	Mitre gates	Steel	16
17	Sluis 4	Mitre gates	Timber	12.6
18	Sluis Amerongen	Mitre gates	Steel	18
19	Sluis Heel oost	Mitre gates	Steel	16
20	Schutsluis Belfeld midden	Mitre gates	Steel	16
21	Sluis I	Mitre gates	Steel	14
22	Sluis Lith noord (nieuw)	Mitre gates	Steel	18.1
23	Sluis Hagestein	Mitre gates	Steel	18
24	Sluis V	Mitre gates	Demolished	8.95
25	Sluis Hintham	Mitre gates	Steel	12.8
26	Schutsluis Sambeek west	Mitre gates	Steel	16
27	Oostersluis	Mitre gates	Steel	16

Cluster 2

The lock characteristics in this cluster are:

- Monodirectional water retention
- Single head high water retention
- Lock chamber width smaller than 10 metre
- Mitre gates (primarily electro-hydraulic driving mechanism)
- Gate openings (primarily electro-hydraulic driven)

	Name	Type of gate	Material	Chamber Width
28	Groevesluis-Zuid	Mitre gates	Steel	6
29	Noordersluis Kleine westelijke sluis	Mitre gates	Timber	7
30	Biesboschsluis	Mitre gates	Timber	7
31	Sluis 0	Mitre gates	Steel	8
32	Sluis 13	Mitre gates	Steel	9.8
33	Sluis 11	Mitre gates	Timber	9.8
34	Ottersluis	Mitre gates	Timber	7.3
35	Helsluis	Mitre gates	Timber	7.3
36	Slochtersluis	Mitre gates	Steel	6
37	Sluis 12	Mitre gates	Timber	9.8
38	Sluis 10	Mitre gates	Timber	9.8
39	Groevesluis-Noord	Mitre gates	Timber	8.6

Cluster 3

The lock characteristics in this cluster are:

- Bidirectional water retention
- Single head high water retention
- Fresh and salt water separation
- Lock chamber width larger than 20 metre
- Rolling gates (primarily electro-hydraulic driving mechanism)
- Culverts (primarily electromechanical driven)

	Name	Type of gate	Material	Chamber Width
40	Prins Willem Alexander sluis	Rolling gates	Steel	24.1
41	Krammersluizencomplex 2e Duwvaartsluis (Noord)	Rolling gates	Steel	24
42	Hansweert Westelijke sluis	Rolling gates	Steel	24
43	Krammersluizencomplex 2e Jachtensluis (Noord)	Rolling gates	Steel	9
44	Kreekraksluizen (Westsluis)	Rolling gates	Steel	24
45	Hansweert Oostelijke sluis	Rolling gates	Steel	24
46	Kreekraksluizen (Oostsluis)	Rolling gates	Steel	24
47	Middensluis, Terneuzen	Rolling gates	Steel	18
48	Noordersluis	Rolling gates	Steel	50
49	Sluis Weurt oost	Rolling gates	Steel	16
50	Krammersluizencomplex 1e Duwvaartsluis (Zuid)	Rolling gates	Steel	24.1
51	Krammersluizencomplex 1e Jachtensluis (Zuid)	Rolling gates	Steel	9
52	Westsluis, Terneuzen	Rolling gates	Steel	40
53	Roompotsluis	Rolling gates	Steel	16

Cluster 4

The lock characteristics in this cluster are:

- Bidirectional water retention
- Single head high water retention
- Lock chamber width between 10 and 20 metre
- Lift gates (electromechanical driving mechanism)
- Gate openings/under gate (primarily electro-hydraulic driven)

	Name	Type of gate	Material	Chamber Width
54	Sluis Eefde	Lift gates	Steel	12
55	Sluis Delden	Lift gates	Steel	12
56	Sluis Hengelo	Lift gates	Steel	12
57	Sluis Lith zuid (oud)	Lift gates	Steel	14
58	Sluis Weurt west	Lift gates	Steel	16
59	Sluis 16	Lift gates	Steel	7.5
60	Prins Bernhardsluis (Oostelijke sluis - sluis 2)	Lift gates	Steel	24
61	Sluis Bosscherveld	Lift gates	Steel	14
62	Prinses Irenesluis Duwvaartsluis (sluis 2)	Lift gates	Steel	24
63	Prinses Beatrixsluis oostelijke sluis	Lift gates	Steel	18
64	Sluis Empel	Mitre gates	Steel	12.9
65	Prins Bernhardsluis (Westelijke sluis - sluis 1)	Lift gates	Steel	18
66	Sluis St. Andries	Lift gates	Steel	14
67	Prinses Beatrixsluis Westerlijke sluis	Lift gates	Steel	18
68	Prinses Irenesluis Oude sluis (sluis 1)	Lift gates	Steel	18

Cluster 5

The lock characteristics in this cluster are:

- Monodirectional water retention
- Single head high water retention
- Lock chamber width between 10 and 20 metre
- Mitre gates (primarily electromechanical driving mechanism)
- Gate openings (primarily electromechanical driven)

	Name	Type of gate	Material	Chamber Width
69	Wilhelminasluis, Andel	Mitre gates	Steel	12.9
70	Sluis Schijndel	Mitre gates	Steel	12.6
71	Zandkreeksluis	Squared Mitre gates	Steel	20
72	Spieringsluis	Mitre gates	Plastic	6
73	Sluis bij Den Hommel	Mitre gates	Timber	7
74	Schutsluis Sambeek oost	Mitre gates	Steel	16
75	Prinses Marijkesluis westelijke sluis	Mitre gates	Steel	18
76	Marksluis	Mitre gates	Steel	14
77	Terhorne sluis	Mitre gates	Steel	16
78	Prinses Marijkesluis oostelijke sluis	Mitre gates	Steel	18
79	Grote Kolksluis	Mitre gates	Timber	8.5
80	Prinses Margrietsluis	Mitre gates	Steel	16
81	2e Sluis Bewesten Utrecht (Muntsluis)	Mitre gates	Steel	14

Cluster 6

The lock characteristics in this cluster are:

- Monodirectional water retention
- Single head high water retention
- Lock chamber width between 10 and 20 metre
- Mitre gates (electromechanical and hydraulic driving mechanism)
- Culverts (electromechanical and hydraulic driven)

	Name	Type of gate	Material	Chamber Width
82	Sluis Heumen	Mitre gates	Steel	16
83	Sluis Panheel (oude kolk, noord)	Mitre gates	Steel	7.5
84	Henriettesluis (Schutsluis Engelen)	Mitre gates	Timber	13
85	Dorkwerdersluis	Rolling gate	Steel	8.6
86	Sluis IV	Mitre gates	Timber	10
87	Sluis Hulsen	Mitre gates	Timber	7.5
88	Sluis Born west	Lifiting gate	Steel	16
89	Sluis Linne	Mitre gates	Steel	14
90	Sluis Born oost	Mitre gates	Steel	16
91	Sluis III	Mitre gates	Timber	9
92	Sluis 15	Mitre gates	Steel	7.5
93	Driewegsluis	Rolling gate[2]	Timber	14
94	Sluis II	Mitre gates	Timber	9
95	Sluis Born midden	Mitre gates	Steel	16
96	Sluis Maasbracht west	Mitre gates	Steel	16
97	Sluis III	Mitre gates	Composite	16
98	Sluis Maasbracht oost	Mitre gates	Steel	16
99	Sluis Roermond	Mitre gates	Steel	14
100	Sluis Maasbracht midden	Mitre gates	Steel	16

[2] According to street view it looks like a rolling gate

Cluster 7

The lock characteristics in this cluster are:

- Bidirectional water retention
- Double head high water retention
- Fresh and salt water separation
- Lock chamber width between 10 and 20 metre
- Square mitre gates (primarily electro-hydraulic driving mechanism)
- Gate openings and culverts (primarily electro-hydraulic driven)

	Name	Type of gate	Material	Chamber Width
101	Houtribsluizen	Square mitre gates	Steel	18
102	Noordersluis	Square mitre gates	Steel	14
103	Zeesluizen Farmsum kamer 2	Square mitre gates	Steel	7
104	Grevelingensluis	Square mitre gates	Steel	16
105	Stevinsluizen	Square mitre gates	Steel	13
106	Oostsluis, Terneuzen	Square mitre gates	Steel	24
107	Sluis 2	Square mitre gates	Steel	24
108	Naviduct Krabbersgat	Square mitre gates	Steel	12
109	Houtribsluizen	Square mitre gates	Steel	18
110	Zeesluizen Farmsum kamer 1	Square mitre gates	Steel	16
111	Lorentzsluizen kamer 1	Square mitre gates	Steel	14
112	Middensluis	Square mitre gates	Steel	18
113	Algerasluis	Square mitre gates	Steel	24
114	Nijkerkersluis	Square mitre gates	Timber	10
115	Goereese sluis	Square mitre gates	Timber	16
116	Zuidersluis	Square mitre gates	Steel	14
117	Naviduct Krabbersgat	Square mitre gates	Steel	12.5
118	Sluis 3	Square mitre gates	Steel	24
119	Sluis 1	Square mitre gates	Steel	24
120	Krabbersgatsluis	Square mitre gates	Steel	12.5
121	Koninginnensluis	Square mitre gates	Steel & Timber	11.9
122	Lorentzsluizen kamer 2	Square mitre gates	Timber	9
123	Bergsediepsluis	Square mitre gates	Steel	6.5
124	Roggebotsluis	Square mitre gates	Steel & Timber	10
125	Jachtensluis sluizencomplex Volkerak	Square mitre gates	Steel	16
126	Middensluis	Square mitre gates	Steel	24

A.1 Mitre gates in the scope of the thesis

The 38 mitre gates that fit in the scope of this thesis are shown below in the table, the location of the navigation locks are pictured in Figure 92.

	Name	Type of gate	Material	Chamber Width
1	Sluis Heel west	Mitre gates	Steel	16
3	Sluis Driel	Mitre gates	Steel	18
4	Schutsluis Belfeld oost (oude sluis)	Mitre gates	Steel	16
5	Zuidersluis	Mitre gates	Steel	18.1
7	Schutsluis Belfeld west	Mitre gates	Steel	16
8	Sluis Grave noord (nieuw)	Mitre gates	Steel	16
9	Sluis Panheel (nieuwe kolk)	Mitre gates	Steel	18.1
12	Schutsluis Sambeek midden	Mitre gates	Steel	16
14	Spooldersluis	Mitre gates	Steel	14
15	Sluis Helmond	Mitre gates	Steel	12.6
16	Gaarkeuken	Mitre gates	Steel	16
17	Sluis Amerongen	Mitre gates	Steel	18
19	Sluis Heel oost	Mitre gates	Steel	16
20	Schutsluis Belfeld midden	Mitre gates	Steel	16
21	Sluis I	Mitre gates	Steel	14
22	Sluis Lith noord (nieuw)	Mitre gates	Steel	18.1
23	Sluis Hagestein	Mitre gates	Steel	18
25	Sluis Hintham	Mitre gates	Steel	12.8
26	Schutsluis Sambeek west	Mitre gates	Steel	16
27	Oostersluis	Mitre gates	Steel	16
64	Sluis Empel	Mitre gates	Steel	12.9
69	Wilhelminasluis, Andel	Mitre gates	Steel	12.9
70	Sluis Schijndel	Mitre gates	Steel	12.6
74	Schutsluis Sambeek oost	Mitre gates	Steel	16
75	Prinses Marijkesluis westelijke sluis	Mitre gates	Steel	18
76	Marksluis	Mitre gates	Steel	14
77	Terhorne sluis	Mitre gates	Steel	16
78	Prinses Marijkesluis oostelijke sluis	Mitre gates	Steel	18
80	Prinses Margrietsluis	Mitre gates	Steel	16
81	2e Sluis Bewesten Utrecht (Muntsluis)	Mitre gates	Steel	14
82	Sluis Heumen	Mitre gates	Steel	16
89	Sluis Linne	Mitre gates	Steel	14
90	Sluis Born oost	Mitre gates	Steel	16
95	Sluis Born midden	Mitre gates	Steel	16
96	Sluis Maasbracht west	Mitre gates	Steel	16
98	Sluis Maasbracht oost	Mitre gates	Steel	16
99	Sluis Roermond	Mitre gates	Steel	14
100	Sluis Maasbracht midden	Mitre gates	Steel	16

Table 20: Mitre gates in the scope of this thesis

Figure 92: Location of the mitre gates in the scope

B. Load distribution in the different types of gates

In this appendix, the simplified load distribution of each type of lock gates is given. The simplified design of each lock gate consists of two parts. The skin plate of the lock gate is to retain the water and the structure behind the skin plate gives stability, stiffness and strength to the lock gate. Every type of gate has its characteristic design. Therefore the load distribution in the lock gate is not identical for the gates. An overview of the load distribution for each gate type is given below. For each gate the hydrostatic load on the gate is mainly dependent on the water level difference. Other hydraulic loading is discussed in detail in Section 3.1.

Figure 93 illustrates the hydrostatic load on the gate due to the water level difference.

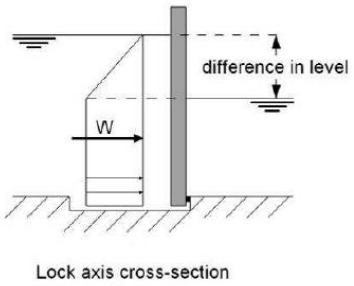

Figure 93: Hydrostatic pressure on a navigation lock gate from Molenaar and Voorendt (2020)

Mitre gate

The mitre gate is pointed towards the high water level. If closed, the loads on a single mitre gate seen from above can be seen Figure 94. In here the Fw is the resultant load of the water pressure. Fs is the spalling force and Fl is the force of the two gates leaning to each other.

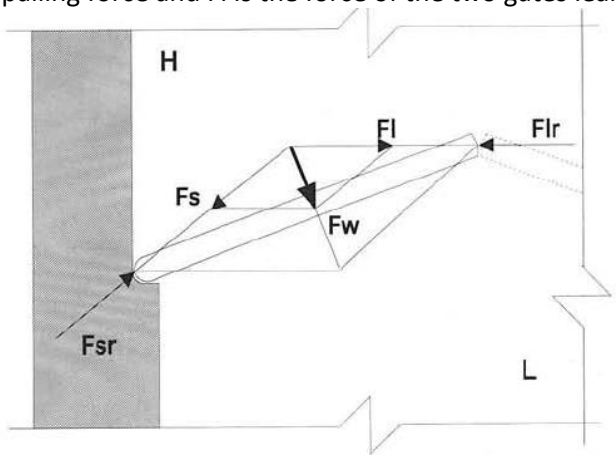

Figure 94: Top view of loads in a mitre gate (Molenaar and Voorendt, 2020)

In Figure 95 a more detailed overview with load vectors for a mitre gate in closed situation is shown.

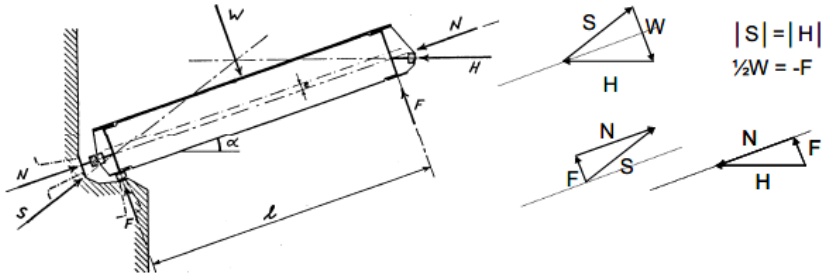

Figure 95: Top view of loads and resultants of loads in a mitre gate (Molenaar and Voorendt, 2020)

In here, W is the resultant force of the hydraulic load on the mitre gate. H is the resulting force of the 2 doors leaning to each other and S is the spalling force acting on the lock head. The contact point of the two mitre gates is chosen deliberately. As can be seen, the contact point is not in the centre line of the mitre gate. This eccentricity is constructed on purpose to counteract the bending moment caused by the water level difference.

An eccentricity is added in the design of the turning point of the mitre gate as well as can be seen in Figure 96. The dashed lines show the opened position of the mitre gate, in that case the water can flow along the gate. The solid lines show the closed position of the mitre gate wherein the water retaining function is preserved. This design avoids wear of the end post and reduce the required energy to rotated the mitre gate.

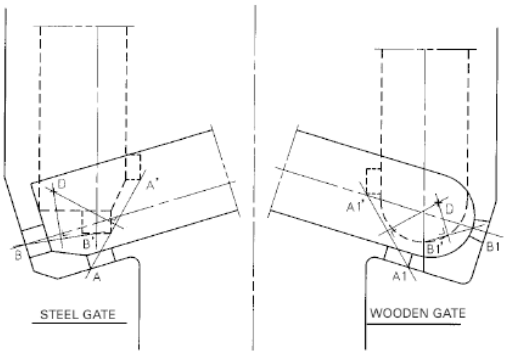

Figure 96: Free turning point in mitre gates (Ministerie van Verkeer en Waterstaat, 2000)

The load distribution through the mitre gates depends on the design of the lock gate. There are two most used alternatives, the first alternative is with clearance of the hinge at the end post and the second alternative is without clearance of the hinge at the end post. In case of clearance in the hinge, the hinge is lifted up by the hydraulic load if the door is closed. When the mitre gate is constructed without any clearance the hinges have no freedom to move. The installation of the end post should be done very precisely to avoid leakage and wear.

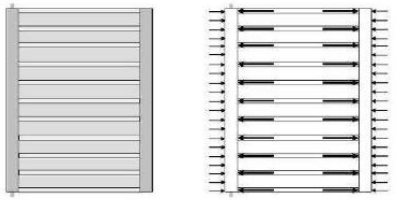

Figure 97: Schematized load distribution to the lock chamber of a mitre gate with clearance (Molenaar and Voorendt, 2020)

In case of construction of the mitre gate with clearance the load is transferred to the lock chamber wall as a distributed load along the height of the end post, this is shown in Figure 97. To do so the spacing between the horizontal girders should not be too big. Advantage of the distributed transfer is that the peaks loads is relatively small, which results in a less heavy gate.

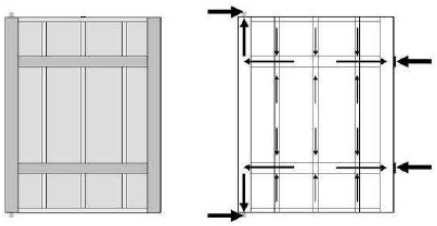

Figure 98: Schematized load distribution to the lock chamber of a mitre gate without clearance (Molenaar and Voorendt, 2020)

Without clearance the load is distributed to the two hinges that are the supports of the system. These two supports transfer all the load to the lock chamber. An advantage of this is that the system is statically determined, which makes it more easy to determine the load transfer to the lock chamber. Disadvantage is the locally high loads at the supports. According to Daniel and Paulus (2019) it is more straightforward and cost effective to use the principle with some clearance. Most of the mitre gates in the Netherlands therefore are constructed with some clearance at the hinges and can be schematized as simply supported beams.

Lift gate

The load distribution through the lift gate is similar to a mitre gate due to the similar layout of the gate. The load distribution from the gate to the lock head is fully done through the piers(a) or through the piers in combination with the sill(b).

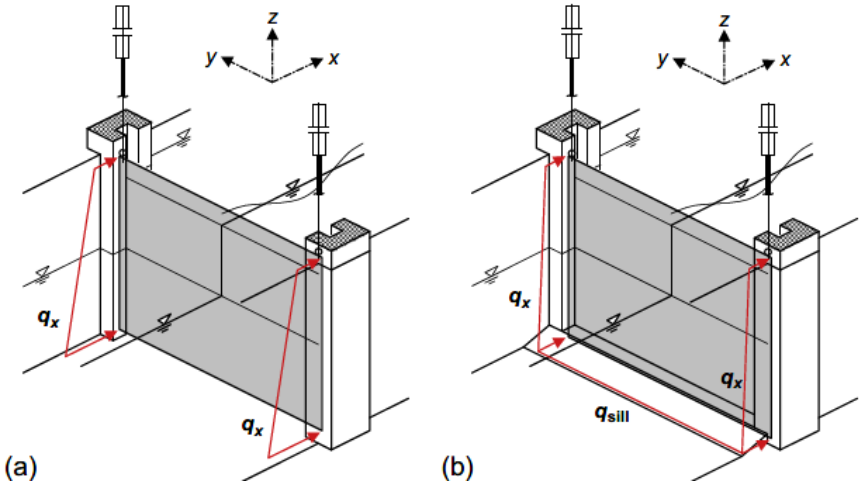

Figure 99: Load distribution on a lift gate (Daniel and Paulus, 2019)

In closed situation the lift gate is schematized as a simply supported beam. The water pushes the lift gate towards the support in the recess. If the lift gate is constructed for double-sided retaining the support is constructed on both sides of the recess.

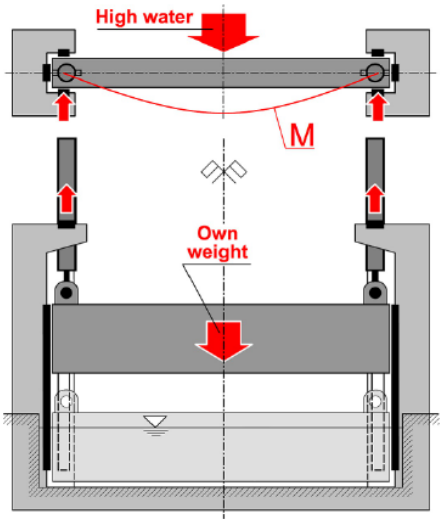

Figure 100: Global moment and load distribution on a lift gate (Daniel and Paulus, 2019)

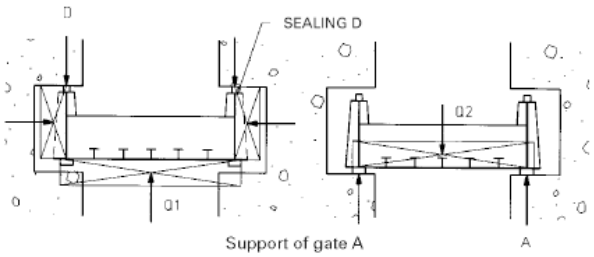

Figure 101: Top view load distribution on a lift gate (Daniel and Paulus, 2019)

If water is flowing into the recess a normal force in the lift gate can occur and have to be taken into account when constructing the lift gate.

Rolling gate

The rolling gate is schematized as two connected doors on roller carriages. According to Glerum, et al. (2000) the roller carriages mainly determine the thickness of the rolling gates. The doors are connected by a collection of girders and posts which give the door the required strength, stiffness and stability. The space between the skin plates is divided into multiple boxes and these are called float control chamber. The introduction of float control chambers to reduce the weight of the gate contribute to a lighter operating mechanism.

The placement of the roller carriages is done in different ways. Figure 102 shows five support systems for the rolling gate. The most favoured systems are (a), (b) and (c).

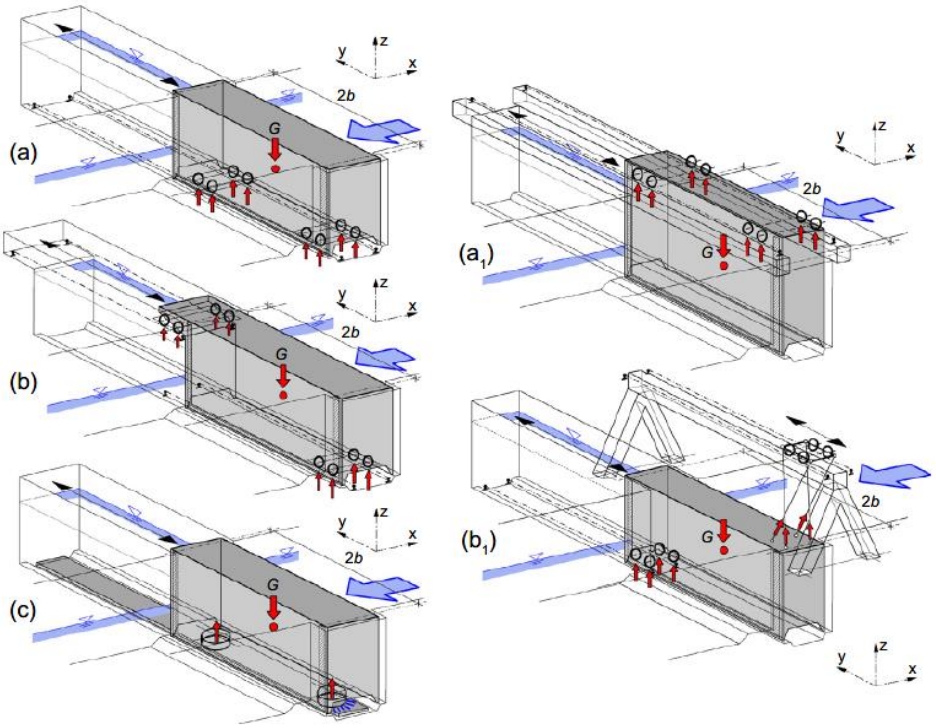

Figure 102: Main support systems of rolling gates (Daniel and Paulus, 2019)

C. Appearance and characteristics of timber

In this appendix, the maximum dimensions of available solid timber beams is shown and the characteristic strength and stiffness values for timber are shown:

C.1 Availability of solid Azobé beam elements

The maximum dimensions of solid Azobé elements are shown in the figure below. The available length is plotted against the cross section of the solid Azobé beam.

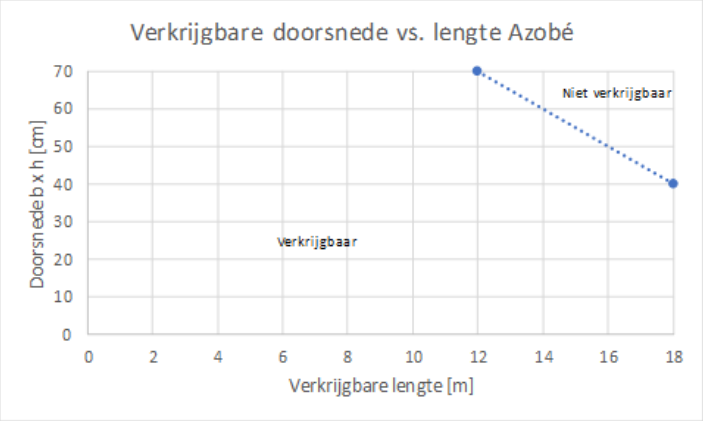

Figure 103: Availability of solid Azobé beams (Wijma Kampen B.V., 2020)

As can be seen the maximum length of an azobé beam is 18 metres, the cross section of the longest beam is maximum 400x400 millimetres. The maximum cross section of an azobé beam is 700x700 millimetres with a maximum length of 12 metres. The maximum dimensions are available, but are not very wide applicable and therefore have a long delivery time which is costly.

C.2 Timber strength classes

The characteristic strength, stiffness and density per strength classes according to NEN-EN 338 are shown below. The bold printed strength classes are the most common used classes in Europe. The strength classes for softwoods are based on bending and tension tests. For hardwoods the classification is only based on bending tests.

Strength classes for softwood based on edgewise bending tests – strength, stiffness and density values

	Class	C14	**C16**	**C18**	C20	C22	**C24**	C27	**C30**	C35	C40	C45	C50
Strength properties in N/mm²													
Bending	$f_{m,k}$	14	**16**	**18**	20	22	**24**	27	**30**	35	40	45	50
Tension parallel	$f_{t,0,k}$	7,2	**8,5**	**10**	11,5	13	**14,5**	16,5	**19**	22,5	26	30	33,5
Tension perpendicular	$f_{t,90,k}$	0,4	**0,4**	**0,4**	0,4	0,4	**0,4**	0,4	**0,4**	0,4	0,4	0,4	0,4
Compression parallel	$f_{c,0,k}$	16	**17**	**18**	19	20	**21**	22	**24**	25	27	29	30
Compression perpendicular	$f_{c,90,k}$	2,0	**2,2**	**2,2**	2,3	2,4	**2,5**	2,5	**2,7**	2,7	2,8	2,9	3,0
Shear	$f_{v,k}$	3,0	**3,2**	**3,4**	3,6	3,8	**4,0**	4,0	**4,0**	4,0	4,0	4,0	4,0
Stiffness properties in kN/mm²													
Mean modulus of elasticity parallel bending	$E_{m,0,mean}$	7,0	**8,0**	**9,0**	9,5	10,0	**11,0**	11,5	**12,0**	13,0	14,0	15,0	16,0
5 percentile modulus of elasticity parallel bending	$E_{m,0,k}$	4,7	**5,4**	**6,0**	6,4	6,7	**7,4**	7,7	**8,0**	8,7	9,4	10,1	10,7
Mean modulus of elasticity perpendicular	$E_{m,90,mean}$	0,23	**0,27**	**0,30**	0,32	0,33	**0,37**	0,38	**0,40**	0,43	0,47	0,50	0,53
Mean shear modulus	G_{mean}	0,44	**0,50**	**0,56**	0,59	0,63	**0,69**	0,72	**0,75**	0,81	0,88	0,94	1,00
Density in kg/m³													
5 percentile density	ρ_k	290	**310**	**320**	330	340	**350**	360	**380**	390	400	410	430
Mean density	ρ_{mean}	350	**370**	**380**	400	410	**420**	430	**460**	470	480	490	520

NOTE 1 Values given above for tension strength, compression strength, shear strength, char. modulus of elasticity in bending, mean modulus of elasticity perpendicular to grain and mean shear modulus have been calculated using the equations given in EN 384.
NOTE 2 The tension strength values are conservatively estimated since grading is done for bending strength.
NOTE 3 The tabulated properties are compatible with timber at moisture content consistent with a temperature of 20 °C and a relative humidity of 65 %, which corresponds to a moisture content of 12 % for most species.
NOTE 4 Characteristic values for shear strength are given for timber without fissures, according to EN 408.
NOTE 5 These classes may also be used for hardwoods with similar strength and density profiles such as e.g. poplar or chestnut.
NOTE 6 The edgewise bending strength may also be used in the case of flatwise bending.

Strength classes for softwood based on tension tests – strength, stiffness and density values

	Class	T 8	T 9	T 10	**T 11**	T 12	T 13	**T 14**	T 14,5	T 15	T 16	**T 18**	**T 21**	**T 22**	T 24	T 26	T 27	T 28	T 30
Strength properties in N/mm²																			
Bending	$f_{m,k}$	13,5	14,5	16	**17**	18	19,5	**20,5**	21	22	23	**25,5**	**29**	**30,5**	33	35	36,5	37,5	40
Tension parallel	$f_{t,0,k}$	8	9	10	**11**	12	13	**14**	14,5	15	16	**18**	**21**	**22**	24	26	27	28	30
Tension perpendicular	$f_{t,90,k}$	0,4	0,4	0,4	**0,4**	0,4	0,4	**0,4**	0,4	0,4	0,4	**0,4**	**0,4**	**0,4**	0,4	0,4	0,4	0,4	0,4
Compression parallel	$f_{c,0,k}$	16	17	17	**18**	19	20	**21**	21	21	22	**23**	**25**	**26**	27	28	29	29	30
Compression perpendicular	$f_{c,90,k}$	2,0	2,1	2,2	**2,2**	2,3	2,4	**2,5**	2,5	2,5	2,6	**2,7**	**2,7**	**2,7**	2,8	2,9	2,9	2,9	3,0
Shear	$f_{v,k}$	2,8	3,0	3,2	**3,4**	3,6	3,8	**4,0**	4,0	4,0	4,0	**4,0**	**4,0**	**4,0**	4,0	4,0	4,0	4,0	4,0
Stiffness properties in kN/mm²																			
Mean modulus of elasticity parallel tension	$E_{t,0,mean}$	7,0	7,5	8,0	**9,0**	9,5	10,0	**11,0**	11,0	11,5	11,5	**12,0**	**13,0**	**13,0**	13,5	14,0	15,0	15,0	15,5
5 percentile modulus of elasticity parallel tension	$E_{t,0,k}$	4,7	5,0	5,4	**6,0**	6,4	6,7	**7,4**	7,4	7,7	7,7	**8,0**	**8,7**	**8,7**	9,0	9,4	10,1	10,1	10,4
Mean modulus of elasticity perpendicular	$E_{t,90,mean}$	0,23	0,25	0,27	**0,30**	0,32	0,33	**0,37**	0,37	0,38	0,38	**0,40**	**0,43**	**0,43**	0,45	0,47	0,50	0,50	0,52
Mean shear modulus	G_{mean}	0,44	0,47	0,50	**0,56**	0,59	0,63	**0,69**	0,69	0,72	0,72	**0,75**	**0,81**	**0,81**	0,84	0,88	0,94	0,94	0,97
Density in kg/m³																			
5 percentile density	ρ_k	290	300	310	**320**	330	340	**350**	350	360	370	**380**	**390**	**390**	400	410	410	420	430
Mean density	ρ_{mean}	350	360	370	**380**	400	410	**420**	420	430	440	**460**	**470**	**470**	480	490	490	500	520

NOTE 1 Values given above for bending strength, compression strength, shear strength, char. modulus of elasticity in tension, mean modulus of elasticity perpendicular to grain and mean shear modulus have been calculated using the equations given in EN 384.
NOTE 2 The bending strength values are conservatively estimated since grading is done for tension strength.
NOTE 3 The tabulated properties are compatible with timber at moisture content consistent with a temperature of 20 °C and a relative humidity of 65 %, which corresponds to a moisture content of 12 % for most species.
NOTE 4 Characteristic values for shear strength are given for timber without fissures, according to EN 408.
NOTE 5 These classes may also be used for hardwoods with similar strength and density profiles such as e.g. poplar or chestnut.
NOTE 6 The bending strength may be used in the case of edgewise or flatwise bending.

Figure 104: Strength classes of softwood based on bending tests (top) and tension (bottom) tests with their characteristic values retrieved from NEN-EN 338.

Strength classes for hardwoods based on edgewise bending tests – strength, stiffness and density values

	Class	D18	**D24**	D27	**D30**	D35	**D40**	D45	**D50**	D55	**D60**	D65	**D70**	D75	D80
Strength properties in N/mm²															
Bending	$f_{m,k}$	18	**24**	27	**30**	35	**40**	45	**50**	55	**60**	65	**70**	75	80
Tension parallel	$f_{t,0,k}$	11	**14**	16	**18**	21	**24**	27	**30**	33	**36**	39	**42**	45	48
Tension perpendicular	$f_{t,90,k}$	0,6	**0,6**	0,6	**0,6**	0,6	**0,6**	0,6	**0,6**	0,6	**0,6**	0,6	**0,6**	0,6	0,6
Compression parallel	$f_{c,0,k}$	18	**21**	22	**24**	25	**27**	29	**30**	32	**33**	35	**36**	37	38
Compression perpendicular	$f_{c,90,k}$	4,8	**4,9**	5,1	**5,3**	5,4	**5,5**	5,8	**6,2**	6,6	**10,5**	11,3	**12,0**	12,8	13,5
Shear	$f_{v,k}$	3,5	**3,7**	3,8	**3,9**	4,1	**4,2**	4,4	**4,5**	4,7	**4,8**	5,0	**5,0**	5,0	5,0
Stiffness properties in kN/mm²															
Mean modulus of elasticity parallel bending	$E_{m,0,mean}$	9,5	**10,0**	10,5	**11,0**	12,0	**13,0**	13,5	**14,0**	15,5	**17,0**	18,5	**20,0**	22,0	24,0
5 percentile modulus of elasticity parallel bending	$E_{m,0,k}$	8,0	**8,4**	8,8	**9,2**	10,1	**10,9**	11,3	**11,8**	13,0	**14,3**	15,5	**16,8**	18,5	20,2
Mean modulus of elasticity perpendicular	$E_{m,90,mean}$	0,63	**0,67**	0,70	**0,73**	0,80	**0,87**	0,90	**0,93**	1,03	**1,13**	1,23	**1,33**	1,47	1,60
Mean shear modulus	G_{mean}	0,59	**0,63**	0,66	**0,69**	0,75	**0,81**	0,84	**0,88**	0,97	**1,06**	1,16	**1,25**	1,38	1,50
Density in kg/m³															
5 percentile density	ρ_k	475	**485**	510	**530**	540	**550**	580	**620**	660	**700**	750	**800**	850	900
Mean density	ρ_{mean}	570	**580**	610	**640**	650	**660**	700	**740**	790	**840**	900	**960**	1020	1080

NOTE 1 Values given above for tension strength, compression strength, shear strength, char. modulus of elasticity in bending, mean modulus of elasticity perpendicular to grain and mean shear modulus, have been calculated using the equations given in EN 384.
NOTE 2 The tabulated properties are compatible with timber at moisture content consistent with a temperature of 20 °C and a relative humidity of 65 %, which corresponds to a moisture content of 12 % for most species.
NOTE 3 Characteristic values for shear strength are given for timber without fissures, according to EN 408.
NOTE 4 The edgewise bending strength may also be used in the case of flatwise bending.

Figure 105: Strength classes of hardwood based on bending tests with their characteristic values retrieved from NEN-EN 338.

C.3 Minimum spacings and edges for fasteners

The minimum spacings for dowels and bolts are shown below. These spacings are important for the minimum thickness of the web plate.

Spacing and end/edge distances (see Figure 8.7)	Angle	Minimum spacing or distance
a_1 (parallel to grain)	$0^\circ \le \alpha \le 360^\circ$	$(4 + \lvert\cos\alpha\rvert)\, d$
a_2 (perpendicular to grain)	$0^\circ \le \alpha \le 360^\circ$	$4\, d$
$a_{3,t}$ (loaded end)	$-90^\circ \le \alpha \le 90^\circ$	max (7 d; 80 mm)
$a_{3,c}$ (unloaded end)	$90^\circ \le \alpha < 150^\circ$ $150^\circ \le \alpha < 210^\circ$ $210^\circ \le \alpha \le 270^\circ$	[A1] $(1 + 6 \sin\alpha)\, d$ $4\, d$ $(1 + 6 \lvert\sin\alpha\rvert)\, d$ [A1]
$a_{4,t}$ (loaded edge)	$0^\circ \le \alpha \le 180^\circ$	max [$(2 + 2 \sin\alpha)\, d$; $3d$]
$a_{4,c}$ (unloaded edge)	$180^\circ \le \alpha \le 360^\circ$	$3\, d$

Figure 106: Minimum distance of bolts retrieved from NEN-EN 1995

Spacing and edge/end distances (see Figure 8.7)	Angle	Minimum spacing or edge/end distance
a_1 (parallel to grain)	$0^\circ \le \alpha \le 360^\circ$	$(3 + 2\lvert\cos\alpha\rvert)\, d$
a_2 (perpendicular to grain)	$0^\circ \le \alpha \le 360^\circ$	$3\, d$
$a_{3,t}$ (loaded end)	$-90^\circ \le \alpha \le 90^{0^\circ}$	max (7 d; 80 mm)
$a_{3,c}$ (unloaded end)	$90^{0^\circ} \le \alpha < 150^\circ$ $150^\circ \le \alpha < 210^\circ$ $210^\circ \le \alpha \le 270^\circ$	$\max(a_{3,t} \lvert\sin\alpha\rvert)\, d; 3d)$ $3\, d$ $\max(a_{3,t} \lvert\sin\alpha\rvert)\, d; 3d)$
$a_{4,t}$ (loaded edge)	$0^\circ \le \alpha \le 180^\circ$	$\max([2 + 2 \sin\alpha)\, d; 3d)$
$a_{4,c}$ (unloaded edge)	$180^\circ \le \alpha \le 360^\circ$	$3\, d$

Figure 107: Minimum distance of dowels retrieved from NEN-EN 1995

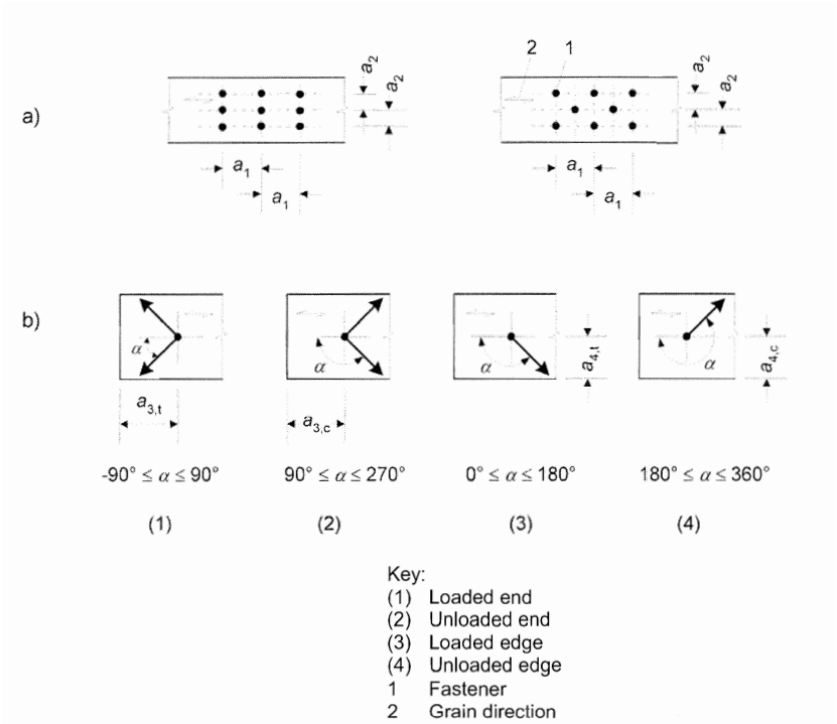

Figure 108: Illustration of minimum distance of fasteners retrieved from NEN-EN 1995

D. Hydraulic boundaries of the case study navigation lock

This appendix shows the hydraulic boundaries of the navigation lock of the case study. The eastern Sambeek navigation lock is chosen as case study location. The information is retrieved from Rijkswaterstaat, the Dutch directorate-general for public works and water management, and therefore written in Dutch.

Voor Sambeek geldt:

bovenhoofd Belfeld / Bovenhoofd Sambeek	waterstand boven [NAP + m]	waterstand beneden [NAP + m]	verval [m]
schutsluis in bedrijf			
waterkeren	11,90[1] (= 11,10 + 0,80[1])	7,70 (= 7,95 - 0,25)	4,20
nivelleren (vullen) in 12 min.	11,10	8,00	3,10

- *De genoemde waarden zijn conform tabel 3.3 van RWS/DMW-2009/4388, de hydraulische randvoorwaarden Oostsluizen Sambeek en Belfeld. Daarnaast geldt nog de volgende toevoeging:*

[1]) Stuwpeil + waterstandvariaties/windopzet/translatiegolven 0,30m + windgolven/scheepsgolven 0,60m (inclusief reflectie).

bovenhoofd Belfeld / Benedenhoofd Sambeek	waterstand boven [NAP + m]	waterstand beneden [NAP + m]	verval [m]
schutsluis in bedrijf			
waterkeren	11,90[1]	7,70	4,20
nivelleren (ledigen) in 9 min.	11,10	8,00	3,10

Feitelijk komt dit neer op;

Keren	11m90+NAP – 7m70+NAP
Nivelleren	11m10+NAP – 8m00+NAP

Figure 109: Information of case study location eastern Sambeek navigation lock (Rijkswaterstaat, unpublished)

The figure shows that the maximum differential head (verval) is 4.2 metres. With red characters it is pointed out that this differential head contains the water level difference, wind waves, translatory waves and ship waves.

E. Python scripts

This appendix shows the calculation of the loss factor of the mechanically jointed theory in the preliminary design.
As the preliminary design is iterative the calculation of the gamma factors is done in Python, the input and output is shown below.

```
import numpy as np
import matplotlib.pyplot as plt
%matplotlib inline
import pandas as pd
from pandas import read_csv
import math
```

```
#Input parameters:
rho = 800
d = 30
s = 200
L = 9470
A1 = 1500*150
A2 = 150*300
A3 = 300*300
E=20000
```

```
#total cross section
Ksls = rho**1.5*d/23
Kuls = 2/3*Ksls
kuls = Kuls/(s/1000)
gamma1 = 1/(1+(math.pi**2*E*A1*s/(kuls*L**2)))
gamma3 = 1/(1+(math.pi**2*E*A3*s/(kuls*L**2)))
ksls = Ksls/(s/1000)
gamma1sls = 1/(1+(math.pi**2*E*A1*s/(ksls*L**2)))
gamma3sls = 1/(1+(math.pi**2*E*A3*s/(ksls*L**2)))
```

```
print('Gamma1 and Gamma3 for ULS are',gamma1, gamma3)
print('Gamma1 and Gamma3 for SLS are',gamma1sls, gamma3sls)
```

```
Gamma1 and Gamma3 for ULS are 0.4983103969191456 0.7129044460688646
Gamma1 and Gamma3 for SLS are 0.5983768840737118 0.7883482005072818
```

```
#6 layered element ULS
E0 = 20000
E90 = 1330
alpha = 45
Ealpha = (E0*E90)/(E0*np.sin(alpha*math.pi/180)**2+E90*np.cos(alpha*math.pi/180)**2)
print('Ealpha is:',Ealpha)
E45 = Ealpha
A1 = 1500*25
A2 = 1500*25
A3 = 1500*25
Ksls = rho**1.5*d/23
Kuls = 2/3*Ksls
k = Kuls/(s/1000)
gamma1 = (k*L**2*(A1**2*E0**2*math.pi**2 + 5*A1*k*E0*L**2*math.pi**2 + 5*k**2*L**4))/\
(5*(A1**3*E0**3*math.pi**6 + A1**2*k*E0**2*L**2*math.pi**4 + 9*A1*k**2*E0*L**4*math.pi**2 + 2*k**3*L**6))
gamma2 = (2*k**3*L**6)/\
(A2**3*E90**3*math.pi**6 + A2**2*k*E90**2*L**2*math.pi**4 + 9*A2*k**2*E90*L**4*math.pi**2 + 2*k**3*L**6)
gamma3 = (2*(math.pi**2*E45*A3 + 3*k*L)*k**2*L**4)/\
(3*(A1**3*E45**3*math.pi**6 + A1**2*k*E45**2*L**2*math.pi**4 + 9*A1*k**2*E45*L**4*math.pi**2 + 2*k**3*L**6))
```

```
Ealpha is: 2494.13970933
```

```
print('Gamma1 is',gamma1)
print('Gamma2 is',gamma2)
print('Gamma3 is',gamma3)
```

```
Gamma1 is 0.49853713171290664
Gamma2 is 0.9997489953690293
Gamma3 is 0.000140406253833
```

```
# Laminated girder ULS 3 elements
rho = 800
d = 30
s = 200
E = 20000
A = 300*100
L = 9470
```

```
Ksls = rho**1.5*d/23
Kuls = 2/3*Ksls
k = Kuls/(s/1000)
gamma13 = 1/(1+(math.pi**2*E*A*s/(k*L**2)))
print('Gamma13 is',gamma13)
```

```
Gamma13 is 0.8816495582724433
```

```
#6 layers element SLS
Ksls = rho**1.5*d/23
k = Ksls/s
gamma1 = (k*L**2*(A1**2*E0**2*math.pi**2 + 5*A1*k*E0*L**2*math.pi**2 + 5*k**2*L**4))/\
(5*(A1**3*E0**3*math.pi**6 + A1**2*k*E0**2*L**2*math.pi**4 + 9*A1*k**2*E0*L**4*math.pi**2 + 2*k**3*L**6))
gamma2 = (2*k**3*L**6)/\
(A2**3*E90**3*math.pi**6 + A2**2*k*E90**2*L**2*math.pi**4 + 9*A2*k**2*E90*L**4*math.pi**2 + 2*k**3*L**6)
gamma3 = (2*(math.pi**2*E45*A3 + 3*k*L)*k**2*L**4)/\
(3*(A1**3*E45**3*math.pi**6 + A1**2*k*E45**2*L**2*math.pi**4 + 9*A1*k**2*E45*L**4*math.pi**2 + 2*k**3*L**6))
print('Gamma1 is',gamma1)
print('Gamma2 is',gamma2)
print('Gamma3 is',gamma3)
```

```
Gamma1 is 0.05641251816895296
Gamma2 is 0.8320205225767451
Gamma3 is 0.0185890240242
```

```
#Laminated girder SLS
Ksls = rho**1.5*d/23
k = Ksls/(s/1000)
gamma13 = 1/(1+(math.pi**2*E*A*s/(k*L**2)))
print('Gamma13 is',gamma13)
```

```
Gamma13 is 0.9178592404563529
```

```
#Equivalente girder
rho = 800
d = 30
s = 200
E = 20000
A = 300*100
L = 9400
Ksls = rho**(1.5)*d/23
Kuls =Ksls*2/3
k = Kuls/(s/1000)
gamma13 = 1/(1+((np.pi**2*E*A*s)/(k*L**2)))
print(k)
print('Gamma13 is',gamma13)
```

```
98380.07390421531
Gamma13 is 0.8800924729072689
```

F. Preliminary design calculations

This appendix shows the extended calculation and the outcomes of the preliminary design. The preliminary design consists of a global design, local design and fastener verification. The verification locations and a legend for the cross sections of the design verifications are shown in the figures below.

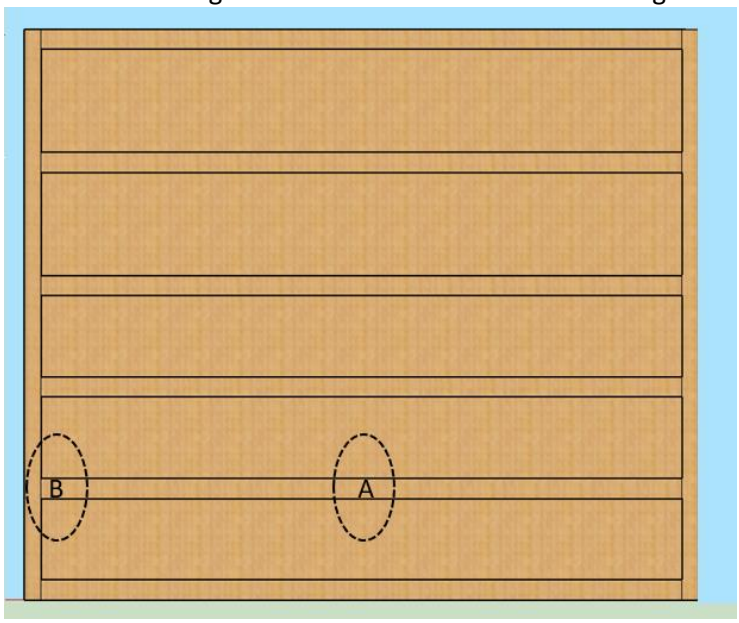

Figure 110: Verification locations of global preliminary design

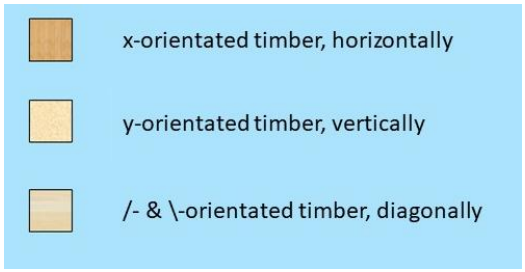

Figure 111: Legend for cross sections of preliminary design

Location A: Halfway the mitre gate (maximum distance between girder and skin plate)
The cross section halfway the mitre gate is shown in Figure 112.

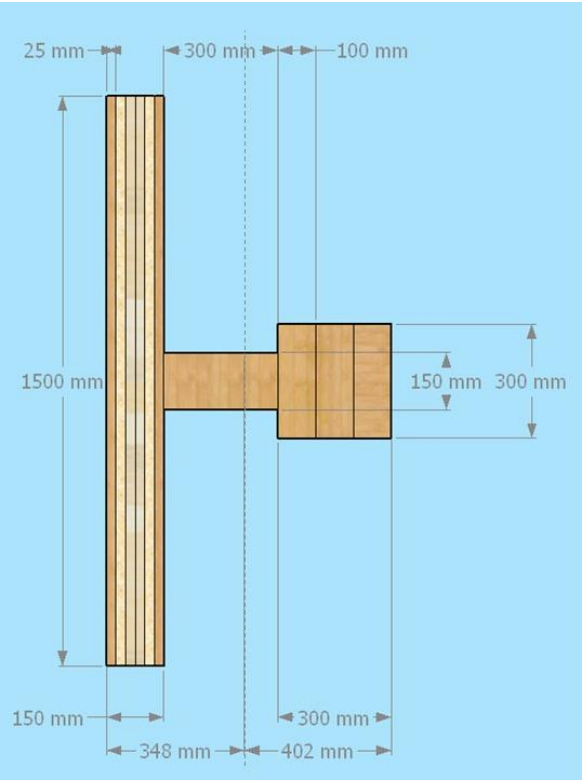

Figure 112: Side view of cross section halfway the mitre gate

The dimensions of the cross section are listed in Table 21.

	Height (mm)	Width (mm)
Skin layer 1 (effective)	1500	25
Skin layers 2-5	1500	100
Skin layer 6 (effective)	1500	25
Connection plate	150	300
Girder	300	300

Table 21: Dimensions of the cross section halfway the mitre gate

With the dimensions listed above, the characteristics are:

$$A_{eff} = 2.1 * 10^5 \text{ mm}^2$$
$$z_1 = 348 \text{ mm}$$
$$z_2 = 402 \text{ mm}$$
$$I_{eff} = 5.20 * 10^8 \text{ mm}^4$$
$$W_{eff,1} = 1.49 * 10^6 \text{ mm}^3$$
$$W_{eff,2} = 1.29 * 10^6 \text{ mm}^3$$

Where:
A [mm^2] = effective area
z_i [mm] = distance to the centre of gravity
I_i[mm^4] = moment of inertia around the i-axis
W_i[mm^3] = section modulus around the i-axis
For a three layered mechanically jointed beam NEN-EN 1995 shows the following stress distribution.

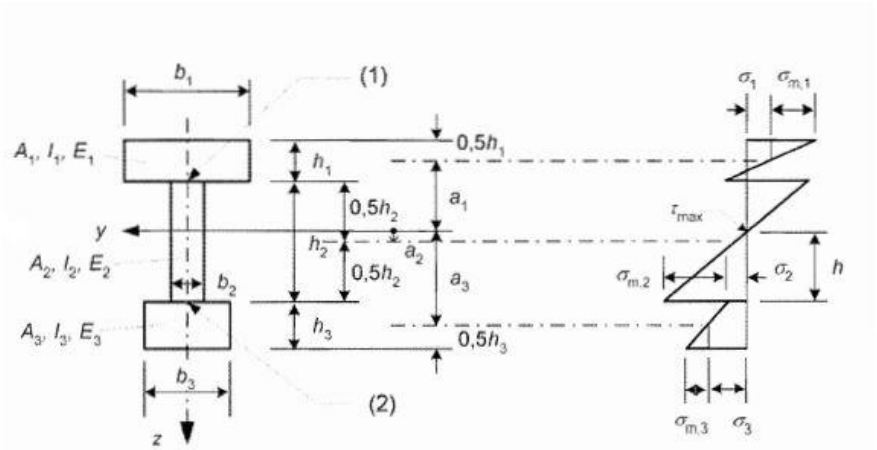

Figure 113: Cross section (left) and bending stress (right of mechanically jointed theory

The formula for the stress due to the bending moment is:

$$\sigma_{m,i,d} = E_i * \frac{M_{max}}{(EI)_{eff}} * \gamma_i * z$$

Where:
E_i [N/mm^2] = modulus of elasticity of the element
M_{max} [N/mm^2] = maximum bending moment
γ [-] = shear deformation reduction factor
z [mm] = maximum distance to the centre of gravity
This results in a maximum bending moment in the girder of:

$$\sigma_{m,y,d} = 12.1 \text{ N/mm}^2$$

And in the cross laminated skin plate:

$$\sigma_{m,y,d} = 7.9 \text{ N/mm}^2$$

The compressive stress is determined by:

$$\sigma_{c,0,d} = \frac{N}{A} = 6.0 \text{ N/mm}^2$$

Halfway the mitre gate the shear force is zero and therefore the shear stress halfway the mitre gate is zero too.

Not only cross sectional checks are given in the Eurocode, but stability checks and curving checks are prescribed too. The combined compression and bending verification taken from section 6.3.2 of NEN-EN 1995 contains the following instability factors:

$$k_m = 0.7$$

$$k_{c,y} = \frac{1}{k_y + \sqrt{k_y^2 - \lambda_{rel,y}^2}} = 1.0$$

$$k_{c,z} = \frac{1}{k_z + \sqrt{k_z^2 - \lambda_{rel,z}^2}} = 1.0$$

$$k_y = 0.5\left(1 + \beta_c\left(\lambda_{rel,y} - 0.3\right) + \lambda_{rel,y}^2\right) = 0.49$$

$$k_z = 0.5\left(1 + \beta_c\left(\lambda_{rel,z} - 0.3\right) + \lambda_{rel,z}^2\right) = 0.49$$

k_y or k_z [-] = instability factor
β_c [-] = straightness factor, 0.1

$$\lambda_{rel,y} = \frac{\lambda_y}{\pi}\sqrt{\frac{f_{c,0,k}}{E_{0.05}}} = 0.22$$

$$\lambda_{rel,z} = \frac{\lambda_z}{\pi}\sqrt{\frac{f_{c,0,k}}{E_{0.05}}} = 0.08$$

$$\lambda_y = \frac{L_y}{i_y} = 13.25$$

$$\lambda_z = \frac{L_z}{i_z} = 5.12$$

λ_y or λ_z [-]= slenderness of cross section

i_y or i_z [mm] = radius of gyration

For the curved laminated girder the flexural buckling is described in Section 6.3.3 of NEN-EN 1995.

$$\lambda_{rel,m} = \sqrt{\frac{f_{m,k}}{\sigma_{m,crit}}} = 0.35$$

$$\sigma_{m,crit} = \frac{\pi * \sqrt{E_{0.05} I_z G_{0.05} I_{tor}}}{l_{ef} W_y} = 599.3 \text{ N/mm}^2$$

$G_{0.05}$ [N/mm^2] = 5th percentile shear modulus

I_t [mm^4] = torsional moment of inertia

The curving factors are obtained from Section 6.4.3 of NEN-EN 1995:

$$k_r = \begin{cases} 1, for\ \frac{r_{in}}{t} \geq 240 \\ 0.76 + 0.001\frac{r_{in}}{t}, for\ \frac{r_{in}}{t} \leq 240 \end{cases} = 0.85$$

$$k_l = k_1 + k_2\left(\frac{h_{ap}}{r}\right) + k_3\left(\frac{h_{ap}}{r}\right)^2 + k_4\left(\frac{h_{ap}}{r}\right)^3 = 1.0$$

α_{ap} [rad] = angle in the middle of tapered beam

r [mm] = radius of curvature from half the height of the beam

h_{ap} [mm] = height of the laminated beam

$$k_1 = 1 + 1.4\tan(\alpha_{ap}) + 5.4\tan^2(\alpha_{ap}) = 1$$

$$k_2 = 0.35 - 8\tan(\alpha_{ap}) = 0.4$$

$$k_3 = 0.6 + 8.3\tan(\alpha_{ap}) - 7.8\tan^2(\alpha_{ap}) = 0.6$$

$$k_4 = 6\tan^2(\alpha_{ap}) = 0$$

$$r = r_{in} + 0.5h_{ap} = 28393 \text{ mm}$$

r_{in} [mm] = inner radius of curvature

For the preliminary design the stability verification and curvature verification is not checked further. As can be seen in the formulas above the stability factor, k_c, and curving factor, k_l, are equal to 1 and therefore not significant in the preliminary design. Therefore the cross sectional checks are from importance in this thesis.

B: At side of mitre gate (minimum distance between beam and skin plate)

The outcome of the preliminary design for the cross section at the side of the mitre gate is shown below.

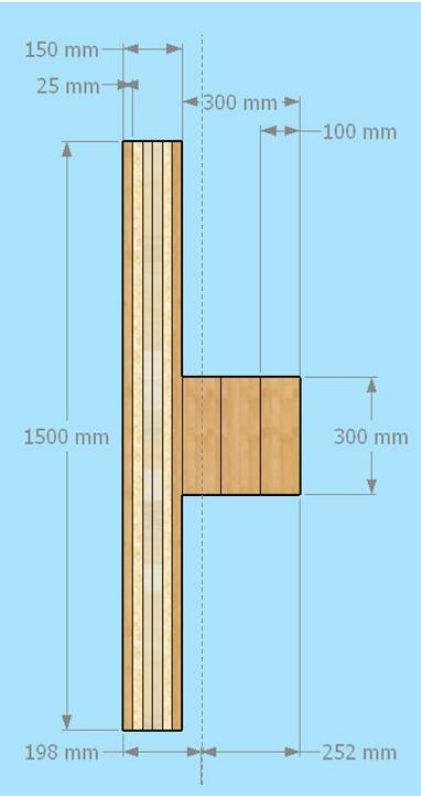

Figure 114: Side view of cross section at the side of mitre gate

The dimensions of the cross section are shown in Table 22.

	Height (mm)	Width (mm)
Skin layer 1 (effective)	1500	25
Skin layer 2-5	1500	100
Skin layer 6 (effective)	1500	25
Web plate	0	0
Girder	300	300

Table 22: Dimensions of the cross section at the side of mitre gate

With the dimensions listed above, the characteristics are:

$$A = 1.65 * 10^5 \text{ mm}^2$$
$$z_1 = 198 \text{ mm}$$
$$z_2 = 252 \text{ mm}$$
$$I_{eff} = 1.37 * 10^9 \text{ mm}^4$$
$$W_{eff,1} = 6.93 * 10^6 \text{ mm}^3$$
$$W_{eff,2} = 5.43 * 10^6 \text{ mm}^3$$

The bending moment at the side of the mitre gate is introduced by the eccentric loaded normal force. This results in a stress in the girder of:

$$\sigma_{m,y,d} = 11.4 \text{ N/mm}^2$$

And in the cross laminated skin plate:

$$\sigma_{m,y,d} = 8.7 \text{ N/mm}^2$$

The compressive stress is determined by:

$$\sigma_{c,0,d} = \frac{N}{A} = 7.7 \text{ N/mm}^2$$

The shear stress at the side of the mitre is determined by:

$$\tau_d = \frac{V * S_a}{b_{ef} I} = 1.3 \text{ N/mm}^2$$

Where:
S_a [mm^3] = the statical moment of area
b_{ef} [mm] = effective width of the cross section

C: Local design of skin plate
The outcome of the preliminary design for the cross section of the skin plate of the mitre gate is shown below. These characteristics are used for the local design.
As told in Section 5.4.4 a slice of one metre width is taken to perform the local design on. The dimensions of the cross section are b = 1000 millimetres, h = 25 millimetres. Because the supports of the continuous beam are at the connection of the web the skin plate, the girder and web plate are not taken into account for the local calculation. For this calculation the two outer (layer 1 & 6, horizontally orientated) and two inner (layer 3 & 4, diagonally orientated) layers of the cross laminated timber plate have no contribution in the strength of the plate and are therefore not taken into account in the cross section. The effective layers and taken slice for the calculation can be seen in Figure 45.

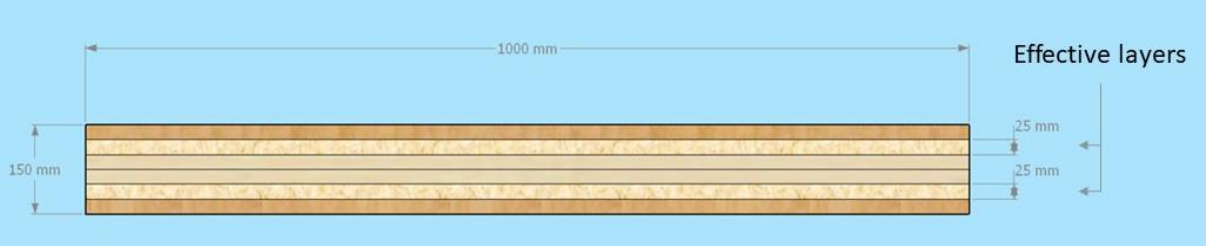

Figure 115: Top view of cross section of skin plate for local design, side view

The dimensions of the cross section are shown in Table 23.

	Height (mm)	Width (mm)
Skin layer 1	1000	25
Skin layer 2 (effective)	1000	25
Skin layer 3 & 4	1000	50
Skin layer 5 (effective)	1000	25
Skin layer 6	1000	25

Table 23: Dimensions of the cross section of the skin plate for local design

With the dimensions listed above, the characteristics are:

$$A_{eff} = 5 * 10^4 \text{ mm}^2$$
$$z = 50 \text{ mm}$$
$$I_{eff} = 7.29 * 10^7 \text{ mm}^4$$
$$W_{eff} = 1.46 * 10^6 \text{ mm}^3$$

The stress due to the local bending moment in the cross laminated skin plate is:

$$\sigma_{m,z,d} = 6.7 \text{ N/mm}^2$$

In the schematization of the local design no normal force is present. The compressive stress therefore is zero. The shear stress in the local design of the mitre is determined by:

$$\tau_d = \frac{\gamma_{11} * E_1 * A_{11} * z_{11} + \gamma_{12} * E_2 * A_{12} * z_{12} + \gamma_{13} * E_3 * A_{13} * z_{13}}{b_{skinplate} * EI_{eff}} * V = 0.74 \text{ N/mm}^2$$

Fastener verification
For the calculation of the load on the fastener the input values for the formula of the load on the fastener are given in Table 24. The formula for the load on the fastener is: $F = \frac{\gamma_i E_i A_i a_i s_i}{EI_{eff}} V$

	value	Unit
$(EI)_{eff}$	$3.8*10^{14}$	Nmm^2
V_d	438770	N

E	20000	Nmm^2
s	200	mm
γ_1	1	-
A_1	30000	mm^2
a_1	100	mm

Table 24: Values for the load on the fastener

G. Detailing joint post, girder and skin plate

This appendix shows the detailing of the preliminary design. First, the now common connection of the girder with the post, the mortise and tenon joint is shown and is demonstrated why this connection is not used for the renewed design of the mitre gate. Second, the replacement design of the mortise and tenon joint is shown.

Mortise and tenon joint

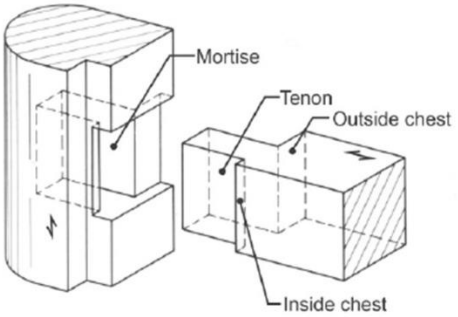

Figure 116: Design mortise and tenon joint (Van Leusen, 1991)

In the current design the total normal force in the structure is transferred by the girder. This girder is acting perpendicular on the fibres of the post and therefore the strength of the girder is relatively low compared to the strongest axis, $f_{c,90,d} = 6.5\ \mathrm{N/mm^2}$ and $f_{c,0,d} = 19.4\ \mathrm{N/mm^2}$. The design value of the normal force of the mitre gate in the preliminary design is 1267 kN. First hand calculations prove that the minimum required contact area to withstand the normal force is.

$$A_{req} = \frac{N_d}{f_{c,90,d}} = 194923\ \mathrm{mm^2}$$

This requires a 442 x 422 mm squared or 300 x 650 mm rectangular cross section of the post by only verifying the compression. The mortise and tenon also contains a bending moment by the eccentricity of the normal force. If the eccentricity for example is 200 mm, this results in a bending moment of 253 kNm.

$$\frac{\frac{N_d}{A}}{f_{c,0,d}} + \frac{\frac{N * e * z}{I}}{f_{m,y,d}} \leq 1$$

Filling in the formula below this requires a squared cross section of 540 x 540 mm. For this design only an average differential head and average navigation lock width is used. In case of widener mitre gates or bigger differential heads the cross sections should be even bigger and thus the expectation is that the available dimensions are not existing.

Continuous girder design

To implement the renewed design in the new application range up to 24 metres wide navigation locks, another solution for the mortise and tenon joint is used. The girder of the redesign is continued and directly supporting the lock chamber wall. The post of the mitre gate is interrupted at the location of the girder. With this design the girder is loaded in the direction of the fibre, which is preferable as it is the strongest direction of timber. In the figures below an overview and top views of the continuous girder are shown.

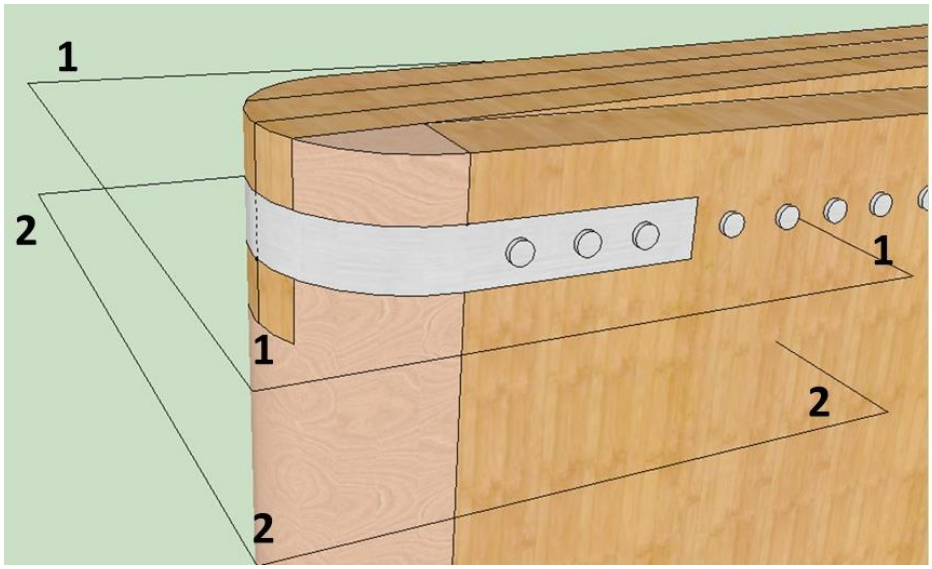

Figure 117: Overview joint post, girder and skin plate with indicated sections

The first section of the joint of the post, girder and skin plate is shown below.

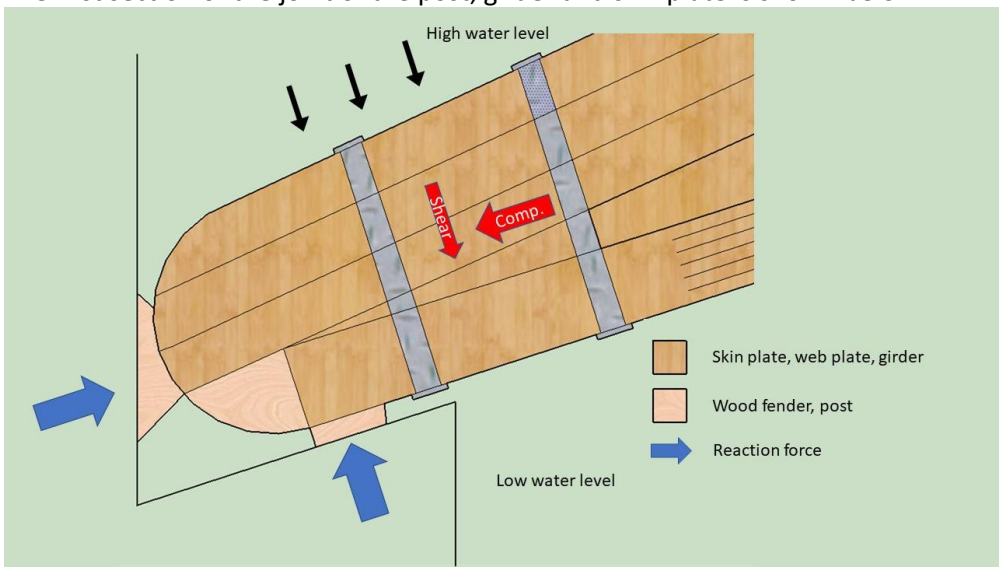

Figure 118: Top view detail end post girder and skin plate detail

A top view of the second section is shown in Figure 119. As can be seen this is at the location where the girder is not present in the cross section, as the girder and web plate are indicated with different colours.

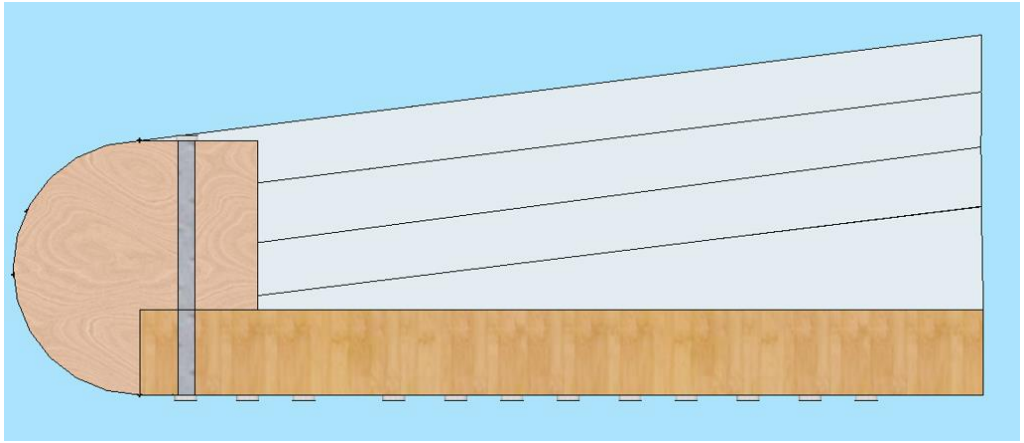
Figure 119: Top view joint laminated skin plate and end post

The force on the lock chamber wall caused by the girder is equal to the normal force in the girder:

$$N_{lock,d} = \frac{N}{A_{eff,cross\ section}} * A_{girder} = \frac{-1267}{2.1 * 10^5} * (300 * 300) = -543\ \text{kN}$$

The required contact area of the girder with the lock chamber wall for the renewed design becomes:

$$A_{req} = \frac{N_{lock,d}}{f_{c,0,d}} = \frac{543 * 10^3}{19.4} = 27989\ \text{mm}^2$$

This requires a squared contact area of 167x167mm or a contact area of 93 mm width over the total height of the girder, 300 mm, to transfer the force of the girder to the concrete lock chamber wall. Furthermore, as concrete has a higher resistance than timber the concrete lock chamber wall is not governing. For the verification of the normal force on the post the skin plate, the effective normal force on the post caused by the skin plate is:

$$N_{post,d} = \frac{N}{A_{eff,cross\ section}} * A_{eff,skin\ plate} = \frac{-1267}{1.65 * 10^5} * (2 * 1500 * 25) = -165\ \text{kN}$$

$$\sigma_{N,post,d} = \frac{N_{post,d}}{A_{eff,skin\ plate}} = \frac{-165 * 10^3}{2 * 1500 * 25} = 2.2\ \text{N/mm}^2$$

$$f_{c,90,d} = 6.5\ \text{N/mm}^2 < \sigma_{N,post}$$

The shear force of the skin plate is transferred before reaching the end post and therefore this check is not required.

The transfer of the normal force in the girder at the connecting mitre gate side is based on the same principle, but the layout is slightly different as can be seen in Figure 120.

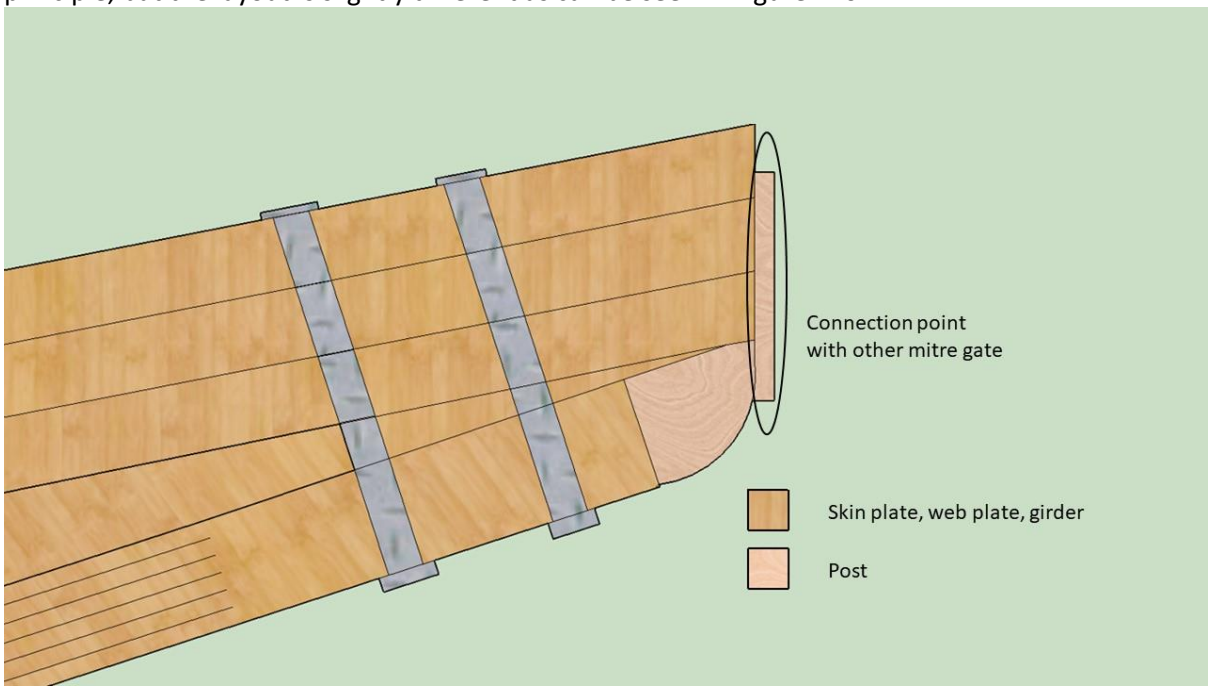

Figure 120: Top view front post, girder and skin plate detail.

H. SCIA results of test models A and B

In this appendix, the outcomes of the test models made in SCIA are shown. These test models simulate dowel cross laminated panels of 2 x 2 metres. First, the outcome of the different type of loading on the structure is shown. After that the results of the test panels, model A and B are shown.

Different type of loading

The transfer of the load to the underlying layers of the laminated panels is done through the dowels. To check if the load distribution is actually through the dowels and not through the beams, two different types of loading are set up on the test model and compared to each other. The first type of loading, LC2 is with a distributed load over the span. The second type of loading, LC_3, is with point loads on the location of dowels. In Figure 121 negligible difference in the bending moment diagrams can be seen on the different type of loading.

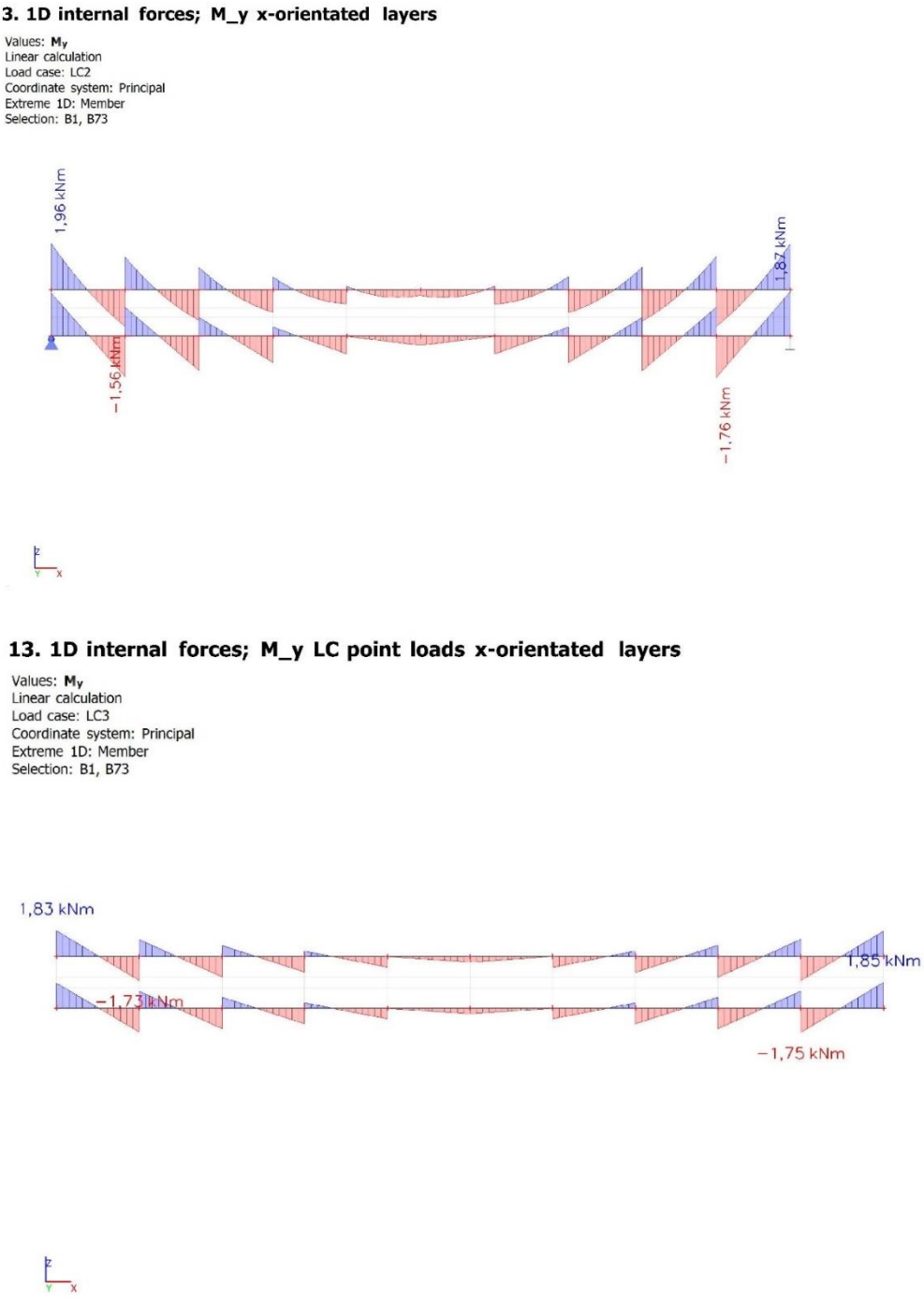

Figure 121: Bending moment diagrams by uniform loading (top) and point loading (bottom) on the test panel

For the shear force distribution initially it seems that there is a difference between uniform loading and point loading. The maximum shear force of the first type of loading is higher, however this load is decreasing towards the first dowel. The mean shear force between the dowels of LC2 is equal to the shear force of LC3.

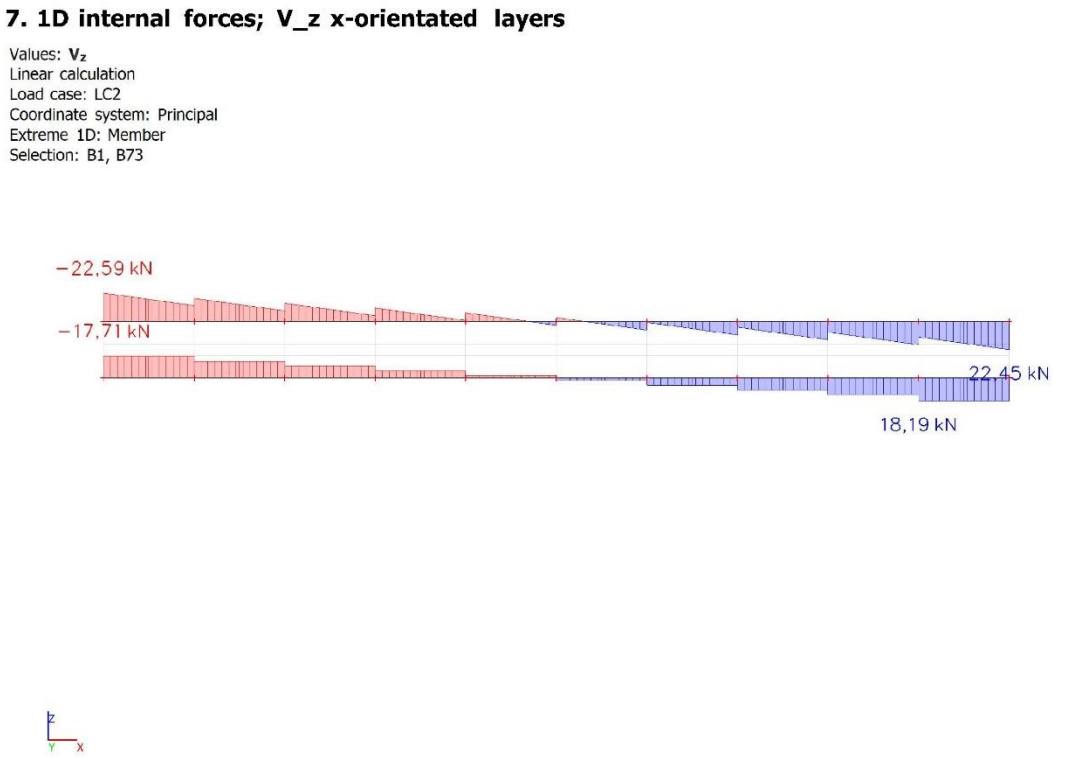

Figure 122: Shear force diagrams by uniform loading (top) and point loading (bottom) on the test panel

H.1 Results test model A

The results of SCIA for the totally fixed connected model, modal A are shown below.

1. Dowel with fixed links

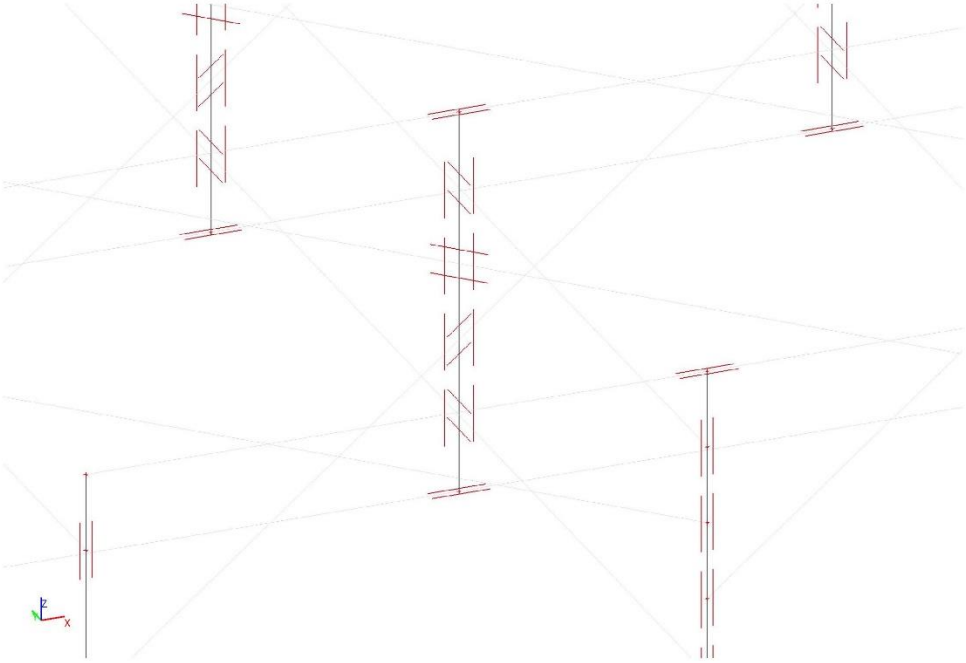

A. Laminated plate test:

Reactions
Values: **Rz**
Linear calculation
Load case: LC2
System: Global
Extreme: Member
Selection: All

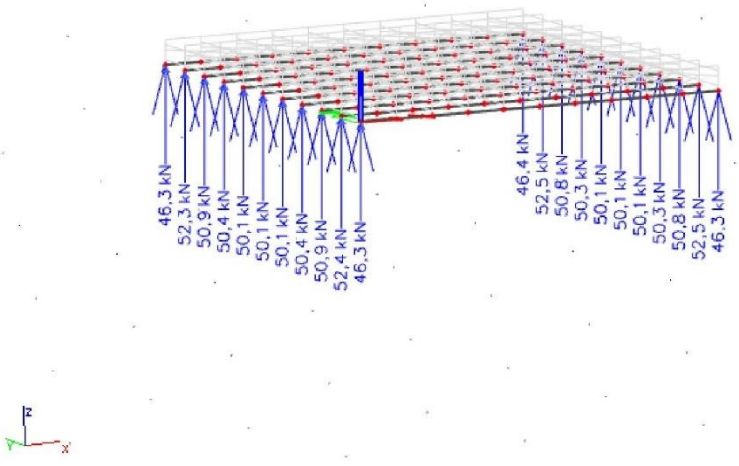

2. 3D displacement; u_z

Values: u_z
Linear calculation
Load case: LC2
Selection: All
Location: In nodes avg. on macro.
System: LCS mesh element

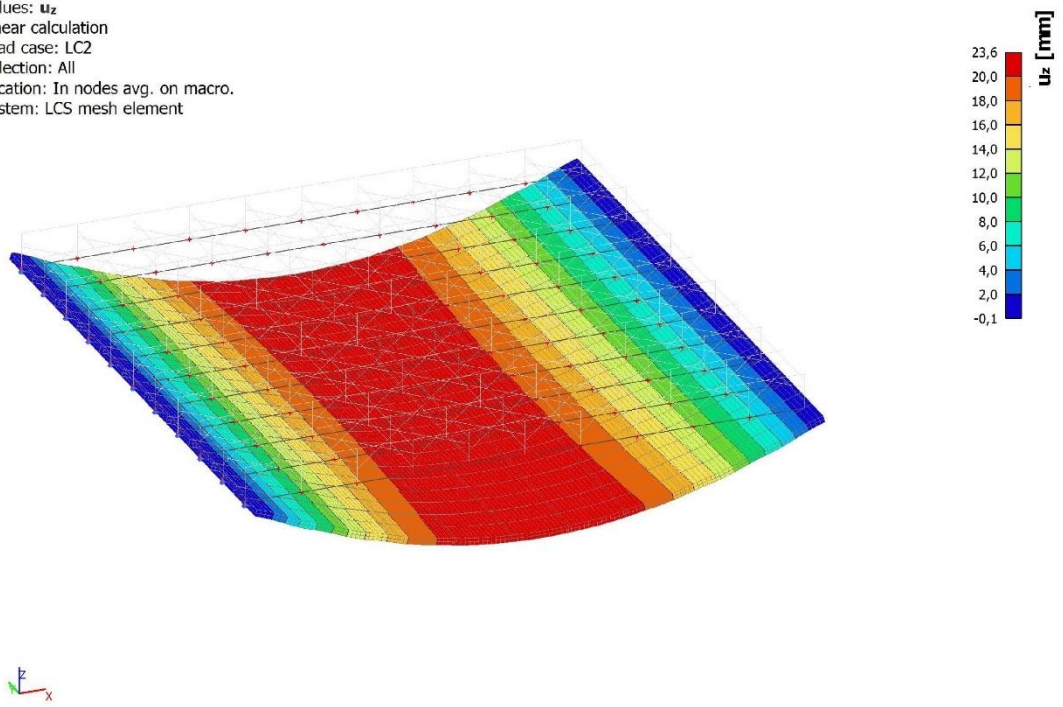

3. 1D internal forces; M_y x-orientated layers

Values: M_y
Linear calculation
Load case: LC2
Coordinate system: Principal
Extreme 1D: Member
Selection: B1, B73

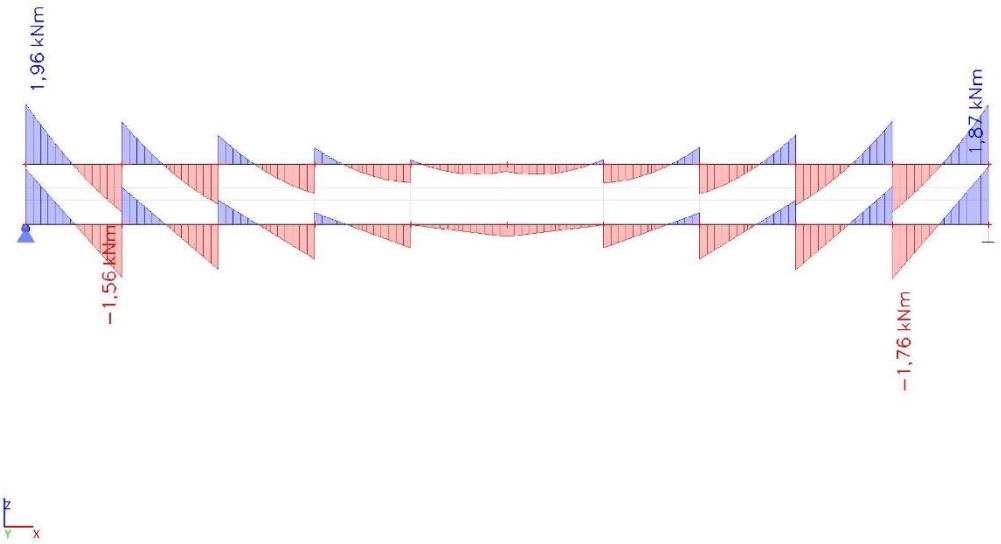

4. 1D internal forces; M_y y-orientated layers

Values: M_y
Linear calculation
Load case: LC2
Coordinate system: Principal
Extreme 1D: Cross-section
Selection: All

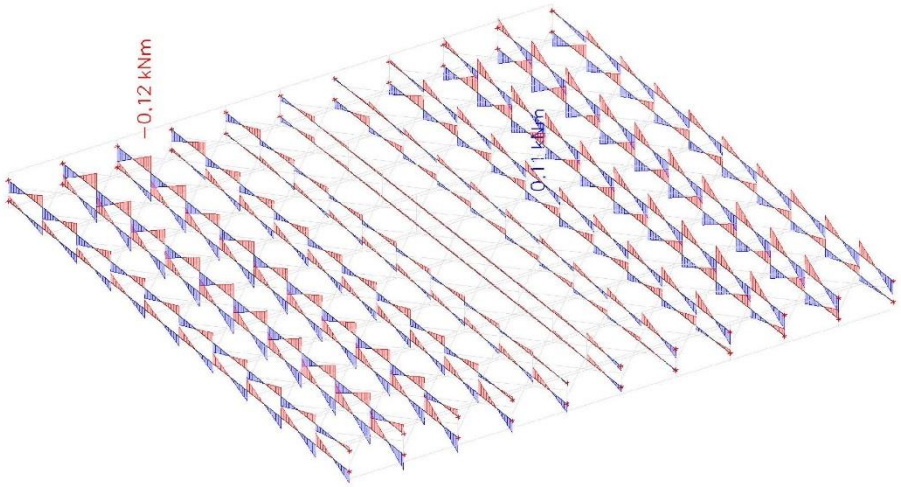

5. 1D internal forces; M_y \-orientated diagonal

Values: M_y
Linear calculation
Load case: LC2
Coordinate system: Principal
Extreme 1D: Cross-section
Selection: All

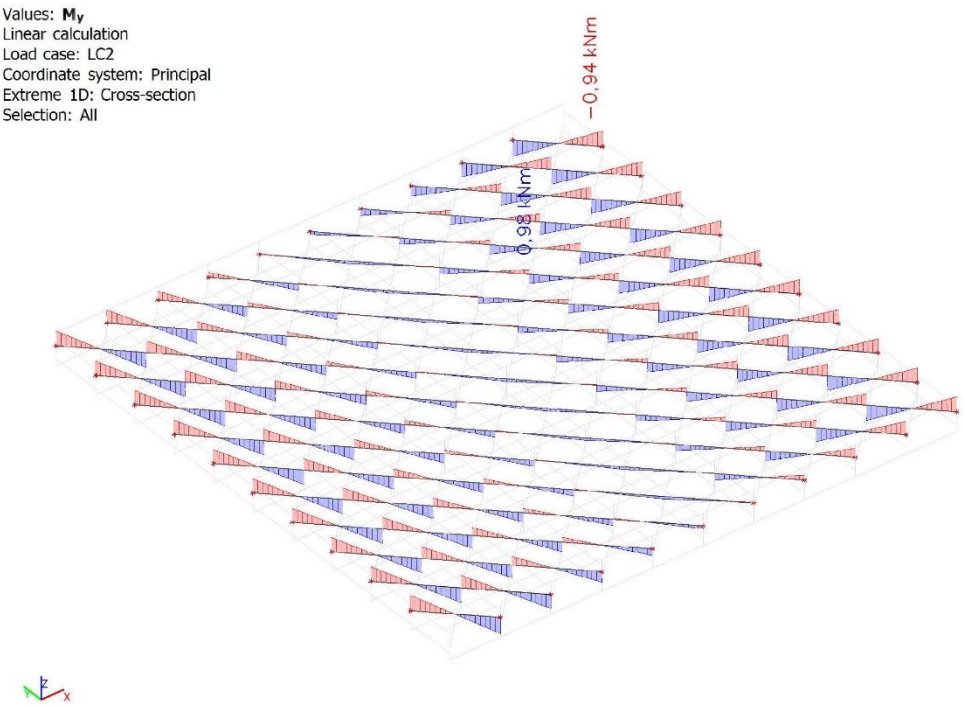

6. 1D internal forces; M_y /-orientated diagonal

Values: M_y
Linear calculation
Load case: LC2
Coordinate system: Principal
Extreme 1D: Cross-section
Selection: All

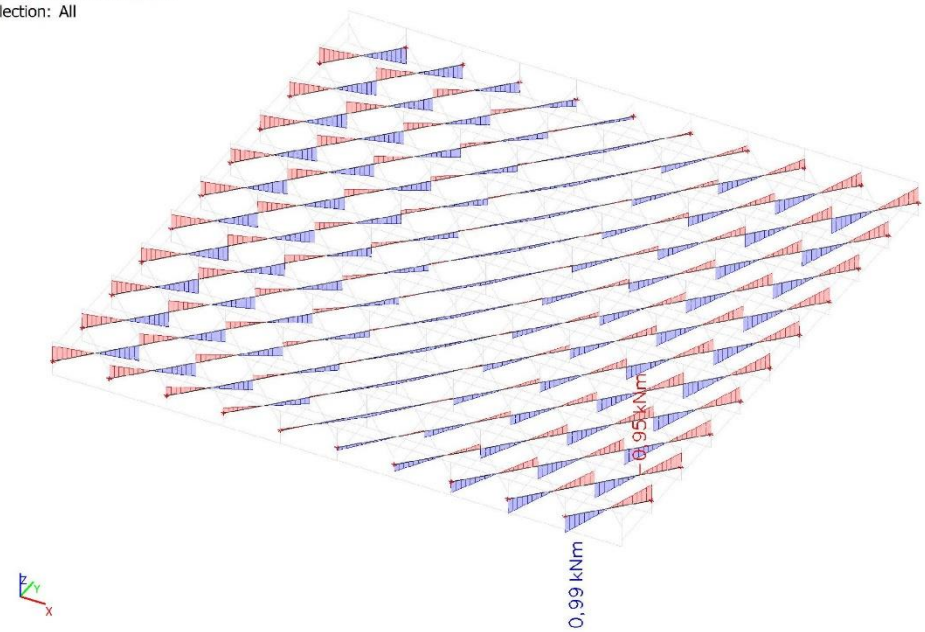

7. 1D internal forces; V_z x-orientated layers

Values: V_z
Linear calculation
Load case: LC2
Coordinate system: Principal
Extreme 1D: Member
Selection: B1, B73

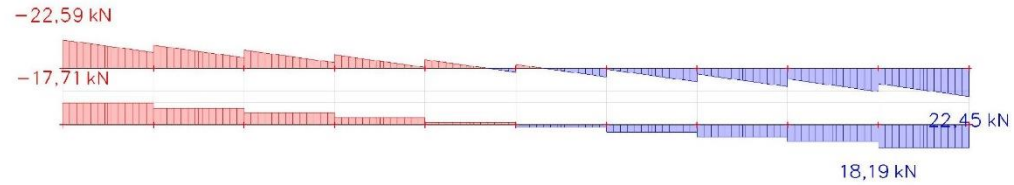

8. 1D internal forces; V_z y-orientated layers

Values: V_z
Linear calculation
Load case: LC2
Coordinate system: Principal
Extreme 1D: Cross-section
Selection: B12, B63

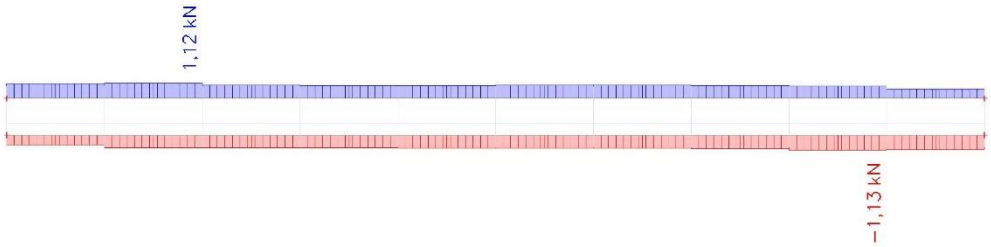

9. 1D internal forces; V_z \-orientated layers

Values: V_z
Linear calculation
Load case: LC2
Coordinate system: Principal
Extreme 1D: Cross-section
Selection: All

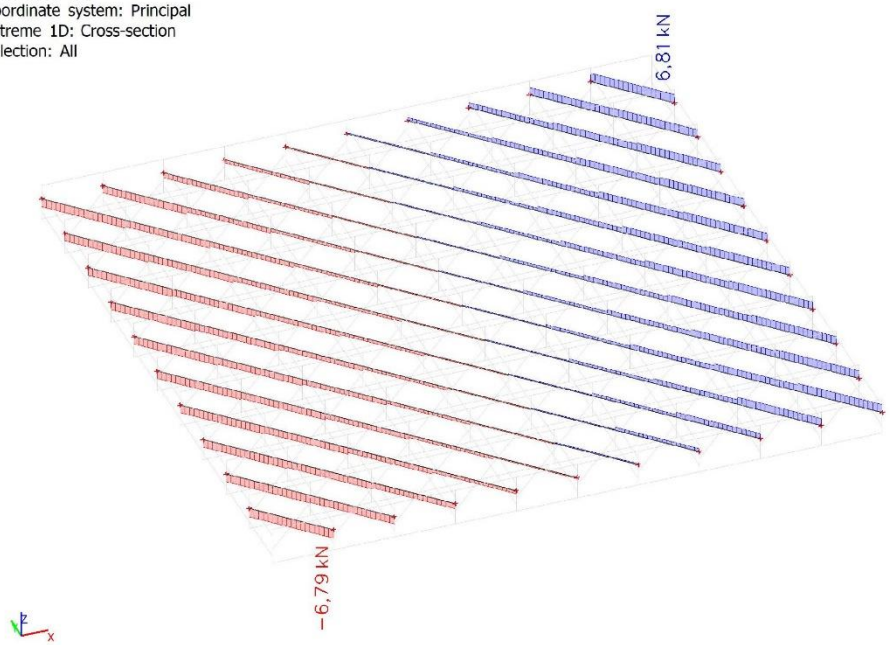

10. 1D internal forces; V_z /-orientated diagonal

Values: V_z
Linear calculation
Load case: LC2
Coordinate system: Principal
Extreme 1D: Cross-section
Selection: All

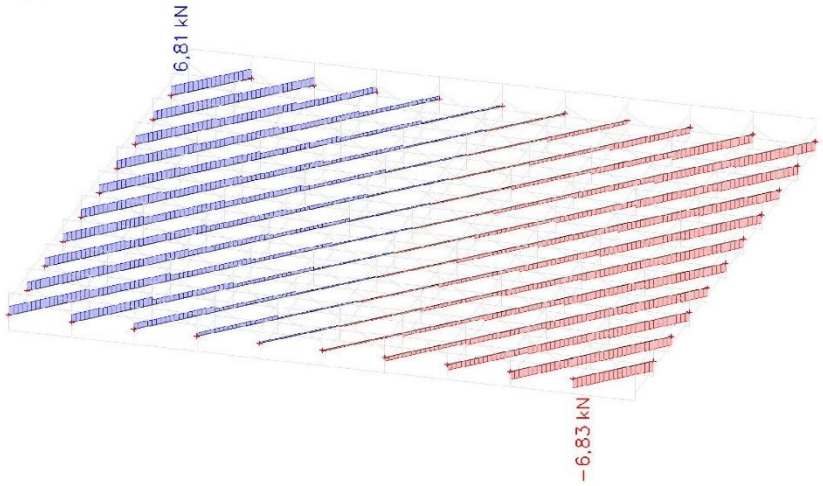

1. 1D internal forces; N x-orientated layer 1

Values: **N**
Linear calculation
Load case: LC2
Coordinate system: Principal
Extreme 1D: Member
Selection: All

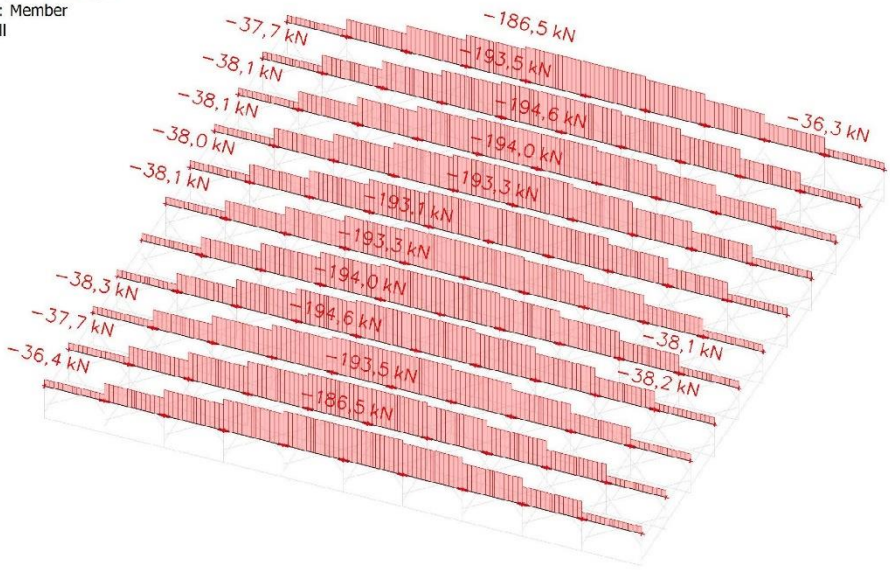

2. 1D internal forces; N y-orientated layer 2

Values: **N**
Linear calculation
Load case: LC2
Coordinate system: Principal
Extreme 1D: Member
Selection: All

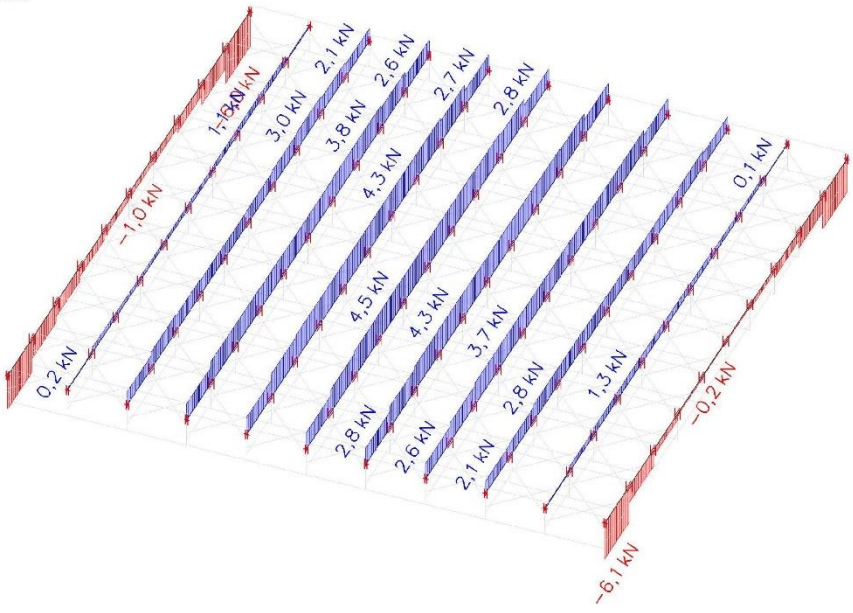

3. 1D internal forces; N \-orientated layer

Values: **N**
Linear calculation
Load case: LC2
Coordinate system: Principal
Extreme 1D: Member
Selection: All

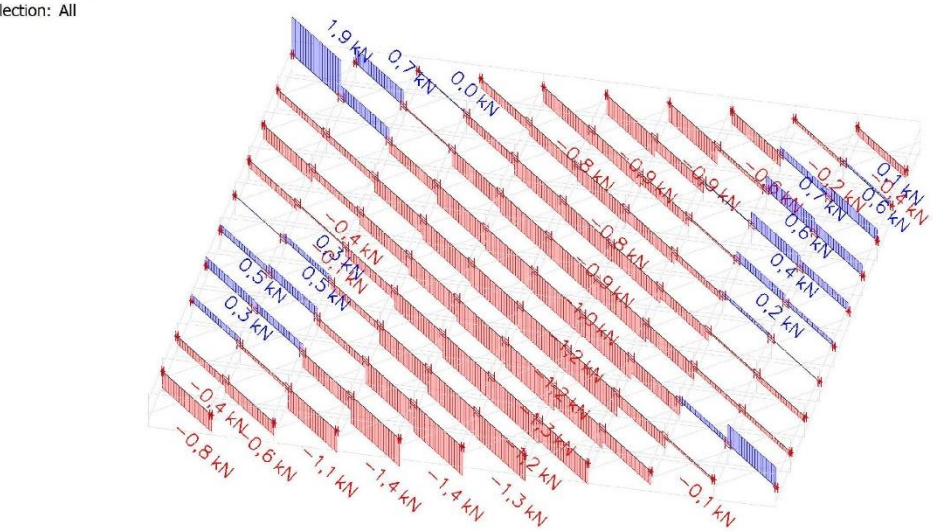

4. 1D internal forces; N /-orientated diagonal

Values: **N**
Linear calculation
Load case: LC2
Coordinate system: Principal
Extreme 1D: Member
Selection: All

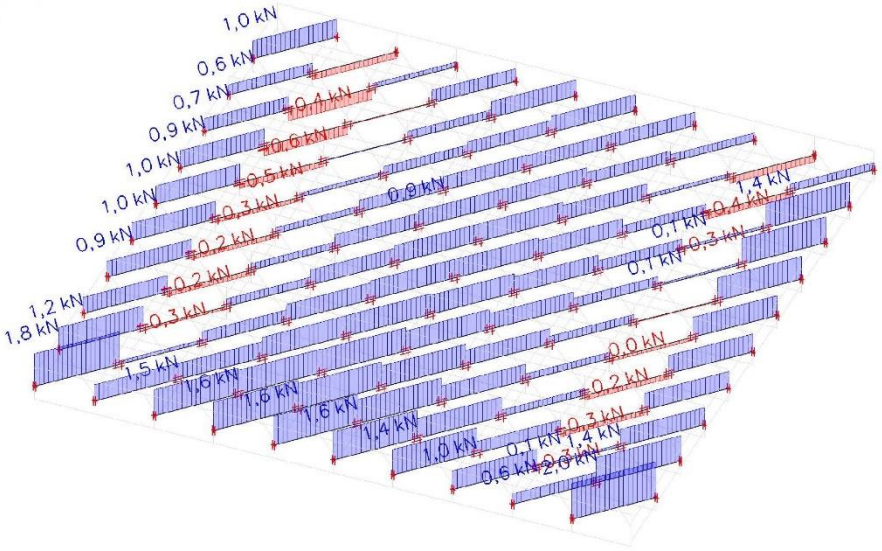

5. 1D internal forces; N y-orientated layer 5

Values: **N**
Linear calculation
Load case: LC2
Coordinate system: Principal
Extreme 1D: Member
Selection: All

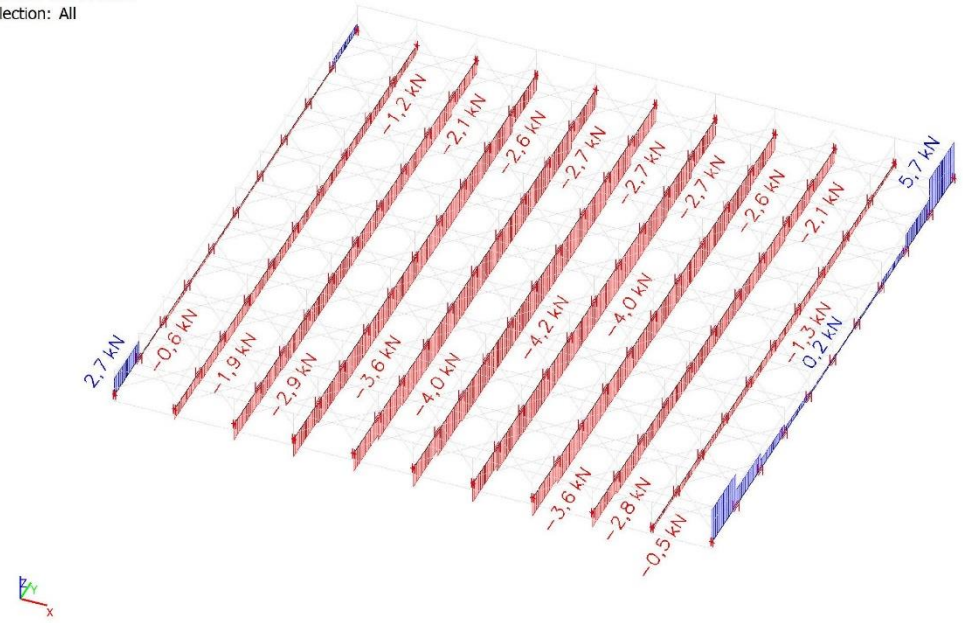

6. 1D internal forces; N x-orientated layer 6

Values: **N**
Linear calculation
Load case: LC2
Coordinate system: Principal
Extreme 1D: Member
Selection: All

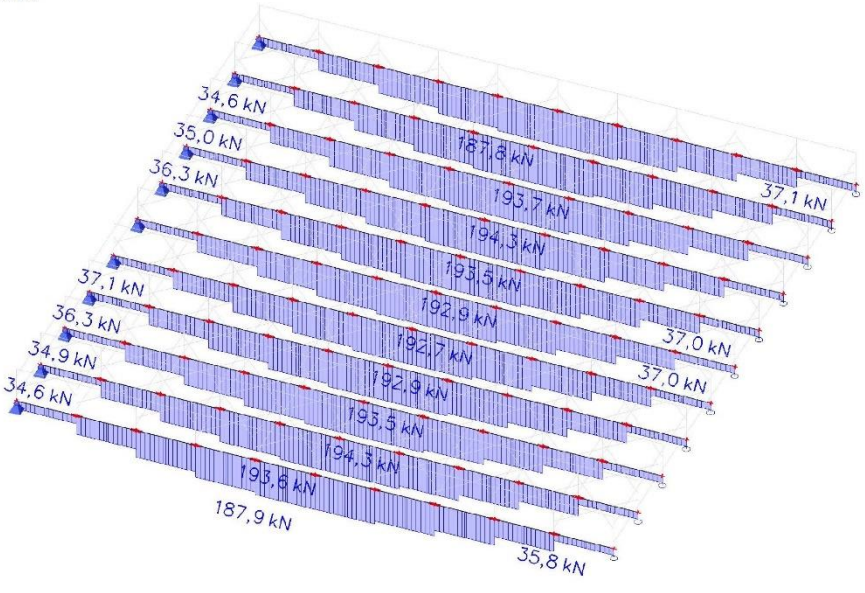

11. 1D internal forces; M_y Dowels

Values: M_y
Linear calculation
Load case: LC2
Coordinate system: Principal
Extreme 1D: Member
Selection: B84..B87, B90..B94

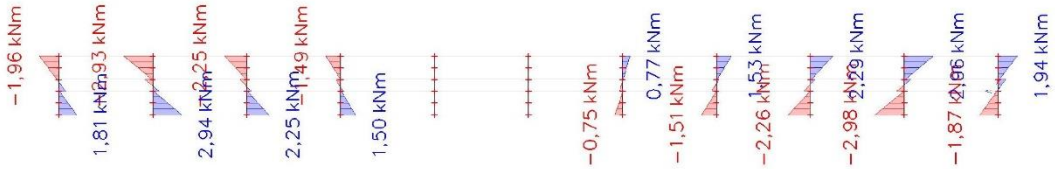

12. 1D internal forces; V_z Dowels

Values: V_z
Linear calculation
Load case: LC2
Coordinate system: Principal
Extreme 1D: Global
Selection: B84..B94

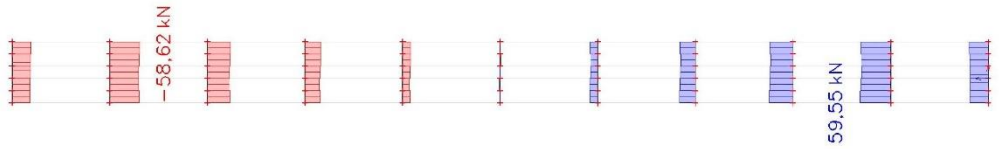

1. Displacement of nodes; U_x

Values: $\mathbf{U_x}$
Linear calculation
Load case: LC2
Extreme: Global
Selection: N1..N40, N43..N49, N51, N53, N55, N57, N59, N61, N63, N65, N67..N373

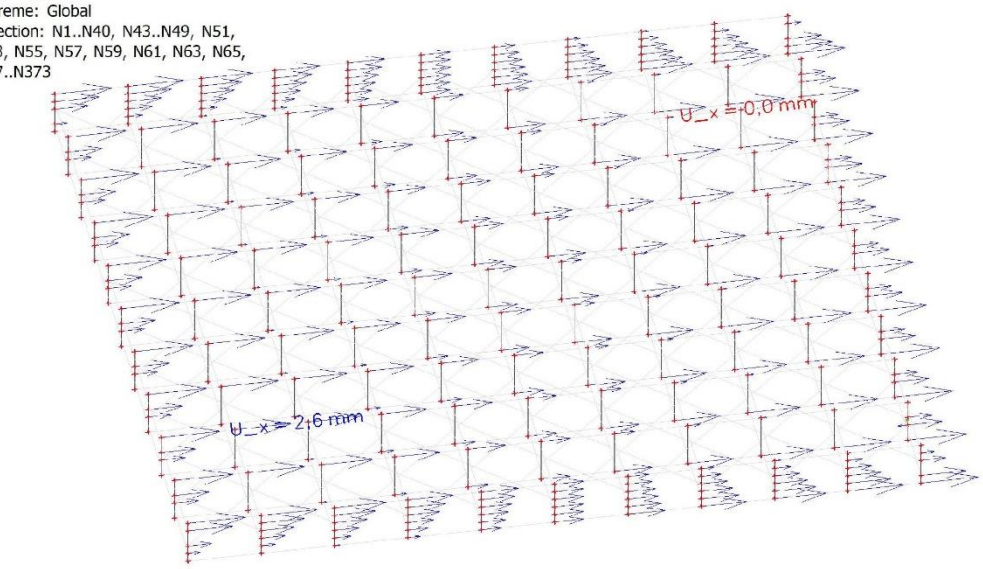

2. Displacement of nodes; U_x Dowels 1, 3, 5, 6

Values: $\mathbf{U_x}$
Linear calculation
Load case: LC2
Extreme: Node
Selection: N1, N21, N25, N29, N31, N47, N77, N79, N80, N94, N97, N106, N108, N132, N136, N140, N142, N154, N178, N179, N182..N185

3. Displacement of nodes; U_x Dowels 6, 7, 9, 11

Values: U_x
Linear calculation
Load case: LC2
Extreme: Node
Selection: N2, N31, N33, N37, N45,
N48, N80, N81, N83, N96, N100,
N104, N106, N142, N144, N148, N152,
N155, N184..N187, N190, N191

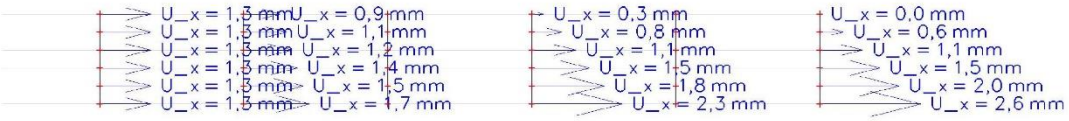

H.2 Results test model B

The results of SCIA for the model with the interaction of the dowel with panel based on the slip modulus of dowels from the NEN-EN 1995 are shown below.

1. Dowel layout

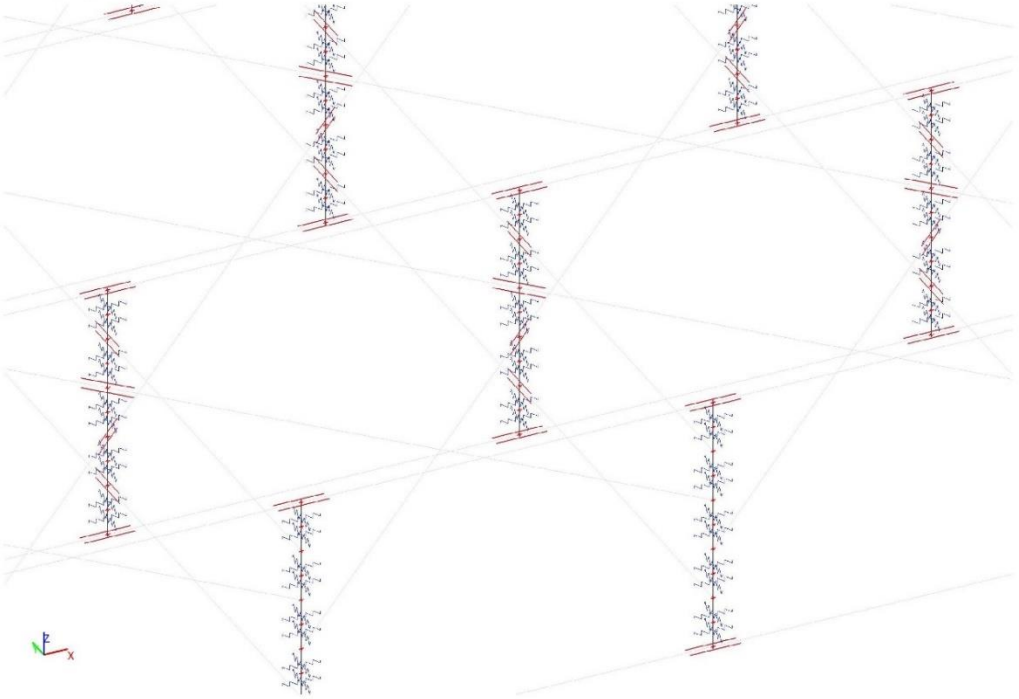

Reactions
Values: R_z
Linear calculation
Load case: LC2
System: Global
Extreme: Member
Selection: All

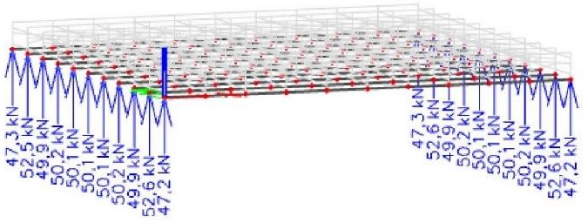

2. 3D displacement; u_z

Values: u_z
Linear calculation
Load case: LC2
Selection: All
Location: In nodes avg.. System: Global

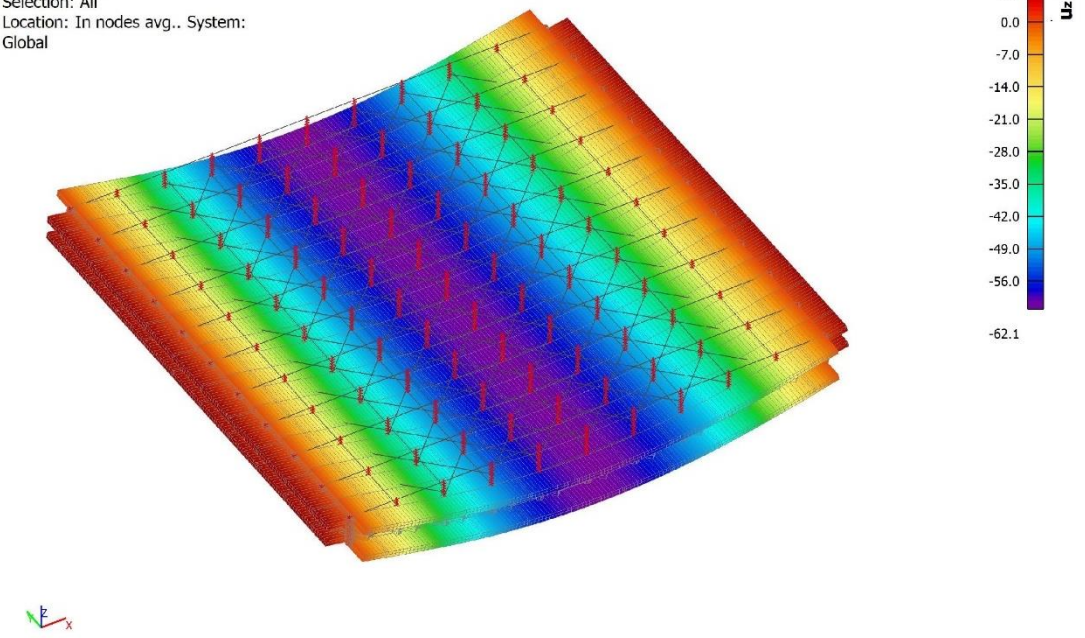

3. 1D internal forces; M_y x-orientated layers

Values: $\mathbf{M_y}$
Linear calculation
Load case: LC2
Coordinate system: Principal
Extreme 1D: Member
Selection: B1, B73

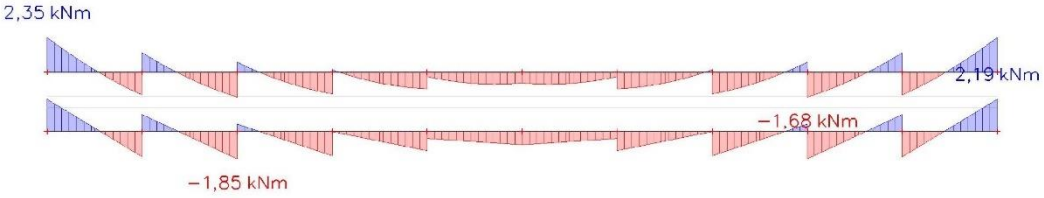

4. 1D internal forces; M_y y-orientated layers

Values: $\mathbf{M_y}$
Linear calculation
Load case: LC2
Coordinate system: Principal
Extreme 1D: Global
Selection: B11..B20, B23, B62..B72

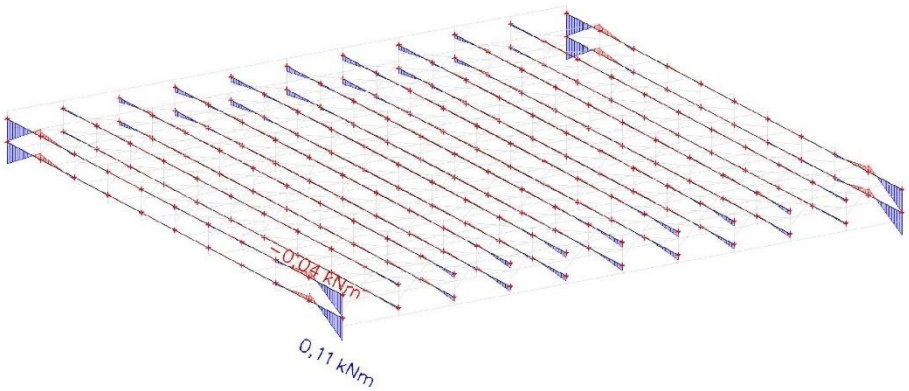

5. 1D internal forces; M_y \-orientated diagonal

Values: M_y
Linear calculation
Load case: LC2
Coordinate system: Principal
Extreme 1D: Member
Selection: All

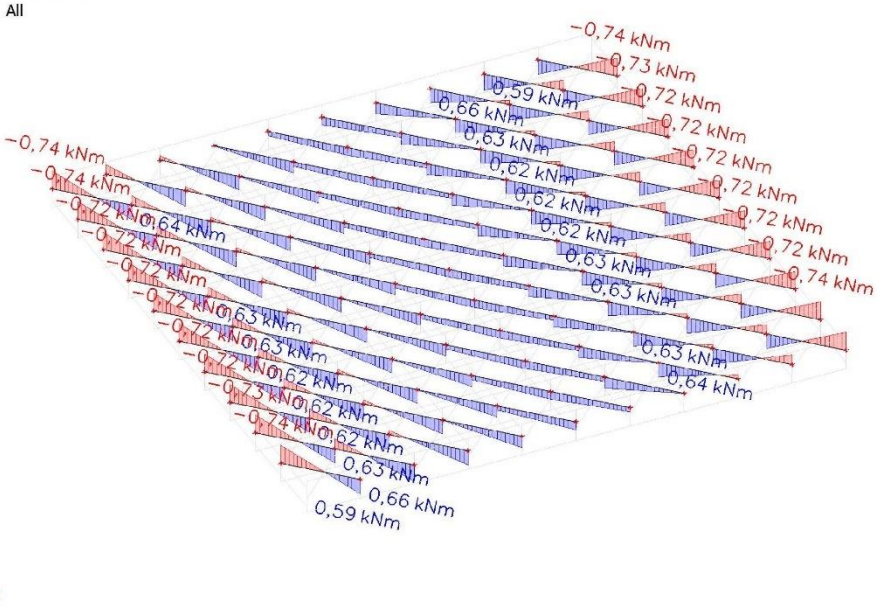

6. 1D internal forces; M_y /-orientated diagonal

Values: M_y
Linear calculation
Load case: LC2
Coordinate system: Principal
Extreme 1D: Member
Selection: All

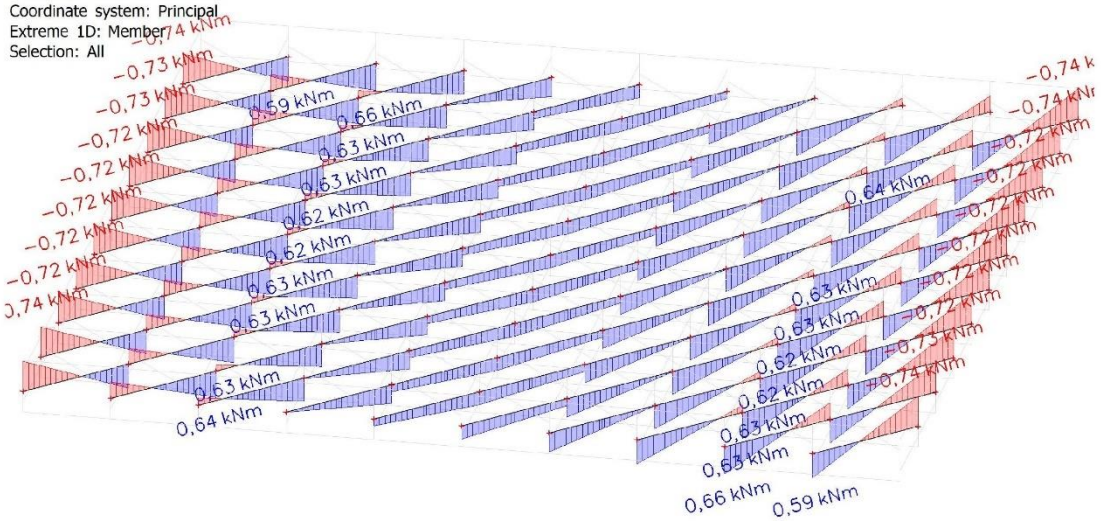

7. 1D internal forces; V_z x-orientated layers

Values: V_z
Linear calculation
Load case: LC2
Coordinate system: Principal
Extreme 1D: Member
Selection: B1, B73

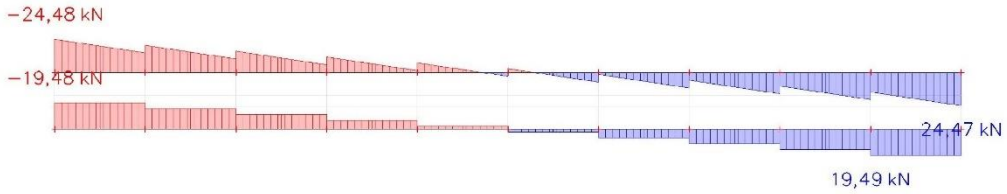

8. 1D internal forces; V_z y-orientated layers

Values: V_z
Linear calculation
Load case: LC2
Coordinate system: Principal
Extreme 1D: Member
Selection: All

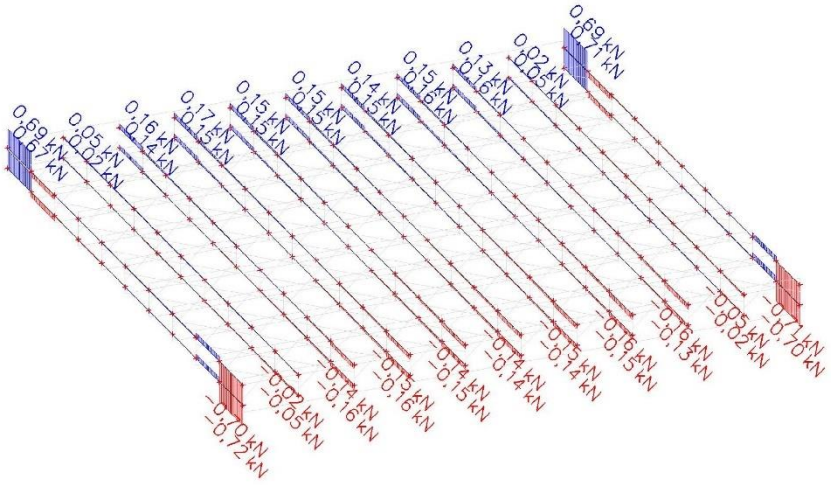

9. 1D internal forces; V_z \-orientated layers

Values: V_z
Linear calculation
Load case: LC2
Coordinate system: Principal
Extreme 1D: Member
Selection: All

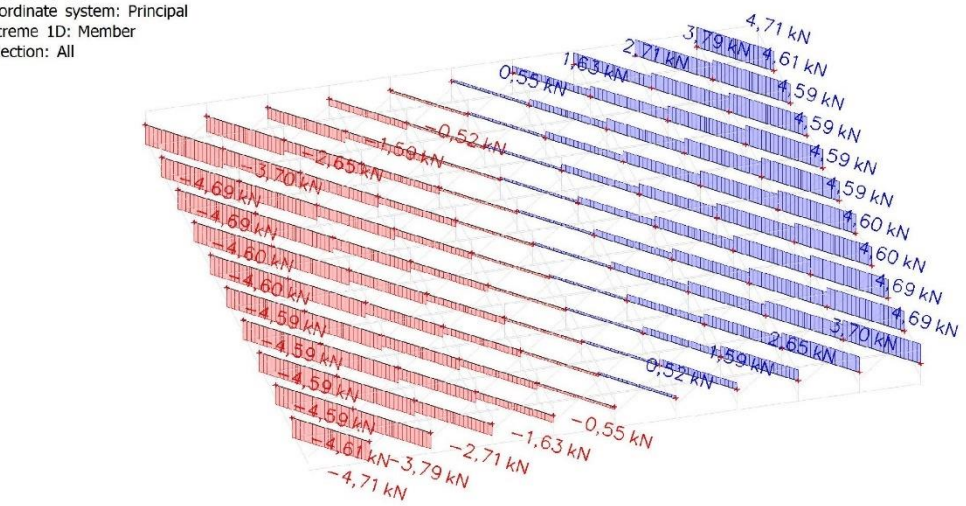

10. 1D internal forces; V_z /-orientated layers

Values: V_z
Linear calculation
Load case: LC2
Coordinate system: Principal
Extreme 1D: Member
Selection: All

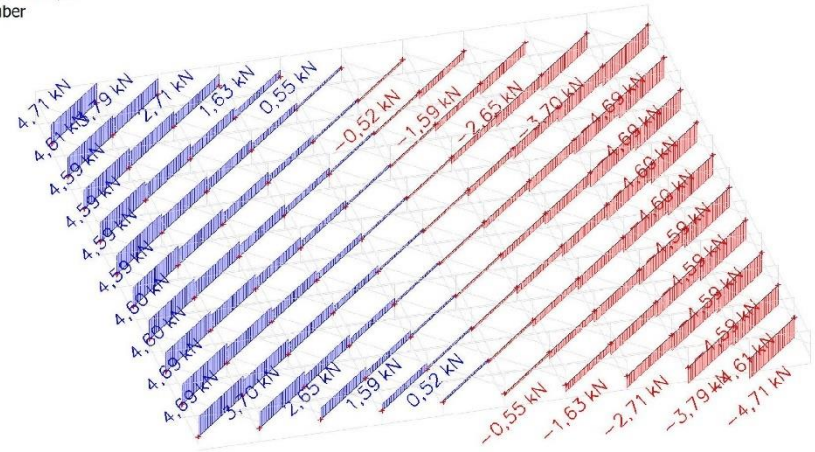

1. 1D internal forces; N x-orientated layer 1

Values: **N**
Linear calculation
Load case: LC2
Coordinate system: Principal
Extreme 1D: Member
Selection: All

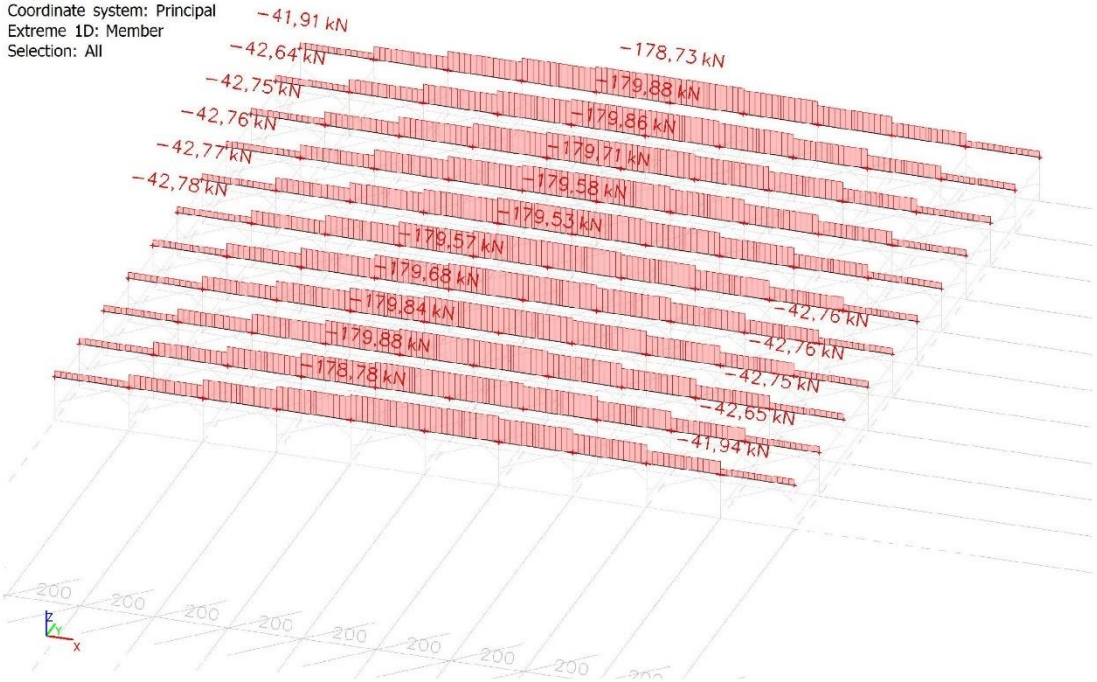

2. 1D internal forces; N y-orientated layer 2

Values: **N**
Linear calculation
Load case: LC2
Coordinate system: Principal
Extreme 1D: Member
Selection: All

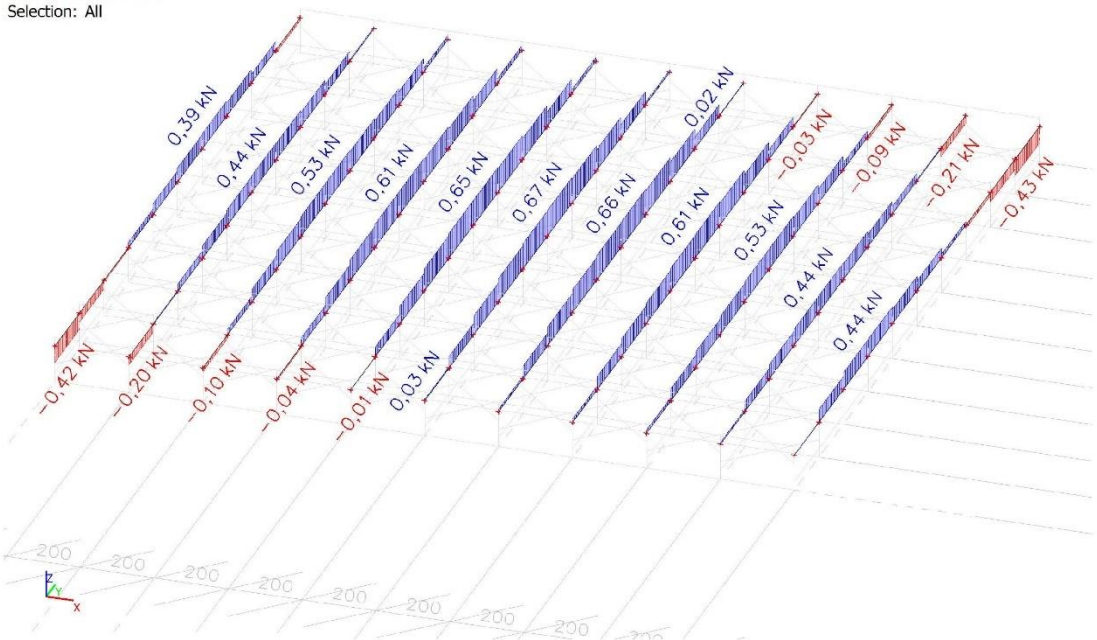

3. 1D internal forces; N \-orientated diagonal

Values: **N**
Linear calculation
Load case: LC2
Coordinate system: Principal
Extreme 1D: Member
Selection: All

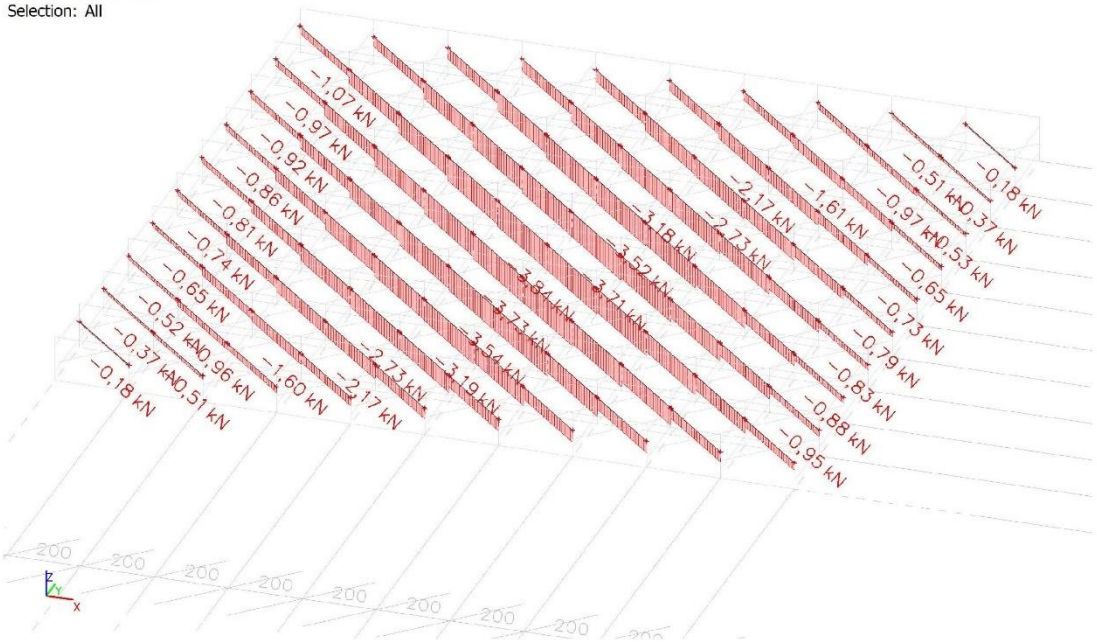

4. 1D internal forces; N /-orientated layer

Values: **N**
Linear calculation
Load case: LC2
Coordinate system: Principal
Extreme 1D: Member
Selection: All

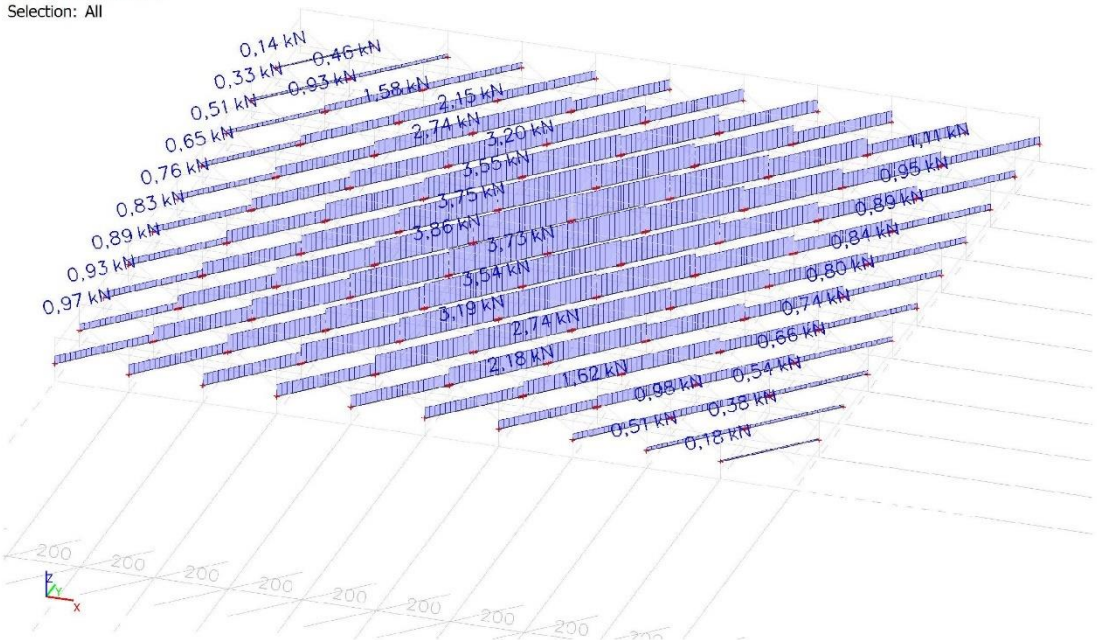

5. 1D internal forces; N y-orientated layer 5

Values: **N**
Linear calculation
Load case: LC2
Coordinate system: Principal
Extreme 1D: Member
Selection: All

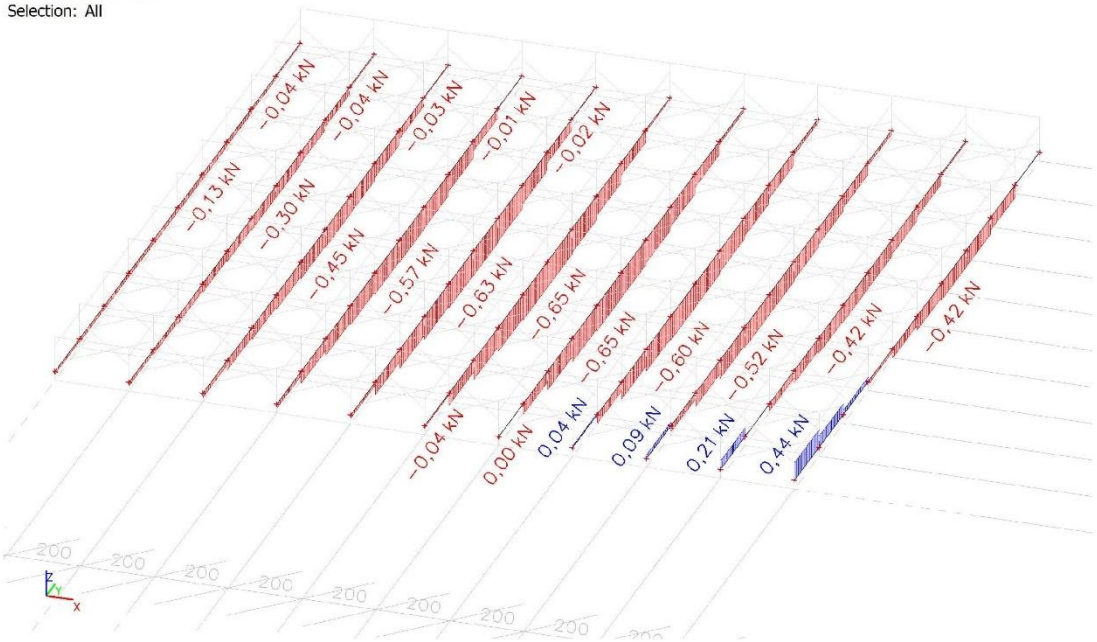

6. 1D internal forces; N x-orientated layer 6

Values: **N**
Linear calculation
Load case: LC2
Coordinate system: Principal
Extreme 1D: Member
Selection: All

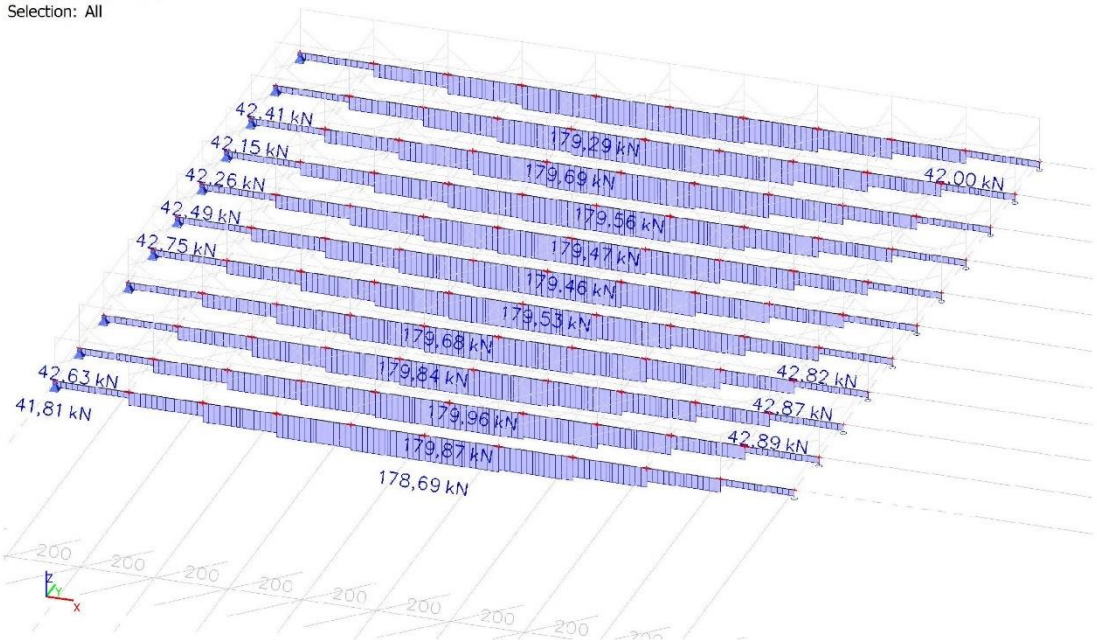

11. 1D internal forces; M_y Dowels

Values: M_y
Linear calculation
Load case: LC2
Coordinate system: Principal
Extreme 1D: Global
Selection: B1376..B1397,
B1618..B1625, B1646, B1647, B1668,
B1669, B1690, B1691, B1712, B1713,
...

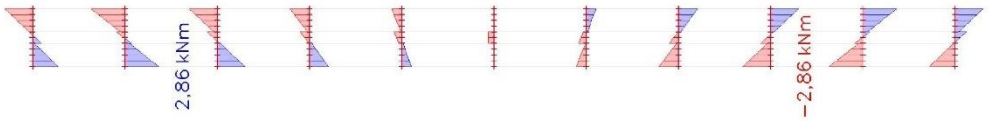

12. 1D internal forces; V_z Dowels

Values: V_z
Linear calculation
Load case: LC2
Coordinate system: Principal
Extreme 1D: Global
Selection: B1376..B1397,
B1618..B1625, B1646, B1647, B1668,
B1669, B1690, B1691, B1712, B1713,
...

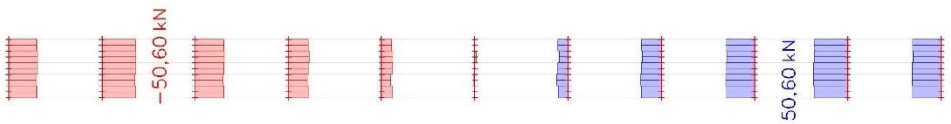

1D internal forces
Values: V_z
Linear calculation
Load case: LC2
Coordinate system: Principal
Extreme 1D: Member
Selection: B1377, B1379, B1381,
B1383, B1385, B1387, B1389, B1391,
B1393, B1395, B1397, B1618, B1620,
...

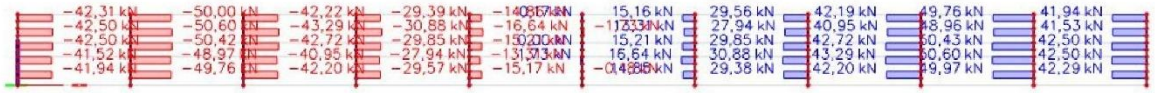

13. Displacement of nodes; U_x Dowels

Values: U_x
Linear calculation
Load case: LC2
Extreme: Global
Selection: N1..N40, N43..N49, N51, N53, N55, N57, N59, N61, N63, N65, N67..N373, N375..N455, N458..N637, N639..N1346

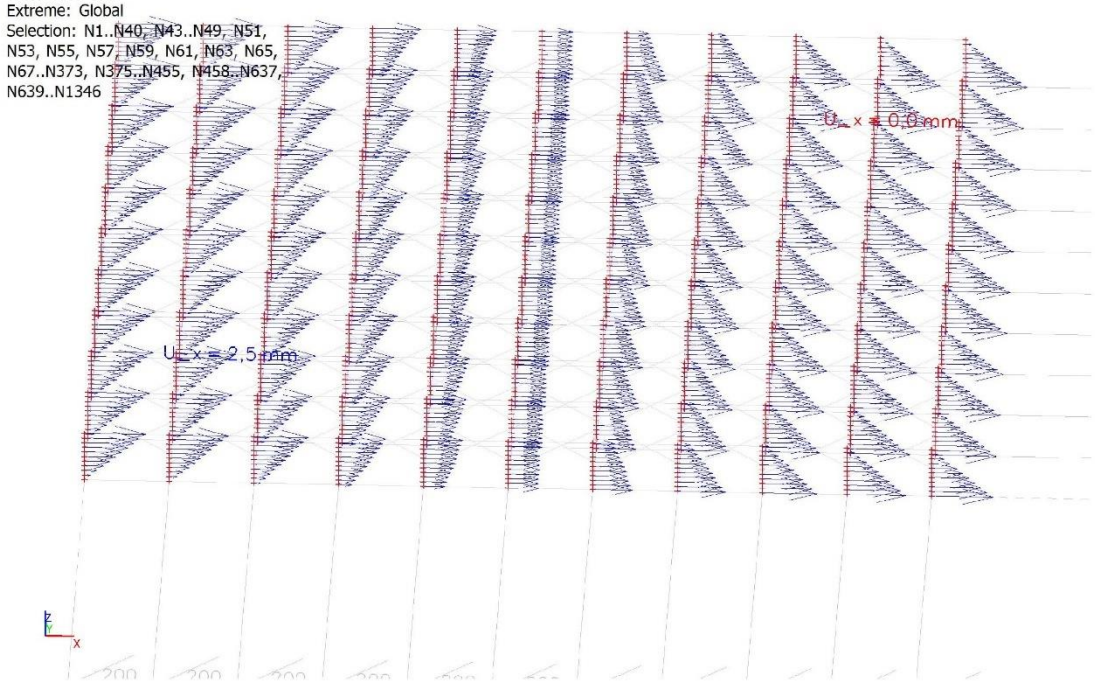

14. Displacement of nodes; U_x Dowel 1,3,5,6

Values: U_x
Linear calculation
Load case: LC2
Extreme: Node
Selection: N1, N21, N25, N29, N31, N47, N77, N79, N80, N94, N106, N108, N132, N136, N140, N142, N154, ...

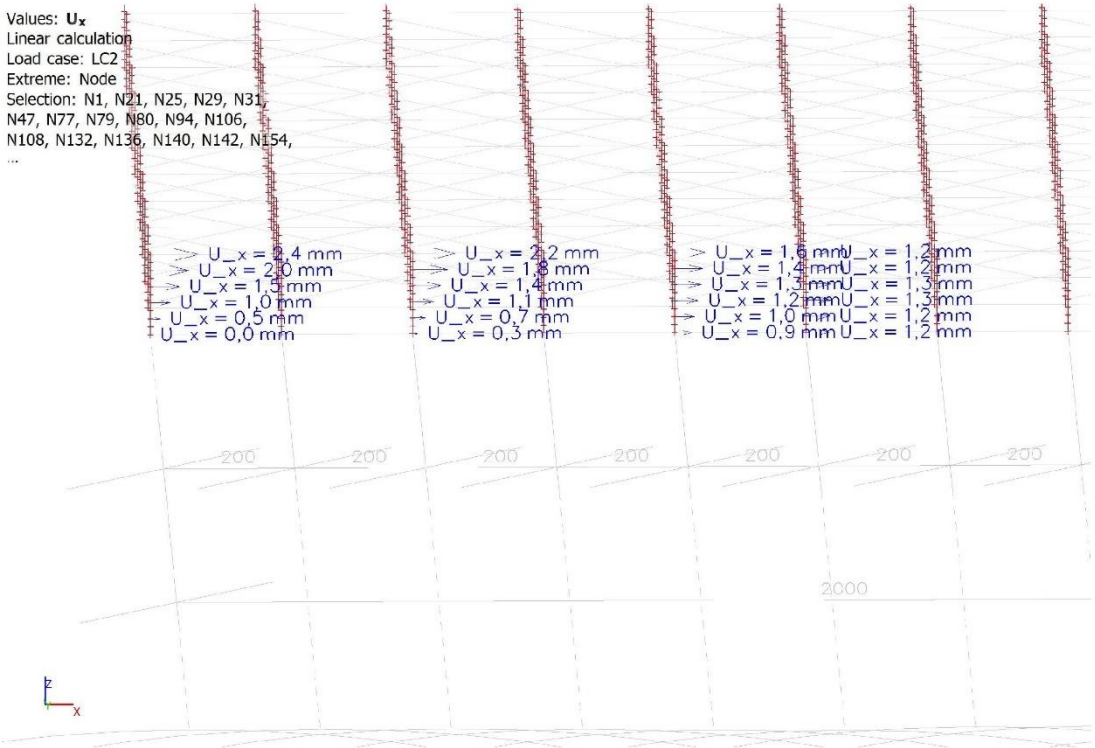

15. Displacement of nodes; U_x Dowels 6, 7, 9, 11

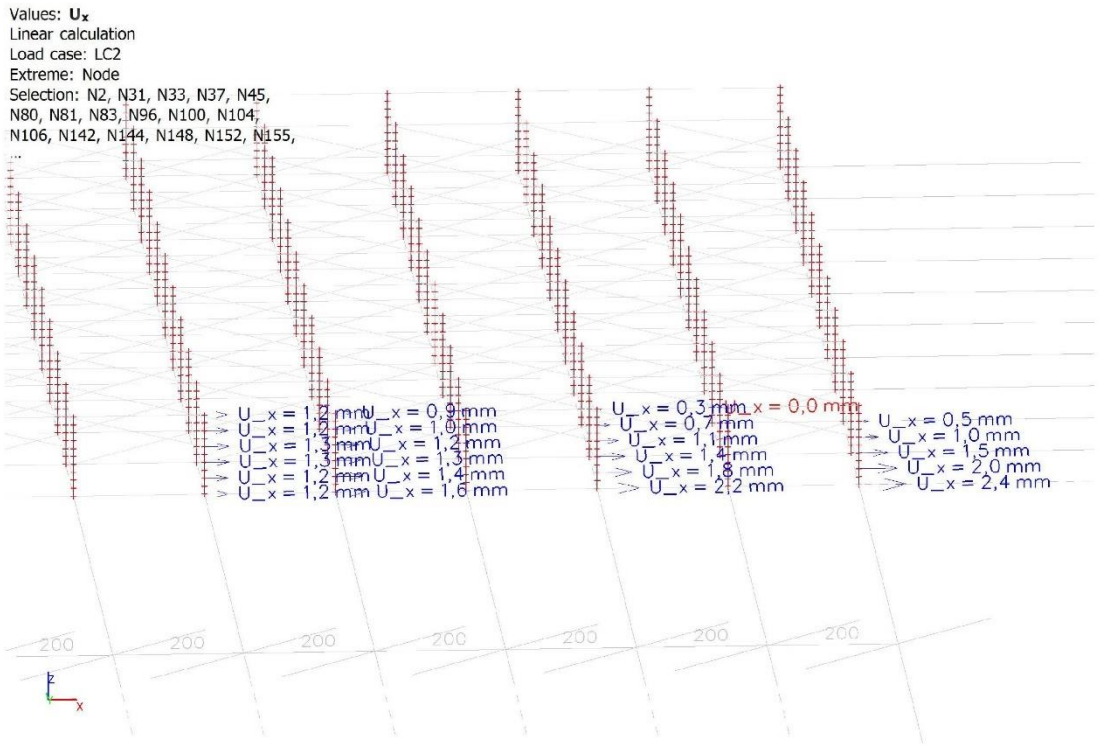

I. Comparison test panel and preliminary design assumption

In this appendix, the model outcomes of the test panel in SCIA Engineer are compared to a dowel cross laminated beam. The test model is a panel of 2x2 meters with lamellae of 200 millimetres in the x- and y-direction and 141 millimetres in the diagonal directions. The dowel laminated beam is calculated with the loss factor of the method of Schelling obtained by Mulder (2019). As the finite element panel is simply supported along the two edges, a simply supported beam of 200 millimetres width loaded by the same uniform load of 50 kN/m is designed. The width of the beam is taken as 200 mm, as it is the distance of the supports and the width of one lamellae of the panel.

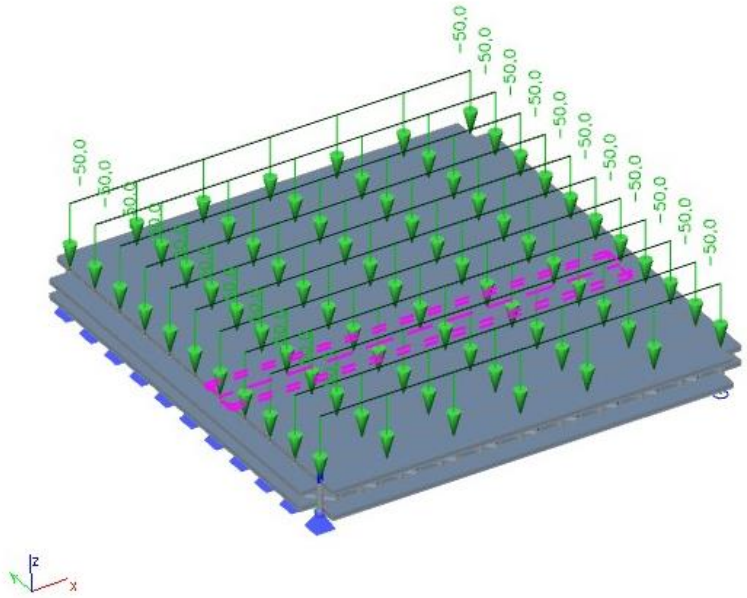

Figure 123: Selected beam for comparison of test model panel and preliminary design

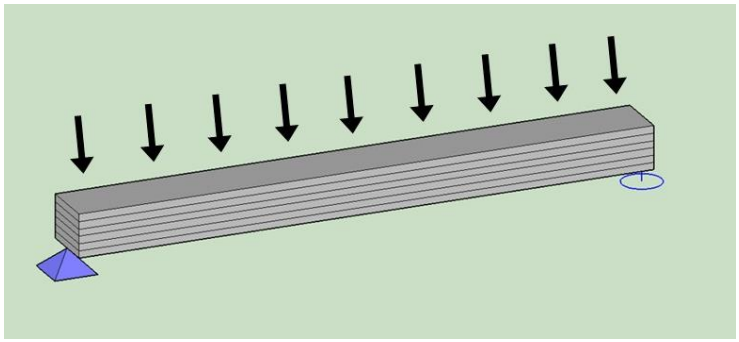

Figure 124: Impression of dowel cross laminated beam

The loss factor for beams with 6 components obtained by Mulder (2019) are:

$$\gamma_1 = \gamma_6 = \frac{k * L^2 * (A_i^2 * E_i^2 * \pi^2 + 5 * A_i * k * E_i * L^2 * \pi^2 + 5 * k^2 * L^4)}{5 * (A_i^3 * E^3 * \pi^6 + A_i^2 * k * E_i^2 * L^2 * \pi^4 + 9 * A_i * k^2 * E_i * L^4 * \pi^2 + 2 * k^3 * L^6)}$$

$$\gamma_2 = \gamma_5 = \frac{2 * k^3 * L^6}{A_i^3 * E^3 * \pi^6 + A_i^2 * k * E_i^2 * L^2 * \pi^4 + 9 * A_i * k^2 * E_i * L^4 * \pi^2 + 2 * k^3 * L^6}$$

$$\gamma_3 = \gamma_4 = \frac{2 * (\pi^2 * E * A + 3 * k * L) * k^2 * L^4}{3 * (A_i^3 * E^3 * \pi^6 + A_i^2 * k * E_i^2 * L^2 * \pi^4 + 9 * A_i * k^2 * E_i * L^4 * \pi^2 + 2 * k^3 * L^6)}$$

For the deflection the serviceable limit state values are used to perform the comparison on. For the shear modulus of the fastener K_{SLS} is used, $k = \frac{K_{SLS}}{s}$. The loss factors are:

$$\gamma_1 = \gamma_6 = 0.483$$

$$\gamma_2 = \gamma_5 = 0.997$$
$$\gamma_3 = \gamma_4 = 0.001$$

The bending stiffness of the panel becomes:

$$EI_{eff,panel} = 2 * \sum_{i=1}^{3} (E_i * I_i + \gamma_i E_i A_i a_i^2) = 4.09 * 10^{11} \mathrm{N/mm^2}$$

	***i*=1**		***i*=2**		***i*=3**
E_i	20000	**E_i**	1330	**E_i**	2494
I_i	260417	**I_i**	260417	**I_i**	260417
A_i	5000	**A_i**	5000	**A_i**	5000
a_i	62.5	**a_i**	37.5	**a_i**	12.5
γ_i	0.483	**γ_i**	0.997	**γ_i**	0.001

Table 25: Characteristics verification beam

For the deflection the formulas of structural mechanics, 'forget-me-nots' are used. The maximum deflection halfway the beam is: $u_{fin,panel} = \frac{5ql^4}{384EI_{eff,panel}}\left(1 + \Psi_{2,1}k_{def}\right) = 66.2$ mm. This is consistent with the deflection of the test model, which is 62.1 millimetres.

However the bending moments in the layers of the model are not consistent. The bending moment diagram has a maximum bending moment of 3 kNm, which is not similar to the expected $\frac{1}{8}ql^2 = 25\ kNm$. The reason for this is the input of the dowels. At the location of the dowel a jump in the bending moment diagram is observed. Although the dowels are infinite stiff, these contain big bending moments. The shear force diagram of the model is consistent. The orientated layers in the direction of the beam together almost distribute the total shear force $\frac{1}{2}ql = 50\ kNm$. The innovation of a dowel cross laminated beam is new and therefore laboratory test provide a definitive answer on the behaviour of dowel cross laminated timber.

J. SCIA results of final models

The SCIA input and results of the closed and opened mitre gate model are shown in this appendix.

J.1 Closed mitre gate

The input and results of the closed mitre gate are shown below.

1. Reacties; Ry

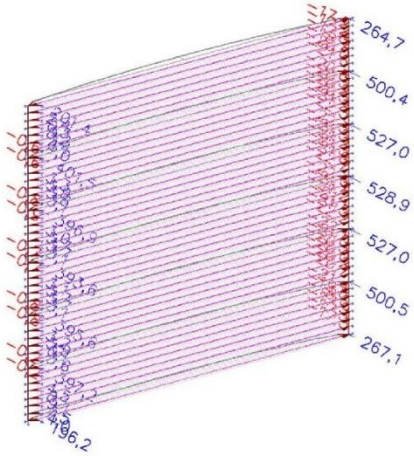

2. Reacties; Ry

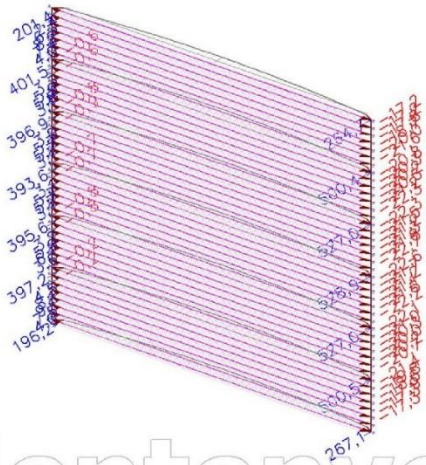

3. Reacties; Rx

4. Verplaatsing van knopen; Uy

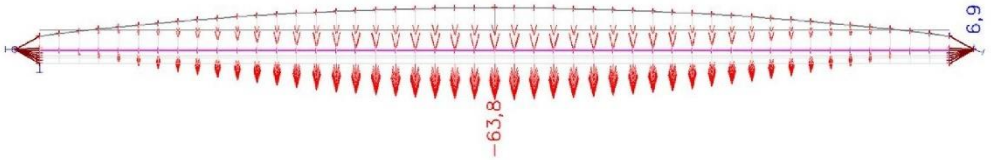

5. Verplaatsing van knopen; Uy

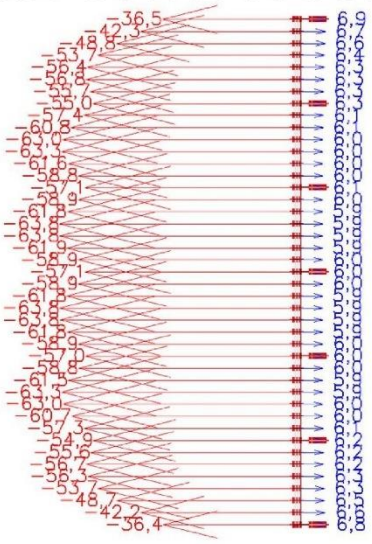

6. Verplaatsing van knopen; Uy halfway plate field

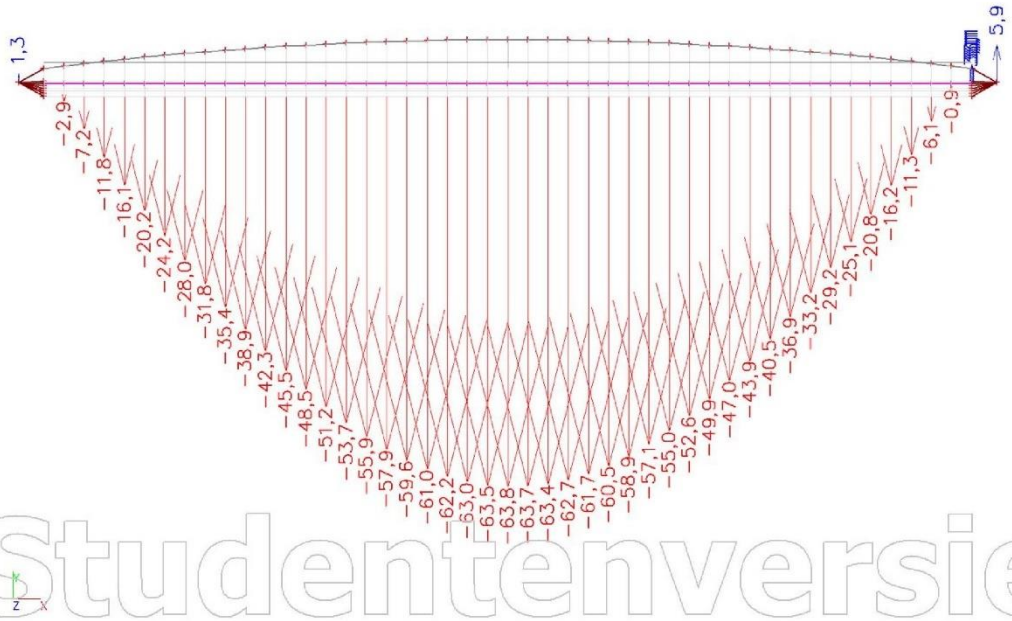

7. Verplaatsing van knopen; Uy height of girder

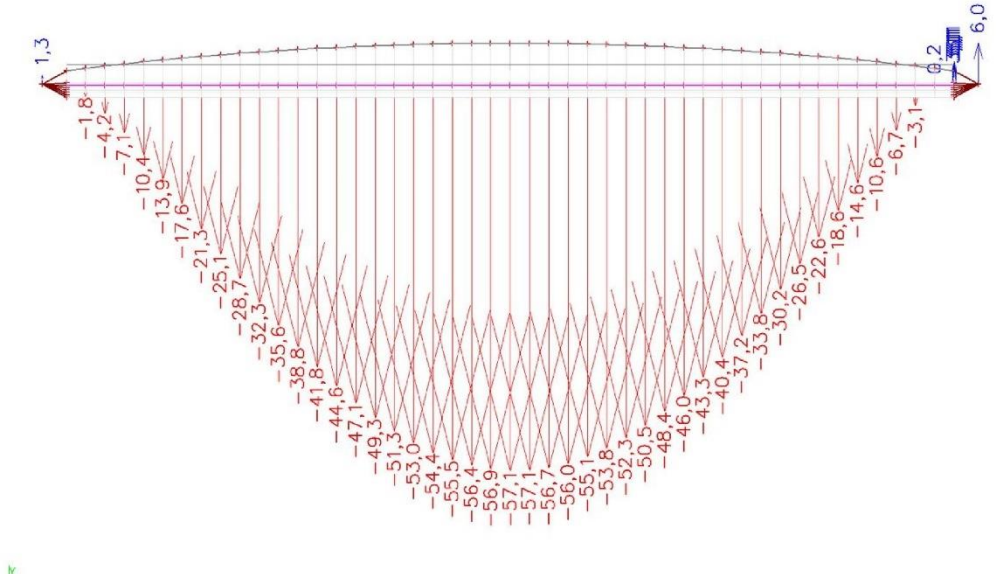

8. Interne krachten in staaf; N upper/lower girder

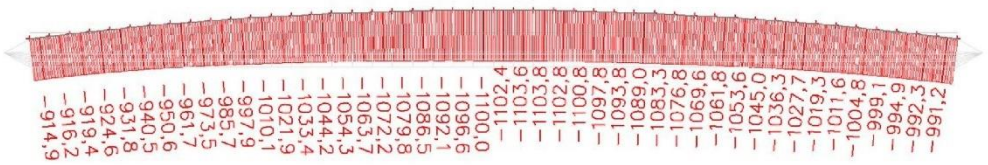

9. Interne krachten in staaf; N inner girders

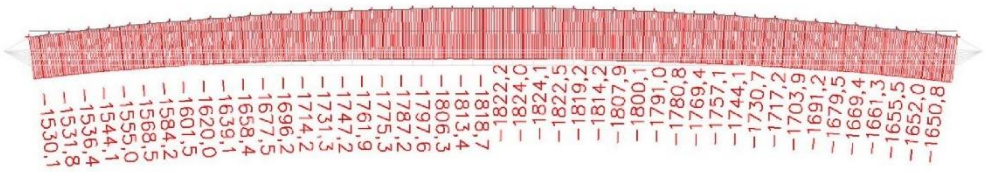

10. Interne krachten in staaf; My girders

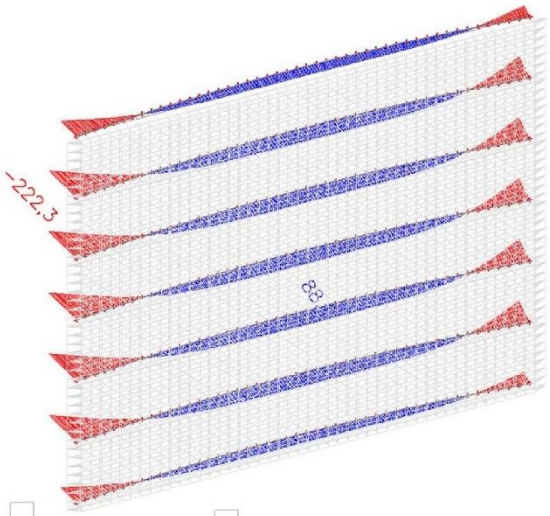

11. Interne krachten in staaf; My inner girders

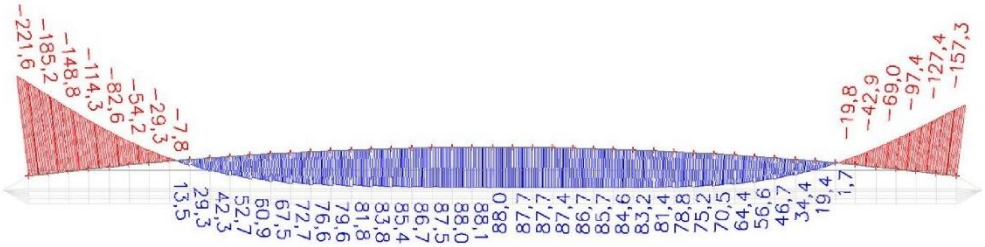

12. Interne krachten in staaf; My upper/lower girder

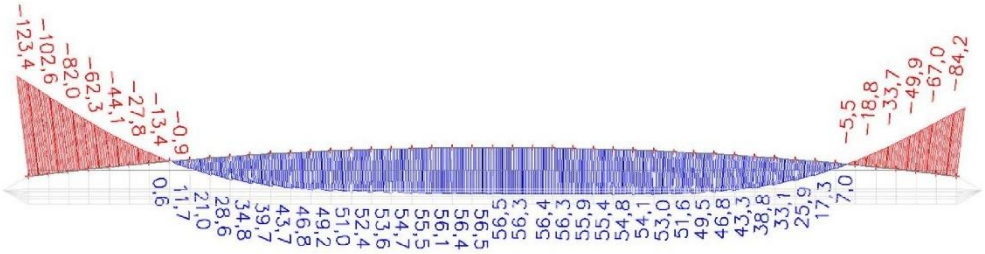

1. Hout UGT controle; Upper/lower girder

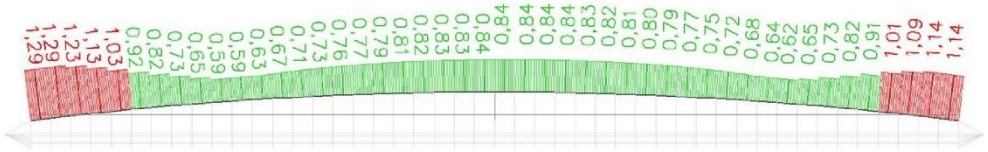

2. Hout UGT controle Extreme upper/lower girder

Lineaire berekening, Extreem : Staaf
Selectie : S400
Belastingsgevallen : BG2

EN 1995-1-1 Normcontrole

Ligger S400	**0,201 m**	**Girder - RECT (300; 289)**	**D70 (EN 338)**	**BG2**	**1,29 -**

Basisgegevens	
Partiële veiligheidsfactor γM – Massief hout	1,30

Materiaalgegevens		
Buigend (fm,k)	70,0	MPa
Spanning (ft,0,k)	42,0	MPa
Spanning (ft,90,k)	0,6	MPa
Compressie (fc,0,k)	36,0	MPa
Compressie (fc,90,k)	12,0	MPa
Afschuiving (fv,k)	5,0	MPa
Houtsoort	Vast	

De kritische controle is op positie **0,201** m.

Interne krachten		
NEd	-916,3	kN
Vy,Ed	-99,2	kN
Vz,Ed	42,5	kN
TEd	-12,0	kNm
My,Ed	47,9	kNm
Mz,Ed	-123,4	kNm

Opmerking: Asdefinitie:
- y-hoofdas in deze normcontrole verwijst naar de z-hoofdas in SCIA Engineer
- z-hoofdas in deze normcontrole verwijst naar de y-hoofdas in SCIA Engineer

Modificatiefactor	
Service Klasse	3
Belastingsduur	Korte termijn
Modificatie factor kmod	0,70

..:: DOORSNEDE CONTROLE ::..

Compressie parallel aan de vezel
Volgens EN 1995-1-1 artikel 6.1.4 en formule (6.2)

σc,0,d	10,6	MPa
fc,0,d	19,4	MPa
Eenheidscontrole	0,55	-

Druk loodrecht op de vezel
Volgens EN 1995-1-1 artikel 6.1.5 en formule (6.3)

Fc,90,d	42,5	kN
l	100	mm
lef	130	mm
b	300	mm
Aef	39000	mm^2
σc,90,d	1,1	MPa
Steunpunt Voorwaarde	Discreet	
h	289	mm
kc,90	1,00	-
fc,90,d	6,5	MPa
Eenheidscontrole	0,17	-

Buiging
Volgens EN 1995-1-1 artikel 6.1.6 en formule (6.11),(6.12)

σm,y,d	11,0	MPa
kh,y	1,00	
fm,y,d	37,7	MPa
σm,z,d	29,6	MPa
kh,z	1,00	
fm,z,d	37,7	MPa
km	0,70	

Eenheidscontrole (6.11) = 0,29 + 0,55 = 0,84 -
Eenheidscontrole (6.12) = 0,21 + 0,78 = 0,99 -

Afschuiving
Volgens EN 1995-1-1 artikel 6.1.7 en formule (6.13)

kcr	1,00	
τy,d	1,7	MPa
τz,d	0,7	MPa
fv,d	2,7	MPa
Eenheidscontrole τy	0,64	-
Eenheidscontrole τz	0,27	-
Eenheidscontrole Interactie	0,48	-

Opmerking: De interactie vergelijking is toegevoegd als een NCCI.

Torsie
Volgens EN 1995-1-1 artikel 6.1.8 en formule (6.14)

τtor,d	2,3	MPa
kshape	1,05	
fv,d	2,7	MPa
Eenheidscontrole	0,80	-
Eenheidscontrole Interactie Afschuiving	**1,28**	-

Opmerking: De interactie vergelijking is toegevoegd als een NCCI.

Gecombineerde Buiging en Axiale druk
Volgens EN 1995-1-1 artikel 6.2.4 en formule (6.19),(6.20)

fc,0,d	19,4	MPa
fm,y,d	37,7	MPa
fm,z,d	37,7	MPa
km	0,70	

Eenheidscontrole (6.19) = 0,30 + 0,29 + 0,55 = **1,14** -
Eenheidscontrole (6.20) = 0,30 + 0,21 + 0,78 = **1,29** -

De staaf voldoet NIET aan de doorsnedecontrole!

..:: STABILITEITSCONTROLE ::..

Opmerking: Alleen de doorsnede controle wordt uitgevoerd voor deze staaf.

3. Hout UGT controle; Inner girders

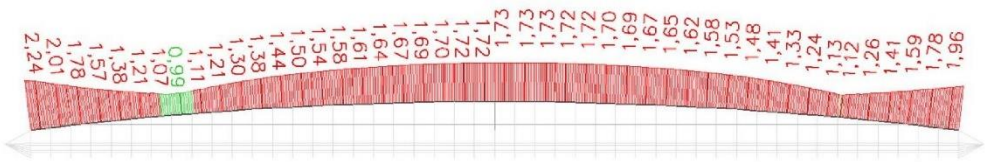

4. Hout UGT controle Extreme inner girders

Lineaire berekening, Extreem : Staaf
Selectie : S492
Belastingsgevallen : BG2

EN 1995-1-1 Normcontrole

Ligger S492	0,201 m	Girder - RECT (300; 289)	D70 (EN 338)	BG2	2,24 -

Basisgegevens	
Partiële veiligheidsfactor γM – Massief hout	1,30

Materiaalgegevens		
Buigend (fm,k)	70,0	MPa
Spanning (ft,0,k)	42,0	MPa
Spanning (ft,90,k)	0,6	MPa
Compressie (fc,0,k)	36,0	MPa
Compressie (fc,90,k)	12,0	MPa
Afschuiving (fv,k)	5,0	MPa
Houtsoort	Vast	

De kritische controle is op positie **0,201** m.

Interne krachten		
NEd	-1524,3	kN
Vy,Ed	-174,6	kN
Vz,Ed	1,0	kN
TEd	-0,1	kNm
My,Ed	1,2	kNm
Mz,Ed	-221,8	kNm

Opmerking: Asdefinitie:
- y-hoofdas in deze normcontrole verwijst naar de z-hoofdas in SCIA Engineer
- z-hoofdas in deze normcontrole verwijst naar de y-hoofdas in SCIA Engineer

Modificatiefactor	
Service Klasse	3
Belastingsduur	Korte termijn
Modificatie factor kmod	0,70

..:: DOORSNEDE CONTROLE ::..

Compressie parallel aan de vezel
Volgens EN 1995-1-1 artikel 6.1.4 en formule (6.2)

σc,0,d	17,6	MPa
fc,0,d	19,4	MPa
Eenheidscontrole	0,91	-

Druk loodrecht op de vezel
Volgens EN 1995-1-1 artikel 6.1.5 en formule (6.3)

Fc,90,d	1,0	kN
l	100	mm
lef	130	mm
b	300	mm
Aef	39000	mm^2
σc,90,d	0,0	MPa
Steunpunt Voorwaarde	Discreet	
h	289	mm
kc,90	1,00	-
fc,90,d	6,5	MPa
Eenheidscontrole	0,00	-

Buiging
Volgens EN 1995-1-1 artikel 6.1.6 en formule (6.11),(6.12)

σm,y,d	0,3	MPa
kh,y	1,00	
fm,y,d	37,7	MPa
σm,z,d	53,1	MPa
kh,z	1,00	
fm,z,d	37,7	MPa
km	0,70	

Eenheidscontrole (6.11) = 0,01 + 0,99 = 0,99 -
Eenheidscontrole (6.12) = 0,00 + 1,41 = **1,41** -

Afschuiving
Volgens EN 1995-1-1 artikel 6.1.7 en formule (6.13)

kcr	1,00	
τy,d	3,0	MPa
τz,d	0,0	MPa
fv,d	2,7	MPa
Eenheidscontrole τy	1,12	-
Eenheidscontrole τz	0,01	-
Eenheidscontrole Interactie	1,26	-

Opmerking: De interactie vergelijking is toegevoegd als een NCCI.

Torsie
Volgens EN 1995-1-1 artikel 6.1.8 en formule (6.14)

τtor,d	0,0	MPa
kshape	1,05	
fv,d	2,7	MPa
Eenheidscontrole	0,01	-
Eenheidscontrole Interactie Afschuiving	**1,26**	-

Opmerking: De interactie vergelijking is toegevoegd als een NCCI.

Gecombineerde Buiging en Axiale druk
Volgens EN 1995-1-1 artikel 6.2.4 en formule (6.19),(6.20)

fc,0,d	19,4	MPa
fm,y,d	37,7	MPa
fm,z,d	37,7	MPa
km	0,70	

Eenheidscontrole (6.19) = 0,82 + 0,01 + 0,99 = **1,82** -
Eenheidscontrole (6.20) = 0,82 + 0,00 + 1,41 = **2,24** -

De staaf voldoet NIET aan de doorsnedecontrole!

..:: STABILITEITSCONTROLE ::..

Opmerking: Alleen de doorsnede controle wordt uitgevoerd voor deze staaf.

15. Interne krachten in staaf; N layer 6

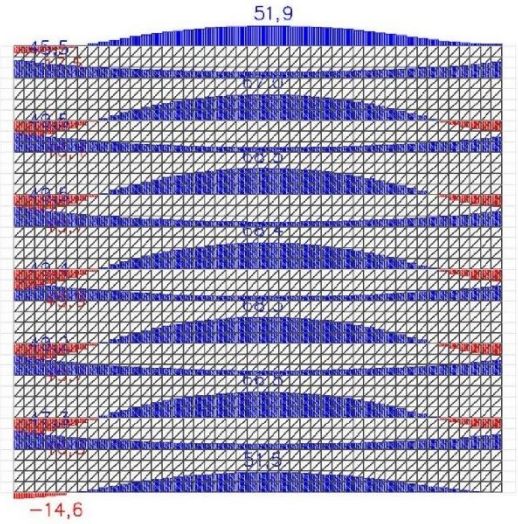

16. Interne krachten in staaf; N layer 5

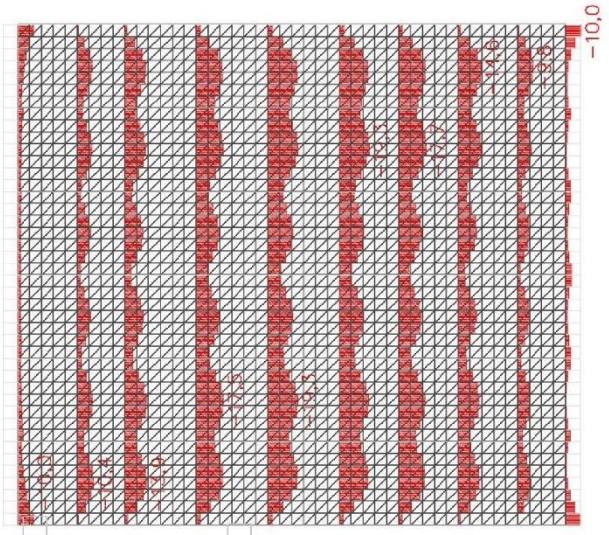

17. Interne krachten in staaf; N layer 4

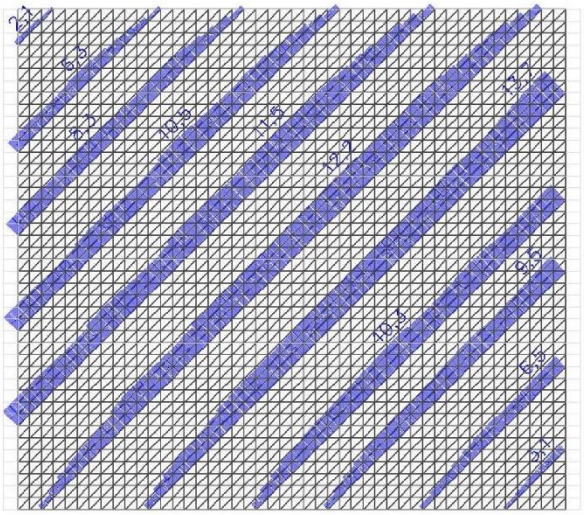

18. Interne krachten in staaf; N layer 3

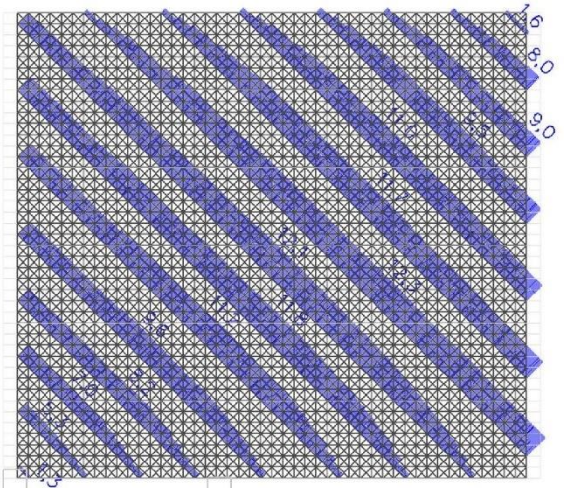

19. Interne krachten in staaf; N Layer 2

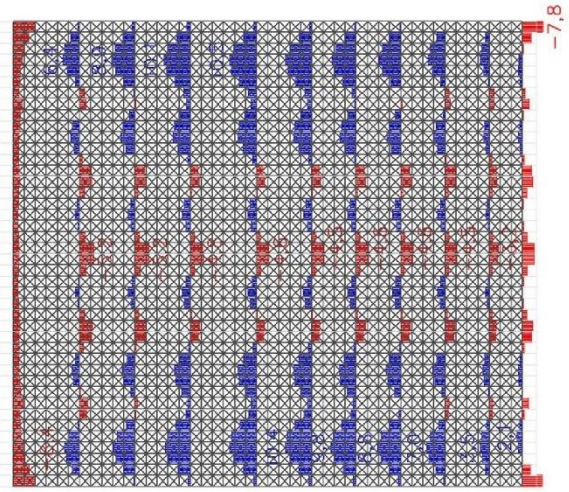

20. Interne krachten in staaf; N Layer 1

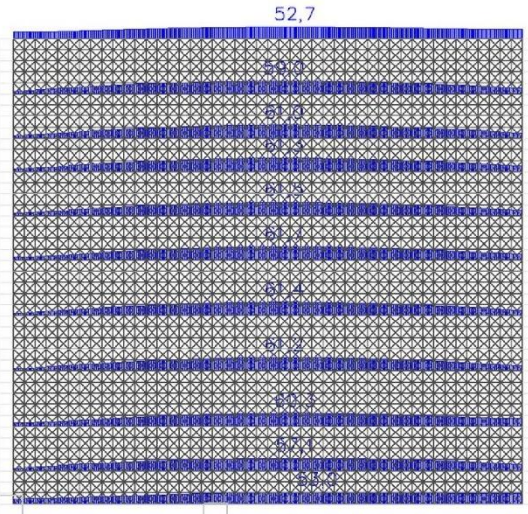

13. Interne krachten in staaf; N Web plate

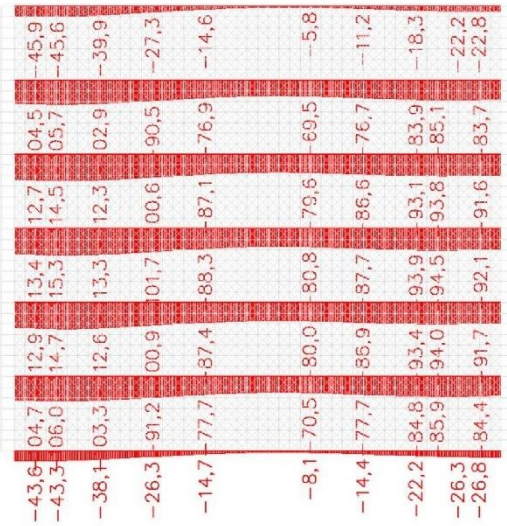

14. Interne krachten in staaf; Vy Web plate

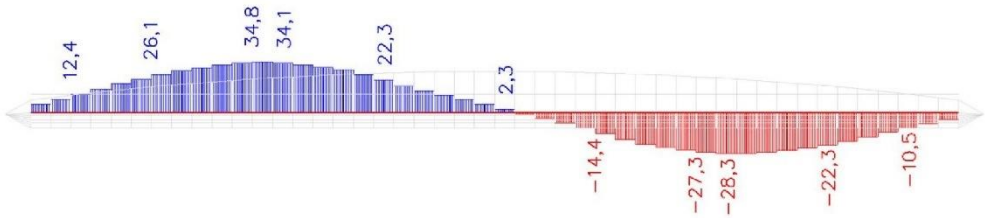

5. Hout UGT controle; Layer 6

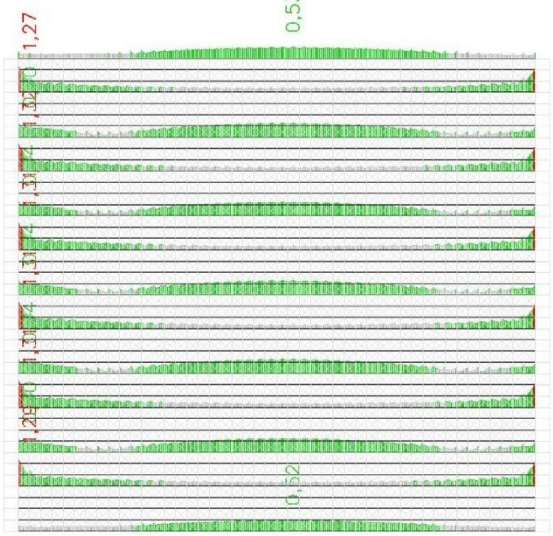

6. Hout UGT controle Extreme layer 6

Lineaire berekening, Extreem : Staaf
Selectie : S351
Belastingsgevallen : BG2

EN 1995-1-1 Normcontrole

Ligger S351	**9,200 m**	**Skin plate - RECT (25; 200)**	**D70 (EN 338)**	**BG2**	**1,27 -**

Basisgegevens		
Partiële veiligheidsfactor γM – Massief hout	1,30	

Materiaalgegevens		
Buigend (fm,k)	70,0	MPa
Spanning (ft,0,k)	42,0	MPa
Spanning (ft,90,k)	0,6	MPa
Compressie (fc,0,k)	36,0	MPa
Compressie (fc,90,k)	12,0	MPa
Afschuiving (fv,k)	5,0	MPa
Houtsoort	Vast	

De kritische controle is op positie **0,000** m.

Interne krachten		
NEd	45,5	kN
Vy,Ed	4,1	kN
Vz,Ed	0,9	kN
TEd	0,0	kNm
My,Ed	0,0	kNm
Mz,Ed	-0,7	kNm

Modificatiefactor	
Service Klasse	3
Belastingsduur	Korte termijn
Modificatie factor kmod	0,70

..:: DOORSNEDE CONTROLE ::..

Spanning parallel aan de vezel

Volgens EN 1995-1-1 artikel 6.1.2 en formule (6.1)

σt,0,d	9,1	MPa
kh	1,00	
ft,0,d	22,6	MPa
Eenheidscontrole	0,40	-

Druk loodrecht op de vezel
Volgens EN 1995-1-1 artikel 6.1.5 en formule (6.3)

Fc,90,d	0,9	kN
l	100	mm
lef	130	mm
b	25	mm
Aef	3250	mm^2
σc,90,d	0,3	MPa
Steunpunt Voorwaarde	Discreet	
h	200	mm
kc,90	1,00	-
fc,90,d	6,5	MPa
Eenheidscontrole	0,04	-

Buiging
Volgens EN 1995-1-1 artikel 6.1.6 en formule (6.11),(6.12)

σm,y,d	0,1	MPa
kh,y	1,00	
fm,y,d	37,7	MPa
σm,z,d	32,5	MPa
kh,z	1,00	
fm,z,d	37,7	MPa
km	0,70	

Eenheidscontrole (6.11) = 0,00 + 0,60 = 0,61 -
Eenheidscontrole (6.12) = 0,00 + 0,86 = 0,87 -

Afschuiving
Volgens EN 1995-1-1 artikel 6.1.7 en formule (6.13)

kcr	1,00	
τy,d	1,2	MPa
τz,d	0,3	MPa
fv,d	2,7	MPa
Eenheidscontrole τy	0,45	-
Eenheidscontrole τz	0,10	-
Eenheidscontrole Interactie	0,22	-

Opmerking: De interactie vergelijking is toegevoegd als een NCCI.

Torsie
Volgens EN 1995-1-1 artikel 6.1.8 en formule (6.14)

τtor,d	0,1	MPa
kshape	1,30	
fv,d	2,7	MPa
Eenheidscontrole	0,04	-
Eenheidscontrole Interactie Afschuiving	0,26	-

Opmerking: De interactie vergelijking is toegevoegd als een NCCI.

Gecombineerd Buig- en Axiale trek
Volgens EN 1995-1-1 artikel 6.2.3 en formule (6.17),(6.18)

ft,0,d	22,6	MPa
fm,y,d	37,7	MPa
fm,z,d	37,7	MPa
km	0,70	

Eenheidscontrole (6.17) = 0,40 + 0,00 + 0,60 = **1,01** -
Eenheidscontrole (6.18) = 0,40 + 0,00 + 0,86 = **1,27** -

De staaf voldoet NIET aan de doorsnedecontrole!

..:: STABILITEITSCONTROLE ::..

Opmerking: Alleen de doorsnede controle wordt uitgevoerd voor deze staaf.

7. Hout UGT controle; Layer 5

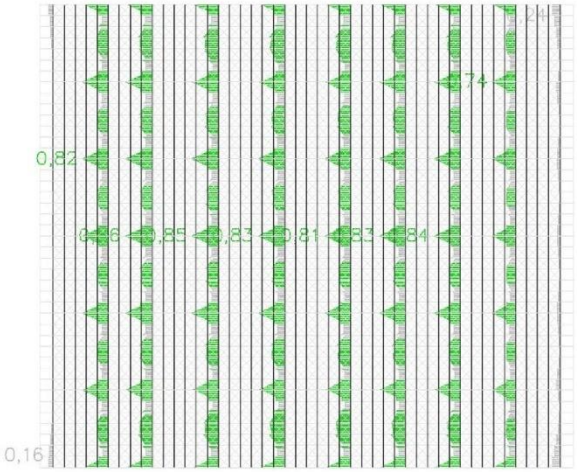

8. Hout UGT controle Extreme layer 5

Lineaire berekening, Extreem : Staaf
Selectie : S347, S286
Belastingsgevallen : BG2

EN 1995-1-1 Normcontrole

Ligger S347	**9,200 m**	**Skin plate - RECT (25; 200)**	**D70 (EN 338)**	**BG2**	**0,70 -**

Basisgegevens	
Partiële veiligheidsfactor γM – Massief hout	1,30

Materiaalgegevens		
Buigend (fm,k)	70,0	MPa
Spanning (ft,0,k)	42,0	MPa
Spanning (ft,90,k)	0,6	MPa
Compressie (fc,0,k)	36,0	MPa
Compressie (fc,90,k)	12,0	MPa
Afschuiving (fv,k)	5,0	MPa
Houtsoort	Vast	

De kritische controle is op positie **0,000** m.

Interne krachten		
NEd	-46,4	kN
Vy,Ed	3,5	kN
Vz,Ed	0,1	kN
TEd	0,0	kNm
My,Ed	0,0	kNm
Mz,Ed	-0,4	kNm

Modificatiefactor	
Service Klasse	3
Belastingsduur	Korte termijn
Modificatie factor kmod	0,70

..:: DOORSNEDE CONTROLE ::..

Compressie parallel aan de vezel

Volgens EN 1995-1-1 artikel 6.1.4 en formule (6.2)

σc,0,d	9,3	MPa
fc,0,d	19,4	MPa
Eenheidscontrole	0,48	-

Druk loodrecht op de vezel
Volgens EN 1995-1-1 artikel 6.1.5 en formule (6.3)

Fc,90,d	0,1	kN
l	100	mm
lef	130	mm
b	25	mm
Aef	3250	mm^2
σc,90,d	0,0	MPa
Steunpunt Voorwaarde	Discreet	
h	200	mm
kc,90	1,00	-
fc,90,d	6,5	MPa
Eenheidscontrole	0,00	-

Buiging
Volgens EN 1995-1-1 artikel 6.1.6 en formule (6.11),(6.12)

σm,y,d	0,2	MPa
kh,y	1,00	
fm,y,d	37,7	MPa
σm,z,d	17,6	MPa
kh,z	1,00	
fm,z,d	37,7	MPa
km	0,70	

Eenheidscontrole (6.11) = 0,01 + 0,33 = 0,33 -
Eenheidscontrole (6.12) = 0,00 + 0,47 = 0,47 -

Afschuiving
Volgens EN 1995-1-1 artikel 6.1.7 en formule (6.13)

kcr	1,00	
τy,d	1,1	MPa
τz,d	0,0	MPa
fv,d	2,7	MPa
Eenheidscontrole τy	0,39	-
Eenheidscontrole τz	0,01	-
Eenheidscontrole Interactie	0,16	-

Opmerking: De interactie vergelijking is toegevoegd als een NCCI.

Torsie
Volgens EN 1995-1-1 artikel 6.1.8 en formule (6.14)

τtor,d	0,0	MPa
kshape	1,30	
fv,d	2,7	MPa
Eenheidscontrole	0,01	-
Eenheidscontrole Interactie Afschuiving	0,16	-

Opmerking: De interactie vergelijking is toegevoegd als een NCCI.

Gecombineerde Buiging en Axiale druk
Volgens EN 1995-1-1 artikel 6.2.4 en formule (6.19),(6.20)

fc,0,d	19,4	MPa
fm,y,d	37,7	MPa
fm,z,d	37,7	MPa
km	0,70	

Eenheidscontrole (6.19) = 0,23 + 0,01 + 0,33 = 0,56 -
Eenheidscontrole (6.20) = 0,23 + 0,00 + 0,47 = 0,70 -

De staaf voldoet aan de doorsnedecontrole.

..:: STABILITEITSCONTROLE ::..

Opmerking: Alleen de doorsnede controle wordt uitgevoerd voor deze staaf.

EN 1995-1-1 Normcontrole

Ligger S286	**8,400 m**	**Skin plate - RECT (25; 200)**	**D70 (EN 338)**	**BG2**	**0,83 -**

Basisgegevens		
Partiële veiligheidsfactor	γM -- Massief hout	1,30

Materiaalgegevens		
Buigend (fm,k)	70,0	MPa
Spanning (ft,0,k)	42,0	MPa
Spanning (ft,90,k)	0,6	MPa
Compressie (fc,0,k)	36,0	MPa
Compressie (fc,90,k)	12,0	MPa
Afschuiving (fv,k)	5,0	MPa
Houtsoort	Vast	

De kritische controle is op positie **4,200** m.

Interne krachten		
NEd	-8,4	kN
Vy,Ed	2,8	kN
Vz,Ed	1,6	kN
TEd	0,0	kNm
My,Ed	-0,2	kNm
Mz,Ed	-0,6	kNm

Modificatiefactor	
Service Klasse	3
Belastingsduur	Korte termijn
Modificatie factor kmod	0,70

..:: DOORSNEDE CONTROLE ::..

Compressie parallel aan de vezel
Volgens EN 1995-1-1 artikel 6.1.4 en formule (6.2)

σc,0,d	1,7	MPa
fc,0,d	19,4	MPa
Eenheidscontrole	0,09	-

Druk loodrecht op de vezel
Volgens EN 1995-1-1 artikel 6.1.5 en formule (6.3)

Fc,90,d	3,0	kN
l	100	mm
lef	160	mm
b	25	mm
Aef	4000	mm²
σc,90,d	0,7	MPa
Steunpunt Voorwaarde	Discreet	
h	200	mm
kc,90	1,00	-
fc,90,d	6,5	MPa
Eenheidscontrole	0,11	-

Buiging
Volgens EN 1995-1-1 artikel 6.1.6 en formule (6.11),(6.12)

σm,y,d	1,4	MPa
kh,y	1,00	
fm,y,d	37,7	MPa
σm,z,d	30,1	MPa
kh,z	1,00	
fm,z,d	37,7	MPa
km	0,70	

Eenheidscontrole (6.11) = 0,04 + 0,56 = 0,60 -
Eenheidscontrole (6.12) = 0,03 + 0,80 = 0,82 -

Afschuiving
Volgens EN 1995-1-1 artikel 6.1.7 en formule (6.13)

kcr	1,00	
τy,d	0,8	MPa
τz,d	0,5	MPa
fv,d	2,7	MPa
Eenheidscontrole τy	0,31	-
Eenheidscontrole τz	0,18	-
Eenheidscontrole Interactie	0,13	-

Opmerking: De interactie vergelijking is toegevoegd als een NCCI.

Torsie
Volgens EN 1995-1-1 artikel 6.1.8 en formule (6.14)

τtor,d	0,0	MPa
kshape	1,30	
fv,d	2,7	MPa
Eenheidscontrole	0,01	
Eenheidscontrole Interactie Afschuiving	0,13	-

Opmerking: De interactie vergelijking is toegevoegd als een NCCI.

Gecombineerde Buiging en Axiale druk
Volgens EN 1995-1-1 artikel 6.2.4 en formule (6.19),(6.20)

fc,0,d	19,4	MPa
fm,y,d	37,7	MPa
fm,z,d	37,7	MPa
km	0,70	

Eenheidscontrole (6.19) = 0,01 + 0,04 + 0,56 = 0,60 -
Eenheidscontrole (6.20) = 0,01 + 0,03 + 0,80 = 0,83 -

De staaf voldoet aan de doorsnedecontrole.

..:: STABILITEITSCONTROLE ::..

Opmerking: Alleen de doorsnede controle wordt uitgevoerd voor deze staaf.

9. Hout UGT controle; Layer 4

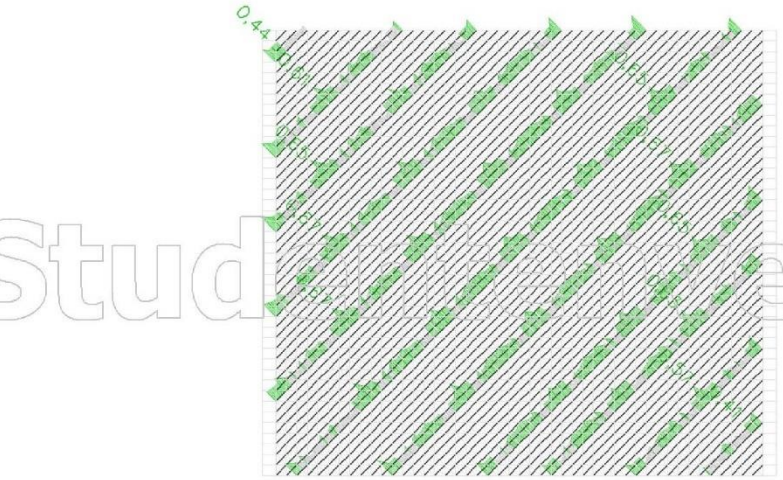

10. Hout UGT controle Extreme layer 4

Lineaire berekening, Extreem : Staaf
Selectie : S220
Belastingsgevallen : BG2

EN 1995-1-1 Normcontrole

Ligger S220	**11,879 m**	**Skin plate diagonals - RECT (25; 141)**	**D70 (EN 338)**	**BG2**	**0,65 -**

Basisgegevens	
Partiële veiligheidsfactor γM – Massief hout	1,30

Materiaalgegevens		
Buigend (fm,k)	70,0	MPa
Spanning (ft,0,k)	42,0	MPa
Spanning (ft,90,k)	0,6	MPa
Compressie (fc,0,k)	36,0	MPa
Compressie (fc,90,k)	12,0	MPa
Afschuiving (fv,k)	5,0	MPa
Houtsoort	Vast	

De kritische controle is op positie **1,980** m.

Interne krachten		
NEd	11,5	kN
Vy,Ed	-1,0	kN
Vz,Ed	-0,8	kN
TEd	0,0	kNm
My,Ed	0,2	kNm
Mz,Ed	0,3	kNm

Modificatiefactor	
Service Klasse	3
Belastingsduur	Korte termijn
Modificatie factor kmod	0,70

..:: DOORSNEDE CONTROLE ::..

Spanning parallel aan de vezel
Volgens EN 1995-1-1 artikel 6.1.2 en formule (6.1)

σt,0,d	3,3	MPa
kh	1,00	
ft,0,d	22,6	MPa
Eenheidscontrole	0,14	-

Druk loodrecht op de vezel
Volgens EN 1995-1-1 artikel 6.1.5 en formule (6.3)

Fc,90,d	0,2	kN
l	100	mm
lef	160	mm
b	25	mm
Aef	4000	mm²
σc,90,d	0,1	MPa
Steunpunt Voorwaarde	Discreet	
h	141	mm
kc,90	1,00	-
fc,90,d	6,5	MPa
Eenheidscontrole	0,01	-

Buiging
Volgens EN 1995-1-1 artikel 6.1.6 en formule (6.11),(6.12)

σm,y,d	2,0	MPa
kh,y	1,00	
fm,y,d	37,7	MPa
σm,z,d	17,7	MPa
kh,z	1,00	
fm,z,d	37,7	MPa
km	0,70	

Eenheidscontrole (6.11) = 0,05 + 0,33 = 0,38 -
Eenheidscontrole (6.12) = 0,04 + 0,47 = 0,51 -

Afschuiving
Volgens EN 1995-1-1 artikel 6.1.7 en formule (6.13)

kcr	1,00	
τy,d	0,4	MPa
τz,d	0,4	MPa
fv,d	2,7	MPa
Eenheidscontrole τy	0,16	-
Eenheidscontrole τz	0,13	-
Eenheidscontrole Interactie	0,04	-

Opmerking: De interactie vergelijking is toegevoegd als een NCCI.

Torsie
Volgens EN 1995-1-1 artikel 6.1.8 en formule (6.14)

τtor,d	1,0	MPa
kshape	1,28	
fv,d	2,7	MPa
Eenheidscontrole	0,30	-
Eenheidscontrole Interactie Afschuiving	0,34	-

Opmerking: De interactie vergelijking is toegevoegd als een NCCI.

Gecombineerd Buig- en Axiale trek
Volgens EN 1995-1-1 artikel 6.2.3 en formule (6.17),(6.18)

ft,0,d	22,6	MPa
fm,y,d	37,7	MPa
fm,z,d	37,7	MPa
km	0,70	

Eenheidscontrole (6.17) = 0,14 + 0,05 + 0,33 = 0,52 -
Eenheidscontrole (6.18) = 0,14 + 0,04 + 0,47 = 0,65 -

De staaf voldoet aan de doorsnedecontrole.

..:: STABILITEITSCONTROLE ::..

Opmerking: Alleen de doorsnede controle wordt uitgevoerd voor deze staaf.

11. Hout UGT controle; Layer 3

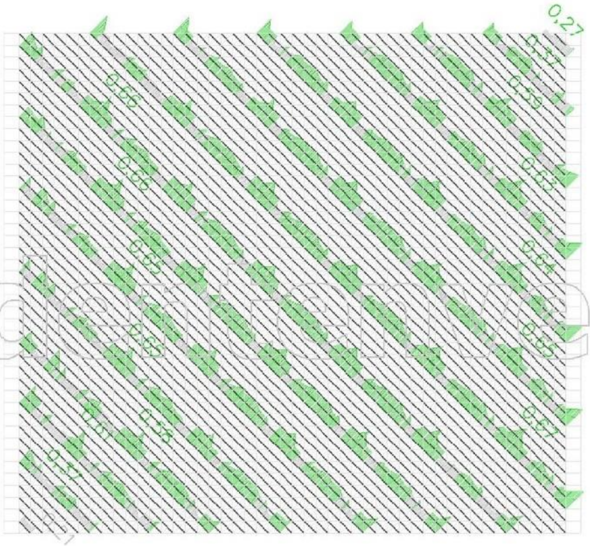

12. Hout UGT controle Extreme layer 3

Lineaire berekening, Extreem : Staaf
Selectie : S134
Belastingsgevallen : BG2

EN 1995-1-1 Normcontrole

Ligger S134	**11,314 m**	**Skin plate diagonals - RECT (25; 141)**	**D70 (EN 338)**	**BG2**	**0,67 -**

Basisgegevens	
Partiële veiligheidsfactor γM – Massief hout	1,30

Materiaalgegevens		
Buigend (fm,k)	70,0	MPa
Spanning (ft,0,k)	42,0	MPa
Spanning (ft,90,k)	0,6	MPa
Compressie (fc,0,k)	36,0	MPa
Compressie (fc,90,k)	12,0	MPa
Afschuiving (fv,k)	5,0	MPa
Houtsoort	Vast	

De kritische controle is op positie **9,899** m.

Interne krachten		
NEd	11,8	kN
Vy,Ed	-1,0	kN
Vz,Ed	-0,6	kN
TEd	0,0	kNm
My,Ed	-0,1	kNm
Mz,Ed	-0,3	kNm

Modificatiefactor	
Service Klasse	3
Belastingsduur	Korte termijn
Modificatie factor kmod	0,70

..:: DOORSNEDE CONTROLE ::..

Spanning parallel aan de vezel
Volgens EN 1995-1-1 artikel 6.1.2 en formule (6.1)

σt,0,d	3,3	MPa
kh	1,00	
ft,0,d	22,6	MPa
Eenheidscontrole	0,15	-

Druk loodrecht op de vezel
Volgens EN 1995-1-1 artikel 6.1.5 en formule (6.3)

Fc,90,d	0,0	kN
l	100	mm
lef	160	mm
b	25	mm
Aef	4000	mm²
σc,90,d	0,0	MPa
Steunpunt Voorwaarde	Discreet	
h	141	mm
kc,90	1,00	-
fc,90,d	6,5	MPa
Eenheidscontrole	0,00	-

Buiging
Volgens EN 1995-1-1 artikel 6.1.6 en formule (6.11),(6.12)

σm,y,d	1,4	MPa
kh,y	1,00	
fm,y,d	37,7	MPa
σm,z,d	18,6	MPa
kh,z	1,00	
fm,z,d	37,7	MPa
km	0,70	

Eenheidscontrole (6.11) = 0,04 + 0,35 = 0,38 -
Eenheidscontrole (6.12) = 0,03 + 0,49 = 0,52 -

Afschuiving
Volgens EN 1995-1-1 artikel 6.1.7 en formule (6.13)

kcr	1,00	
τy,d	0,4	MPa
τz,d	0,3	MPa
fv,d	2,7	MPa
Eenheidscontrole τy	0,16	-
Eenheidscontrole τz	0,10	-
Eenheidscontrole Interactie	0,03	-

Opmerking: De interactie vergelijking is toegevoegd als een NCCI.

Torsie
Volgens EN 1995-1-1 artikel 6.1.8 en formule (6.14)

τtor,d	0,9	MPa
kshape	1,28	
fv,d	2,7	MPa
Eenheidscontrole	0,27	-
Eenheidscontrole Interactie Afschuiving	0,31	-

Opmerking: De interactie vergelijking is toegevoegd als een NCCI.

Gecombineerd Buig- en Axiale trek
Volgens EN 1995-1-1 artikel 6.2.3 en formule (6.17),(6.18)

ft,0,d	22,6	MPa
fm,y,d	37,7	MPa
fm,z,d	37,7	MPa
km	0,70	

Eenheidscontrole (6.17) = 0,15 + 0,04 + 0,35 = 0,53 -
Eenheidscontrole (6.18) = 0,15 + 0,03 + 0,49 = 0,67 -

De staaf voldoet aan de doorsnedecontrole.

..:: STABILITEITSCONTROLE ::..

Opmerking: Alleen de doorsnede controle wordt uitgevoerd voor deze staaf.

13. Hout UGT controle; Layer 2

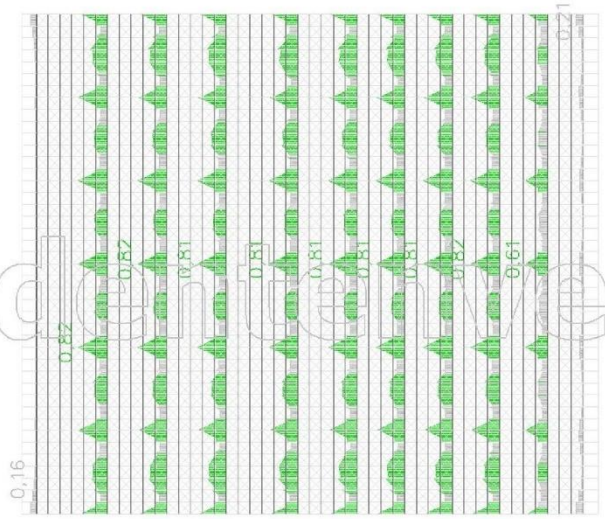

14. Hout UGT controle Extreme layer 2

Lineaire berekening, Extreem : Staaf
Selectie : S79
Belastingsgevallen : BG2

EN 1995-1-1 Normcontrole

Ligger S79	**8,400 m**	**Skin plate - RECT (25; 200)**	**D70 (EN 338)**	**BG2**	**0,82 -**

Basisgegevens		
Partiële veiligheidsfactor	γM – Massief hout	1,30

Materiaalgegevens		
Buigend (fm,k)	70,0	MPa
Spanning (ft,0,k)	42,0	MPa
Spanning (ft,90,k)	0,6	MPa
Compressie (fc,0,k)	36,0	MPa
Compressie (fc,90,k)	12,0	MPa
Afschuiving (fv,k)	5,0	MPa
Houtsoort	Vast	

De kritische controle is op positie **4,200** m.

Interne krachten		
NEd	-5,1	kN
Vy,Ed	2,8	kN
Vz,Ed	0,0	kN
TEd	0,0	kNm
My,Ed	-0,1	kNm
Mz,Ed	-0,6	kNm

Modificatiefactor	
Service Klasse	3
Belastingsduur	Korte termijn
Modificatie factor kmod	0,70

..:: DOORSNEDE CONTROLE ::..

Compressie parallel aan de vezel
Volgens EN 1995-1-1 artikel 6.1.4 en formule (6.2)

σc,0,d	1,0	MPa
fc,0,d	19,4	MPa
Eenheidscontrole	0,05	-

Druk loodrecht op de vezel
Volgens EN 1995-1-1 artikel 6.1.5 en formule (6.3)

Fc,90,d	0,1	kN
l	100	mm
lef	160	mm
b	25	mm
Aef	4000	mm²
σc,90,d	0,0	MPa
Steunpunt Voorwaarde	Discreet	
h	200	mm
kc,90	1,00	-
fc,90,d	6,5	MPa
Eenheidscontrole	0,01	-

Buiging
Volgens EN 1995-1-1 artikel 6.1.6 en formule (6.11),(6.12)

σm,y,d	0,6	MPa
kh,y	1,00	
fm,y,d	37,7	MPa
σm,z,d	30,2	MPa
kh,z	1,00	
fm,z,d	37,7	MPa
km	0,70	

Eenheidscontrole (6.11) = 0,02 + 0,56 = 0,58 -
Eenheidscontrole (6.12) = 0,01 + 0,80 = 0,81 -

Afschuiving
Volgens EN 1995-1-1 artikel 6.1.7 en formule (6.13)

kcr	1,00	
τy,d	0,8	MPa
τz,d	0,0	MPa
fv,d	2,7	MPa
Eenheidscontrole τy	0,31	-
Eenheidscontrole τz	0,00	-
Eenheidscontrole Interactie	0,10	-

Opmerking: De interactie vergelijking is toegevoegd als een NCCI.

Torsie
Volgens EN 1995-1-1 artikel 6.1.8 en formule (6.14)

τtor,d	0,1	MPa
kshape	1,30	
fv,d	2,7	MPa
Eenheidscontrole	0,02	
Eenheidscontrole Interactie Afschuiving	0,12	-

Opmerking: De interactie vergelijking is toegevoegd als een NCCI.

Gecombineerde Buiging en Axiale druk
Volgens EN 1995-1-1 artikel 6.2.4 en formule (6.19),(6.20)

fc,0,d	19,4	MPa
fm,y,d	37,7	MPa
fm,z,d	37,7	MPa
km	0,70	

Eenheidscontrole (6.19) = 0,00 + 0,02 + 0,56 = 0,58 -
Eenheidscontrole (6.20) = 0,00 + 0,01 + 0,80 = 0,82 -

De staaf voldoet aan de doorsnedecontrole.

..:: STABILITEITSCONTROLE ::..

Opmerking: Alleen de doorsnede controle wordt uitgevoerd voor deze staaf.

15. Hout UGT controle; Upper/lower web plate

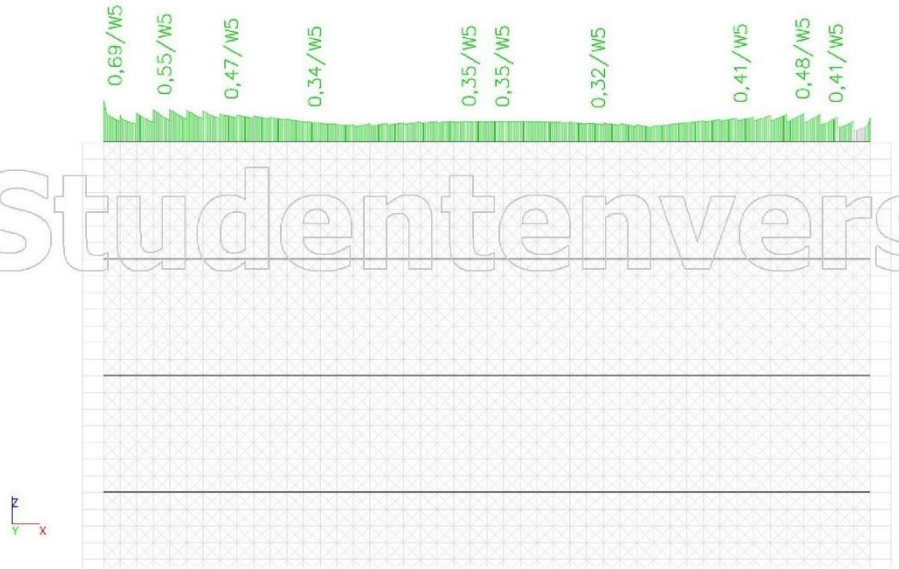

16. Hout UGT controle Extreme upper/lower web plate

Lineaire berekening, Extreem : Staaf
Selectie : S21294
Belastingsgevallen : BG2

EN 1995-1-1 Normcontrole

Ligger S21294	**0,600 m**	**Web plate - RECT (30; 150)**	**D70 (EN 338)**	**BG2**	**0,69 -**

Waarschuwing: Deze variabele doorsnede wordt niet beschouwd als Enkel Tapse Ligger of Dubbele Tapse Ligger volgens EN 1995-1-1. Als resultaat hiervan zijn er geen specifieke controles voor tapse liggers uitgevoerd. Gelieve de geometrie van deze ligger te herzien en de additionele uitvoertabellen van Tapse liggers te controleren.

Basisgegevens		
Partiële veiligheidsfactor	γM -- Massief hout	1,30

Materiaalgegevens		
Buigend (fm,k)	70,0	MPa
Spanning (ft,0,k)	42,0	MPa
Spanning (ft,90,k)	0,6	MPa
Compressie (fc,0,k)	36,0	MPa
Compressie (fc,90,k)	12,0	MPa
Afschuiving (fv,k)	5,0	MPa
Houtsoort	Vast	

De kritische controle is op positie **0,000** m.

Interne krachten		
NEd	-45,5	kN
Vy,Ed	3,0	kN
Vz,Ed	-0,6	kN
TEd	0,0	kNm
My,Ed	-0,1	kNm
Mz,Ed	-0,4	kNm

Modificatiefactor	
Service Klasse	3
Belastingsduur	Korte termijn
Modificatie factor kmod	0,70

..:: DOORSNEDE CONTROLE ::..

Compressie parallel aan de vezel
Volgens EN 1995-1-1 artikel 6.1.4 en formule (6.2)

σc,0,d	10,1	MPa
fc,0,d	19,4	MPa
Eenheidscontrole	0,52	-

Druk loodrecht op de vezel
Volgens EN 1995-1-1 artikel 6.1.5 en formule (6.3)

Fc,90,d	0,6	kN
l	100	mm
lef	130	mm
b	30	mm
Aef	3900	mm^2
σc,90,d	0,2	MPa
Steunpunt Voorwaarde	Discreet	
h	150	mm
kc,90	1,00	-
fc,90,d	6,5	MPa
Eenheidscontrole	0,02	-

Buiging
Volgens EN 1995-1-1 artikel 6.1.6 en formule (6.11),(6.12)

σm,y,d	0,5	MPa
kh,y	1,00	
fm,y,d	37,7	MPa
σm,z,d	15,6	MPa
kh,z	1,00	
fm,z,d	37,7	MPa
km	0,70	

Eenheidscontrole (6.11) = 0,01 + 0,29 = 0,30 -
Eenheidscontrole (6.12) = 0,01 + 0,41 = 0,42 -

Afschuiving
Volgens EN 1995-1-1 artikel 6.1.7 en formule (6.13)

kcr	1,00	
τy,d	1,0	MPa
τz,d	0,2	MPa
fv,d	2,7	MPa
Eenheidscontrole τy	0,38	-
Eenheidscontrole τz	0,08	-
Eenheidscontrole Interactie	0,15	-

Opmerking: De interactie vergelijking is toegevoegd als een NCCI.

Torsie
Volgens EN 1995-1-1 artikel 6.1.8 en formule (6.14)

τtor,d	0,6	MPa
kshape	1,25	
fv,d	2,7	MPa
Eenheidscontrole	0,19	
Eenheidscontrole Interactie Afschuiving	0,33	-

Opmerking: De interactie vergelijking is toegevoegd als een NCCI.

Gecombineerde Buiging en Axiale druk
Volgens EN 1995-1-1 artikel 6.2.4 en formule (6.19),(6.20)

fc,0,d	19,4	MPa
fm,y,d	37,7	MPa
fm,z,d	37,7	MPa
km	0,70	

Eenheidscontrole (6.19) = 0,27 + 0,01 + 0,29 = 0,57 -
Eenheidscontrole (6.20) = 0,27 + 0,01 + 0,41 = 0,69 -

De staaf voldoet aan de doorsnedecontrole.

..:: STABILITEITSCONTROLE ::..

Opmerking: Alleen de doorsnede controle wordt uitgevoerd voor deze staaf.

17. Hout UGT controle; Inner web plates

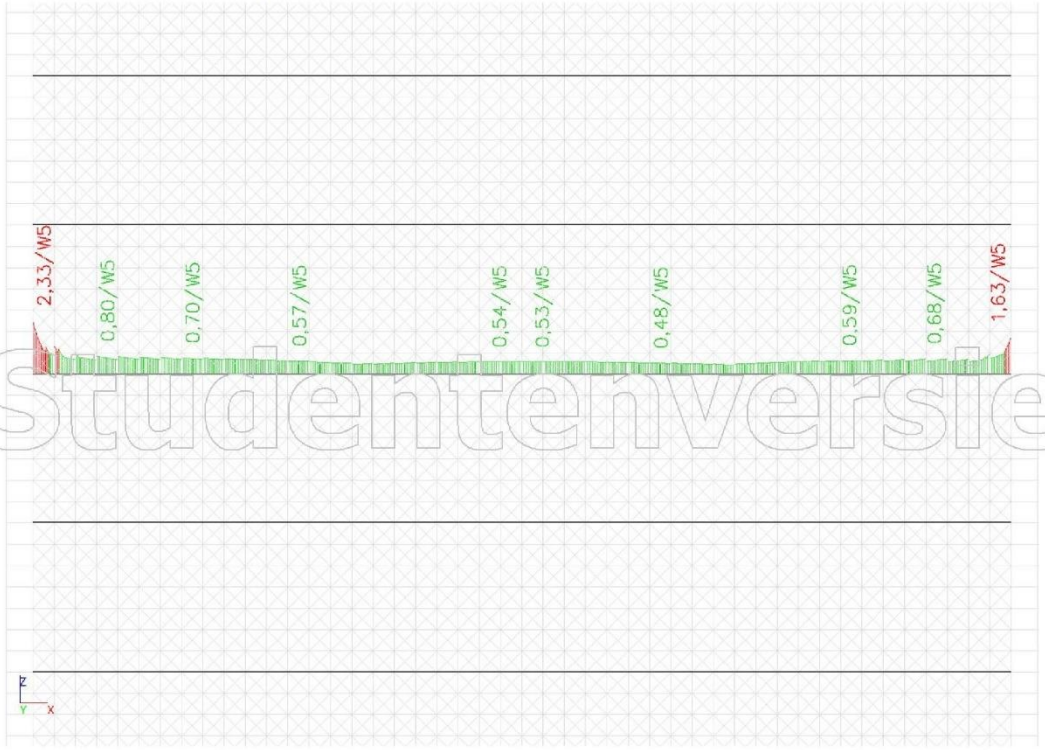

18. Hout UGT controle Extreme inner web plate

Lineaire berekening, Extreem : Staaf
Selectie : S22285
Belastingsgevallen : BG2

EN 1995-1-1 Normcontrole

Ligger S22285	**0,600 m**	**Web plate - RECT (30; 150)**	**D70 (EN 338)**	**BG2**	**2,33 -**

Waarschuwing: Deze variabele doorsnede wordt niet beschouwd als Enkel Tapse Ligger of Dubbele Tapse Ligger volgens EN 1995-1-1. Als resultaat hiervan zijn er geen specifieke controles voor tapse liggers uitgevoerd. Gelieve de geometrie van deze ligger te herzien en de additionele uitvoertabellen van Tapse liggers te controleren.

Basisgegevens		
Partiële veiligheidsfactor	γM - Massief hout	1,30

Materiaalgegevens		
Buigend (fm,k)	70,0	MPa
Spanning (ft,0,k)	42,0	MPa
Spanning (ft,90,k)	0,6	MPa
Compressie (fc,0,k)	36,0	MPa
Compressie (fc,90,k)	12,0	MPa
Afschuiving (fv,k)	5,0	MPa
Houtsoort	Vast	

De kritische controle is op positie **0,000** m.

Interne krachten		
NEd	-110,2	kN
Vy,Ed	5,7	kN
Vz,Ed	0,0	kN
TEd	0,0	kNm
My,Ed	0,0	kNm
Mz,Ed	-0,6	kNm

Modificatiefactor	
Service Klasse	3
Belastingsduur	Korte termijn
Modificatie factor kmod	0,70

..:: DOORSNEDE CONTROLE ::..

Compressie parallel aan de vezel
Volgens EN 1995-1-1 artikel 6.1.4 en formule (6.2)

σc,0,d	24,5	MPa
fc,0,d	19,4	MPa
Eenheidscontrole	**1,26**	-

Buiging
Volgens EN 1995-1-1 artikel 6.1.6 en formule (6.11),(6.12)

σm,y,d	0,0	MPa
kh,y	1,00	
fm,y,d	37,7	MPa
σm,z,d	27,5	MPa
kh,z	1,00	
fm,z,d	37,7	MPa
km	0,70	

Eenheidscontrole (6.11) = 0,00 + 0,51 = 0,51 -
Eenheidscontrole (6.12) = 0,00 + 0,73 = 0,73 -

Afschuiving
Volgens EN 1995-1-1 artikel 6.1.7 en formule (6.13)

kcr	1,00	
τy,d	1,9	MPa
τz,d	0,0	MPa
fv,d	2,7	MPa
Eenheidscontrole τy	0,71	-
Eenheidscontrole τz	0,00	-
Eenheidscontrole Interactie	0,50	-

Opmerking: De interactie vergelijking is toegevoegd als een NCCI.

Torsie
Volgens EN 1995-1-1 artikel 6.1.8 en formule (6.14)

τtor,d	0,0	MPa
kshape	1,25	
fv,d	2,7	MPa
Eenheidscontrole	0,00	-
Eenheidscontrole Interactie Afschuiving	0,50	-

Opmerking: De interactie vergelijking is toegevoegd als een NCCI.

Gecombineerde Buiging en Axiale druk
Volgens EN 1995-1-1 artikel 6.2.4 en formule (6.19),(6.20)

fc,0,d	19,4	MPa
fm,y,d	37,7	MPa
fm,z,d	37,7	MPa
km	0,70	

Eenheidscontrole (6.19) = 1,60 + 0,00 + 0,51 = **2,11** -
Eenheidscontrole (6.20) = 1,60 + 0,00 + 0,73 = **2,33** -

De staaf voldoet NIET aan de doorsnedecontrole!

..:: STABILITEITSCONTROLE ::..

Opmerking: Alleen de doorsnede controle wordt uitgevoerd voor deze staaf.

1. Hout UGT controle; Layer 1

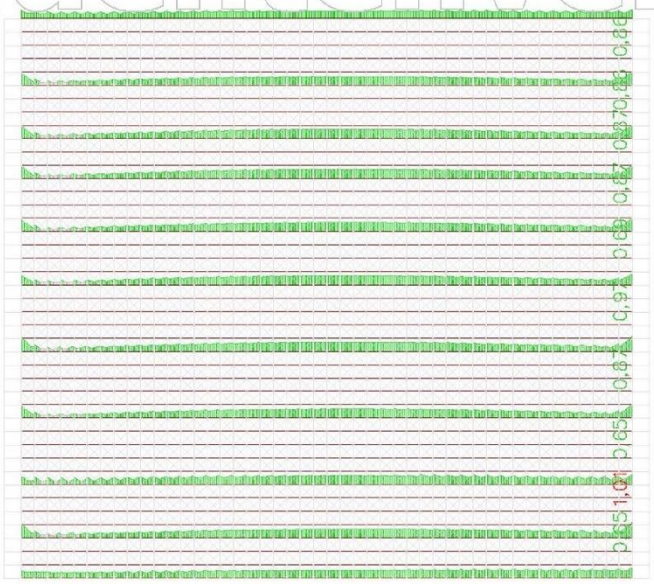

2. Hout UGT controle Extreme layer 1

Lineaire berekening, Extreem : Staaf
Selectie : S4
Belastingsgevallen : BG2

EN 1995-1-1 Normcontrole

Ligger S4	**9,200 m**	**Skin plate - RECT (25; 200)**	**D70 (EN 338)**	**BG2**	**1,01 -**

Basisgegevens	
Partiële veiligheidsfactor γM – Massief hout	1,30

Materiaalgegevens		
Buigend (fm,k)	70,0	MPa
Spanning (ft,0,k)	42,0	MPa
Spanning (ft,90,k)	0,6	MPa
Compressie (fc,0,k)	36,0	MPa
Compressie (fc,90,k)	12,0	MPa
Afschuiving (fv,k)	5,0	MPa
Houtsoort	Vast	

De kritische controle is op positie **9,200** m.

Interne krachten		
NEd	27,8	kN
Vy,Ed	-2,7	kN
Vz,Ed	-1,2	kN
TEd	0,0	kNm
My,Ed	-0,2	kNm
Mz,Ed	-0,6	kNm

Modificatiefactor	
Service Klasse	3
Belastingsduur	Korte termijn
Modificatie factor kmod	0,70

..:: DOORSNEDE CONTROLE ::..

Spanning parallel aan de vezel

Volgens EN 1995-1-1 artikel 6.1.2 en formule (6.1)

σt,0,d	5,6	MPa
kh	1,00	
ft,0,d	22,6	MPa
Eenheidscontrole	0,25	-

Druk loodrecht op de vezel
Volgens EN 1995-1-1 artikel 6.1.5 en formule (6.3)

Fc,90,d	1,2	kN
l	100	mm
lef	130	mm
b	25	mm
Aef	3250	mm^2
σc,90,d	0,4	MPa
Steunpunt Voorwaarde	Discreet	
h	200	mm
kc,90	1,00	-
fc,90,d	6,5	MPa
Eenheidscontrole	0,06	-

Buiging
Volgens EN 1995-1-1 artikel 6.1.6 en formule (6.11),(6.12)

σm,y,d	0,9	MPa
kh,y	1,00	
fm,y,d	37,7	MPa
σm,z,d	28,3	MPa
kh,z	1,00	
fm,z,d	37,7	MPa
km	0,70	

Eenheidscontrole (6.11) = 0,02 + 0,53 = 0,55 -
Eenheidscontrole (6.12) = 0,02 + 0,75 = 0,77 -

Afschuiving
Volgens EN 1995-1-1 artikel 6.1.7 en formule (6.13)

kcr	1,00	
τy,d	0,8	MPa
τz,d	0,4	MPa
fv,d	2,7	MPa
Eenheidscontrole τy	0,30	-
Eenheidscontrole τz	0,13	-
Eenheidscontrole Interactie	0,11	-

Opmerking: De interactie vergelijking is toegevoegd als een NCCI.

Torsie
Volgens EN 1995-1-1 artikel 6.1.8 en formule (6.14)

τtor,d	0,2	MPa
kshape	1,30	
fv,d	2,7	MPa
Eenheidscontrole	0,06	-
Eenheidscontrole Interactie Afschuiving	0,17	-

Opmerking: De interactie vergelijking is toegevoegd als een NCCI.

Gecombineerd Buig- en Axiale trek
Volgens EN 1995-1-1 artikel 6.2.3 en formule (6.17),(6.18)

ft,0,d	22,6	MPa
fm,y,d	37,7	MPa
fm,z,d	37,7	MPa
km	0,70	

Eenheidscontrole (6.17) = 0,25 + 0,02 + 0,53 = 0,80 -
Eenheidscontrole (6.18) = 0,25 + 0,02 + 0,75 = **1,01** -

De staaf voldoet NIET aan de doorsnedecontrole!

..:: STABILITEITSCONTROLE ::..

Opmerking: Alleen de doorsnede controle wordt uitgevoerd voor deze staaf.

J.2 Opening or closing mitre gate

The input and results of the mitre gate during opening or closing are shown here.

Materiaallijst

Selectie: Alle
Sorteertype: Materiaal

Samenvatting

Materiaal	Massa [kg]	Oppervlak [mm²]	Volume [m³]
Staal	79223,8	134555941,7	1,0092e+01
Hout	4032,0	33600000,0	4,2000e+00
Totaal	83255,8	168155941,7	1,4292e+01

Opmerking: De waarde 'Oppervlak' vertegenwoordigt voor 1D-elementen de totale blootgestelde oppervlakte, en voor 2D-elementen correspondeert deze alleen met de oppervlakte van het vlak met het zwaartepunt.

Staal (1D)

Materiaal	Dichtheid [kg/m³]	Massa [kg]	Oppervlak [mm²]	Volume [m³]
S 235 inf stiff	7850,0	79223,8	134555941,7	1,0092e+01
Totaal		79223,8	134555941,7	1,0092e+01

Hout (1D)

Materiaal	Dichtheid [kg/m³]	Massa [kg]	Oppervlak [mm²]	Volume [m³]
D70 (EN 338)	960,0	4032,0	33600000,0	4,2000e+00
Totaal		4032,0	33600000,0	4,2000e+00

1. Reacties; Rx

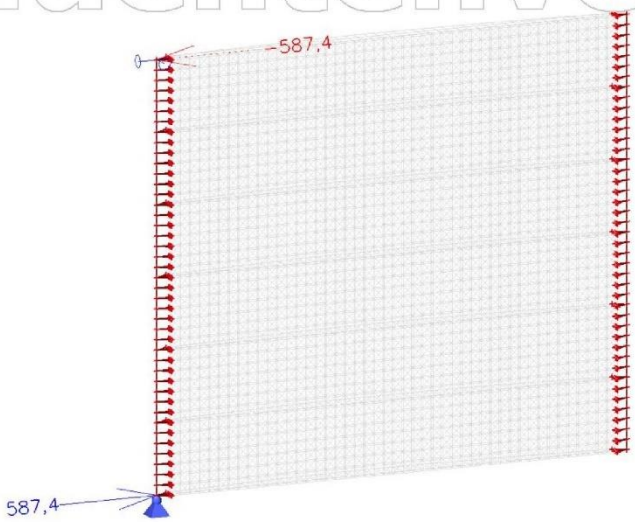

2. Reacties; Ry

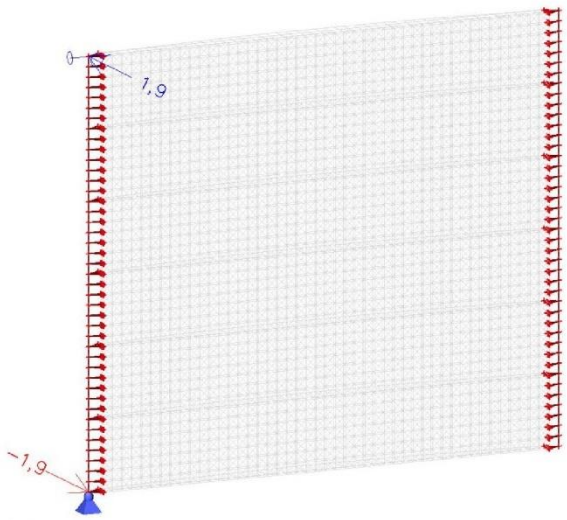

3. Reacties; Rz

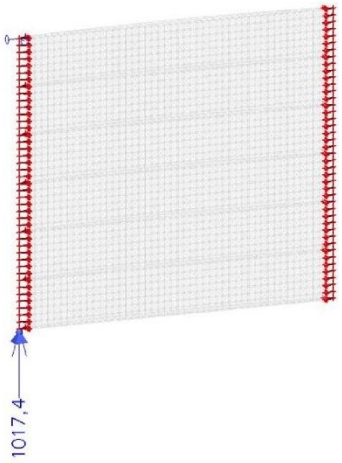

4. Vervormingen van staaf; uz Skin plate

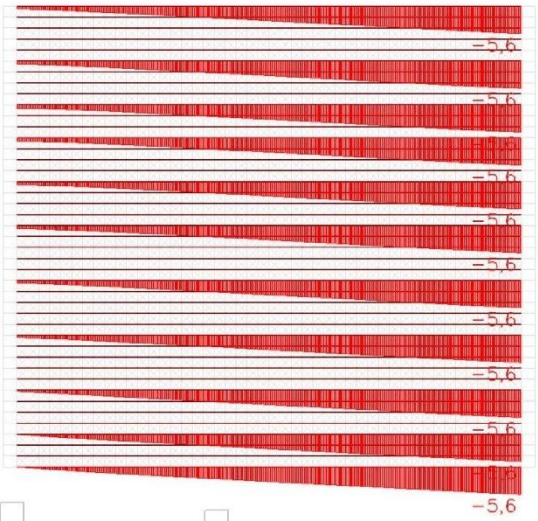

5. Interne krachten in staaf; N Layer 1

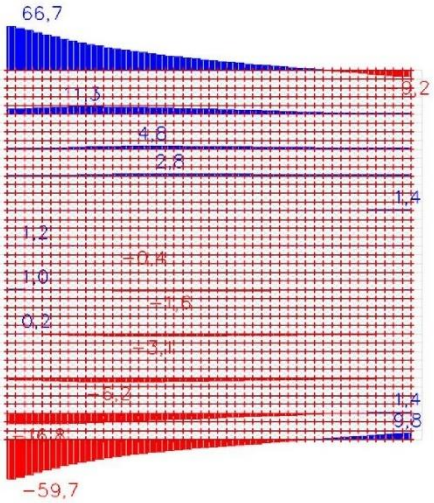

6. Interne krachten in staaf; N Layer 2

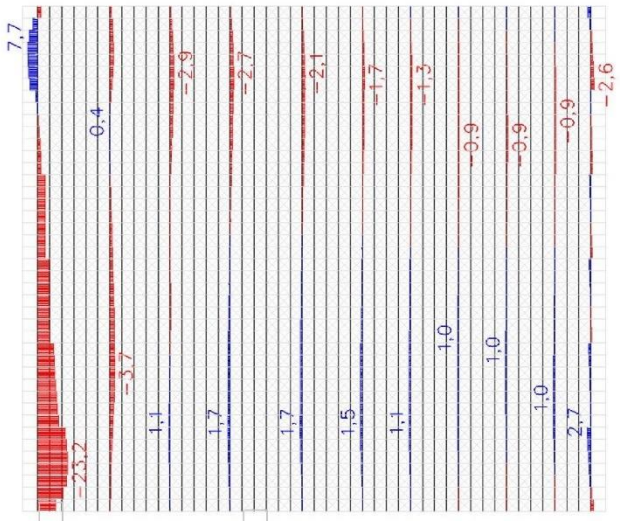

7. Interne krachten in staaf; N Layer 3

8. Interne krachten in staaf; N Layer 4

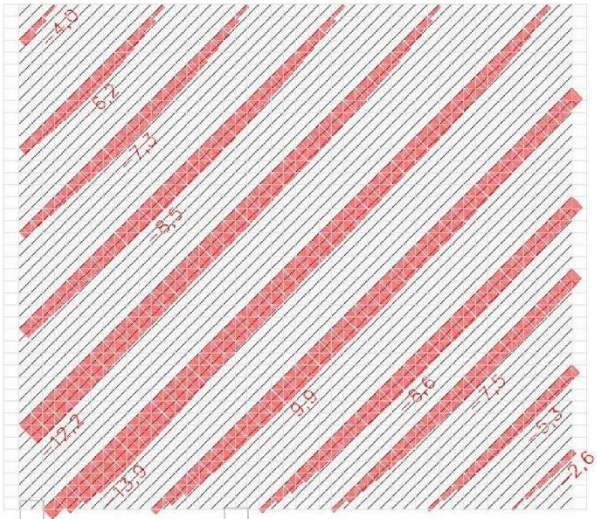

9. Interne krachten in staaf; N Layer 5

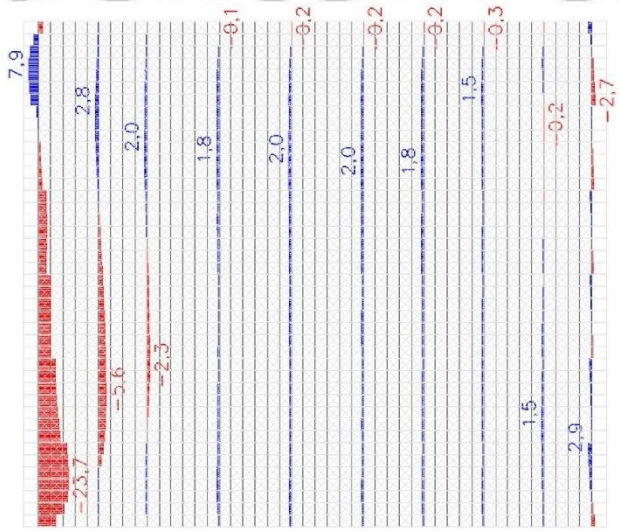

10. Interne krachten in staaf; N Layer 6

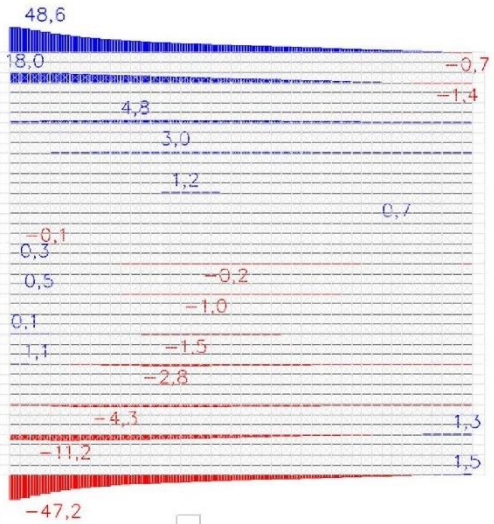

11. Interne krachten in staaf; N Web plate

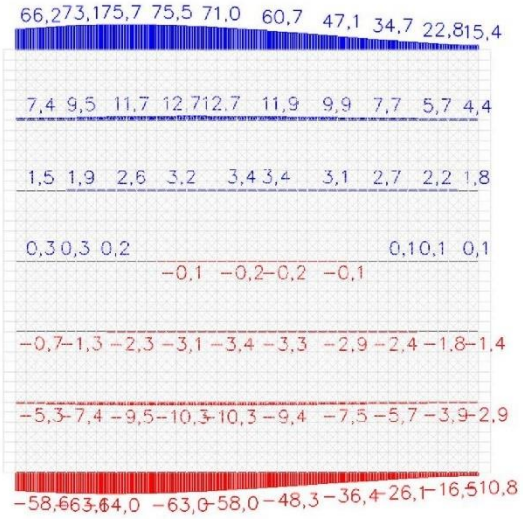

12. Interne krachten in staaf; N Girder

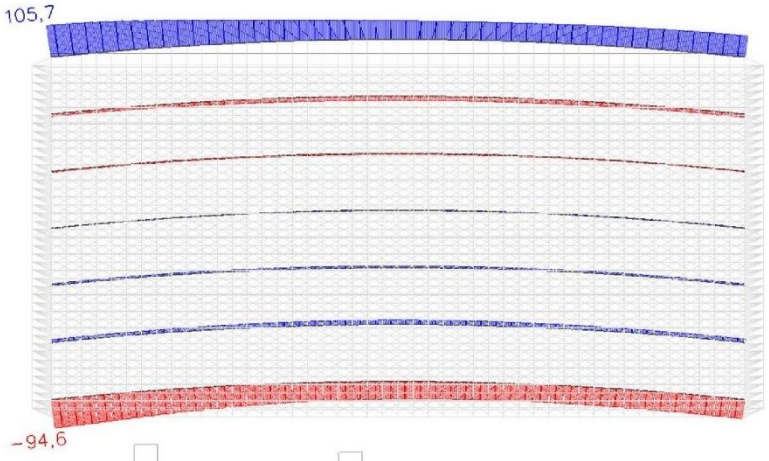

17. Hout UGT controle; Girders

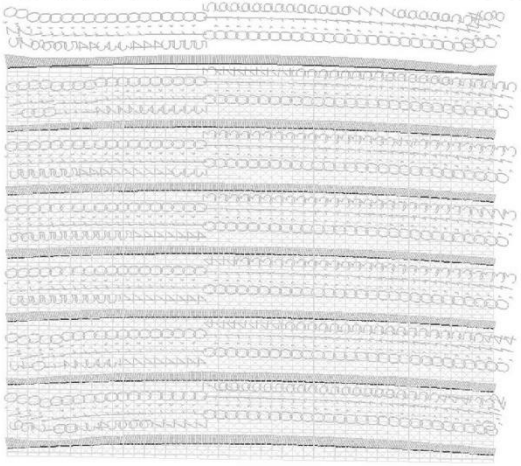

18. Hout UGT controle; Web plate

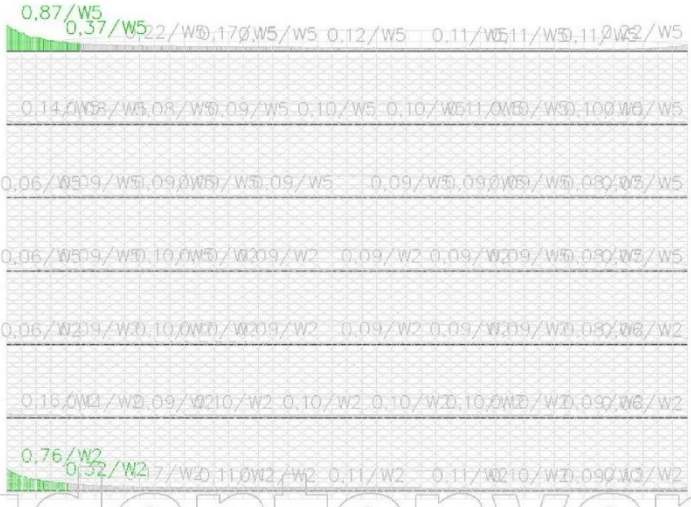

19. Hout UGT controle; Layer 1

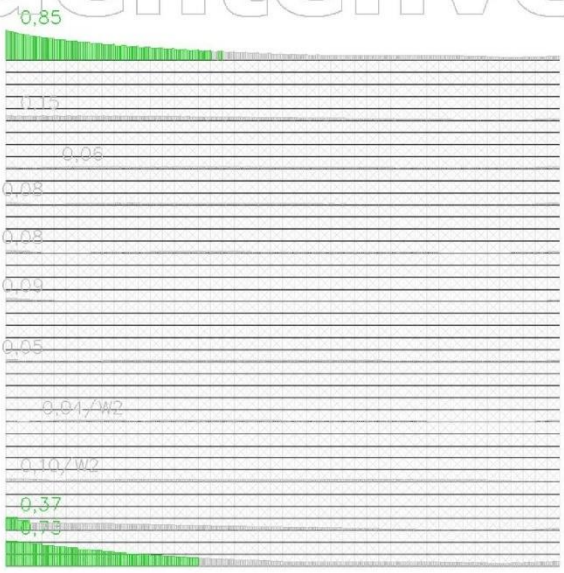

20. Hout UGT controle; Layer 2

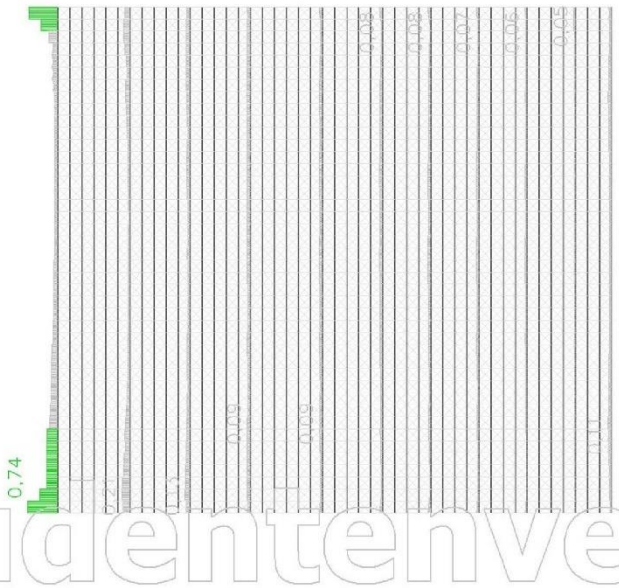

21. Hout UGT controle; Layer 3

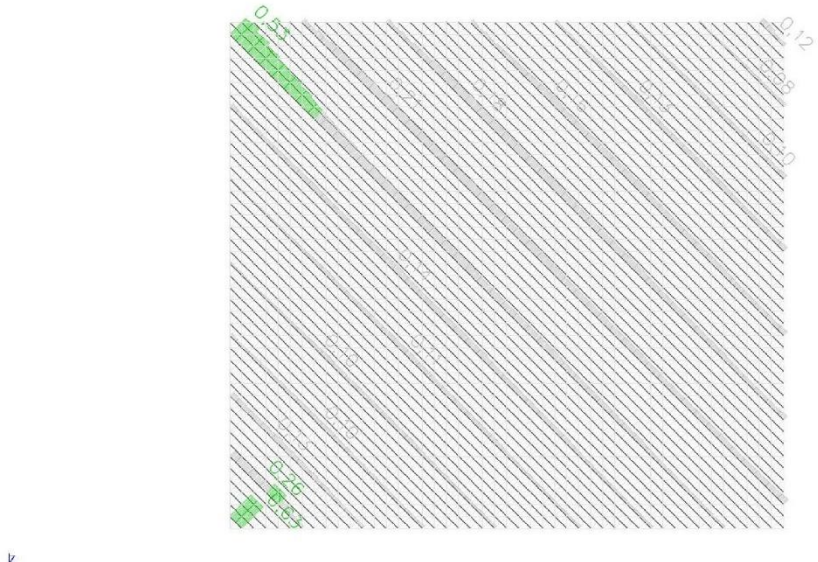

22. Hout UGT controle; Layer 4

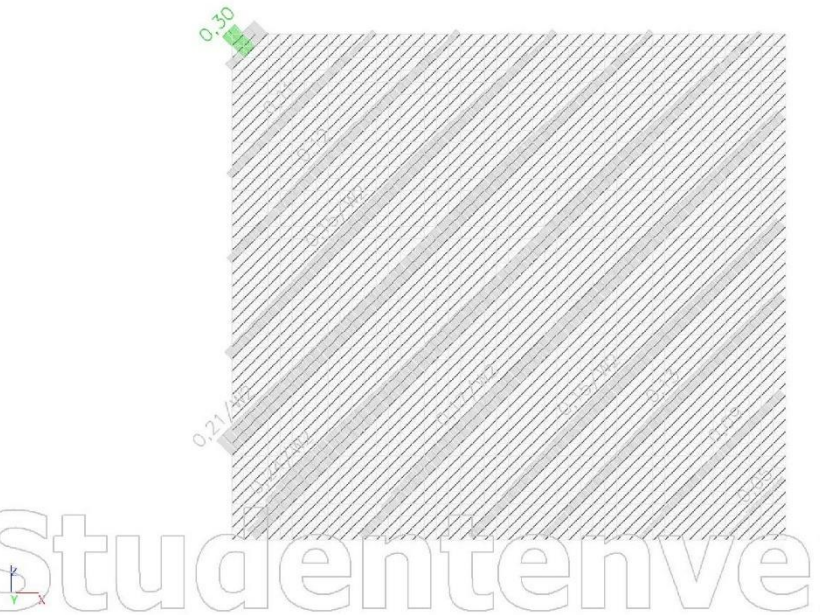

23. Hout UGT controle; Layer 5

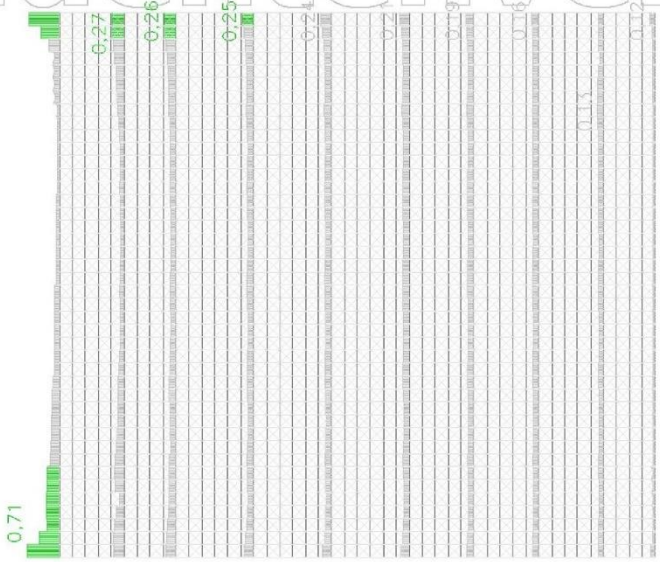

24. Hout UGT controle; Layer 6

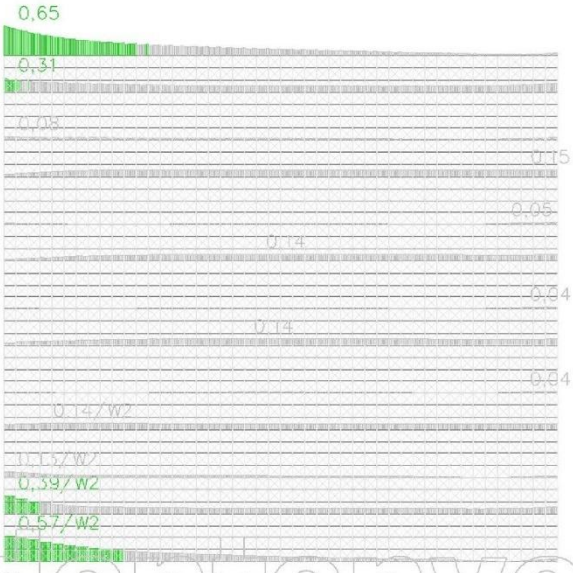

1. Hout UGT controle Extreme layer 1

Lineaire berekening, Extreem : Staaf
Selectie : S1
Belastingsgevallen : BG1

EN 1995-1-1 Normcontrole

Ligger S1	**9,200 m**	**Skin plate - RECT (25; 200)**	**D70 (EN 338)**	**BG1**	**1,00 -**

Basisgegevens		
Partiële veiligheidsfactor γM – Massief hout	1,30	

Materiaalgegevens		
Buigend (fm,k)	70,0	MPa
Spanning (ft,0,k)	42,0	MPa
Spanning (ft,90,k)	0,6	MPa
Compressie (fc,0,k)	36,0	MPa
Compressie (fc,90,k)	12,0	MPa
Afschuiving (fv,k)	5,0	MPa
Houtsoort	Vast	

De kritische controle is op positie **0,000** m.

Interne krachten		
NEd	-59,7	kN
Vy,Ed	-0,1	kN
Vz,Ed	3,4	kN
TEd	0,0	kNm
My,Ed	-1,1	kNm
Mz,Ed	0,0	kNm

Modificatiefactor	
Service Klasse	3
Belastingsduur	Permanent
Modificatie factor kmod	0,50

..:: DOORSNEDE CONTROLE ::..

Compressie parallel aan de vezel
Volgens EN 1995-1-1 artikel 6.1.4 en formule (6.2)

σc,0,d	11,9	MPa
fc,0,d	13,8	MPa
Eenheidscontrole	0,86	-

Druk loodrecht op de vezel
Volgens EN 1995-1-1 artikel 6.1.5 en formule (6.3)

Fc,90,d	3,4	kN
l	100	mm
lef	130	mm
b	25	mm
Aef	3250	mm^2
σc,90,d	1,1	MPa
Steunpunt Voorwaarde	Discreet	
h	200	mm
kc,90	1,00	-
fc,90,d	4,6	MPa
Eenheidscontrole	0,23	-

Buiging
Volgens EN 1995-1-1 artikel 6.1.6 en formule (6.11),(6.12)

σm,y,d	6,5	MPa
kh,y	1,00	
fm,y,d	26,9	MPa
σm,z,d	0,5	MPa
kh,z	1,00	
fm,z,d	26,9	MPa
km	0,70	

Eenheidscontrole (6.11) = 0,24 + 0,01 = 0,25 -
Eenheidscontrole (6.12) = 0,17 + 0,02 = 0,19 -

Afschuiving
Volgens EN 1995-1-1 artikel 6.1.7 en formule (6.13)

kcr	1,00	
τy,d	0,0	MPa
τz,d	1,0	MPa
fv,d	1,9	MPa
Eenheidscontrole τy	0,01	-
Eenheidscontrole τz	0,54	-
Eenheidscontrole Interactie	0,29	-

Opmerking: De interactie vergelijking is toegevoegd als een NCCI.

Torsie
Volgens EN 1995-1-1 artikel 6.1.8 en formule (6.14)

τtor,d	0,0	MPa
kshape	1,30	
fv,d	1,9	MPa
Eenheidscontrole	0,00	-
Eenheidscontrole Interactie Afschuiving	0,29	-

Opmerking: De interactie vergelijking is toegevoegd als een NCCI.

Gecombineerde Buiging en Axiale druk
Volgens EN 1995-1-1 artikel 6.2.4 en formule (6.19),(6.20)

fc,0,d	13,8	MPa
fm,y,d	26,9	MPa
fm,z,d	26,9	MPa
km	0,70	

Eenheidscontrole (6.19) = 0,74 + 0,24 + 0,01 = 1,00 -
Eenheidscontrole (6.20) = 0,74 + 0,17 + 0,02 = 0,93 -

De staaf voldoet aan de doorsnedecontrole.

..:: STABILITEITSCONTROLE ::..

Opmerking: Alleen de doorsnede controle wordt uitgevoerd voor deze staaf.

2. Hout UGT controle Extreme layer 4

Lineaire berekening, Extreem : Staaf
Selectie : S9, S178, S219
Belastingsgevallen : BG1

EN 1995-1-1 Normcontrole

Ligger S9	**9,200 m**	**Skin plate - RECT (25; 200)**	**D70 (EN 338)**	**BG1**	**0,09 -**

Basisgegevens		
Partiële veiligheidsfactor	γM – Massief hout	1,30

Materiaalgegevens		
Buigend (fm,k)	70,0	MPa
Spanning (ft,0,k)	42,0	MPa
Spanning (ft,90,k)	0,6	MPa
Compressie (fc,0,k)	36,0	MPa
Compressie (fc,90,k)	12,0	MPa
Afschuiving (fv,k)	5,0	MPa
Houtsoort	Vast	

De kritische controle is op positie **0,200** m.

Interne krachten		
NEd	-1,4	kN
Vy,Ed	0,0	kN
Vz,Ed	0,6	kN
TEd	0,0	kNm
My,Ed	-0,2	kNm
Mz,Ed	0,0	kNm

Modificatiefactor	
Service Klasse	3
Belastingsduur	Permanent
Modificatie factor kmod	0,50

..:: DOORSNEDE CONTROLE ::..

Compressie parallel aan de vezel
Volgens EN 1995-1-1 artikel 6.1.4 en formule (6.2)

σc,0,d	0,3	MPa
fc,0,d	13,8	MPa
Eenheidscontrole	0,02	-

Druk loodrecht op de vezel
Volgens EN 1995-1-1 artikel 6.1.5 en formule (6.3)

Fc,90,d	0,0	kN
l	100	mm
lef	160	mm
b	25	mm
Aef	4000	mm²
σc,90,d	0,0	MPa
Steunpunt Voorwaarde	Discreet	
h	200	mm
kc,90	1,00	-
fc,90,d	4,6	MPa
Eenheidscontrole	0,00	-

Buiging
Volgens EN 1995-1-1 artikel 6.1.6 en formule (6.11),(6.12)

σm,y,d	1,0	MPa
kh,y	1,00	
fm,y,d	26,9	MPa
σm,z,d	0,1	MPa
kh,z	1,00	
fm,z,d	26,9	MPa
km	0,70	

Eenheidscontrole (6.11) = 0,04 + 0,00 = 0,04 -
Eenheidscontrole (6.12) = 0,03 + 0,00 = 0,03 -

Afschuiving
Volgens EN 1995-1-1 artikel 6.1.7 en formule (6.13)

kcr	1,00	
τy,d	0,0	MPa
τz,d	0,2	MPa
fv,d	1,9	MPa
Eenheidscontrole τy	0,00	-
Eenheidscontrole τz	0,09	-
Eenheidscontrole Interactie	0,01	-

Opmerking: De interactie vergelijking is toegevoegd als een NCCI.

Torsie
Volgens EN 1995-1-1 artikel 6.1.8 en formule (6.14)

τtor,d	0,0	MPa
kshape	1,30	
fv,d	1,9	MPa
Eenheidscontrole	0,01	-
Eenheidscontrole Interactie Afschuiving	0,02	-

Opmerking: De interactie vergelijking is toegevoegd als een NCCI.

Gecombineerde Buiging en Axiale druk
Volgens EN 1995-1-1 artikel 6.2.4 en formule (6.19),(6.20)

fc,0,d	13,8	MPa
fm,y,d	26,9	MPa
fm,z,d	26,9	MPa
km	0,70	

Eenheidscontrole (6.19) = 0,00 + 0,04 + 0,00 = 0,04 -
Eenheidscontrole (6.20) = 0,00 + 0,03 + 0,00 = 0,03 -

De staaf voldoet aan de doorsnedecontrole.

..:: STABILITEITSCONTROLE ::..

Opmerking: Alleen de doorsnede controle wordt uitgevoerd voor deze staaf.

EN 1995-1-1 Normcontrole

Ligger S178	**11,879 m**	**Skin plate diagonals - RECT (25; 141)**	**D70 (EN 338)**	**BG1**	**1,30 -**

Basisgegevens	
Partiële veiligheidsfactor γM – Massief hout	1,30

Materiaalgegevens		
Buigend (fm,k)	70,0	MPa
Spanning (ft,0,k)	42,0	MPa
Spanning (ft,90,k)	0,6	MPa
Compressie (fc,0,k)	36,0	MPa
Compressie (fc,90,k)	12,0	MPa
Afschuiving (fv,k)	5,0	MPa
Houtsoort	Vast	

De kritische controle is op positie **11,597** m.

Interne krachten		
NEd	-52,1	kN
Vy,Ed	0,0	kN
Vz,Ed	1,4	kN
TEd	0,0	kNm
My,Ed	-0,3	kNm
Mz,Ed	0,0	kNm

Modificatiefactor	
Service Klasse	3
Belastingsduur	Permanent
Modificatie factor kmod	0,50

..:: DOORSNEDE CONTROLE ::..

Compressie parallel aan de vezel
Volgens EN 1995-1-1 artikel 6.1.4 en formule (6.2)

σc,0,d	14,8	MPa
fc,0,d	13,8	MPa
Eenheidscontrole	**1,07**	-

Druk loodrecht op de vezel
Volgens EN 1995-1-1 artikel 6.1.5 en formule (6.3)

Fc,90,d	0,5	kN
l	100	mm
lef	160	mm
b	25	mm
Aef	4000	mm²
σc,90,d	0,1	MPa
Steunpunt Voorwaarde	Discreet	
h	141	mm
kc,90	1,00	-
fc,90,d	4,6	MPa
Eenheidscontrole	0,03	-

Buiging
Volgens EN 1995-1-1 artikel 6.1.6 en formule (6.11),(6.12)

σm,y,d	4,2	MPa
kh,y	1,00	
fm,y,d	26,9	MPa
σm,z,d	0,3	MPa
kh,z	1,00	
fm,z,d	26,9	MPa
km	0,70	

Eenheidscontrole (6.11) = 0,16 + 0,01 = 0,17 -
Eenheidscontrole (6.12) = 0,11 + 0,01 = 0,12 -

Afschuiving
Volgens EN 1995-1-1 artikel 6.1.7 en formule (6.13)

kcr	1,00	
τy,d	0,0	MPa
τz,d	0,6	MPa
fv,d	1,9	MPa
Eenheidscontrole τy	0,00	-
Eenheidscontrole τz	0,31	-
Eenheidscontrole Interactie	0,10	-

Opmerking: De interactie vergelijking is toegevoegd als een NCCI.

Torsie
Volgens EN 1995-1-1 artikel 6.1.8 en formule (6.14)

τtor,d	0,0	MPa
kshape	1,28	
fv,d	1,9	MPa
Eenheidscontrole	0,01	-
Eenheidscontrole Interactie Afschuiving	0,11	-

Opmerking: De interactie vergelijking is toegevoegd als een NCCI.

Gecombineerde Buiging en Axiale druk
Volgens EN 1995-1-1 artikel 6.2.4 en formule (6.19),(6.20)

fc,0,d	13,8	MPa
fm,y,d	26,9	MPa
fm,z,d	26,9	MPa
km	0,70	

Eenheidscontrole (6.19) = 1,14 + 0,16 + 0,01 = **1,30** -
Eenheidscontrole (6.20) = 1,14 + 0,11 + 0,01 = **1,26** -

De staaf voldoet NIET aan de doorsnedecontrole!

..:: STABILITEITSCONTROLE ::..

Opmerking: Alleen de doorsnede controle wordt uitgevoerd voor deze staaf.

EN 1995-1-1 Normcontrole

Ligger S219	**11,879 m**	**Skin plate diagonals - RECT (25; 141)**	**D70 (EN 338)**	**BG1**	**0,31 -**

Basisgegevens		
Partiële veiligheidsfactor γM – Massief hout	1,30	

Materiaalgegevens		
Buigend (fm,k)	70,0	MPa
Spanning (ft,0,k)	42,0	MPa
Spanning (ft,90,k)	0,6	MPa
Compressie (fc,0,k)	36,0	MPa
Compressie (fc,90,k)	12,0	MPa
Afschuiving (fv,k)	5,0	MPa
Houtsoort	Vast	

De kritische controle is op positie **10,748** m.

Interne krachten		
NEd	-15,4	kN
Vy,Ed	0,0	kN
Vz,Ed	0,3	kN
TEd	0,0	kNm
My,Ed	0,0	kNm
Mz,Ed	0,0	kNm

Modificatiefactor	
Service Klasse	3
Belastingsduur	Permanent
Modificatie factor kmod	0,50

..:: DOORSNEDE CONTROLE ::..

Compressie parallel aan de vezel
Volgens EN 1995-1-1 artikel 6.1.4 en formule (6.2)

σc,0,d	4,4	MPa
fc,0,d	13,8	MPa
Eenheidscontrole	0,31	-

Druk loodrecht op de vezel
Volgens EN 1995-1-1 artikel 6.1.5 en formule (6.3)

Fc,90,d	0,0	kN
l	100	mm
lef	160	mm
b	25	mm
Aef	4000	mm^2
σc,90,d	0,0	MPa
Steunpunt Voorwaarde	Discreet	
h	141	mm
kc,90	1,00	-
fc,90,d	4,6	MPa
Eenheidscontrole	0,00	-

Buiging
Volgens EN 1995-1-1 artikel 6.1.6 en formule (6.11),(6.12)

σm,y,d	0,4	MPa
kh,y	1,00	
fm,y,d	26,9	MPa
σm,z,d	0,1	MPa
kh,z	1,00	
fm,z,d	26,9	MPa
km	0,70	

Eenheidscontrole (6.11) = 0,01 + 0,00 = 0,02 -
Eenheidscontrole (6.12) = 0,01 + 0,00 = 0,01 -

Afschuiving
Volgens EN 1995-1-1 artikel 6.1.7 en formule (6.13)

kcr	1,00	
τy,d	0,0	MPa
τz,d	0,1	MPa
fv,d	1,9	MPa
Eenheidscontrole τy	0,00	-
Eenheidscontrole τz	0,06	-
Eenheidscontrole Interactie	0,00	-

Opmerking: De interactie vergelijking is toegevoegd als een NCCI.

Torsie
Volgens EN 1995-1-1 artikel 6.1.8 en formule (6.14)

τtor,d	0,0	MPa
kshape	1,28	
fv,d	1,9	MPa
Eenheidscontrole	0,00	-
Eenheidscontrole Interactie Afschuiving	0,01	-

Opmerking: De interactie vergelijking is toegevoegd als een NCCI.

Gecombineerde Buiging en Axiale druk
Volgens EN 1995-1-1 artikel 6.2.4 en formule (6.19),(6.20)

fc,0,d	13,8	MPa
fm,y,d	26,9	MPa
fm,z,d	26,9	MPa
km	0,70	

Eenheidscontrole (6.19) = 0,10 + 0,01 + 0,00 = 0,12 -
Eenheidscontrole (6.20) = 0,10 + 0,01 + 0,00 = 0,11 -

De staaf voldoet aan de doorsnedecontrole.

.:: STABILITEITSCONTROLE ::..

Opmerking: Alleen de doorsnede controle wordt uitgevoerd voor deze staaf.

3. Hout UGT controle Extreme layer 6

Lineaire berekening, Extreem : Staaf
Selectie : S312
Belastingsgevallen : BG1

EN 1995-1-1 Normcontrole

Ligger S312	**9,200 m**	**Skin plate - RECT (25; 200)**	**D70 (EN 338)**	**BG1**	**0,71 -**

Basisgegevens	
Partiële veiligheidsfactor γM – Massief hout	1,30

Materiaalgegevens		
Buigend (fm,k)	70,0	MPa
Spanning (ft,0,k)	42,0	MPa
Spanning (ft,90,k)	0,6	MPa
Compressie (fc,0,k)	36,0	MPa
Compressie (fc,90,k)	12,0	MPa
Afschuiving (fv,k)	5,0	MPa
Houtsoort	Vast	

De kritische controle is op positie **0,000** m.

Interne krachten		
NEd	-47,2	kN
Vy,Ed	-0,1	kN
Vz,Ed	3,0	kN
TEd	0,0	kNm
My,Ed	-1,0	kNm
Mz,Ed	0,0	kNm

Modificatiefactor	
Service Klasse	3
Belastingsduur	Permanent
Modificatie factor kmod	0,50

..:: DOORSNEDE CONTROLE ::..

Compressie parallel aan de vezel
Volgens EN 1995-1-1 artikel 6.1.4 en formule (6.2)

σc,0,d	9,4	MPa
fc,0,d	13,8	MPa
Eenheidscontrole	0,68	-

Druk loodrecht op de vezel
Volgens EN 1995-1-1 artikel 6.1.5 en formule (6.3)

Fc,90,d	3,0	kN
l	100	mm
lef	130	mm
b	25	mm
Aef	3250	mm^2
σc,90,d	0,9	MPa
Steunpunt Voorwaarde	Discreet	
h	200	mm
kc,90	1,00	-
fc,90,d	4,6	MPa
Eenheidscontrole	0,20	-

Buiging
Volgens EN 1995-1-1 artikel 6.1.6 en formule (6.11),(6.12)

σm,y,d	6,2	MPa
kh,y	1,00	
fm,y,d	26,9	MPa
σm,z,d	0,5	MPa
kh,z	1,00	
fm,z,d	26,9	MPa
km	0,70	

Eenheidscontrole (6.11) = 0,23 + 0,01 = 0,24 -
Eenheidscontrole (6.12) = 0,16 + 0,02 = 0,18 -

Afschuiving
Volgens EN 1995-1-1 artikel 6.1.7 en formule (6.13)

kcr	1,00	
τy,d	0,0	MPa
τz,d	0,9	MPa
fv,d	1,9	MPa
Eenheidscontrole τy	0,01	-
Eenheidscontrole τz	0,46	-
Eenheidscontrole Interactie	0,21	-

Opmerking: De interactie vergelijking is toegevoegd als een NCCI.

Torsie
Volgens EN 1995-1-1 artikel 6.1.8 en formule (6.14)

τtor,d	0,0	MPa
kshape	1,30	
fv,d	1,9	MPa
Eenheidscontrole	0,00	-
Eenheidscontrole Interactie Afschuiving	0,21	-

Opmerking: De interactie vergelijking is toegevoegd als een NCCI.

Gecombineerde Buiging en Axiale druk
Volgens EN 1995-1-1 artikel 6.2.4 en formule (6.19),(6.20)

fc,0,d	13,8	MPa
fm,y,d	26,9	MPa
fm,z,d	26,9	MPa
km	0,70	

Eenheidscontrole (6.19) = 0,46 + 0,23 + 0,01 = 0,71 -
Eenheidscontrole (6.20) = 0,46 + 0,16 + 0,02 = 0,64 -

De staaf voldoet aan de doorsnedecontrole.

..:: STABILITEITSCONTROLE ::..

Opmerking: Alleen de doorsnede controle wordt uitgevoerd voor deze staaf.

4. Hout UGT controle Extreme Web plate

Lineaire berekening, Extreem : Staaf
Selectie : S21294
Belastingsgevallen : BG1

EN 1995-1-1 Normcontrole

Ligger S21294	**0,600 m**	**Web plate - RECT (30; 150)**	**D70 (EN 338)**	**BG1**	**1,04 -**

Waarschuwing: Deze variabele doorsnede wordt niet beschouwd als Enkel Tapse Ligger of Dubbele Tapse Ligger volgens EN 1995-1-1. Als resultaat hiervan zijn er geen specifieke controles voor tapse liggers uitgevoerd. Gelieve de geometrie van deze ligger te herzien en de additionele uitvoertabellen van Tapse liggers te controleren.

Basisgegevens	
Partiële veiligheidsfactor γM – Massief hout	1,30

Materiaalgegevens		
Buigend (fm,k)	70,0	MPa
Spanning (ft,0,k)	42,0	MPa
Spanning (ft,90,k)	0,6	MPa
Compressie (fc,0,k)	36,0	MPa
Compressie (fc,90,k)	12,0	MPa
Afschuiving (fv,k)	5,0	MPa
Houtsoort	Vast	

De kritische controle is op positie **0,000** m.

Interne krachten		
NEd	63,0	kN
Vy,Ed	-0,7	kN
Vz,Ed	1,3	kN
TEd	0,0	kNm
My,Ed	-0,5	kNm
Mz,Ed	0,0	kNm

Modificatiefactor	
Service Klasse	3
Belastingsduur	Permanent
Modificatie factor kmod	0,50

..:: DOORSNEDE CONTROLE ::..

Spanning parallel aan de vezel
Volgens EN 1995-1-1 artikel 6.1.2 en formule (6.1)

σt,0,d	14,0	MPa
kh	1,00	-
ft,0,d	16,2	MPa
Eenheidscontrole	0,87	-

Druk loodrecht op de vezel
Volgens EN 1995-1-1 artikel 6.1.5 en formule (6.3)

Fc,90,d	1,3	kN
l	100	mm
lef	130	mm
b	30	mm
Aef	3900	mm^2
σc,90,d	0,3	MPa
Steunpunt Voorwaarde	Discreet	
h	150	mm
kc,90	1,00	-
fc,90,d	4,6	MPa
Eenheidscontrole	0,07	-

Buiging
Volgens EN 1995-1-1 artikel 6.1.6 en formule (6.11),(6.12)

σm,y,d	4,4	MPa
kh,y	1,00	
fm,y,d	26,9	MPa
σm,z,d	0,5	MPa
kh,z	1,00	
fm,z,d	26,9	MPa
km	0,70	

Eenheidscontrole (6.11) = 0,17 + 0,01 = 0,18 -
Eenheidscontrole (6.12) = 0,12 + 0,02 = 0,13 -

Afschuiving
Volgens EN 1995-1-1 artikel 6.1.7 en formule (6.13)

kcr	1,00	
τy,d	0,2	MPa
τz,d	0,4	MPa
fv,d	1,9	MPa
Eenheidscontrole τy	0,12	-
Eenheidscontrole τz	0,23	-
Eenheidscontrole Interactie	0,07	

Opmerking: De interactie vergelijking is toegevoegd als een NCCI.

Torsie
Volgens EN 1995-1-1 artikel 6.1.8 en formule (6.14)

τtor,d	0,0	MPa
kshape	1,25	
fv,d	1,9	MPa
Eenheidscontrole	0,02	-
Eenheidscontrole Interactie Afschuiving	0,09	-

Opmerking: De interactie vergelijking is toegevoegd als een NCCI.

Gecombineerd Buig- en Axiale trek
Volgens EN 1995-1-1 artikel 6.2.3 en formule (6.17),(6.18)

ft,0,d	16,2	MPa
fm,y,d	26,9	MPa
fm,z,d	26,9	MPa
km	0,70	

Eenheidscontrole (6.17) = 0,87 + 0,17 + 0,01 = **1,04** -
Eenheidscontrole (6.18) = 0,87 + 0,12 + 0,02 = **1,00** -

De staaf voldoet NIET aan de doorsnedecontrole!

..:: STABILITEITSCONTROLE ::..

Opmerking: Alleen de doorsnede controle wordt uitgevoerd voor deze staaf.

K. Elaboration of modelling with rotational and translational spring

This appendix shows the elaboration of an alternative method to model the interaction of the dowel and lamellae in a cross dowel laminated panel. The exact values of the springs need to be determined by laboratory tests and are therefore not applied in this thesis. The forces in the panel layer result in translational and rotational movement on the dowel. Therefore the interaction between the dowel and panel layers is rationally expected to be modelled with a rotational and translational spring. An example of the modelling of the dowel is shown in Figure 125.

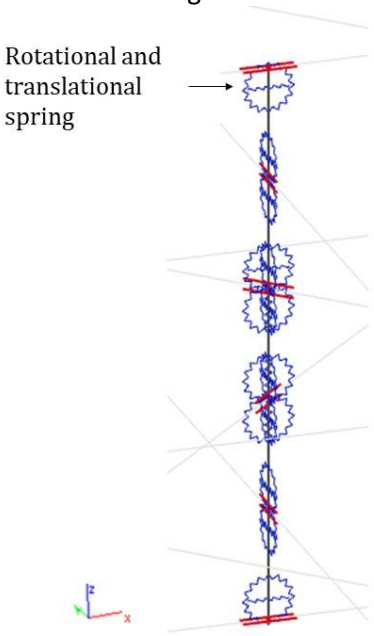

Figure 125: Dowel layout of panel with rotational and translational springs

For a dowel cross laminated panel with 6 layers, the dowel in the panel is divided in 5 part. Each end of the dowel contains a rotational and translational spring. The stiffness of these springs is explained in the following sections.

K.1 Rotational stiffness

The determination of the rotational spring is done in the following manner. Two timber layers connected with a dowel are subjected to shear. As Figure 126 indicates, due to shear forces in the timber layers, the dowel rotates.

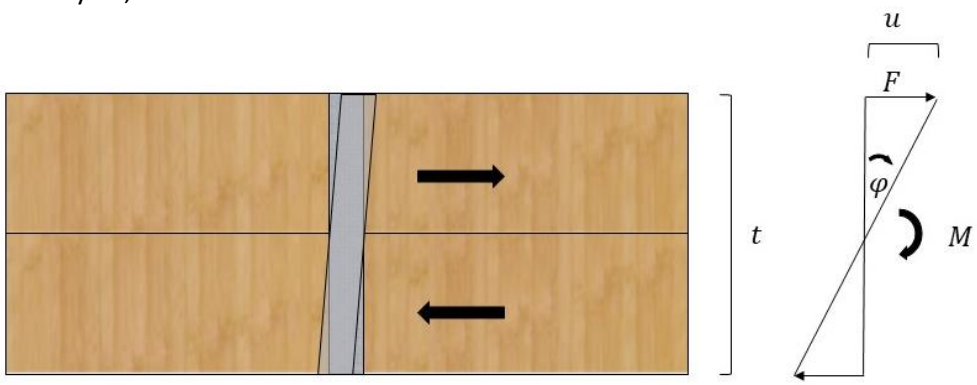

Figure 126: Determination of rotational spring for 2 layers subjected to shear

The derivation of the spring stiffness is given below:

$$k = \frac{M}{\varphi} = \frac{\frac{2}{3}Ft}{\frac{u}{\frac{1}{2}t}} = \frac{\frac{1}{3}Ft^2}{u}$$

$$M = \frac{2}{3}Ft$$

$$\varphi = \frac{u}{\frac{1}{2}t}$$

$$u = \frac{F}{k}$$

$$F = f_{max} * A$$

$$A = d * t$$

$$f_{max} = 0.082 * (1 - 0.01 * d) * \rho_k$$

K.2 Translational stiffness

The stiffness of the translational spring for a doweled cross laminated panel needs to be obtained by tests as well. The stiffness of the translational spring is not equal to the slip modulus of the Eurocode as this slip modulus does not make distinction of the direction of the fibres. As timber is anisotropic, the direction of the fibre is assumed to be important for the stiffness of the translational spring for dowel cross laminated timber.

$$k = \frac{F}{u}$$

u